

MASTER THESIS PROJECT

FLOW FIELD CHARACTERISTICS IN VERTICAL CHANNEL WITH ONE HEATED SURFACE

— OCTOBER 23, 2015 —

Indoor Environmental and Energy Engineering
School of Engineering and Science, Aalborg University

Aalborg University
Engineering and Science
Sofiendalsvej 9-11
9000 Aalborg
Phone No.: 99 40 84 84
<http://www.byggeri.aau.dk>

Synopsis:

Title:

Flow Field Characteristics in Vertical Channel With One Heated Surface.

Project period:

IE, spring-fall 2015

Participant:

Maria Bagge Mikkelsen

Supervisor:

Olena Kalyanova Larsen
Li Liu

Editions: 3

Number of pages: 195

Completed: 23-10-2015

The turbulent natural convection in a vertical parallel-plate channel with one heated surface is studied in the present project. The main objective of this study is to focus on the particular recirculation flow appearing at certain conditions. The project is divided into three main parts; a pre-study, an experimental study and a numerical study. In the pre-study the theory about convective heat transfer is presented and a literature review is conducted regarding the work that has been done up till now. The experimental work includes temperature measurements in a vertical channel and data processing in order to analyze the flow pattern inside the cavity. The experimental results are then compared to the literature. The numerical study contains a complete description of the numerical solution technique, where after the solution is being validated according the results obtained in the experimental work.

The content of the report is available but the publication can only happen in agreement with the authors.



Preface

The following Master Thesis project is completed by student Maria Bagge Mikkelsen at 4th semester of the master education Indoor Environmental and Energy Engineering at Aalborg University. The project is completed in the Fall 2015 and it focuses on the subject convective flow conditions inside a one-sided heated vertical channel. The first six months of experimental work is conducted in cooperation with two other master students, who finished their work in June 2015.

The project contains references, all of which are collected in a bibliography at the end of the report. All the sources in the report are given by Harvard method and divided in books, articles, homepages and reports. Referring to books is done at the following way; author, title, ISBN-number, edition, publisher, year. For articles; author, title, edition, date, year. For homepages; author, title, URL-address, year, date of use. Tables and figures without source reference are self-made. If a source reference is located before the full stop it refers to the concerned sentence, otherwise it is referring to the previous section, if it is located after the full stop.

Maria Bagge Mikkelsen



Resumé

Turbulent naturlig konvektion i en vertikal parallel kanal var studeret i den foreliggende projekt. En litteratur analyse viste, at to mulige typer strømningstilstande kan forekomme udover det fra teorien kendte standard strømningstilstande. Det er, et tilfælde med ekstrem recirculation strømning, som foregår i hele kanalen, hvor luften er varmet op og strømmer langs den varme flade mens den ændrer retning langs den kolde flade. Et andet muligt type flow er også recirculation, men kun i et begrænset område. Det var bevist i den analyserede litteratur, at tilsynskomsten af recirculerende strømninger var afhængig af de dimensionsløse parametre Rayleigh og Reynolds tal samt Gr/Re^2 -forhold. Eksperimentalt arbejde var udført på et forsøgs anlæg konstrueret af to vertikale plader, hvoraf en kunne opvarmes, og et forsøg er gjort på at finde det interval, hvor recirculation forekommer sammenlignet med litteraturen. Temperature var målt i højden og bredden af den vertikale kanal. Målingerne viste flere tegn på recirculation som fx. dynamiske forhold og deformationer på vertikale og horisontale temperatur profiler. Temperaturene i boksen var forventet at variere med meget lille afvigelse, men på grund af usikkerheder forbundet med målingerne og selve setuppet, kunne indikationerne angående recirculation ikke bevises. Til sidst var en numerisk løsning studeret, som var antaget, at være valideret i forhold til de eksperimentelle resultater, da afvigelsen var mindre end 10 %.



Abstract

The turbulent natural convection in a vertical parallel-plate channel has been studied in the present work. A literature study revealed that two types of flow conditions may occur besides from the standard channel flow. That is, a case of extreme recirculation flow occurring in the entire channel with air moving downstream near the heated surface and reversed direction at the colder surface, and another case where the recirculation flow was appearing in limited regions. In the studied literature it was proved that the appearance of recirculation flow was dependent on dimensionless parameters such as Rayleigh and Reynolds number and Gr/Re^2 - ratio. Experiments were conducted on a test facility of a vertical parallel-plate channel with one heated surface, and an effort was being done to find the range of appearance of recirculation flow compared to the literature. Temperatures were measured along the height and the width of the channel. They revealed several indications of occurrence of flow reversal by dynamic behavior and deformations in both vertical and horizontal temperature profiles. The temperature variations were expected to vary within a small deviation, but due to high uncertainty regarding the set up and measurements the implications were not proved. At last, a numerical solution was studied that was validated according to the experiment within a limit less than 10 %.



Table of contents

Chapter 1 Introduction	1
1.1 Aim of this work	6
I Pre-Study	7
Chapter 2 Convective heat transfer	9
Chapter 3 Literature Study	15
3.1 Summary	28
II Experimental Study	30
Chapter 4 Introduction to Experiment	31
4.1 Experimental set-up	31
4.1.1 Equipment list	32
4.1.2 Inlet and outlet	32
4.1.3 Heating system	33
4.1.4 Temperature measurements	34
4.2 Test conditions	35
Chapter 5 Experimental results and Discussion	39
5.1 Review of Test 1	39
5.1.1 Remarks	52
5.2 Rayleigh Number Dependency	55
5.2.1 Group 1: Change of Heated Surface Temperature	55
5.2.2 Group 2: Change of Inlet Temperature	72
5.2.3 Remarks Regarding Rayleigh Number Dependency	83
5.3 Air Change Rate Influence on Channel Flow	85
5.3.1 Group 3: Influence of ACH	85
5.3.2 Remarks Regarding the Influence of ACH	96

Chapter 6	Thickness of Boundary Layer	97
III	Numerical Study	102
Chapter 7	Numerical solution of Flow Inside a Vertical Channel	103
7.1	Numerical Solution Technique	103
7.1.1	Mesh features	104
7.1.2	General decisions	104
7.1.3	Properties of the fluid material	105
7.1.4	Governing Equations	105
7.2	Turbulence Modelling	106
7.2.1	Radiation Model	108
7.3	Boundary Conditions	109
7.4	Discretization Scheme	110
7.5	Numerical Results and Discussion	112
7.5.1	Further investigation of Numerical Results	117
Chapter 8	Conclusion	123
8.1	Future Work	124
	Bibliography	127
	Appendix A	Wide Cavity
	Appendix B	Positions of Thermocouples
	Appendix C	2D Thermal Pictures
	Appendix D	Test 1
	Appendix E	Test 2
	Appendix F	Test 3
	Appendix G	Test 4
	Appendix H	Test 5
	Appendix I	Test 6
	Appendix J	Comparison Close to Glass Surface of Group 3
	Appendix K	First Period of Experimental Work
	Appendix L	Positions of Thermocouples First Measurement Period
	Appendix M	Velocity Measurements
	Appendix N	Electronic Appendix

Introduction

The global warming is a concern for many countries all over the world which are taking action in decreasing the consumption of fossil fuels. The focus on expanding the use of renewable energy and transforming the energy systems to ones that are cleaner and less dependent on coal and other fossil fuels has impacted the building industry, leading to new and improved approaches. Utilization of the sun and wind for natural ventilation, solar collectors, wind mills and many other applications are fast increasing and is therefore an extensive topic in the research field. It is seen that an increasing number of offices and commercial buildings distinguished by the use of natural ventilation systems are being constructed leading to several problems that needs to be solved. The rise of natural ventilation systems is caused by the well-known "sick-building-syndrome" ¹ that may occur in highly air-conditioned high-rise buildings due to insufficient HVAC systems either caused by lack of maintenance, individual conflicting needs or the high costs of having such systems. Natural ventilation may not be an appropriate strategy for a conventional façade in a high-rise building due to high wind pressures occurring in the upper floors or in noise polluted areas. An installation of a second transparent façade in front of the building enables the use of natural ventilation even by wind speeds up to 10 m/s. Such system is the so-called *Double-Skin Façade* (DSF). [Zollner et al., 2002]

The DSF design is a European architectural trend motivated by the aesthetic need for transparent façades, the desire for reducing the energy consumption for HVAC systems and improving the indoor environments both thermal, atmospheric and acoustic. A building with a DSF therefore provides a "green-energy" statement, and the thermal buffer zone created by the additional skin reduces the heat losses and enables passive solar gains. If the DSF is designed and operated properly the heating demand may be reduced during the winter and the cooling demand during the summer. Furthermore the peak heating and cooling loads may be decreased. In order to have a clear overview the advantages and disadvantages of this system are listed below. [Poirazis, 2004]

¹Sick building syndrome is the situation when occupants in a building experience critical health and comfort problems that appear to be related to the time spent in that building, but no specific cause or illness can be explained.

Advantages

- Possibility of natural ventilation
- Acoustic insulation
- Thermal insulation (especially during the winter)
- Night time natural ventilation is possible
- Energy consumption and environmental impact reduced
- Protection of shading device
- Reduce wind pressure effects in high storeys buildings
- Provide better indoor environment

Disadvantages

- Higher construction costs compared to a conventional façade
- Reduction of internal space in building
- Additional maintenance and operating costs
- Problems with overheating if not designed properly
- Sound transmission problems within the building
- Possible decrease of daylight due to the additional skin

A DSF can cover one or more storeys and consists of two layers of glass that is separated by an air gap, see figure 1.1.

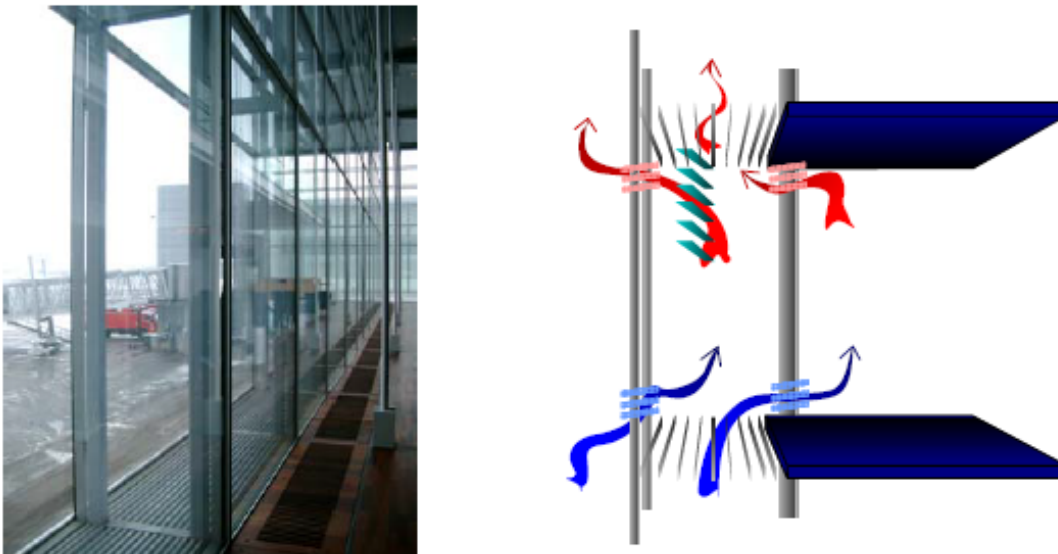


Figure 1.1. Illustration of DSF.

The two layers of glass and air between have an insulating function against extreme temperatures, noise from the outdoors and impact from wind, and the distance may vary between 0.2 to more than 2.0 m [Poirazis, 2004]. The cavity can be mechanically or naturally ventilated, and the ventilation strategy can vary in time. Air may enter the cavity from either outdoors or indoors through an opening and is then extracted to the outdoors or the adjacent room. In order to classify the different types of DSF operations regarding naturally ventilated cavity figure 1.2 on the next page is shown.

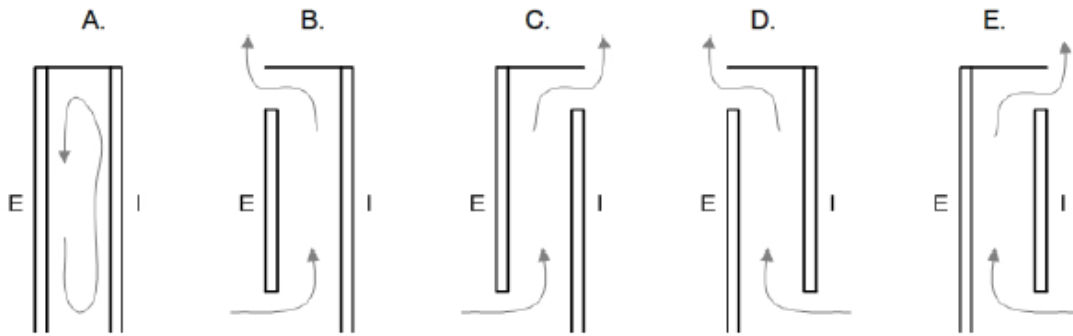


Figure 1.2. Classification of DSF type.

Figure A shows the transparent insulation mode, also called buffer system. Having this system allows daylight into the room and has a benefit in cooler periods, where the DSF increases the insulation ability and radiant temperature in the room. There is no exchange of air to the outdoors or indoors.

The external air curtain mode is shown in figure B. This mode is used to remove excessive heat which occurs in the cavity during warmer periods. The air will enter at the bottom from the outdoors and leave the cavity at the top to the outdoor again; the air is driven by buoyancy and wind forces.

Figure C illustrates the preheating mode that supplies fresh air to the building. This operation mode is often used in the midseason™s where the benefits of the high solar radiation is utilized to heat up the inlet air that has a low temperature due to the outdoor conditions.

Figure D shows the exhaust mode. The air enters the cavity at the bottom from the building and leaves at the top to the exterior. Exploiting the stack effect that is increased due to the solar radiation, the exhaust of air is increased and excessive heat may be removed.

At last the internal air curtain mode is shown in figure E, where air enters and leaves the cavity to the indoors. Internal air curtain mode is preferable during colder periods, where the air is heated while being transported through the cavity and enters the room with a higher temperature. [Larsen, 2008]

As it is recognized by the previous description of different types of DSF ventilation strategies, convection is a significant heat transfer process occurring in the cavity due to temperature differences and possible also by wind induced pressure differences. It is therefore crucial to understand this process in order to evaluate the thermal and energy performance of a building having a DSF.

Convection is the heat transfer mode in fluids when a temperature difference is present and especially the process happening between a surface and a fluid in motion is interesting. Convection involves two mechanism namely the conduction at the boundary and the advection, which happens by bulk fluid flow. The convective heat transfer process is mainly about understanding what is happening at the boundary to the surface; a thermal and velocity boundary layer is formed with increasing thickness in the stream wise direction and the thickness and strength of the boundary layer determines the amount of heat which is being

transferred and therefore the performance of a DSF.

Previous work has been thoroughly investigated both experimentally and numerically regarding laminar convective flow in vertical parallel-plate channels, but there is a lack of experimental data for turbulent natural convection and especially the case of asymmetric heated surfaces, which is most likely to happen in a DSF. The flow in a naturally ventilated cavity is difficult to predict due to the highly fluctuating outdoor conditions that determines the performance of a DSF, and since previous studies show that commercial numerical models have a tendency of predicting the heat transfer and airflow incorrect among others [Yilmaz og Gilchrist, 2007] and [Marcondes et al., 2006], it is crucial to examine and evaluate experimentally possible scenarios that may occur.

Besides from the standard steady channel flow, other possible flow conditions may occur in the cavity like extreme recirculation where the one main recirculation area occupies the entire channel, this is often seen if one surface is heated above the other, it may only be occurring in a certain region of the channel or both types of flow is seen at once. The first type of recirculation happening in the entire channel will in the preceeding report be referred to as extreme recirculation, whereas the recirculation only happening in regions will be referred to as simply only recirculation. The two phenomenoms are illustrated in figures 1.3 and 1.4.

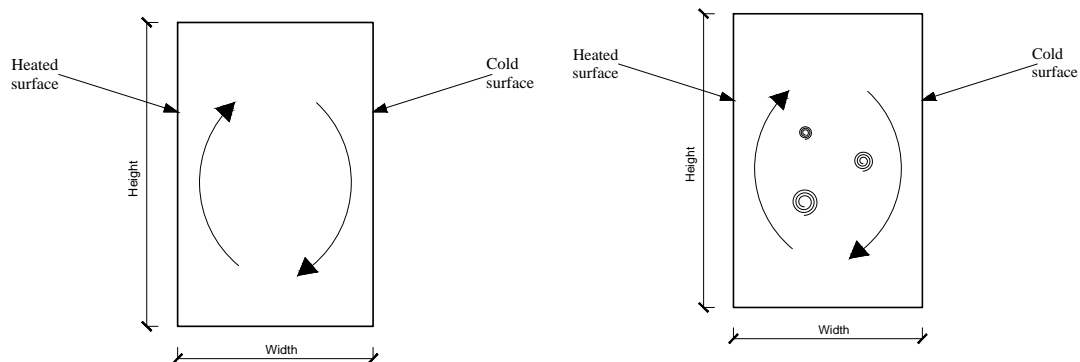


Figure 1.3. Sketch illustrating extreme recirculation. **Figure 1.4.** Sketch illustrating both extreme recirculation and regions with recirculation.

Obtaining this recirculation flow in a channel region means that the air flow acts in an unpredictable and unstable way where the heat transfer is unknown due to little investigation but expectadly different from the standard channel flow. The increased velocities in the boundary layers means a mixing of the air from the boundary layer and the free flow, which leads to increased convective heat transfer and different temperature gradients in the cavity compared to what would have been expected with standard channel flow. The recirculation phenomenon is said to occur when the buoyancy forces are dominating, meaning that the solar radiation is strong and the air flow is small.

[Larsen, 2008] explained a hypothesis regarding this phenomenon, and it is described as followed:

1. First consider the cavity as wide and with two heated surfaces. As explained previous a boundary layer develops due to viscous effects as a fluid flow enters the cavity. The thickness of the boundary layer increases upward as it happens for a standard channel flow as illustrated in figure 1.

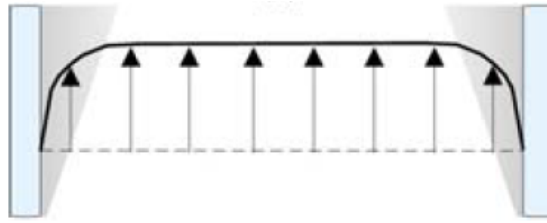


Figure 1.5. Development of recirculation flow step 1.

2. Since the surface temperatures are relatively higher than the air temperature the buoyancy forces will be strong and cause the air velocity at the boundary layers to exceed the velocity in the free flow. The mass balance has to be fulfilled and the air velocity in the free flow will therefore decrease as a consequence of the increase of velocity in the boundary layer, see figure 1.6.

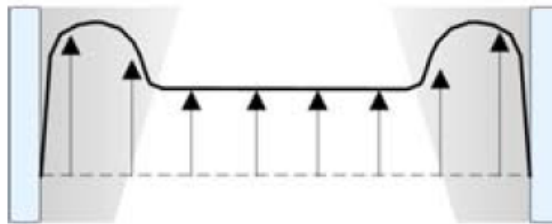


Figure 1.6. Development of recirculation flow step 2.

3. As the boundary layer further develops a situation where the velocity at the boundary layer is the same as at the entrance of the cavity occurs. A neutral plane exists according to the mass balance, where the velocity and mass flow rate is equal to zero, this is called Recirculation Neutral Plane (RNP), and is shown in figure 1.7.



Figure 1.7. Development of recirculation flow step 3.

4. As the boundary layer continuous formation above the neutral plane, the boundary layer mass flow rate exceeds the mass flow rate entering the cavity. As a results, the air to this plane is removed from the zones above causing a region of recirculation flow in the vicinity of the center. The principle is shown in figure 1.8 on the following page.

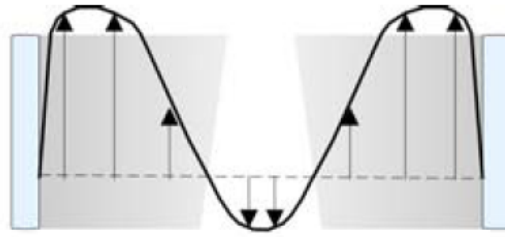


Figure 1.8. Development of recirculation flow step 4.

Although the experimental work presented in [Larsen, 2008] exhibited indication of this phenomenon, the lack of measurements made it impossible to conclude the occurrence.

1.1 Aim of this work

The main idea of this research is to evaluate the convective heat transfer in a DSF constructed as two vertical parallel plates with one heated surface. The vertical parallel-plate channel is representative of many applications such as chimneys, solar panels, trombe walls, room ventilation and air cooling of electronic components that are formed as vertical channels and generates heat etc..

The objective is to contribute to the understanding of turbulent natural convection in vertical channels and an effort is being done to find the range of boundary conditions of where the recirculation phenomenon exists.

During the experimental study the temperatures inside the channel will be measured and evaluated to indicate how the flow develops, and will furthermore provide data for the validation of a numerical solution.

The following report is divided into three main parts. Initially the project starts with a pre-study, where both theory regarding convective heat transfer and a literature study is presented. Next is the experimental part presented and the results are analyzed according to two main studies: Rayleigh number dependency and influence of air flow rate regarding channel flow structure. The last part includes the numerical analysis, where a model is presented and validated according to the experimental results.

Part I

Pre-Study

The report is introduced by a theory study regarding convective heat transfer in order to give the reader an understanding of the main topic of this study. Several dimensionless numbers have been used to quantify the convection effects in the experiment, and are therefore presented in this chapter. Next is the literature study regarding some work conducted until now for this specific topic.

Convective heat transfer

The following chapter is based on [Incopera og Dewitt, 2011] if nothing else is stated.

Convection in general appears in many aspects of the engineering application such as heat transfer in a double skin façade or a trombe wall, room ventilation and many other aspects like i.e. natural convection air cooling of electronic components [Ayinde et al., 2008]. Convection is energy transfer between a surface and a fluid moving over the surface when a temperature gradient is present. It can happen by bulk fluid motion and random fluid motion. Figure 2.1 shows the principle of convection heat transfer between a surface and a fluid.

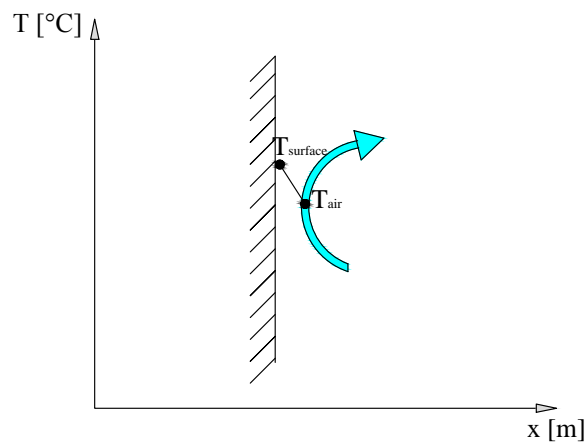


Figure 2.1. Convective heat transfer principle.

Convection happens at the boundary layer at the surface when a fluid is in motion. The heat exchange is a combined interaction between the conductive heat transfer by diffusion in the solid and the heat transfer due to bulk fluid motion.

It is therefore crucial to understand the concept of boundary layers when discussing convective heat transfer, see figure 2.2 on the following page.

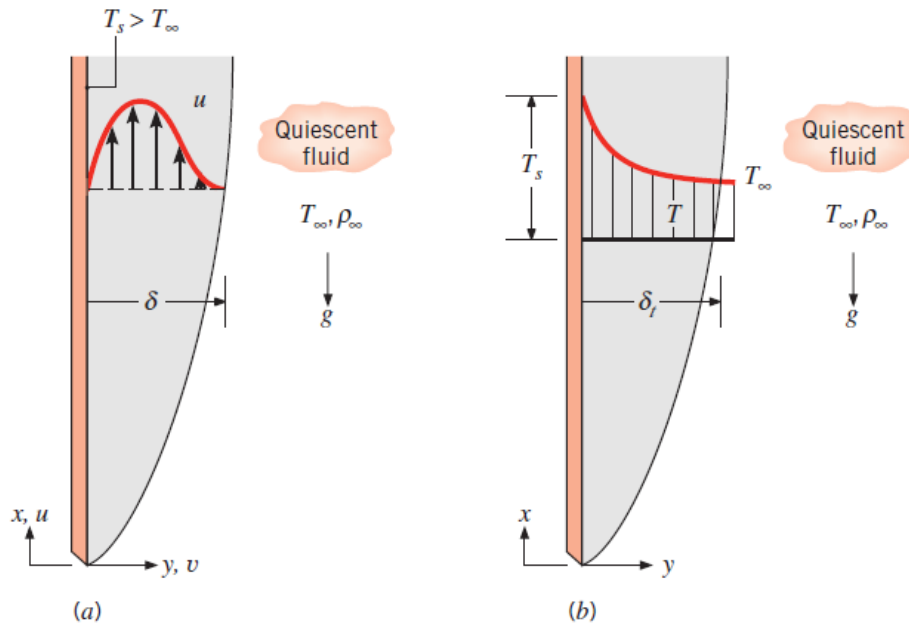


Figure 2.2. Boundary layer development on a heated vertical plate: (a) Velocity boundary layer (b) Thermal boundary layer. [Incopera og Dewitt, 2011]

When convection occurs, a velocity and a thermal boundary layer emerge as a consequence of the interaction between fluid and surface. The velocity boundary layer, also called hydrodynamic boundary layer, emerges due to the delay of fluid particles close to the surface because of sheer stresses acting in planes parallel to the fluid velocity. These particles then delay the particles in the next layer and so on, until the effect becomes insignificant, where the boundary layer velocity has the same value as the free stream. The velocity will vary from zero at the surface to a finite velocity related with the free flow. The thermal boundary layer develops if a temperature difference is present, and the heat transfer will always happen from the surface to the fluid if the surface temperature is higher than the fluid temperature.

Convective heat transfer is classified according to three main principles regarding the nature of the flow:

- Forced convection - when external mechanisms cause the fluid motion i.e. by a fan or a pump.
- Natural convection - when the flow is dominated by buoyancy forces due to density differences caused by the temperature variations.
- Mixed convection - combined forced and natural convection.

The boundary layer development can both have laminar and turbulent flow conditions and is described by the velocity. The laminar flow is characterized by highly ordered components that continues until a transition region, where after the turbulent flow is reached and particles move irregularly by random motion. The transition occurs due to mechanisms that is either triggered naturally within the fluid by unsteady flow conditions or by small disturbances originated from fluctuations within the free fluid flow or induced by surface roughness.

When analyzing the nature of forced convection flow it is customary to look at the dimension-

less Reynolds number, which can be seen in equation 2.1.

$$Re = \frac{u \cdot l}{\nu} \quad (2.1)$$

Where:

Re	Reynolds number [-]
u	Average velocity of the fluid [m/s]
l	Characteristic length [m]
ν	Kinematic viscosity of the fluid [m ² /s]

Reynolds number is a value that relates the ratio of inertia forces to viscous forces. A low Reynolds number indicates laminar flow where viscous forces are dominating, whereas a high Reynolds number point towards a turbulent flow. According to [Incopera og Dewitt, 2011] the transition to turbulent flow will occur at a distance from the leading edge, and the location is determined by the critical Reynolds number, that is assumed to be $5 \cdot 10^5$ for a vertical flat plate [Incopera og Dewitt, 2011]. Furthermore a flow can be fully developed for both laminar and turbulent condition. It is seen when the fluid has the same velocity at each point, hence it is independent of the stream wise coordinate, a fully developed turbulent region can occur and is characterized by the merge of the boundary layer. In this region a fully mixed flow with same velocity and temperature is found.

Grashof number plays the same role in natural convection as Reynolds number when analyzing forced convection; the number indicates whether the flow is laminar or turbulent, and is a ratio between the buoyancy and the viscous forces. It is calculated as shown in equation 2.2.

$$Gr = \frac{g \cdot \beta \cdot (T_s - T_{fluid}) \cdot l^3}{\nu^2} \quad (2.2)$$

Where:

g	Gravitational acceleration [m/s ²]
β	Coefficient of volumetric expansion [1/K]
T_s	Surface temperature [°C]
T_{fluid}	Fluid temperature [°C]

Prandtl number is a measure of the ratio between the momentum diffusivity and the thermal diffusivity. It contains no length scale, and is therefore only dependent on the property of the fluid, in this case the air. The equation for calculating Prandtl number can be seen in 2.3.

$$Pr = \frac{c_p \cdot \mu}{k} \quad (2.3)$$

Where:

c_p	Specific heat [J/kgK]
μ	Dynamic viscosity [Ns/m ²]
k	Thermal conductivity of the fluid [W/mK]

According to this equation the Prandtl number is 0.74 for air, which is relatively close to 1. Having a Prandtl number close to 1 means that the energy diffusion rate is close to the momentum diffusion rate, thus the thickness of the thermal boundary layer is equal to the thickness of the velocity boundary layer [Incopera og Dewitt, 2011].

Rayleigh number is another dimensionless number associated with natural convection, see equation 2.4.

$$Ra = \frac{g \cdot \beta \cdot (T_s - T_{fluid}) \cdot l^3}{\nu \cdot \alpha} = Gr \cdot Pr \quad (2.4)$$

Where:

Ra | Rayleigh number [-]

Rayleigh number is also an indication of whether the flow in the boundary layer is laminar or turbulent. In [Incopera og Dewitt, 2011] it is stated that the transition to turbulent flow on a vertical plate happens at a Rayleigh number of 10^9 .

The modified Rayleigh number will be used in the succeeding report in order to be able to compare the experimental results with the literature. Since the Rayleigh number often is based on the channel height, the modified therefore take the effect of the channel width into account [Badr et al., 2006]. The modified Rayleigh number is calculated according to equation 2.5.

$$Ra^* = Gr \cdot Pr \cdot \frac{b}{H} \quad (2.5)$$

Where:

Ra^* | Modified Rayleigh number [-]
 b | Width of channel [m]
 H | Height of the channel [m]

Classification of the convective flow regime in the boundary layer can be analyzed according to the Gr/Re^2 -ratio, which is an estimation of the strength of the boundary layer flow compared to the bulk flow. The distinction is made according to

$$\frac{Gr}{Re^2} \ll 1 \quad \text{Forced convection} \quad (2.6)$$

$$\frac{Gr}{Re^2} \gg 1 \quad \text{Natural convection} \quad (2.7)$$

$$\frac{Gr}{Re^2} \approx 1 \quad \text{Mixed convection} \quad (2.8)$$

Meaning that the natural convection is negligible for $Gr/Re^2 \ll 1$ and forced convection is negligible for $Gr/Re^2 \gg 1$. Situations where both natural and forced convection effects are comparable may arise and then neither of them must be neglected. The buoyancy forces may vary in this case and is furthermore divided into three possible scenarios: Assisting flow (when buoyancy and forced convection have the same direction), opposing flow (opposite directions) and transverse flow (buoyancy force is normal to the forced motions). It is discovered that assisting and transverse flow enhance the heat transfer process associated with pure forced convection whereas the opposing flow decreases the heat transfer.

Another important issue to mention is the aspect ratio when analyzing the flow in a vertical channel and is defined as the height of the channel divided by the width of the cavity, see equation 2.9.

$$AR = \frac{H}{b} \quad (2.9)$$

Where:

AR | Aspect ratio [-]

As mentioned previously boundary layers develop on each surface of the channel. If the aspect ratio is large (narrow channel) the boundary layers will eventually merge to yield a fully developed flow. However, if the aspect ratio is small (wide channel) the boundary layers develop independently and can in theory take on similar conditions to that of convection on a single vertical plate. A distinction between wide and narrow channels is found by [Sealens, 2002] and is described by

$$\frac{b}{H} > Ra^{-\frac{1}{4}} \quad (2.10)$$

The dimensions of the test facility of this study leads to $\frac{b}{H} = 0.13$ and according to calculations of $Ra^{-\frac{1}{4}}$ for all conducted tests the cavity acts as wide. Graphs showing the results can be found in *appendix A* on page 129 .

The presented dimensionless numbers will be widely used in the succeeding chapters to describe the results obtained in the experimental work in a vertical channel.

Literature Study

[Ayinde et al., 2008] studied experimentally the turbulent natural convection flow in a vertical channel with asymmetric heated walls. The channel was 500 mm high and the experiment was conducted for two aspect ratios 12.5 (narrow) and 6.25 (wide), which was the ratio between the height and the gap between the two walls. The two vertical plates were located inside a test chamber made of plexiglass. The chamber was of much greater size than the channel in order to prevent air stratification and chimney effects, but still allowing the natural convection flow to happen inside the channel by openings at the bottom and top of the chamber. Except from the two different aspect ratios also two different Rayleigh numbers were tested, which were $1.0 \cdot 10^8$ and $2.0 \cdot 10^8$ that provided the modified Rayleigh numbers of $8.0 \cdot 10^6$ and $3.2 \cdot 10^7$ respectively. The Rayleigh numbers are based on the height of the channel and the inlet temperature was taken as the fluid temperature. The two walls were subjected to uniform temperature distribution, one heated above and one maintained below the ambient temperature. Measurements of the velocity field using the Particle Image Velomecity (PIV) system were the foundation of this paper that described the flow pattern due to natural convection.

[Ayinde et al., 2008] found for both aspect ratios and both Rayleigh numbers a flow recirculation occurring in the entire channel. The flow entered the bottom, moved downstream near the heated wall, slowed down near the top exit and turned towards the cooler wall moving upstream and repeated continuously, see figure 3.1 on the next page. These results showed that the temperature difference between the walls and the air in the channel created density differences, which enhanced convective flow with a downstream direction near the heated wall and an upstream direction near the cooler wall, causing a *clockwise natural convection loop*.

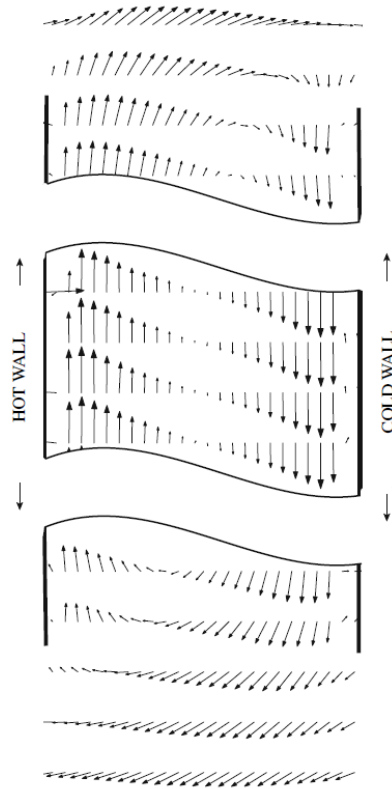


Figure 3.1. Vector plot of the mean velocity for aspect ratio 12.5 at Rayleigh number $2 \cdot 10^8$. [Ayinde et al., 2008]

For wider channel the peak velocities were found to be more pronounced, and the mixing between the fluid and surface parts was less than for the narrow channel. It was also seen that the peak velocities exceeded the inlet and outlet velocity, thus the air accelerated after the inlet, but slowed down before leaving as a consequence of the opposing buoyancy forces. Increasing the Rayleigh number from $1.0 \cdot 10^8$ to $2.0 \cdot 10^8$ caused a 50 % increase in the peak velocity, but also moved the peak velocity closer to the walls, which indicated that the boundary layer became smaller.

Furthermore assuming a two-dimensional flow was proven to be accurate. Measurements was conducted in three different points in the span wise direction (the length of the channel), which showed a close correlation, meaning that correlating velocity profiles were obtained at each point in the span wise direction.

Another study was completed by [Habib et al., 2002] regarding the air flow pattern in a vertical channel that was both symmetrically and asymmetrically heated for natural turbulent convection flow. Velocities in the channel were measured at three different elevations along the channel and presented for the symmetrically heated surfaces, which was 20°C above ambient and for a Rayleigh number of $4.0 \cdot 10^6$ (modified $1.3 \cdot 10^6$), and a case with asymmetrically heated surfaces, where one surface was kept 10°C above and the other 10°C below ambient corresponding to a Rayleigh number of $2.0 \cdot 10^6$ (modified $6.4 \cdot 10^5$). The aspect ratio of the channel was 3.125, and inlet and outlet were openings at the top of bottom allowing a free air flow.

The symmetrically test in general showed that the velocity increased as the air moved downstream the hot wall. At the entrance of the channel the mean velocity across the width was more constant compared to the top, where the velocity was below zero at the vicinity of the centerline and the peak was more distinguished near the hot wall, see figure 3.2. The nearly zero velocities indicated that a region at the top had the characteristics of the phenomenon flow reversal. It was also found that the peak velocities had greater distance from the wall at the top, meaning that the thickness of the boundary layer was increased. A fully developed turbulent flow was not reached due to the small aspect ratio.

For the asymmetrically heated surfaces a case of extreme recirculation was found or as it was referred to previously a clockwise natural convection loop, where the air moved upward near the hot wall and downward near the cold wall, see figure 3.3. The absolute values of the velocity was higher near the cold surface at the entrance, but interchanged at the top of the channel, where the absolute velocity was higher near the heated surface. As before, the thickness of the boundary layer increased at the top near the hot wall, but the opposite was found at the colder wall. In general it could be said that the air accelerated up the heated wall and decelerated down the colder wall. The velocities crossed zero close to the centerline but unlike the symmetrically case it had a gradient.

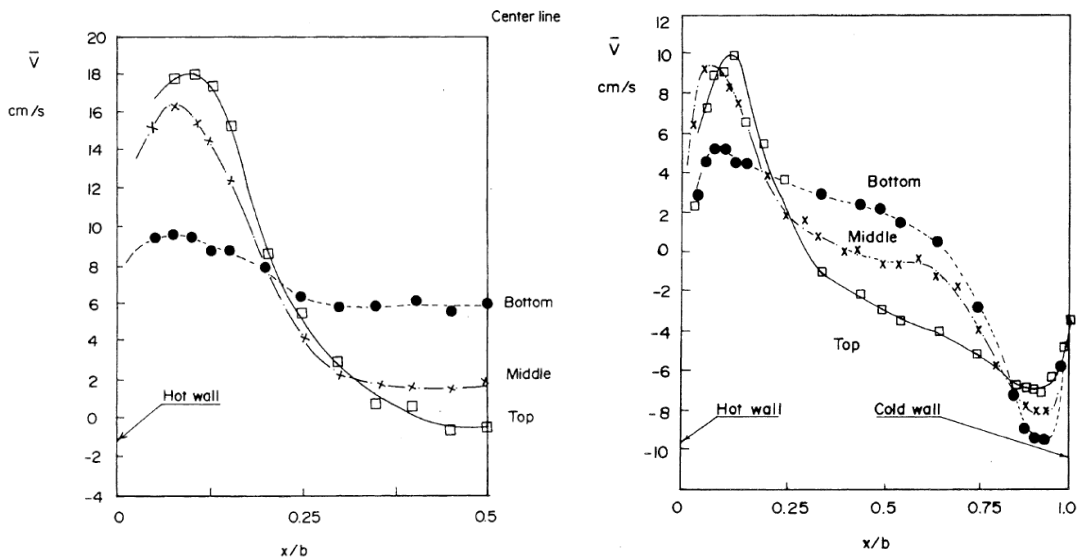


Figure 3.2. Horizontal mean velocity profile of a symmetrically flow case [Habib et al., 2002].

Figure 3.3. Horizontal mean velocity profile of an asymmetrically flow case [Habib et al., 2002].

Furthermore it is worth mentioning that the turbulence intensity, which is calculated based on the mean velocity and the standard deviation, see equation 3.1, was found to be higher in the vicinity of the centerline for both cases in all the heights. This implied that the flow was highly unstable in this region.

$$Tu = \frac{\sigma}{u_{mean}} \cdot 100\% \quad (3.1)$$

Where:

Tu	Turbulence intensity [%]
σ	Standard deviation (RMS) [m/s]
u_{mean}	Mean velocity [m/s]

[Yilmaz og Gilchrist, 2007] also investigated the flow field characteristics of turbulent natural convection in a vertical channel with asymmetric heating by velocity and temperature measurements. The channel was constructed of one heated wall with uniform heat flux and an outer glass wall. The aspect ratio was 20 and covered the modified Rayleigh number of $3.2 \cdot 10^7$.

The velocity measurements of [Yilmaz og Gilchrist, 2007] showed only positive values unlike the previous two studies, meaning there was no backflow at the unheated surface. This could be due to the fact that the channel is considered narrow compared to the other cases of [Ayinde et al., 2008] and [Habib et al., 2002]. The horizontal velocity profiles at the entrance was found to be almost uniform, but moving upward in the channel a peak was found near the heated wall that got more pronounced as moving closer to the top. As in the previous cases it was obvious that the thickness of the velocity boundary layer increased the higher the elevation became. The temperature distribution showed gradients close to the heated wall, but then uniform temperature distribution close to the center and to the unheated glass wall, implicating that the glass wall was essentially adiabatic. Figure 3.4 shows the horizontal velocity and temperature profiles for different heights.

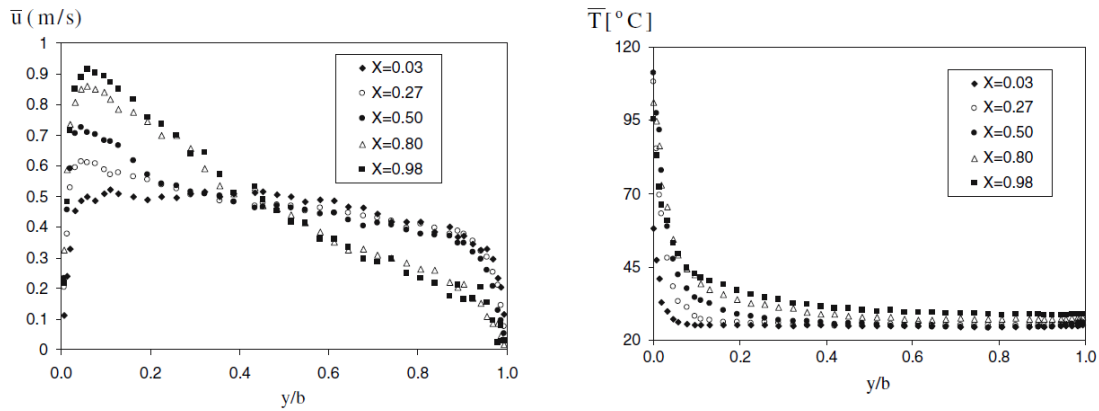


Figure 3.4. Velocity and temperature profiles obtained by [Yilmaz og Gilchrist, 2007].

It is worth mentioning that there was no sign of either extreme recirculation or an area of recirculation in the channel for this setup and tested boundary conditions, but one important difference between this study and the previously mentioned studies is that the present study uses isoflux heating compared to the others using isothermal.

A study was carried out by [Gau et al., 1992] regarding mixed buoyancy-assisted convection in a vertical asymmetrically heated duct, where the object was to visualize and study the reversed flow structure for different Gr/Re^2 -ratio and Reynolds number. The experimental work was performed in a vertical wind tunnel that can provide a uniform air flow with different velocities. The wind tunnel had one isoflux heated side and another adiabatic and the aspect ratio covered

was in total 15.2, but 12 if only the height of the heated section is considered. Table 3.1 shows the covered Reynolds numbers and Gr/Re^2 -ratios, where the hydraulic diameter is used as the characteristic length.

	Re [-]	Gr/Re^2 -ratio [-]
Change of Gr/Re^2 -ratio	514	120
	400	210
	171	1160
Change of Re	200	100
	600	100

Table 3.1. Tested combinations of Reynolds number and Gr/Re^2 -ratio by [Gau et al., 1992].

The study revealed that no recirculation or oscillations were found for Reynolds number 650 and Gr/Re^2 -ratio less than 80. Reducing the inlet velocity leading to a Reynolds number of 514 and Gr/Re^2 -ratio 120 showed that the increase of buoyancy forces generates a case of extreme recirculation; the air moves rapidly downstream close to the heated wall, then decelerates upstream close to the colder wall at a certain height. It is stated that the reversed flow contains lower temperatures than the flow downstream and enters the channel at the outlet. The flow along the heated wall then drives and entrains the reversed flow, so that the flow changes direction once again following downstream the heated wall forming a V-shaped recirculating area. Figure 3.5 shows how the flow developed into a V-shaped recirculation flow in 4 sec.

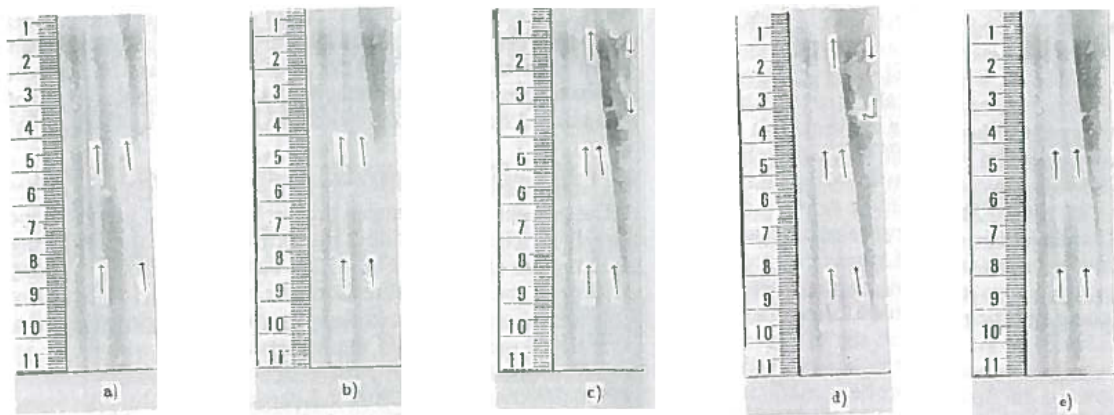


Figure 3.5. Occurrence of the V-shaped recirculation flow for $Re = 514$, $Gr/Re^2 = 120$, at (a) $t = 0$, (b) $t = 1$, (c) $t = 2$, (d) $t = 3$ and (e) $t = 4$. [Gau et al., 1992]

It was further discovered that an increase of Gr/Re^2 -ratio, either achieved by increase of heat supply or decrease of air flow rate, the penetration depth becomes deeper and the recirculation region wider, see figure 3.6 on the next page, that shows the development of the flow for Reynolds number 400 and Gr/Re^2 -ratio 210, and compare to figure 3.5.

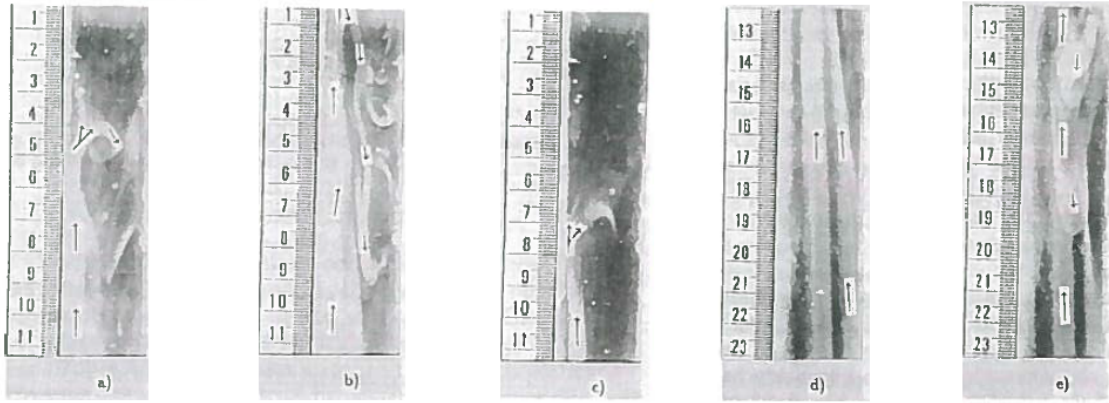


Figure 3.6. Occurrence of the V-shaped recirculation flow for $Re = 171$, $Gr/Re^2 = 1160$: (a) Generation of vortices and eddies, (b) generation of different vortices and eddies, (c) complete mixing of heated buoyant flow with the V-shaped recirculation flow, (d) V-shaped recirculation flow region close to the separation point and (e) upstream motion of eddies and vortices. [Gau et al., 1992]

It was observed that the boundary layer flow started to become distorted and unstable that led to generation of eddies and vortices projected from the buoyant flow into the recirculating area. The reason for this mechanism was the counterflow motion between the downstream heated flow and the colder recirculation flow. At the end the vortices collapsed and was carried away by the recirculating flow leading to the V-shaped flow as first seen.

Figure 3.7 is a visualization of the flow when keeping the Gr/Re^2 -ratio at 100 but changing Reynolds number from 100 to 600.

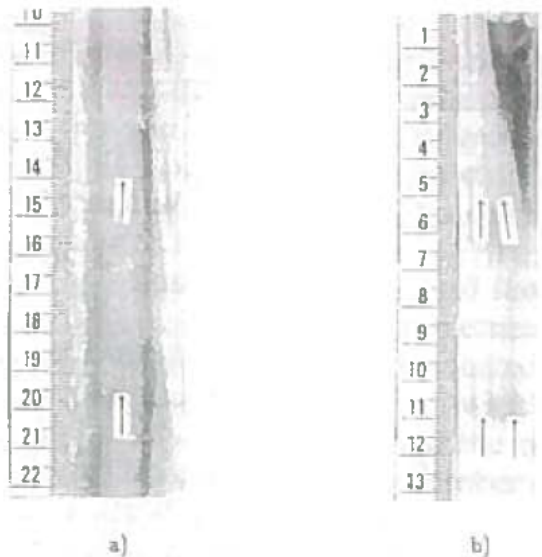


Figure 3.7. Variation of the reversed flow structure with Re : (a) $Re = 200$, $Gr/Re^2 = 100$, smoke on the right side indicates the thin, reversed flow region and (b) $Re = 600$, $Gr/Re^2 = 100$, the V-shaped black region on the upper right corner represents the recirculation flow. [Gau et al., 1992]

It was observed that increasing Reynolds number pushed the recirculating area downstream closer to the outlet but also made the region wider.

In general it was concluded for all conditions that the flow had dynamic behavior that grew and collapsed in a periodic manner based on the visualization and temperature measurements. Another interesting indication in this study was that the heat transfer process was enhanced as the buoyancy-assisted flow increased achieved by increasing Nusselt number¹ with increasing Gr/Re^2 -ratio.

[Ospir et al., 20012] also studied flow visualization of natural convection in a vertical channel with asymmetric heating, but this time with water as the working fluid. The heated wall was supplied with uniform heat flux distribution. The part of the study that concerned influence of the change in Rayleigh number covered an aspect ratio equal to 6, and modified Rayleigh numbers $4.3 \cdot 10^5$, $1.7 \cdot 10^6$ and $4.5 \cdot 10^6$, which were obtained by changing the heat supply. The modified Rayleigh numbers were in this study calculated based on the heat flux and the width of the channel but also takes the aspect ratio into account.

Figure 3.8 on the following page shows the results from the three tests by increasing Rayleigh number.

¹Nusselt number is a dimensionless number associated with the thermal boundary layer, and it provides a measure of the convection heat transfer occurring at the surface. [Incopera og Dewitt, 2011]

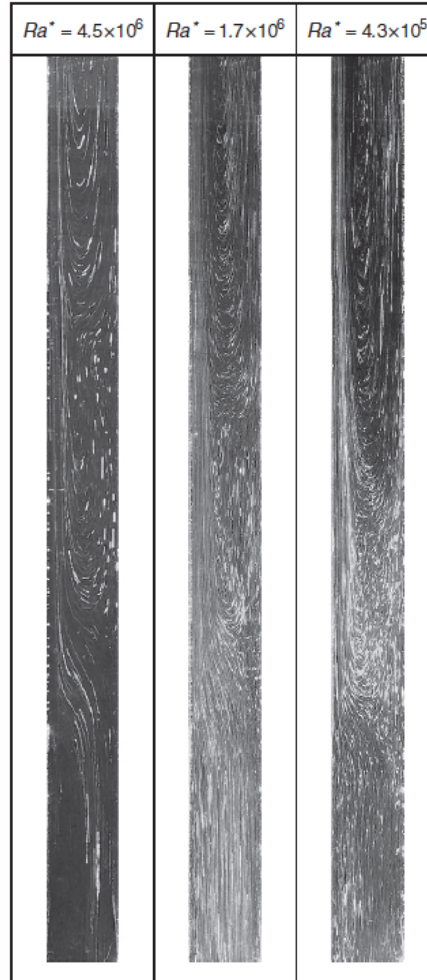


Figure 3.8. Visualization of flow condition in channel by [Ospir et al., 20012].

In all tests it was discovered that an upward boundary layer flow occurred close to the heated wall supplemented by a reversed flow near the colder glass wall. The flow was described as *an elongated eight-shaped structure with two main recirculation cells*, and it was observed that with increasing Rayleigh number the overall recirculating area was reduced mainly by a great reduction of the upper recirculating cell length. A study regarding the dynamic behavior of the flow showed that the flow initially consists of one recirculating cell transforming into having two recirculating cells.

Another study concerning reversed flow for natural convection in a one-sided heated vertical channel with water as working fluid was performed by [Sparrow et al., 1984]. The study was likewise based on flow visualization, where different Rayleigh numbers were tested for different aspect ratios. Initially a test was conducted for modified Rayleigh number $1.22 \cdot 10^6$ and aspect ratio of approximately 15. It should be mentioned that Rayleigh numbers were calculated according to the channel width as the characteristic height. This test showed a V-shaped recirculating flow as it was found in the previous mentioned literature; Due to the aiding buoyancy forces close to the heated wall the fluid was accelerated downstream adjacent to the heated wall. The accelerated fluid was drawn to the heated wall in order to satisfy the

conservation of mass on the behalf of the downstream fluid adjacent to the unheated wall that was depleted, and at some point total depletion occurred. When this phenomenon happened more fluid was needed to fulfill the mass balance of the accelerating fluid adjacent to the heated wall, and this was drawn from the outlet close to the unheated wall. It enters the top of the channel, moving upstream close to the unheated wall and at some distance from the top (penetration depth) the fluid is drawn to the heated surface and changing direction.

Three different aspect ratios were tested with varying Rayleigh numbers. Figure 3.9 illustrates the results obtained from the three different aspect ratios by comparing the Rayleigh number to the penetration depth.

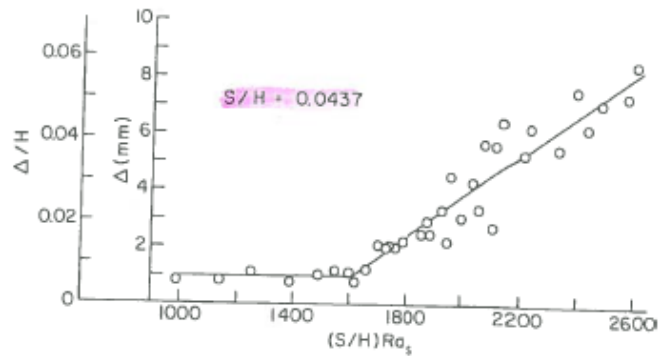


Fig 3 Maximum penetration depth of downflow, $S/H = 0.0437$

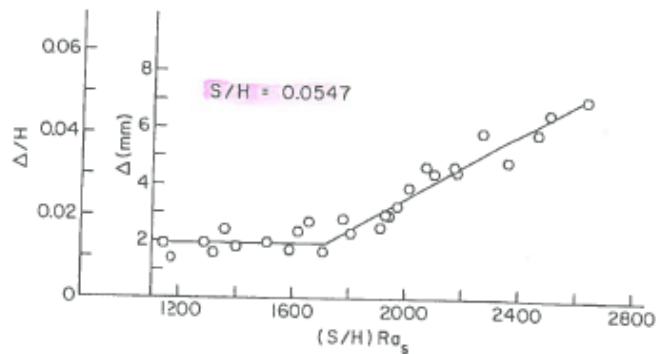


Fig 4 Maximum penetration depth of downflow, $S/H = 0.0547$

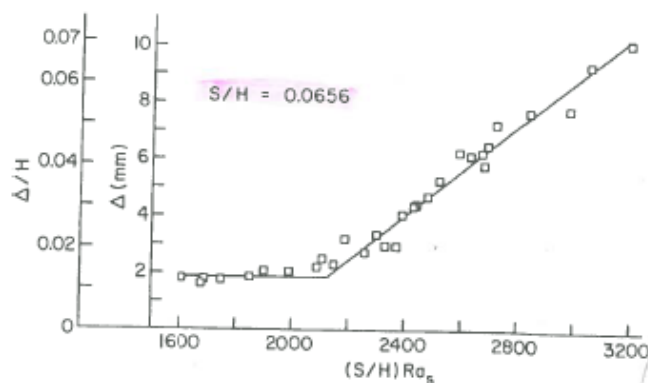


Figure 3.9. Maximum penetration depth of reversed flow. [Sparrow et al., 1984]

All figures show the same tendencies; the penetration depth was seen very small and practically

constant for low Rayleigh numbers, and then from a certain threshold value of Rayleigh number the penetration depth increases almost linear with increasing Rayleigh number.

In general it was concluded that the flow behavior was Rayleigh number-related and that the onset of flow reversal appears for modified Rayleigh numbers between $4.95 \cdot 10^5$ and $8.38 \cdot 10^5$.

At last, the convective flow regime in a double skin façade was studied in [Larsen, 2008] where measurements were conducted on an outdoor test facility. Since the facility was located outdoors it was not possible to control the thermal or wind conditions as in the previous mentioned studies, which is why results for different Rayleigh numbers were achieved. The aspect ratio of the double skin façade was 10 and an analysis of the Rayleigh number showed that the cavity acted as wide, thus the heat transfer could be treated as convection between two infinitely wide heated surfaces. During the experiment the external air curtain mode was examined, see figure 3.10.



Figure 3.10. Ventilation strategy in [Larsen, 2008] (E=external, I=internal).

Temperature and velocity measurements made it possible to analyze the flow pattern caused by convection in the double skin façade by different dimensionless numbers like Reynolds and Rayleigh number, and the Gr/Re^2 -ratio.

The Reynolds numbers were found to be in the range of approximately $1.0 \cdot 10^4$ to $14.0 \cdot 10^4$ leading to the conclusion that the flow in the cavity was either in transition to or was turbulent. Figure 3.11 on the next page shows the Rayleigh numbers obtained by [Larsen, 2008].

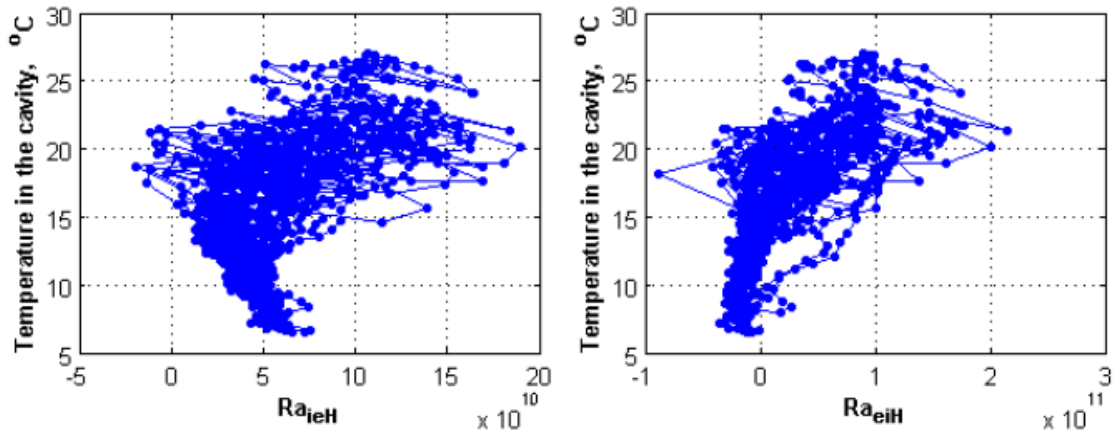


Figure 3.11. Mean Rayleigh numbers found by [Larsen, 2008] (ei=External glass inner surface, ie=Internal glass external surface).

The Rayleigh number showed that the boundary layer flow was in transition to or was turbulent.

The recirculation phenomenon was studied by analyzing vertical temperature profiles and vertical mass flow rates. The phenomenon was said to appear when there was strong solar radiation and weak wind forces, and two periods were therefore selected with these conditions. Figure 3.12 shows the vertical temperature profiles and the dimensionless mass flow rate for those two periods.

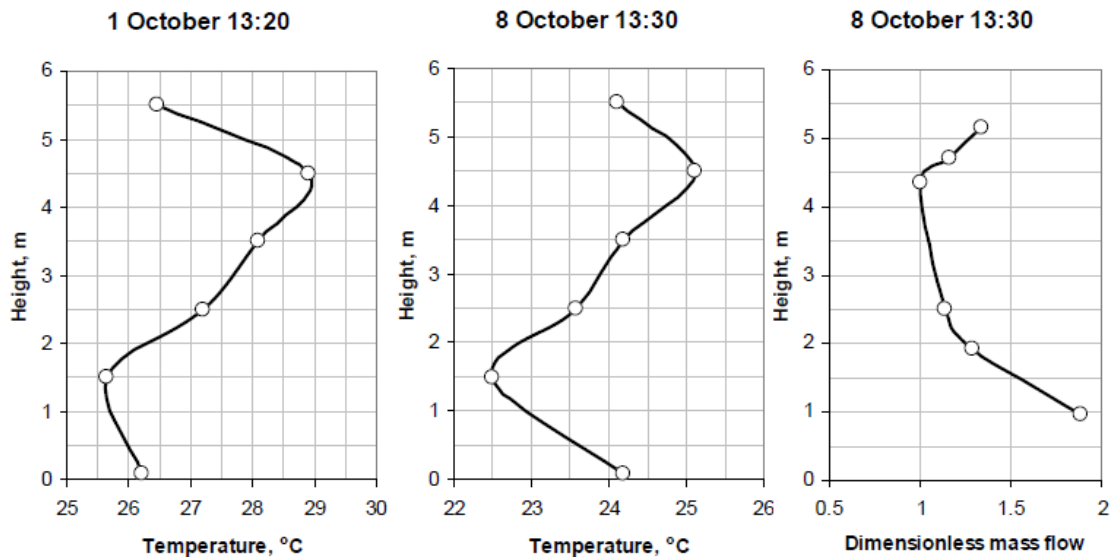


Figure 3.12. Vertical temperature profiles in the cavity and dimensionless mass flow rate [Larsen, 2008].

The known test conditions for these two periods are listed in table 3.2 on the next page.

	1st October	8th October
Outdoor air temperature [°C]	18.5	16.2
Inlet velocity [m/s]	0.24	0.49
External glass (internal surface) temperature [°C]	32.75	27.43
Internal glass (external surface) temperature [°C]	33.47	28.72
Global solar radiation [W/m ²]	452	439
Diffuse solar radiation [W/m ²]	185	169

Table 3.2. Test conditions in [Larsen, 2008].

The appearance of recirculation causes a mixing of the boundary layer flow and the free fluid flow. This leads to a deformation of the vertical temperature profile with a lack of temperature gradient where the phenomenon takes place, as it was found in the two figures illustrating the vertical temperature profile. The increase of mass flow rate measured above 4.50 m supported the statement about appearance of recirculation, since the mass flow rate was found to be increased in the same height as the temperature decreased. It was found that with increasing surface temperatures, the deformation indicating recirculation was increased.

Numerical Literature Study

In addition to the experimental work conducted by [Yilmaz og Gilchrist, 2007] a numerical analysis was also performed using the CFD software PHOENICS. Three different LRN $k - \epsilon$ turbulence models were used; Lam and Bremhorst model (LB), To and Humphrey model (TH) and Davidson LRN $k - \epsilon$ model (DA). It should be noted that the TH and DA models were originally established for natural convection flows, and the LB for forced convection [Yilmaz og Gilchrist, 2007]. The boundary conditions for the model were as followed: The flow was induced entirely by buoyancy forces. The heated surface had a constant uniform heat flux applied and the colder surface was adiabatic, and no-slip condition was assumed for both walls. Air entered at the bottom and assumed the temperature according to the ambient and left at the top. As inlet the ambient pressure was used as a stagnation boundary condition, thus the flow was proportional to the square root of the pressure difference where the stagnation of the pressure was set to zero. As outlet the static pressure option was used. The density change of air due to temperature difference was taken into account. Thermal radiation was neglected. The model was simulated in steady state.

The numerical study showed that none of the models were able to predict the measured velocities, and were almost at all times over-estimated. A single agreement was found at the highest elevation near the heated wall. In the article [Yilmaz og Gilchrist, 2007] it was cited:

The unknown pressure field creates difficulty in the numerical solution of the momentum equations to produce velocity components. There is not an equation for the pressure, unlike velocity, energy, etc., so that it can be calculated from.

Although the model was unable to predict the velocities, a good agreement was found when looking upon the temperatures. All three models were able to estimate the temperature from

the cold surface to the core, but had difficulties near the heated surface at high elevations. The TH model showed the closest correlation of this matter.

A numerical study regarding buoyancy driven turbulent flow in a parallel-plate channel was carried out by [Badr et al., 2006]. The numerical study was conducted in a steady-state, turbulent, 2D channel. The thermophysical fluid properties was assumed constant except the density in the buoyancy term which was modelled according to the Boussinesq approximation. Conservation of mass, energy and momentum was required and the *low-Reynolds number k-ε turbulence model* was used. The walls were assumed to have the no-slip condition, the inlet was those of ambient conditions (temperature and ambient pressure) and the outlet was only imposed by the uniform ambient pressure. At first the model was validated according to the experimental results obtained in [Habib et al., 2002] for the asymmetrically case, see figure 3.13.

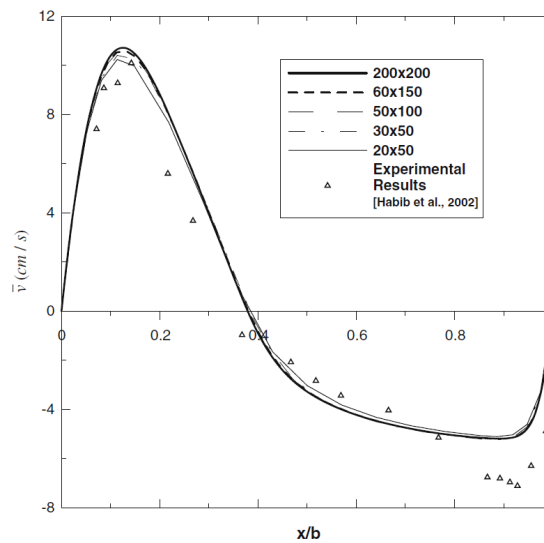


Figure 3.13. Velocity profile obtained with different grid size in numerical model compared with [Habib et al., 2002]. [Badr et al., 2006]

Based on the grid dependency test a cell size of 60x150 was chosen. The model was assumed to be validated and in good agreement with the measured velocity profiles. The numerical results revealed that the model had lower accuracy in the presence of high velocity gradients, where the rate of generation of turbulent kinetic energy was significant. The chosen turbulent model treated the energy generation due to buoyancy forces by an isotropic form of Reynolds stresses, which was found to be inaccurate, because the flow was highly anisotropic in regions with high velocity gradient.

After validating the model more simulations were conducted. One of the studies included the study of influence of Rayleigh number. Figure 3.14 on the next page shows the predicted horizontal velocity profiles for different Rayleigh numbers.

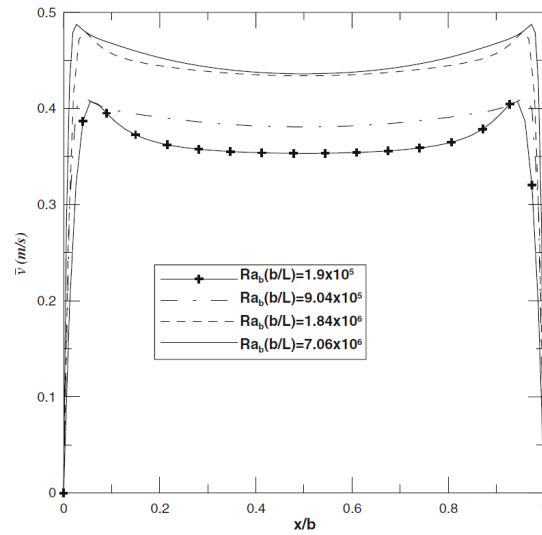


Figure 3.14. Velocity profile for different modified Rayleigh numbers. [Badr et al., 2006]

It was observed that the horizontal velocity component increases with increasing Rayleigh number causing an increase in the mass flow rate as expected. Furthermore, temperature profiles showed that the thermal boundary layer thickness decreased as Rayleigh number increased.

3.1 Summary

Figure 3.15 on the facing page sums up the covered Rayleigh numbers compared to aspect ratio for the aforementioned literature, except from [Gau et al., 1992] and [Larsen, 2008], since it was not presented in the article. Since the Rayleigh numbers found in the literature depends on different choices regarding characteristic length, all Rayleigh numbers are re-calculated and are presented in the graph according to the channel height in order to compare.

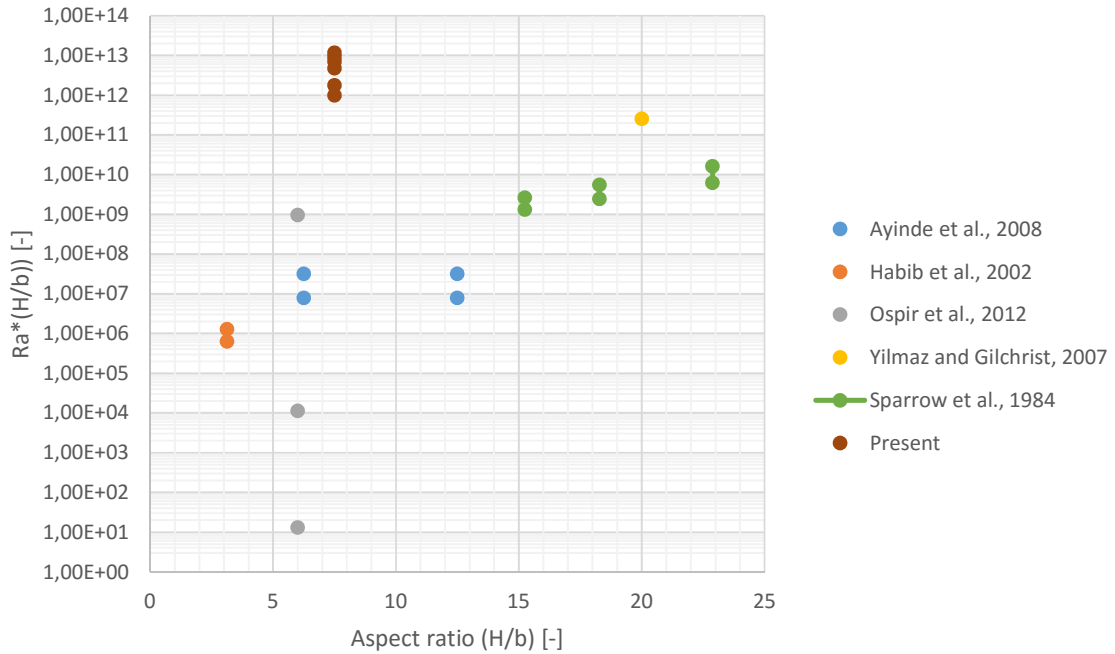


Figure 3.15. Summary of Rayleigh numbers from literature and present study.

Only the study by [Yilmaz og Gilchrist, 2007] did not find any evidence of recirculation.

The following list sums up characteristics of reversed flow found in the literature:

- Flow reversal appears with strong buoyancy forces and low air flow rates
- Recirculations occur in periodic manner within seconds
- Dependent of aspect ratio
- Flow reversal is affected by surface temperatures (symmetrical and asymmetrical heating)
- Flow reversal appears with increasing Rayleigh number
- Penetration length is linked with Gr/Re^2 -ratio and Reynolds number
- Flow reversal takes place at the end of channel and at the colder surface
- Deformations in vertical temperature profiles (the highest temperatures are not found at the outlet)
- Induced mass flow rate
- Enhanced heat transfer due to reversed flow

These are all characteristics that appear for reversed flow in a vertical channel. Due to limitations regarding the present study it is chosen only to study the influence of Rayleigh number and ACH.

Part II

Experimental Study

The experimental results obtained during this study are presented in the following chapters. The experimental study begins with a chapter describing the experimental setup and procedure. Then the discussion about the results is divided into three groups according to change of boundary conditions.

Introduction to Experiment

Experiments are conducted on a parallel-plate vertical channel with one heated surface. The purpose of the experiment is to measure temperature profiles inside a vertical channel and analyze the flow conditions based on the temperature measurements. The experimental work will contribute with a broader range of tested Rayleigh numbers for a different aspect ratio and also different air change rates (ACH) compared to the literature mentioned in *chapter 3 on page 15*.

4.1 Experimental set-up

The description of the experimental set-up is a common part of the work made in cooperation with two other master students, but is then later changed and extended.

For the experimental investigation of the air flow pattern in a vertical channel, a test apparatus of a single box window is designed and constructed in the klima-laboratory at Aalborg University to resemble and represent the smallest subunit of all the double skin façade systems.

The main dimensions of the apparatus are length x height: 1.55 m x 3.03 m. The facility is constructed in such a way that allows the adjustment of the cavity width in a range between 0.05 m and 0.50 m. In order to limit the heat transfer between the test facility and its surroundings, it is enhanced by 100 mm EPS, which is enclosed by 12 mm of plywood. The facility can be seen in figure 4.1 and 4.2 on the following page.



Figure 4.1. Photo of the laboratory test facility.

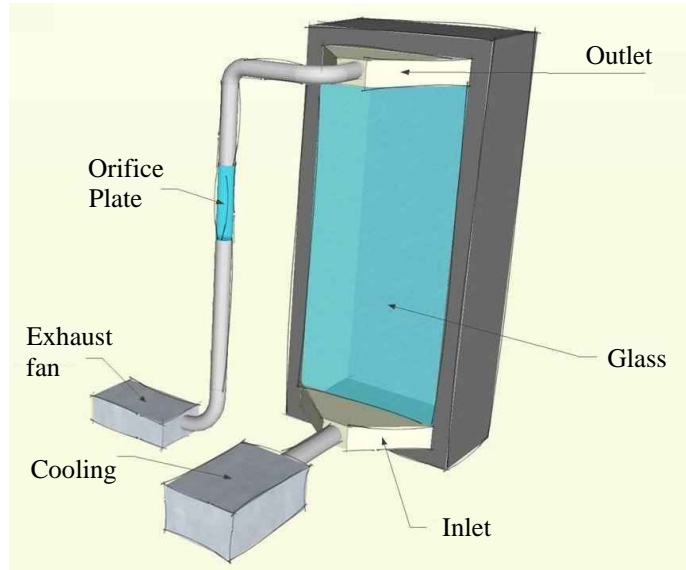


Figure 4.2. Sketch of the test facility.

The front glass surface is 2.73 m high and 1.55 m wide comprising an aluminium frame of 0.025 m. It is made of 3 mm polycarbonate plastic with a density of 1.20 g/cm^3 , and its thermal conductivity is $0.21 \text{ W/m} \cdot \text{K}$.

4.1.1 Equipment list

The following equipment was used in the experimental setup for the vertical channel with one heated surface:

- PC with LabView
- Carawarm heating mats
- Thin type K thermocouples
- Fluke Helios Plus 2287A data logger
- Compensation box
- Ice point reference KAYE K170-6
- Exhaust fan
- Power transducer
- Smoke machine with controller
- Two Dantec Laser Doppler Anemometer
- PC's with BSA flow software
- Mechanical traverse system for LDA

4.1.2 Inlet and outlet

The inlet is designed at the bottom and the outlet at the top of the glass surface, with an area of 0.105 m^2 for both of them. The inlet air has the option of being cooled to certain temperatures, and is found to be dependent on the air flow rate. I.e. the lowest possible inlet temperature for an ACH of 4 h^{-1} is approximately $15 \text{ }^\circ\text{C}$. The outlet is controlled by a fan equipped with an

orifice plate to regulate the flow rate at the exit. This choice of the outlet and inlet are done with respect to the lesser possible influence of the flow inside the cavity from external factors, since the idea of the set up is to investigate the buoyancy effect resulting in a certain air flow pattern for different heat inputs and ACH in a vertical channel. Due to the mass balance of the box and with the assumption of air tight construction, it is assumed that the flow rate exiting the test facility is the same as the flow rate entering. So, in that way the inlet flow rate is known in advance and can be adjusted.

4.1.3 Heating system

For having the heat input gradually or uniformly distributed into the cavity, five electrical heating mats made from Carawarm foils are placed into the back wall (insulated wooden plate). Each electrical heating mat consists of a maze of hot wires, with an area of 600 mm x 1500 mm and a power of 480 W. Their temperatures can be controlled and modulated manually and separately for each one of the five heating mats. By this way, a temperature gradient can be obtained with a maximum of 15 °C difference. Their construction and the way they are placed into wooden back wall is presented in figure 4.3.



Figure 4.3. Placement of the electrical heating mats into the backwall of vertical channel.

During the experimental work it is observed that the heating system is acting highly dynamic, which is a consequence of the ON/OFF control. Analyzing the surface temperature distribution by the measured values it is concluded that the first heater mat closest to the ground was not supplying any heat for three tests (2, 3 and 4). For all tests it is observed that the heater mat located at the top had a temperature decrease compared to the heater below. Figures 4.4 and 4.5 on the following page show the measured surface temperatures for test 1 and 2. From those graphs it can be observed how the heaters acts, and that the first heater mat is not supplying any heat in test 2.

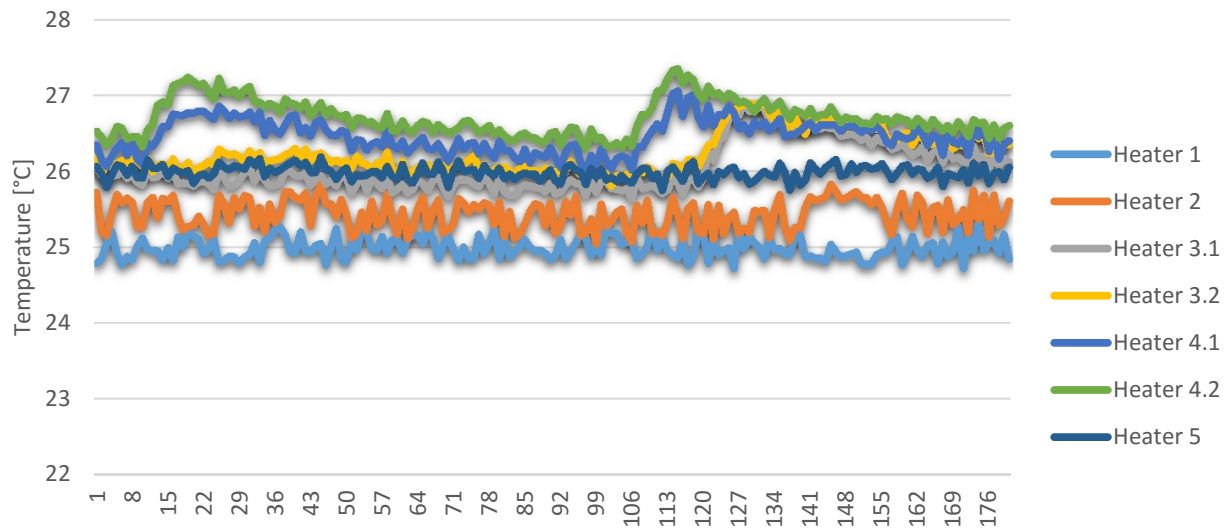


Figure 4.4. Measured surface temperaturesw at the heated wall in test 1 according to time.

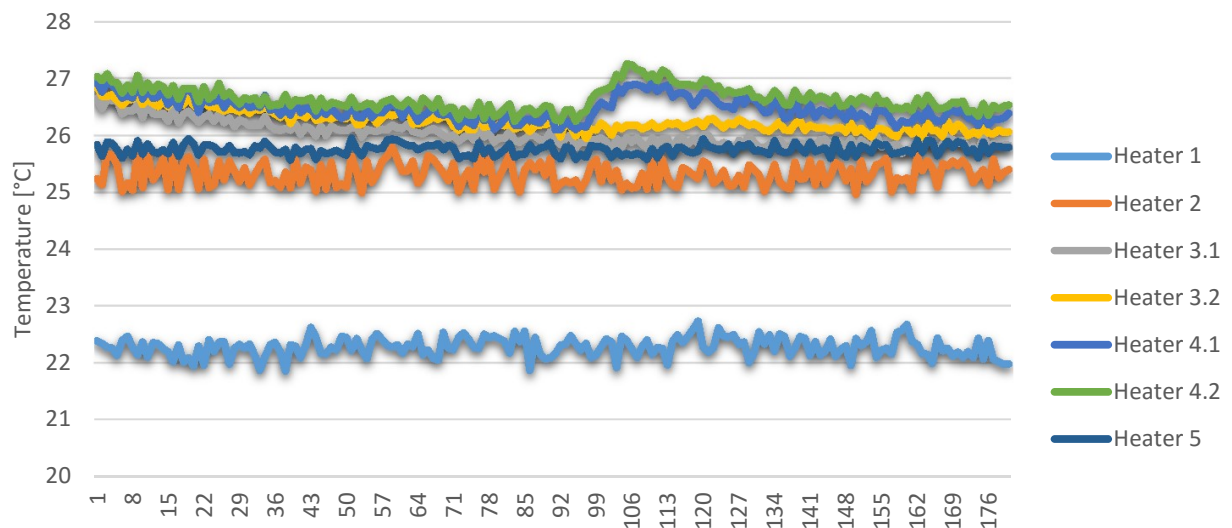


Figure 4.5. Measured surface temperaturesw at the heated wall in test 2 according to time.

Inaccuracy regarding obtained surface temperatures compared to the set point can be caused by the placement of the sensors of the heating system. The placement requires great precision when constructed and can be affected once heating is supplyid due to thermal expansion of the materials that might create small air gaps. Furthermore, it is discovered that the measured surface temperatures at the heated wall are approximately 5 °C lower than the set point.

4.1.4 Temperature measurements

The measurements of the temperature inside the tested cavity are conducted by using thin thermocouples type K for both surfaces and air measurements. 89 measuring locations for a 40 cm cavity are used distributed on different heights and on different positions in each height.

The location of the thermocouples can be found in *appendix B* on page 132. The choice of the locations of the thermocouples is based on previous tests and known theory. Other tests have been conducted with a greater distance between the thermocouples where no good results were obtained, see also *appendix K* on page 173 for further explanation.

The thermocouples on the surfaces are located above thermal paste in order to have good contact with the surface. The material has a high thermal conductivity and will therefore transfer the heat to the thermocouple.

For higher precision in temperature measurements, the thermocouples are calibrated at reference temperatures in ten steps going from 10 °C to 50 °C. The temperatures are registered every 10 s by a Helios data logger which is connected to a KAYE K170-6 ice point reference. All the thermocouples are connected in an isolated compensation box and protected from the ambient conditions, to increase the accuracy of the measurements.

The uncertainties regarding temperature measurements are determined by the *Propagation of Uncertainty* method. From this calculation the intervals of measurement error is found. The uncertainty is calculated according to equation 4.1.

$$\Delta\theta = \sqrt{\Delta\theta_{O,channel}^2 + \Delta\theta_{O,ambient}^2} \quad (4.1)$$

$\theta_{O,channel}$ (Operative temperature in channel) and $\theta_{O,ambient}$ (Operative temperature in ambient zone) are assumed to vary within ± 0.15 K. This leads to an uncertainty according to the equation of 0.42 °C.

Finally, for preventing the noise in the electrical signals of the thermocouples, all the used devices are properly grounded. By grounding, the electric noise is reduced to ± 0.1 K.

4.2 Test conditions

The channel width is set to 40 cm for all experiments which gives an aspect ratio of 7.5 (H/b). The flow is studied in six experiments and a grouping according to temperature and ACH is made, see table 4.1.

	Test number	Temperature [°C]	ACH [h ⁻¹]	Inlet temp. [°C]
Group 1	2	30	4	18.55
	3	35	4	18.00
	4	40	4	17.16
Goup 2	1	30	4	24.59
	5	30	4	15.76
Group 3	1	30	4	24.59
	6	30	8	23.44

Table 4.1. Grouping of tests and conditions.

The temperature in the table refers to the set point of the heaters.

Temperatures are measured for 30 min after achieving steady-state in the channel. Steady-state regime is generally observed after about 1 h to 2 h depending on which boundary condition is modified, and is observed by the surface temperatures of the heated wall and the inlet temperature. Whenever a calculation is based on a temperature measurement in this study, the temperature used is the average of the last 5 min. Since the flow in the channel is expected to be highly unstable both 30 min, 5 min and 1 min averages is analyzed for all measurements, and it is concluded that the difference from taken a 1 min average to a 5 min average is negligible. The transient flow dynamics is presented in the following chapters whenever it is found necessary.

The analysis of the experimental results starts with a complete description of test 1. Then the tests are grouped according to which boundary condition is changed leaning towards two main objectives:

- Study the influence of the change in Rayleigh number
- Study the influence of the change in ACH

Each study is presented with comparisons of the obtained Rayleigh numbers, Gr/Re^2 -ratios and both horizontal and vertical temperature profiles implicating the flow conditions inside the channel. When comparing tests the temperatures are non-dimensionalized according to equation 4.2.

$$T_{dim} = \frac{T - T_{inlet}}{T_{heater} - T_{inlet}} \quad (4.2)$$

Where:

T_{dim}	Dimensionless temperature [-]
T_{inlet}	5 min average measured inlet temperature [°C]
T_{heater}	Average of all measured surface temperatures at the heated wall [°C]

By doing this the values are better measured relative to the unit °C and referred to quantities related to the system. It is chosen to use an average of the last 5 min of measurement each time comparisons are made between the tests. This is done with respect to lesser lines in each figure and therefore allowing a better view for the reader. A test is conducted comparing 5 min and 1 min averages that revealed no great differences, which is why it is assumed to be sufficient with the 5 min average. Since the literature study showed that a recirculation flow rises and collapses in a periodic manner it is chosen to analyze the stability whenever found necessary, and in *appendix* each test is presented with stability for all measurement points if they are not presented in the sections. To understand the graphs it is worth mentioning that whenever the abscissa is x/b it illustrates the distance from the heated wall; $x/b = 0$ is the heated surface and $x/b = 1$ is the glass surface.

Whenever Grashof and Rayleigh numbers are calculated the inlet temperature is chosen as the fluid temperature. This decision is based on a comparison of three calculated Grashof/Rayleigh numbers, where the fluid temperature is set as the inlet temperature, the temperature in the center at each height and a weighted moving average of the center temperatures in all heights respectively, but it is also based on the fact that the studied literature

similarly uses the inlet temperature when having isothermal heating. Moreover, the calculation of Reynolds number is based on an average velocity, which is being calculated by the measured airflow at the outlet and the channel dimensions.

Concluding remarks are found at the end of each section, where the results are compared to the literature.

Experimental results and Discussion

A complete review of the results from test 1 is presented as an introduction to this chapter. As mentioned earlier each section is presented with Rayleigh numbers, Gr/Re^2 -ratio and temperature profiles to understand the flow condition with varying boundary condition. As it is mentioned in *section 4.1* on page 31 temperatures are measured in 89 points divided by 7 different heights. The lowest points are located at 0.25 m and the highest at 2.75 m, and it is chosen not to use those results when analyzing the temperature profiles due to high uncertainty and turbulence at the inlet and outlet, which is why it is supposedly not representative for the general air flow pattern in the channel. The horizontal temperature profiles for these two locations can be found in *appendix D* on page 135.

5.1 Review of Test 1

The test conditions are listed in table 5.1.

	Test 1
Ra_H [-]	$9.98 \cdot 10^{11}$
Gr_H [-]	$1.34 \cdot 10^{12}$
Re_H [-]	$8.03 \cdot 10^5$
$Gr_H/Re_H^2 - ratio$ [-]	2.08
$T_{heater,SP}$ [°C]	30.00
$T_{heater,meas.}$ [°C]	26.08
$T_{inlet,SP}$ [°C]	Ambient air
$T_{inlet,meas.}$ [°C]	24.59
ACH [h^{-1}]	4.00
$T_{heater,meas.} - T_{inlet,meas.}$ [°C]	1.49
$T_{heater,meas.} - T_{glass,meas.}$ [°C]	0.69

Table 5.1. Test conditions for test 1

Some results are not shown in the following section, but they can be found in *appendix D* on page 135.

Dimensionless Numbers to Indicate Flow Condition

Figure 5.1 represents the calculated Rayleigh numbers for test 1 according to height. Recall, that the inlet temperature is used as the fluid temperature and the total height of the channel is used as the characteristic length.

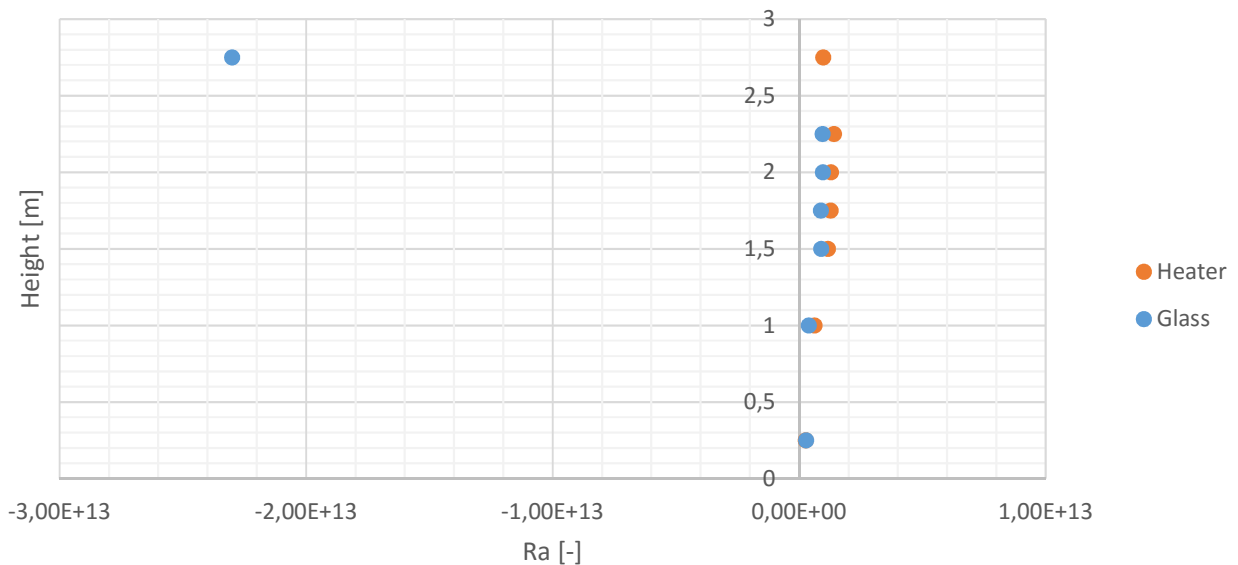


Figure 5.1. Calculated Rayleigh numbers according to height.

The negative value is caused by the negative temperature difference between surfaces and inlet temperature. It is therefore not an indication of the flow condition but instead implicating the flow direction, which is why only the absolute values should be analyzed.

The minimum obtained Rayleigh number is $2.06 \cdot 10^{11}$ and the maximum is $1.71 \cdot 10^{13}$ indicating that the flow in the boundary layer is in transition to or is turbulent, as it is above 10^9 at all times.

The Gr/Re^2 -ratio indicates if the flow is either forced, natural or mixed convection, and is illustrated in figure 5.2 on the next page.

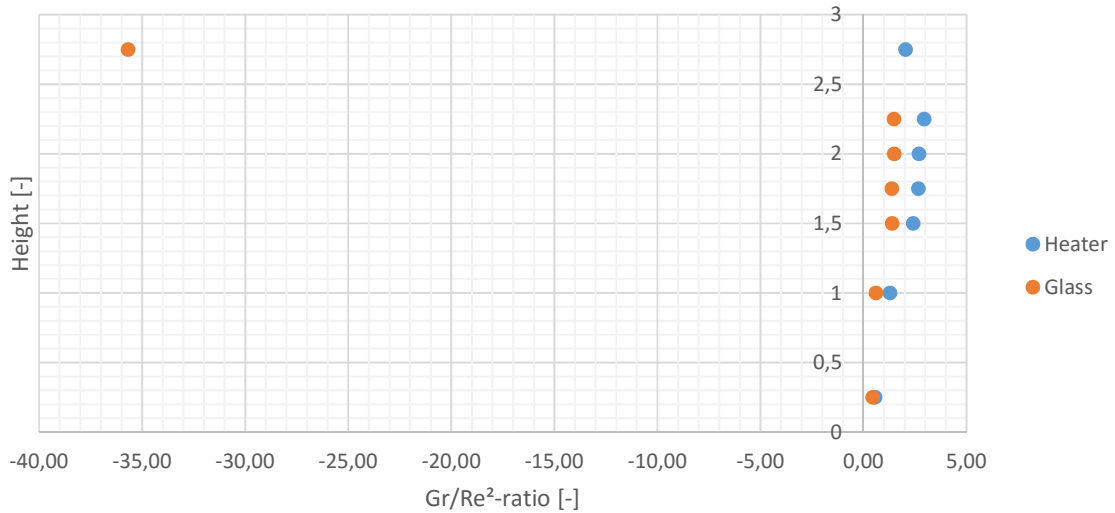


Figure 5.2. Calculated Gr/Re^2 -ratio according to height.

The lowest calculated Gr/Re^2 -ratio is 0.43 in height 0.25 m and the highest number is 35.7 in height 2.75 m. From the graph it is observed like for Rayleigh number that the ratio increases along the height as the temperature difference between the surface and the inlet becomes greater. Besides from the lowest measurement point the flow is assumed to be driven by natural convection.

Temperature Profiles

The horizontal temperature profile in height 1.00 m is shown in figure 5.3.

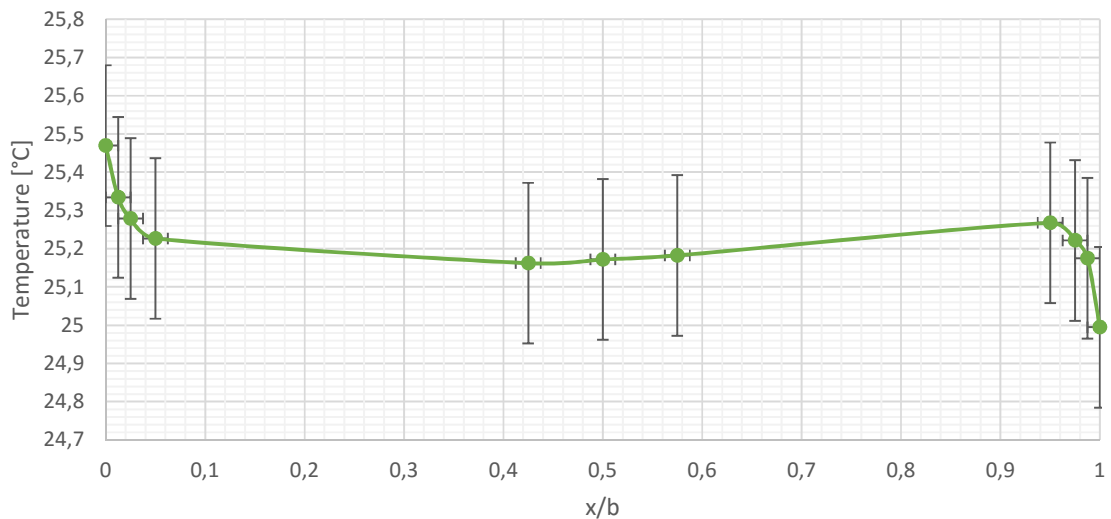


Figure 5.3. 5 min average horizontal temperature profile in height 1.00 m.

The horizontal temperature profile in height 1.00 m shows an example of the temperature distribution when having a standard channel flow with one heated wall (left) and one colder wall (right). The free flow temperature is lower than the heated wall but higher than the colder wall, which creates a downward stream at the colder surface. Figure 5.4 presenting each measurement for 50 s is showing that the fluctuations are within the measurement error, hence the flow is considered stable at this height.

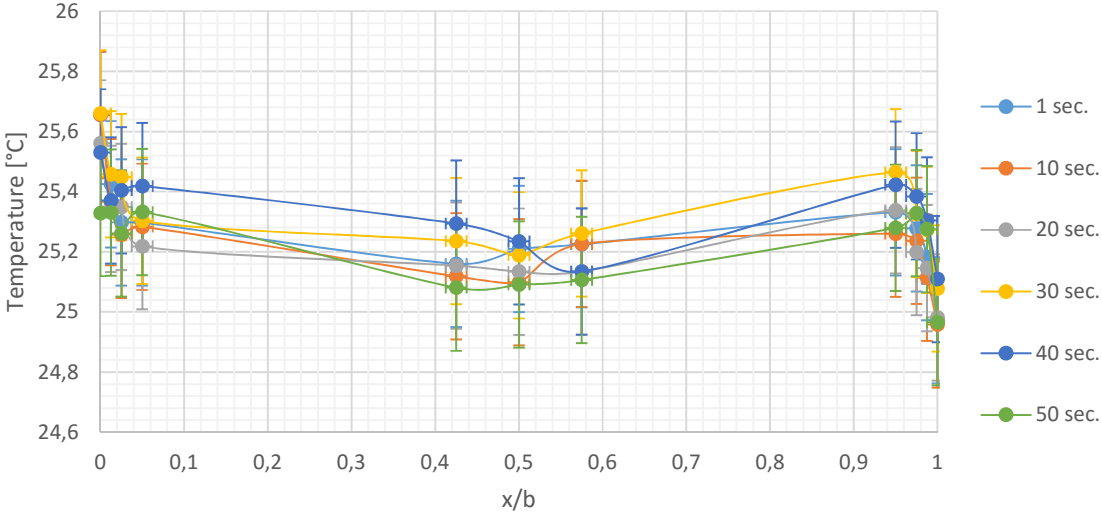


Figure 5.4. Stability in horizontal temperature profile in height 1.00 m.

Although the flow is considered stable it is observed that all temperature profiles in time exhibit the same general flow pattern; air moving upward along the heated wall and downward along the colder surface.

Next is the temperature distribution for height 1.50 m shown in figure 5.5 on the facing page.

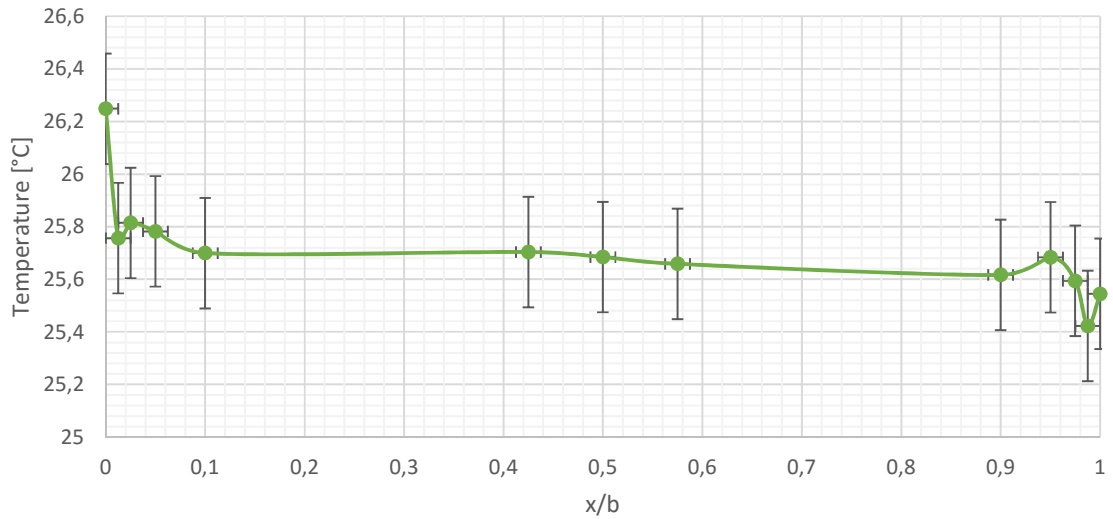


Figure 5.5. 5 min average horizontal temperature profile in height 1.50 m.

It is seen that the flow in the boundary both close to the heated wall and the colder wall have air coming from the upper layer. For this height it is observed that the peaks close to the surfaces does not lie within the measurement error implicating that the measured temperatures are actual fluctuations. Since recirculation is a dynamic phenomenon the stability for this height is given in figure 5.6.

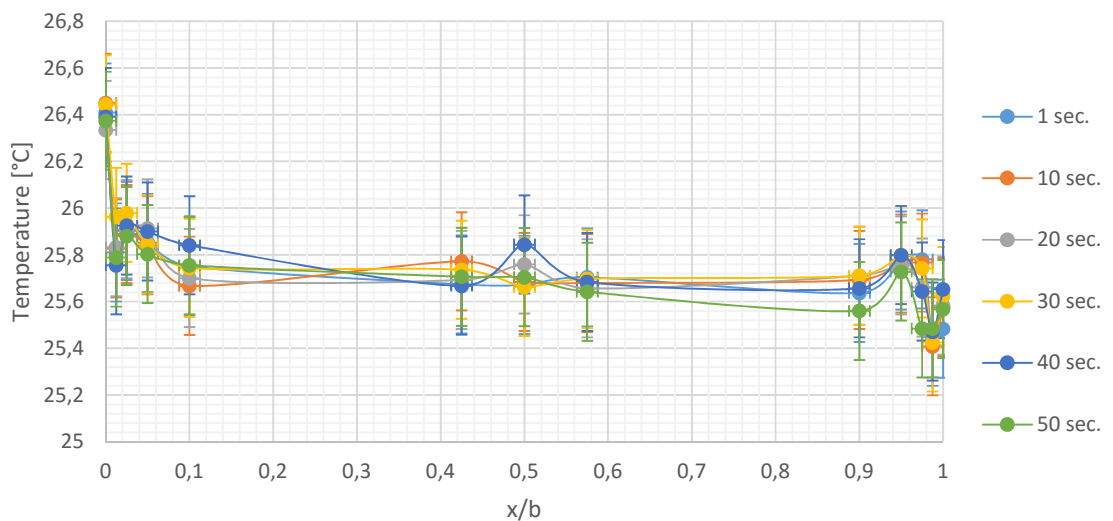


Figure 5.6. Stability in horizontal temperature profile in height 1.50 m.

It is recognized from the figure that the flow is rather steady, which is not expected by theory, as a result the implication of recirculating regions near the boundaries are weakened.

In height 1.75 m the same tendency is found as in height 1.50 m, but the air flow coming from

the upper part at the boundaries seem to have decreased, see figure 5.7.

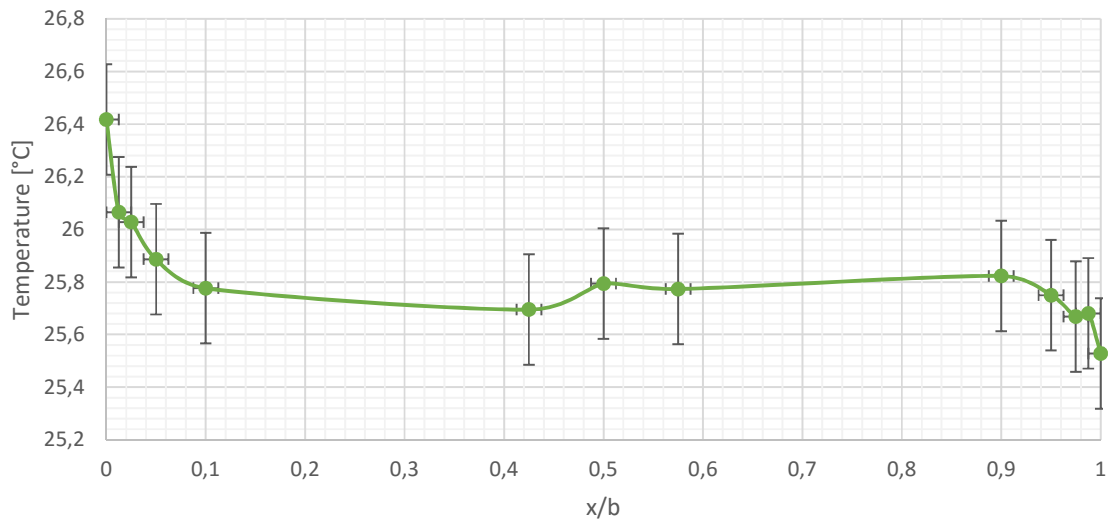


Figure 5.7. 5 min average horizontal temperature profile in height 1.75 m.

The peaks close to the boundaries have decreased and are now within the limit of the measurement error, which is why it can be said that the possible recirculating flow has decreased or even disappeared.

The stability in height 1.75 m is shown in figure 5.8.

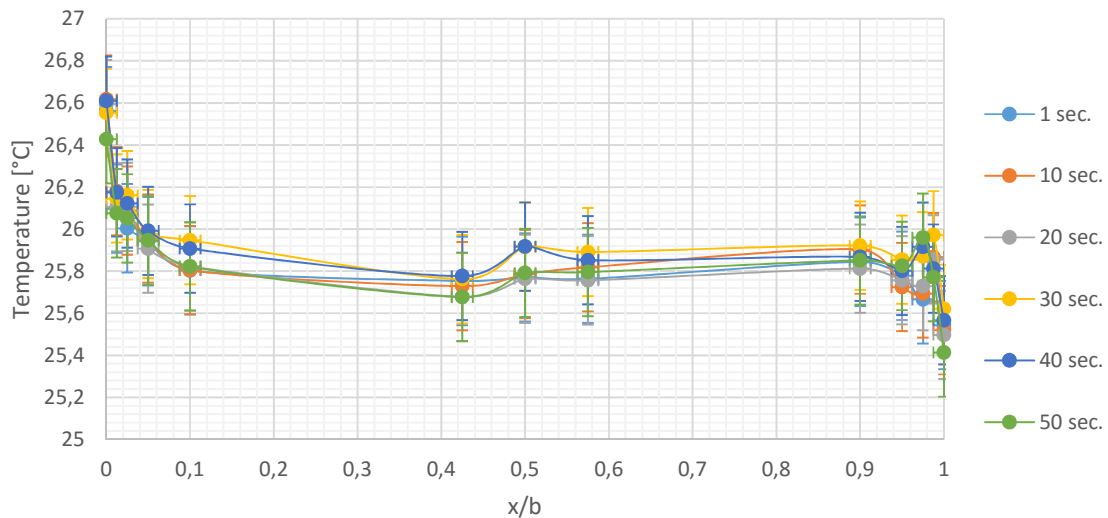


Figure 5.8. Stability in horizontal temperature profile in height 1.75 m.

The stability in height 1.75 m shows a different situation close to the glass surface. I.e. the measurement after 30 s has the highest peak temperature located at $x/b = 0.9875$ and this measurement is outside of the error limit indicating that the flow is dynamic.

The horizontal temperature in height 2.00 m profile is shown in figure 5.9.

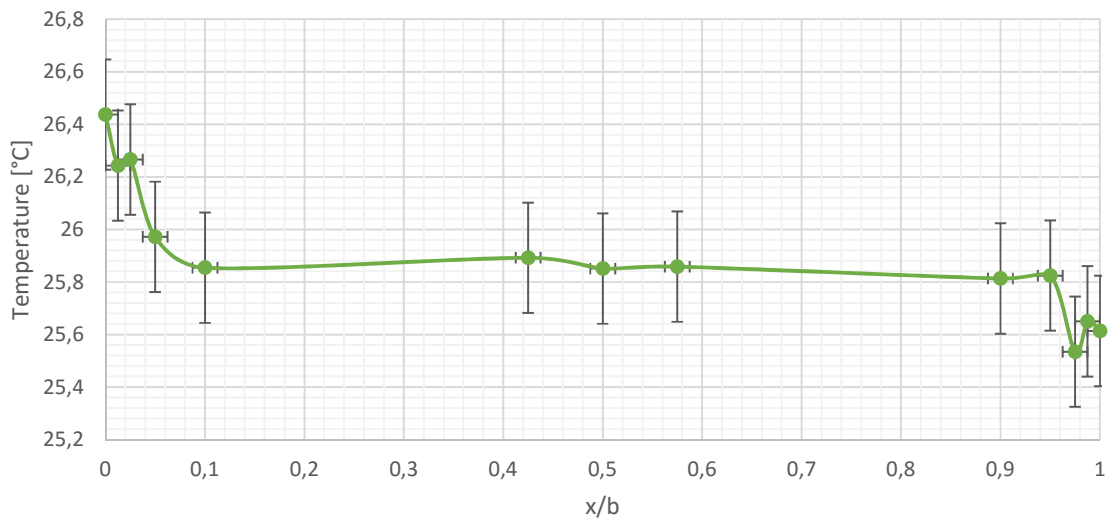


Figure 5.9. 5 min average horizontal temperature profile in height 2.00 m.

The 5 min average again revealed peaks that indicate regions with recirculating flow close to the colder boundary. It may be said that the strong extreme recirculating flow creating a backflow at the cold surface is accompanied with additional effects like a smaller region of recirculating flow.

Figure 5.10 illustrates the stability with measurements taken each 10 s.

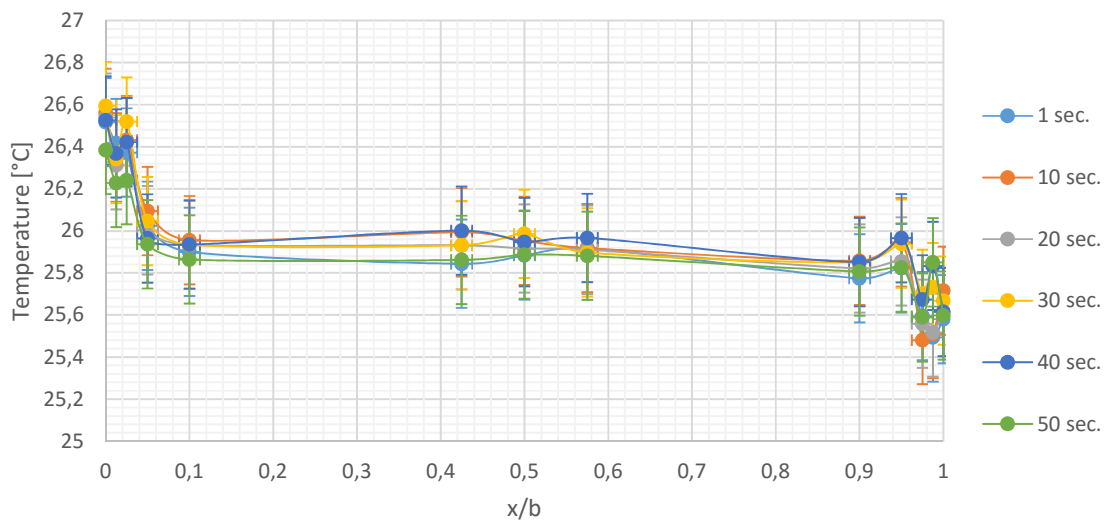


Figure 5.10. Stability in horizontal temperature profile in height 2.00 m.

It is seen that the flow has a steady tendency everywhere but close to the cold surface where the points located $x/b = 0.9875$ displays shift in peak outside of the measurement error.

Next is the horizontal temperature profile presented for height 2.25 m in figure 5.11.

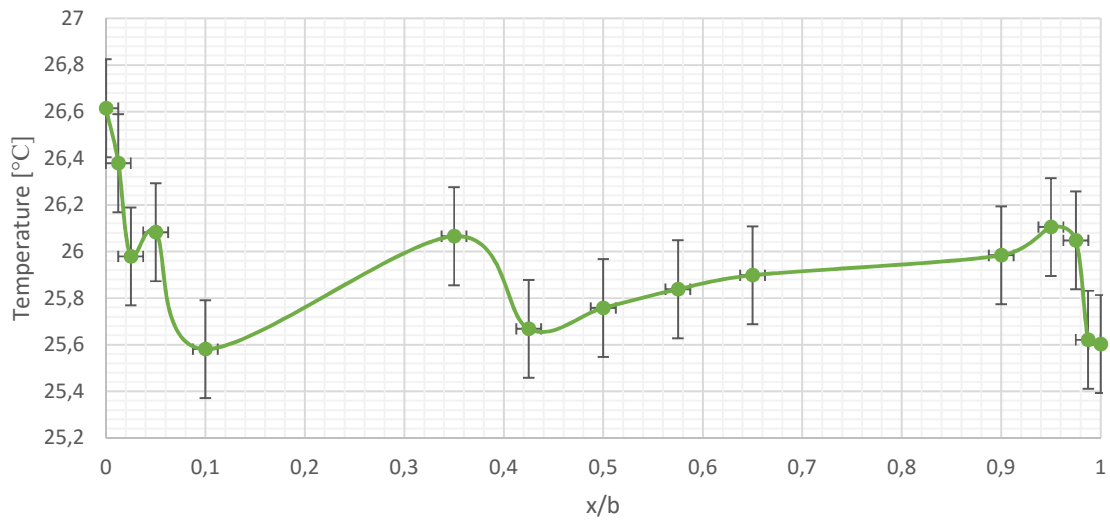


Figure 5.11. 5 min average horizontal temperature profile in height 2.25 m.

As the figure is showing the temperature distribution in the vicinity of the center is different compared to other heights. It should be mentioned that there is an extra measuring point at this height located 6 cm from the center on both sides in $x/b = 0.35$ and $x/b = 0.65$. Peaks close to the boundaries are still happening, but is now moved to the fourth measurement point from the boundaries.

Looking at the stability in figure 5.12 it is seen that the flow is relatively steady although it exhibits several peaks along the width of the channel. The fluctuations are all located within the measurement error.

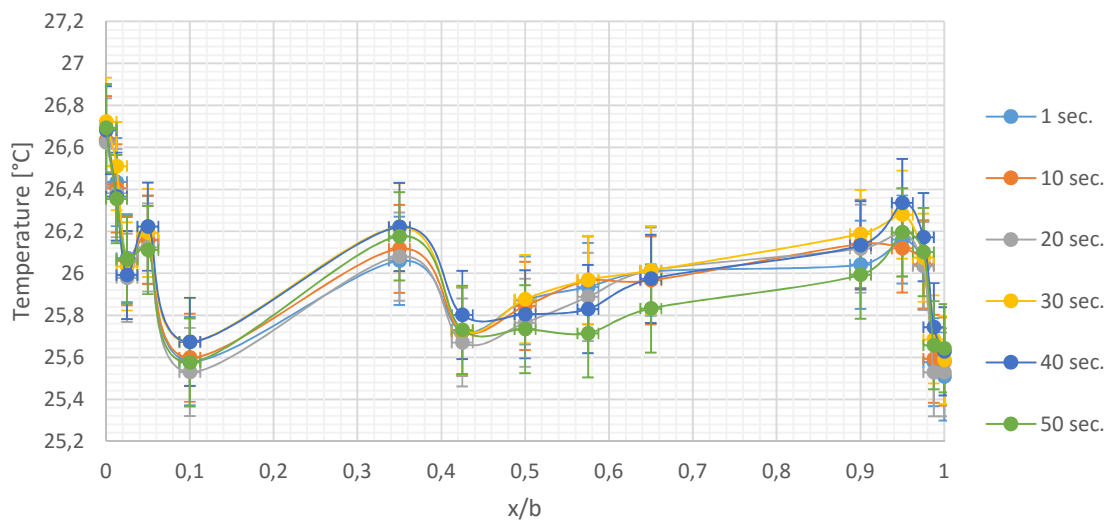


Figure 5.12. Stability in horizontal temperature profile in height 2.25 m.

Another way to describe the flow in the channel is by analyzing the vertical temperature profiles, especially the vertical temperature profile in the center is interesting. Having a standard channel flow the vertical temperature profile will be proportional with the height of the channel; increasing as the height increases. Figure 5.13 is showing the vertical temperature profile with measurements taken each 10 s.

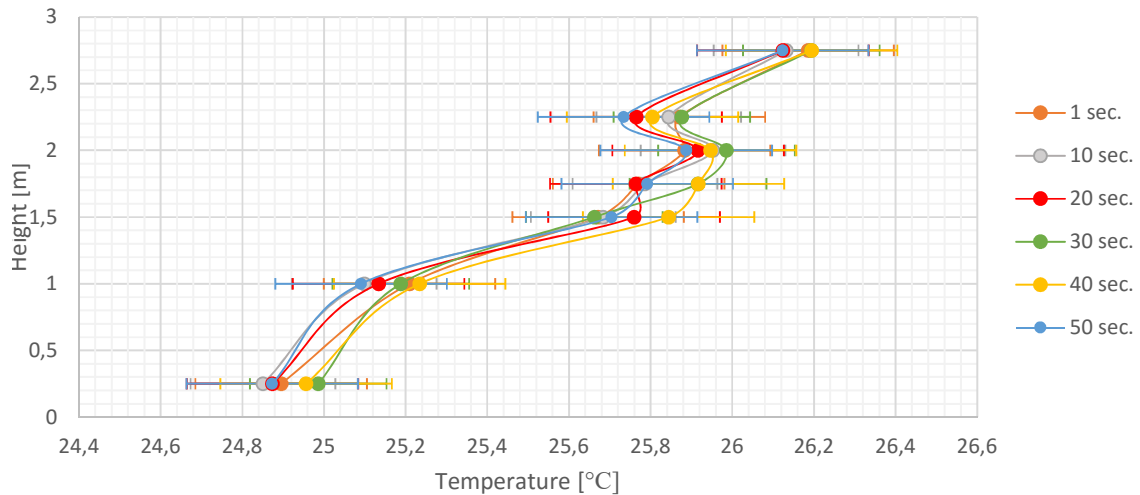


Figure 5.13. Stability of vertical temperature profile in center.

A temperature drop in height 2.25 m indicates that a recirculating flow is appearing in this area. The temperature is also seen fluctuating in heights 1.50 m and 1.75 m, which also agrees with the horizontal profiles. Although this could be a sign of recirculation the points located from 1.50 m to 2.25 m are all within the measurement error bar and can for that reason i.e. have constant temperatures by means.

The horizontal temperature profiles implicated areas of recirculation near the boundaries. Close to the heated surface the horizontal temperature profiles showed that warmer air is measured 1 cm from the wall. This can also be seen in the vertical temperature profiles shown in figure 5.14 on the next page.

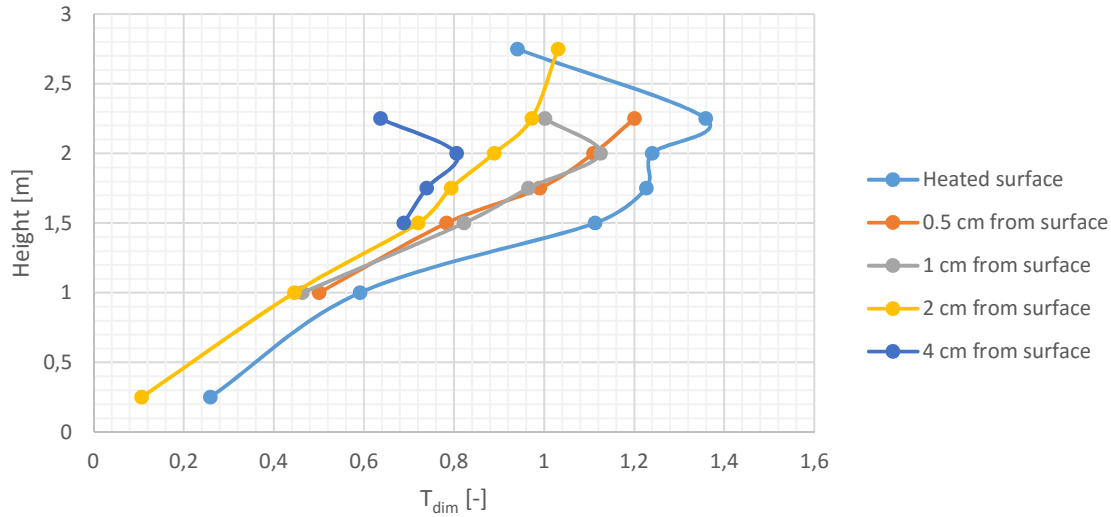


Figure 5.14. Vertical temperature profiles close to heated surface.

The figure is illustrating 5 min average of measurements at different locations in both height and distance from the heated surface. It is chosen to compare only the average since the stability analysis and averages showed the same tendencies.

At the distance of 0.5 cm from the heated surface the temperature is increasing proportional with the height. Then moving to 1 cm from the surface the vertical profile has a temperature drop in height 2.25 m but otherwise having the same temperatures. They are located with a distance of 0.5 cm from each other, and it may be an indication that they are both in the thermal boundary layer until 2.25 m, where the temperature 1 cm from the surface drops. The boundary layer development might not be consistent with the theory of a vertical plate if recirculation is appearing. If this is the case, the boundary layer may have decreased in thickness at this height. At the distance 2 cm from the surface the temperature is again increasing proportional with the height, and 4 cm from the surface the vertical distribution again drops in height 2.25 m.

From the horizontal temperature profiles areas of recirculation is indicated close to the colder glass wall. The next figure 5.15 on the facing page is showing the vertical profile 0.5 cm from the glass.

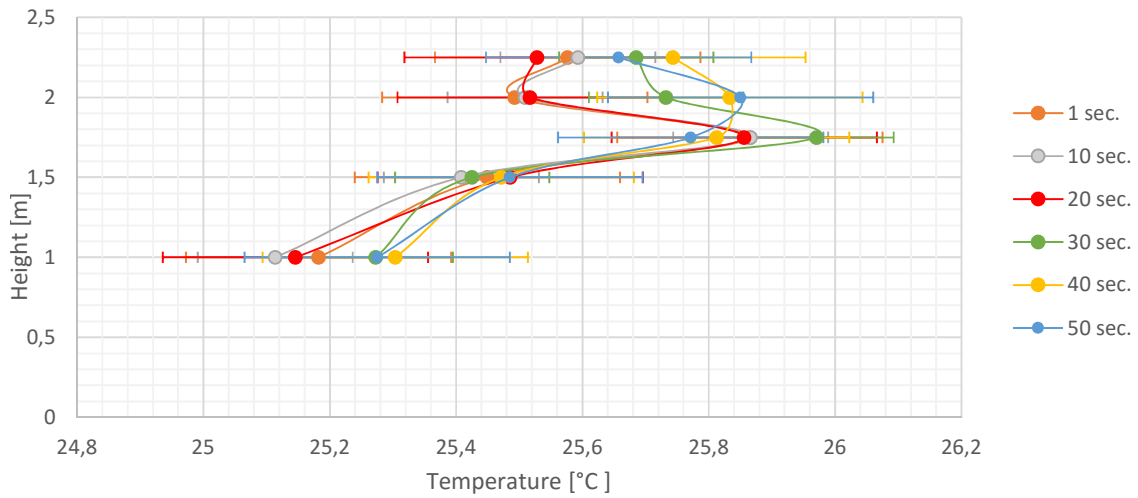


Figure 5.15. Stability of vertical temperature profile 0.5 cm from glass surface.

The interesting part of this graph is the top of the channel. In height 1.75 m and 2.00 m there is a shift in which height the highest temperature is found. I.e. from the 30 sec measurement the peak temperature is found in height 1.75 m but the 50 sec measurement shows a peak in 2.00 m height. The lowest temperature at the top of the channel is also seen varying; from the first measurement to 20 sec the lowest temperature at the top is found in the height of 2.00 m but the rest shows that the lowest temperature is found in 2.25 m. From this graphs it can be concluded that the air is highly unstable having both warmer and colder air coming from different locations in the channel at different times indicating a recirculating flow.

At the lower part of the channel the peak temperatures near the boundary to the glass was found shifting between 1 cm and 2 cm from the surface. Figures 5.16 and 5.17 on the next page represents the instantly taken measurements at the mentioned distances.

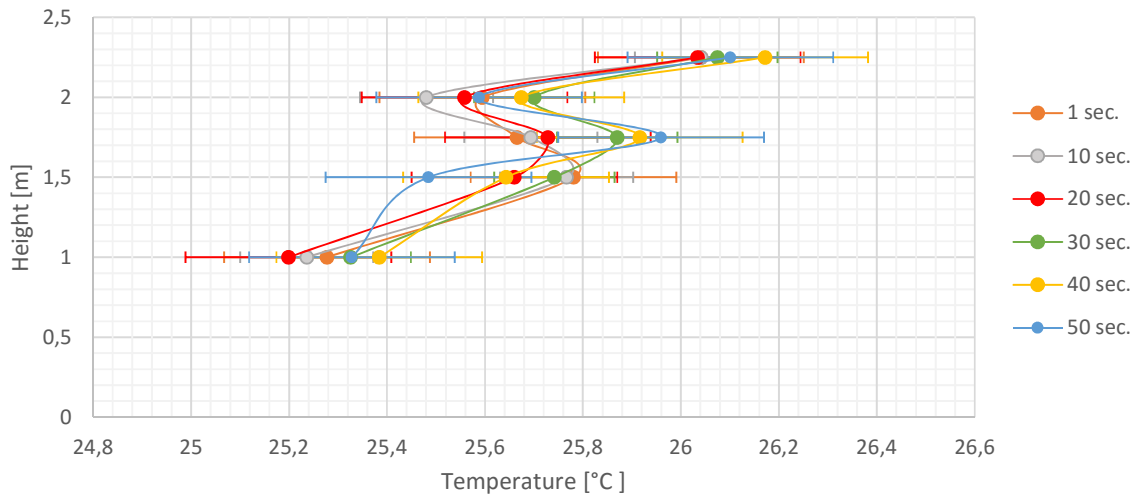


Figure 5.16. Stability of vertical temperature profile 1 cm from glass surface.

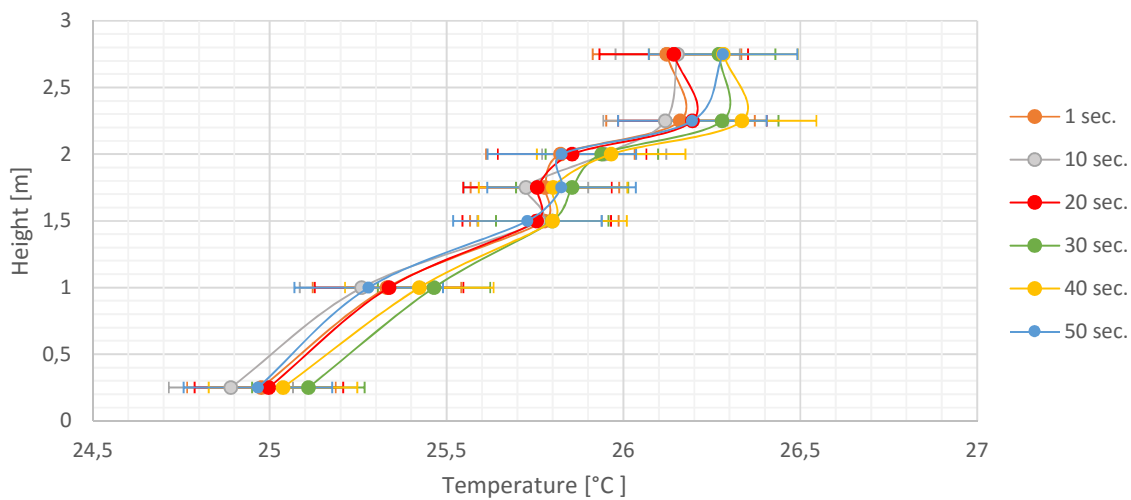


Figure 5.17. Stability of vertical temperature profile 2 cm from glass surface.

A significant temperature drop in height 2.00 m is found in the graph showing the temperature gradient 1 cm from the glass surface. Another notable trend in this graph is the change of peak temperature in heights 1.50 m and 1.75 m. I.e. the first measurement shows that the peak temperature between these heights are found in 1.50 m, the same tendency is found in the 10 sec measurement but with a lower temperature in height 2.00 m. The peak is then moved to height 1.75 in the 20 sec measurement and in the 30 sec to 50 m with even greater temperatures.

2 cm from the glass the difference between the peaks in heights 1.50 m to 2.00 m is lowered and in four of the measurements a constant temperature is found at those previously seen peaks indicating that an area of mixing of the air is occurring. Compared to the temperatures

measured in 1 cm from the surface the heights from 1.50 m to 2.25 m have higher temperatures. The last vertical temperature gradient close to the glass is located with a distance of 4 cm, see figure 5.18.

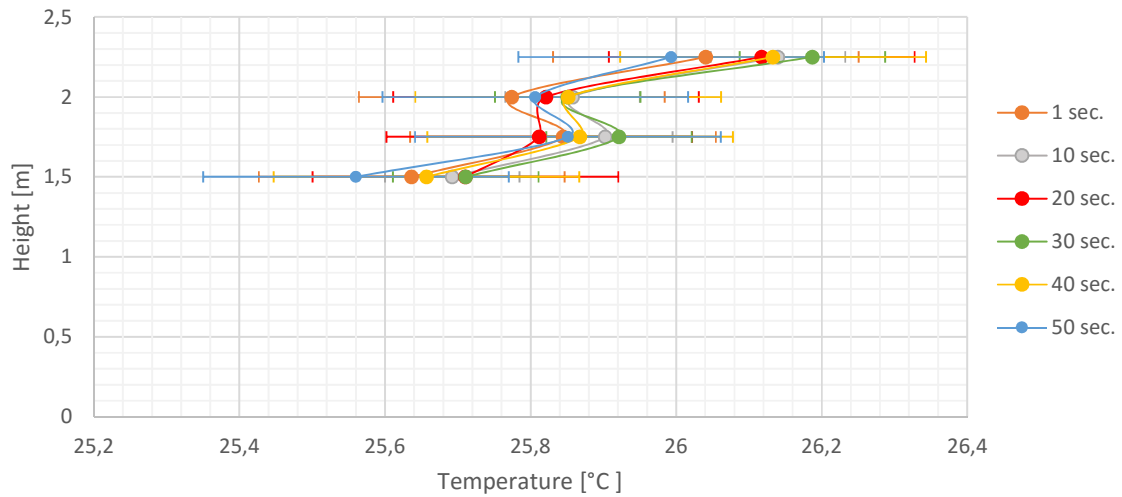


Figure 5.18. Stability of vertical temperature profile 4 cm from glass surface.

The same temperature drop as found in the vertical profile 1 cm from the glass is again clearly distinguished and is still found in height 2.00 m. The 20 sec is especially standing out from the other measurements because of the almost constant temperature in heights 1.75 m and 2.00 m.

Figure 5.19 on the next page is showing a comparison of the 5 min average in each distance from the glass surface. The graph is made to give an overview of how the temperatures develop with increasing distance from the colder surface.

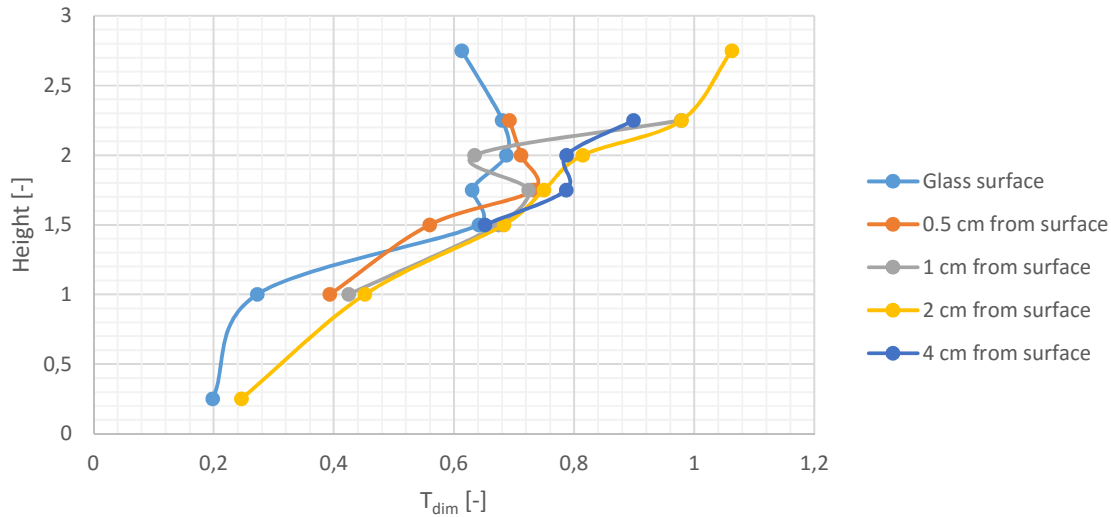


Figure 5.19. Vertical temperature profiles close to glass surface.

This comparison shows that the highest temperatures in height 1.50 m is found 2 cm from the surface. Then in height 1.75 m it is located 4 cm from the surface and at last heights 1.75 m and 2.00 m have the highest temperatures located 2 cm from the surface.

The distance 1 cm from the surface in height 2.00 m has a lowest temperature than all other distances including the glass surface. From this it might be concluded that recirculation is occurring.

5.1.1 Remarks

It is found in the first section of this chapter that the Rayleigh number indicated that the flow is in transition to or is turbulent, and the Gr/Re^2 -ratio proved that the flow is dominated by buoyancy forces. For those two conditions it was found in the literature that recirculation is a possibility.

From the horizontal and vertical temperature profiles it can be concluded that the general air flow pattern within the channel has the conditions similar to the case of extreme recirculation; the air enters the bottom and as it is being heated up by convection it follows an upward direction at the heated surface, and reversed direction close to the glass surface due to lower temperatures. From the literature study it is known that air not only leaves at the outlet, but also enters due to the conservation of the mass balance inside the channel as it is expected to happen for this test as well.

Regarding smaller regions of recirculating flow inside the channel at different heights nothing can truly be concluded, but several indications is found such as peaks close to the surfaces and the transient behavior of the flow. Working with temperature profiles in the measurements are supposed to have only small temperature differences, but scientifically they cannot exclude possible measurement errors.

In the literature the smaller recirculation regions were found to appear and collapse by few

second. As it is mentioned the temperature is logged every 10 s by the datalogger and this option cannot be changed due to the amount of thermocouples. It is therefore possible that the recirculation is not captured very well. For the future work regarding this topic the flow dynamics must be closely studied.

The peaks and fluctuations found in the horizontal and vertical temperature profiles may also be caused by a 3D flow occurring in the channel, and not the assumed 2D flow. The 3D flow is studied in test 1 with a thermal camera. A perforated thin paper is located at height 2.25 m, see figure 5.20.

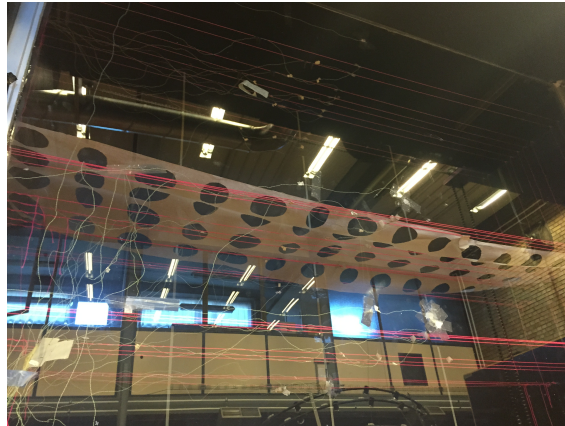


Figure 5.20. Perforated paper located in the channel.

The paper is perforated in order to minimize the disturbance of the flow occurring in the channel.

The thermal camera is located at the bottom of the channel in a position that allowed taking pictures of the perforated paper. Due to the limit of the width of the pictures taken by the camera, three pictures are taken to capture the whole length of the box. Figure 5.21 shows the positions of the camera according to the channel length.

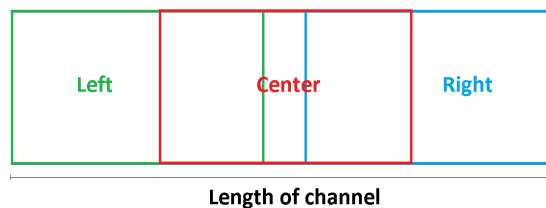


Figure 5.21. Explanation of locations of the three pictures.

Figure 5.22, 5.23 and 5.24 on the following page shows a 3D plot of the temperatures in the channel.

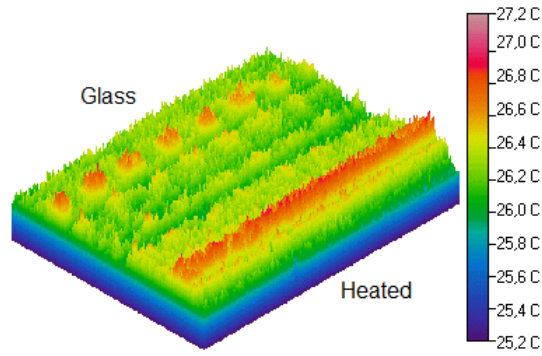


Figure 5.22. Picture captured in the center of the channel.

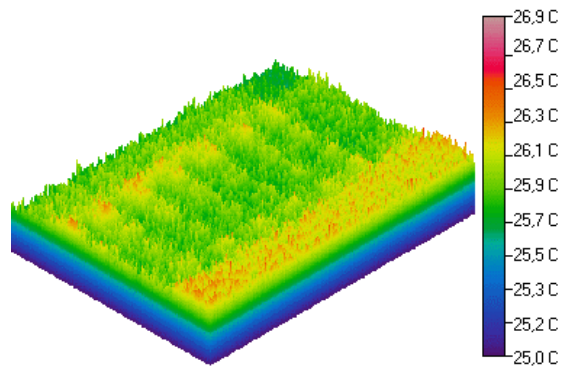


Figure 5.23. Picture captured to the right.

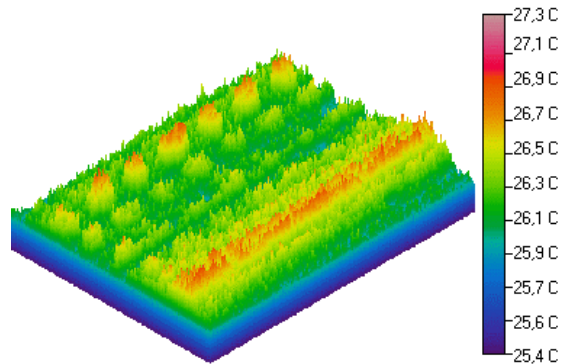


Figure 5.24. Picture captured to the left.

Based on these pictures it is concluded that the flow is in fact 2D in the dimensions channel width and height. 2D pictures can be found in *appendix C* on page 133.

5.2 Rayleigh Number Dependency

In the literature study in *chapter 3* on page 15 evidence was found that proved a change in Rayleigh number influences the flow structure inside a vertical channel, it is therefore chosen to investigate this in the present study but with other boundary conditions. The influence of Rayleigh number can be examined by changing two boundary conditions: the set point of the heaters and the inlet temperature. Changing the set point of the heaters will affect the surface temperature and changing the inlet temperature will have an impact on the temperature of the free fluid inside the channel, and both settings will influence the convective heat transfer. Recall from *chapter 2* on page 9 the equation for calculating the dimensionless Rayleigh number

$$Ra = \frac{g \cdot \beta \cdot (T_s - T_{fluid}) \cdot l^3}{\nu \cdot \alpha} = Gr \cdot Pr \quad (5.1)$$

As it is mentioned Rayleigh number is a dimensionless size which is used to describe the flow in the boundary layer for natural convection. A Rayleigh number above 10^9 indicates that the boundary layer flow is in transition to turbulent conditions [Incopera og Dewitt, 2011].

In the following chapter the influence of different Rayleigh numbers is examined by changing the two mentioned conditions and is named Group 1: Change of heater set point and Group 2: Change of inlet temperature.

Each group is provided with comparisons of Rayleigh numbers, and how the change of Rayleigh number influences Gr/Re^2 -ratio and flow conditions indicated by both horizontal and vertical temperature profiles.

5.2.1 Group 1: Change of Heated Surface Temperature

Group 1 is a comparison of the tests 2, 3 and 4 where the set point of the heaters are modified. Table 5.2 shows the test conditions for this specific group.

	Test 2	Test 3	Test4
Ra_H [-]	$4.81 \cdot 10^{12}$	$9.20 \cdot 10^{12}$	$1.17 \cdot 10^{13}$
Gr_H [-]	$6.46 \cdot 10^{12}$	$1.10 \cdot 10^{13}$	$1.58 \cdot 10^{13}$
Re_H [-]	$8.03 \cdot 10^5$		
Gr_H/Re_H^2 - ratio [-]	10.02	17.09	24.43
$T_{heater,SP}$ [°C]	30.00	35.00	40.00
$T_{heater,meas.}$ [°C]	25.89	30.68	35.38
$T_{inlet,SP}$ [°C]	19.00		
$T_{inlet,meas.}$ [°C]	18.55	18.00	17.16
ACH [h ⁻¹]	4		
$T_{heater,meas.} - T_{inlet,meas.}$ [°C]	7.33	12.68	18.22
$T_{heater,meas.} - T_{glass,meas.}$ [°C]	0.53	3.31	5.81

Table 5.2. Test conditions for group 1. All values are averages of the last 5 min of measurements.

The mean values of the dimensionless numbers are taken according to the heated surface.

First of all a graph presenting the measured surface temperature distributions on the heated wall is shown in figure 5.25.

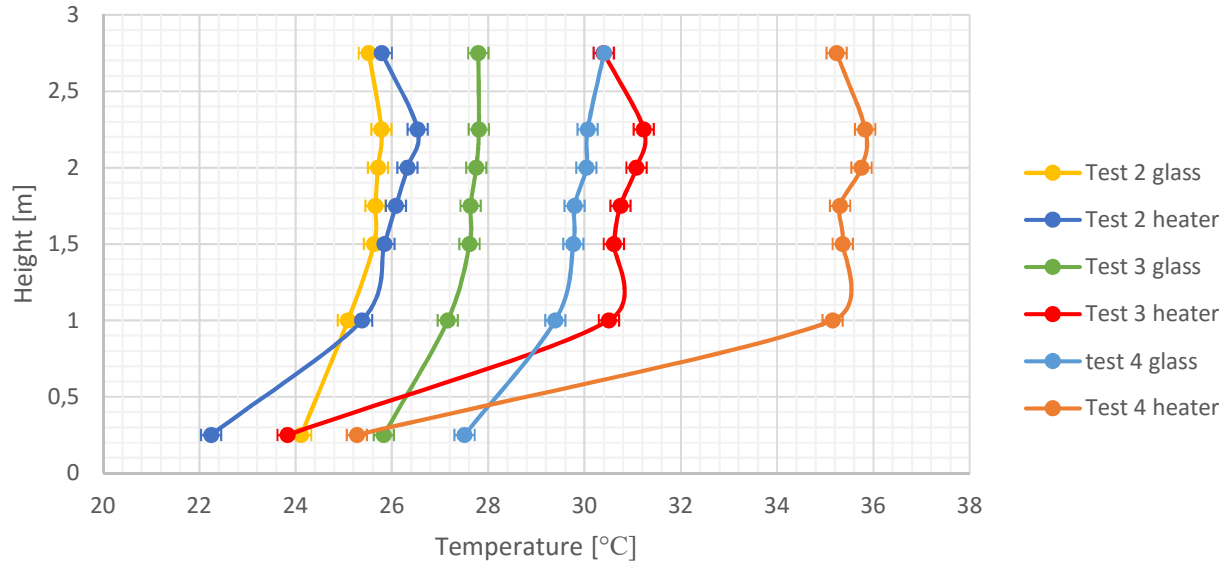


Figure 5.25. Temperature distribution on heated and cold surface.

As it is mentioned in *section 4.1.3* on page 33 the heater mat located at the bottom was not supplying any heat for the tests in this group. A small temperature gradient is obtained from height 1.00 m to 2.25 m even though the set point for all five mats is the same. This may be due to the natural transport of heat on the aluminum plate in front of the heating mats and possible losses. The temperature decrease at the highest point may be due to a measurement error or an error in the way the sensor is setup.

Comparison of Rayleigh Numbers

Rayleigh numbers are calculated according to equation 5.1 using the total height of the channel as the characteristic length and the inlet temperature as the fluid temperature. By looking at the equation it is seen that the only two parameters varying are the surface and fluid temperature. Rayleigh numbers are calculated from both the heated surface and the glass wall.

The results are found in figures 5.26 and 5.27 on the next page.

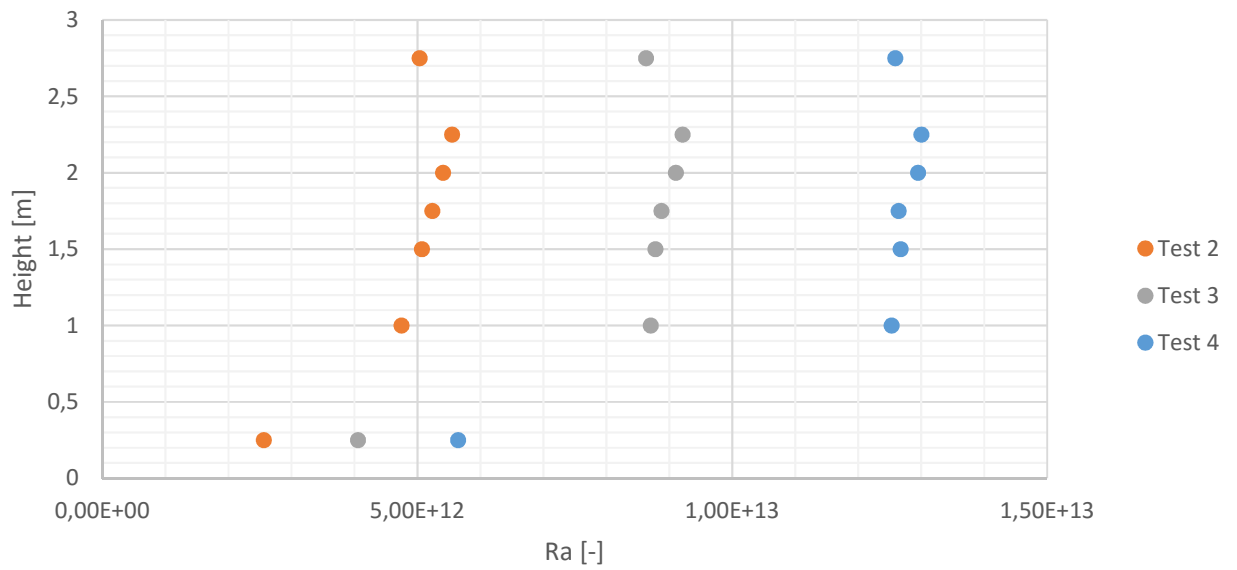


Figure 5.26. Rayleigh numbers according to the heated surface.

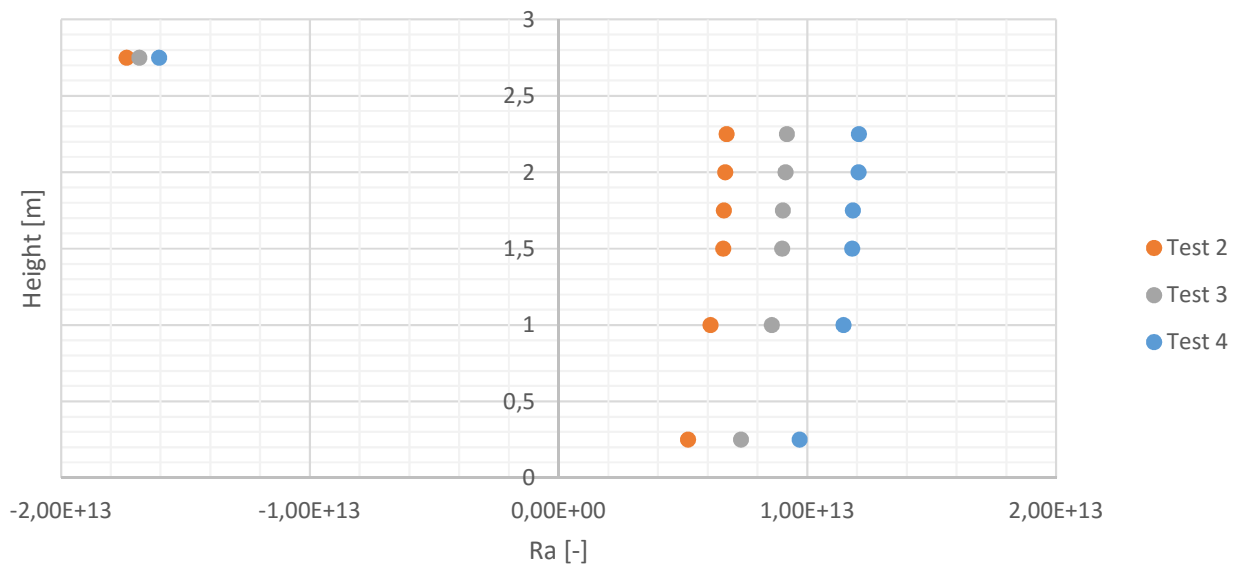


Figure 5.27. Rayleigh numbers according to the glass surface.

As a reminder it should be mentioned that only the absolute values are analyzed.

The Rayleigh number is for that reason found to be at all times above the criterion 10^9 implicating that the boundary layer flow is in transition to or is turbulent. Increasing the set point temperature of the heaters the Rayleigh number increased due to higher temperature differences between the surface and the free fluid. It is also found that the Rayleigh number increases along the height due to enhanced buoyancy forces in all three tests.

Comparison of Gr/Re^2 - ratio

As mentioned in *chapter 2* on page 9 the ratio of Gr/Re^2 is a measure of the strength of the boundary layer flow compared to the bulk flow, and categorizes the flow as either being forced, natural or mixed convection.

Figures 5.28 and 5.29 on the next page illustrates the ratio compared to the Rayleigh number. The ordinate is chosen with respect to the objective of this particular study in this section regarding the influence of the change in Rayleigh number.

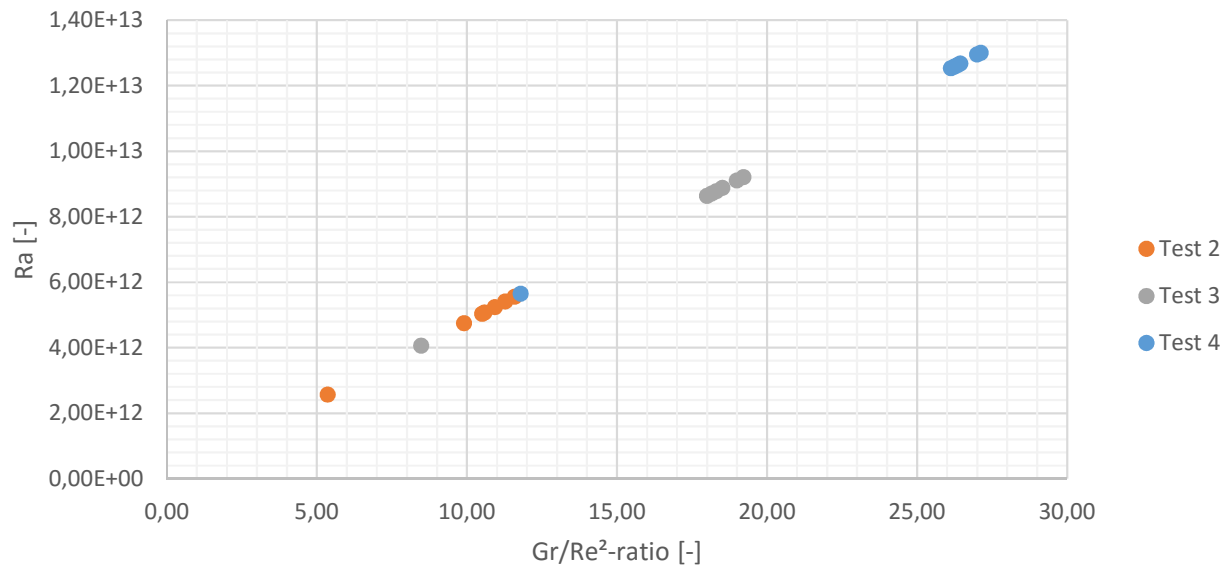


Figure 5.28. Gr/Re^2 -ratios according to the heated surface.

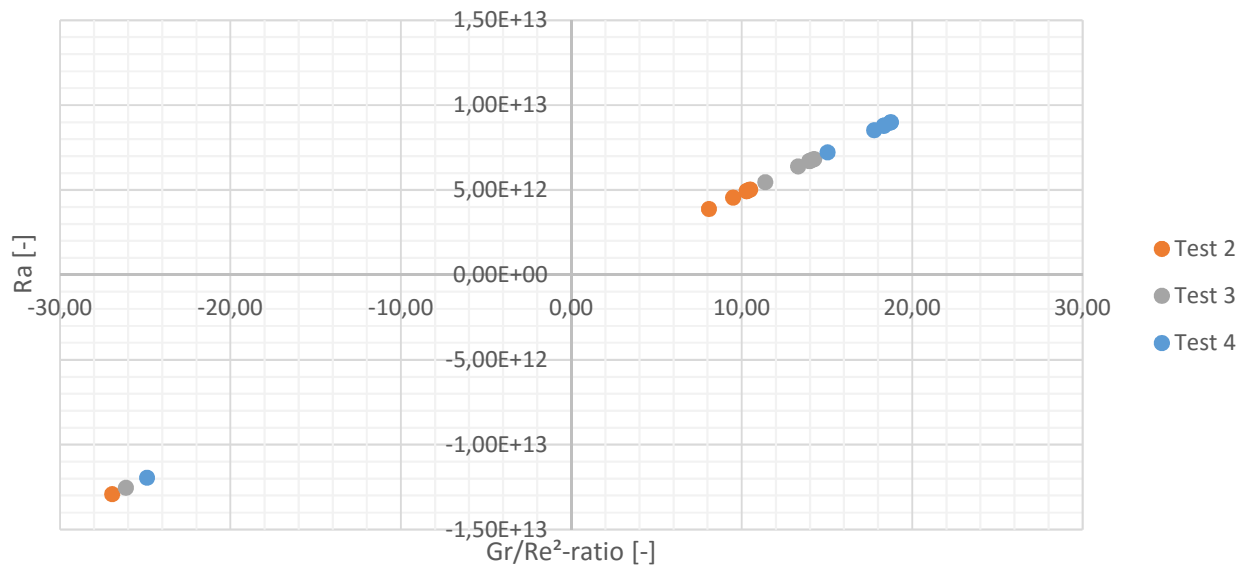


Figure 5.29. Gr/Re^2 -ratios according to the glass surface.

Since Rayleigh number is based on Grashof number and Reynolds number is constant for all three tests, a proportional relation is found; increasing Rayleigh number, hence increasing the surface temperature at the heated wall, also increases the Gr/Re^2 -ratio. Again only absolute values should be studied.

From *chapter 2* on page 9 the distinguishing of forced, natural and mixed convection is explained, and it can be concluded from the graphs that the Gr/Re^2 -ratio is for all tests above 1 indicating that the flow is natural convection dominated. Furthermore, it is observed that increasing the surface temperature increases the buoyancy forces leading to a higher value of Gr/Re^2 -ratio.

Flow Structure Indicated by Temperatures

In order to establish the flow conditions inside the channel with varying Rayleigh number results shown by horizontal temperature profiles and vertical gradients are presented in the following section.

As previously mentioned each temperature profile presented is a 5 min average calculated from the last 5 min of measurements unless else is stated.

First are the horizontal temperature profiles measured in height 1.00 m shown in figure 5.30 on the next page.

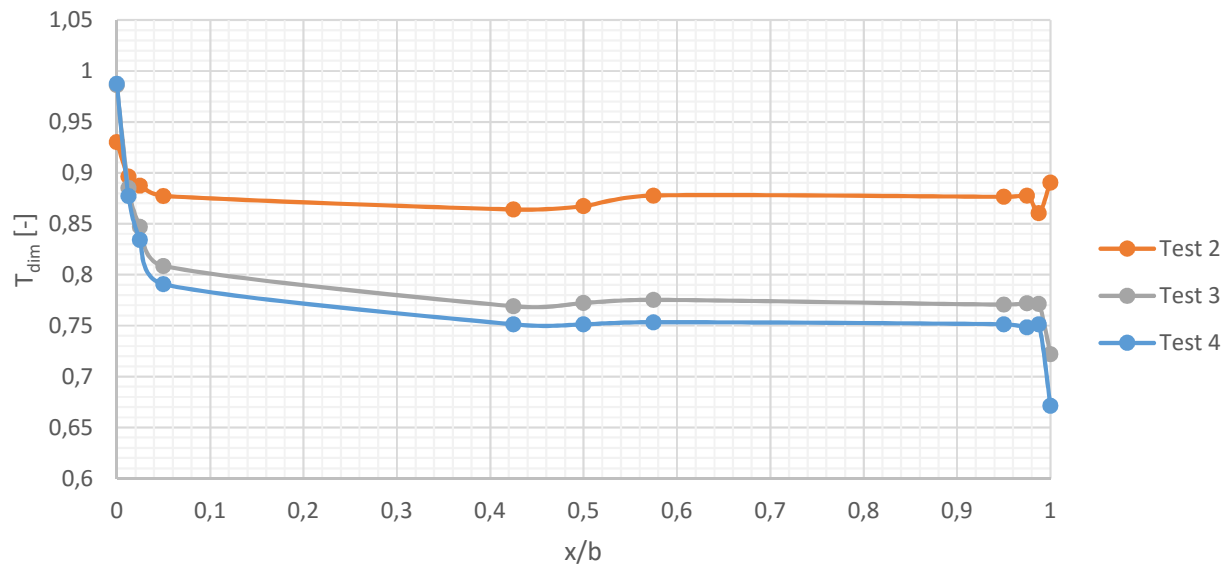


Figure 5.30. Horizontal temperature profiles in height 1.00 m.

Close to the heated wall for all three tests the temperature is distributed as known from theory; the highest temperatures are found at the surface and decreases as one moves away from the surface. At the glass surface different temperatures are seen that may either be due to a measurement error or different surrounding temperatures at the location, which is not being controlled, or due to higher radiation from the heated surface. A temperature drop is found in $x = 0.9875$ from the surface in test 2, which disappears with increasing Rayleigh number in test 3 and 4. Although this temperature drop may be due to a measurement error, it can also be due to a warmer air stream coming from the upper part with increasing effect and moving closer to the glass surface as Rayleigh number is increased. In general the flow pattern for all three tests can be explained as; colder air moving upwards in the channel close to the heated surface and warmer air moving downwards close to the colder surface creating a backflow.

Another interesting difference between these three tests is the dynamic behavior. Figure 5.31 on the facing page illustrates the instantly measurements in height 1.00 m for test 2.

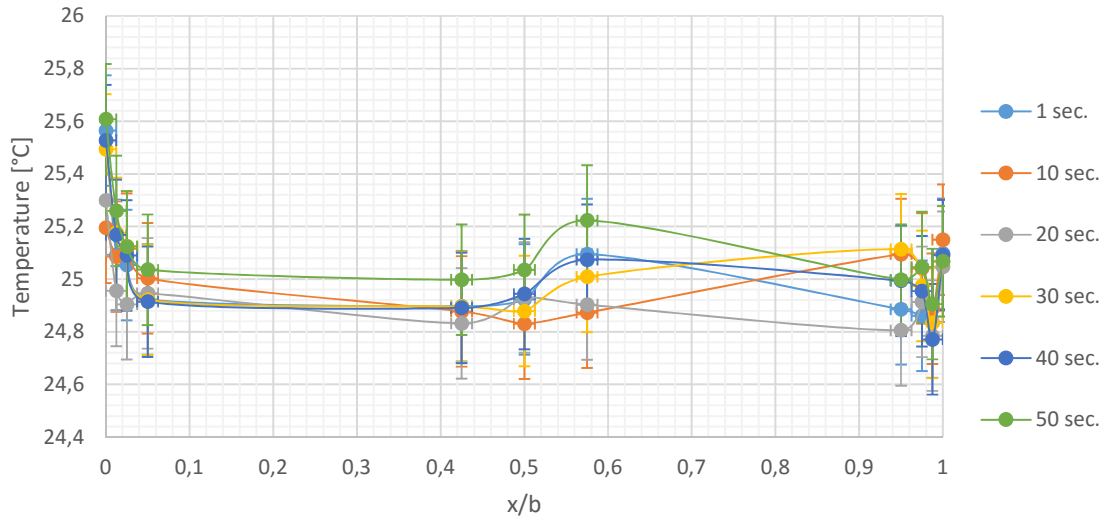


Figure 5.31. Stability in horizontal temperature profile in height 1.00 m for test 2.

As it is seen in test 1, test 2 also exhibits dynamic flow conditions, but here is only shown the first 50 sec and only the right side of the cavity is discussed. At this location the temperature fluctuations extends the measurement error indicating that the flow is dynamic. The first instantly measurement indicates that warm air is coming from the upper part of the cavity but closer to the center than the glass wall and the same temperature is found at this peak as for the surface. Then 10 sec later the warmer air is moved closer to the surface and has a higher temperature than the surface. After 20 sec the colder air arising from the bottom is again dominating, but a peak is found 1 cm from the surface either due to a measurement error or indicating than a small air stream with warmer temperatures is moving downwards close to the surface. And so the flow continues showing shifting temperatures indicating a dynamic flow and a possible area of recirculation or it might also be due to a measurement error since the highest temperature difference in one point is approximately 0.3 °C.

A different situation is seen in both test 3 and 4. Figure 5.32 on the next page shows the instantly measurement for test 3 in 50 sec in height 1.00 m.

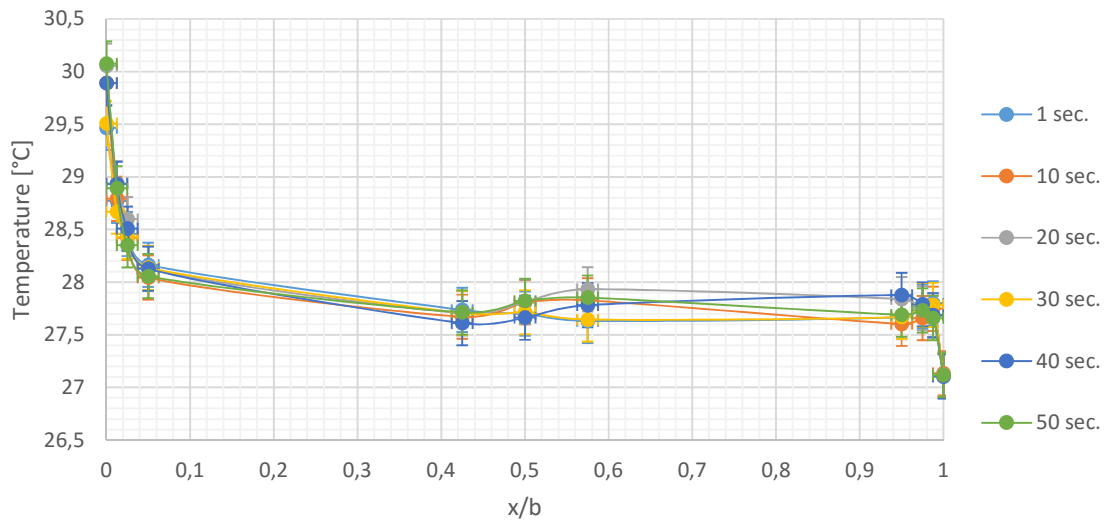


Figure 5.32. Stability in horizontal temperature profile in height 1.00 m for test 3.

It can be said that a much more stable flow regime is achieved by increasing Rayleigh number. Even in test 4 a more stable condition is found, the graph can be found in *appendix G* on page 153. Comparing the stability by the three tests it can be concluded that the dynamic behavior in height 1.00 m in test 3 is caused by fluctuating air movements and not by measurement errors.

The temperature distribution in height 1.50 m shows the same tendencies as in height 1.00 m except a temperature drop is now also occurring close to the heated surface in test 2, see figure 5.33.

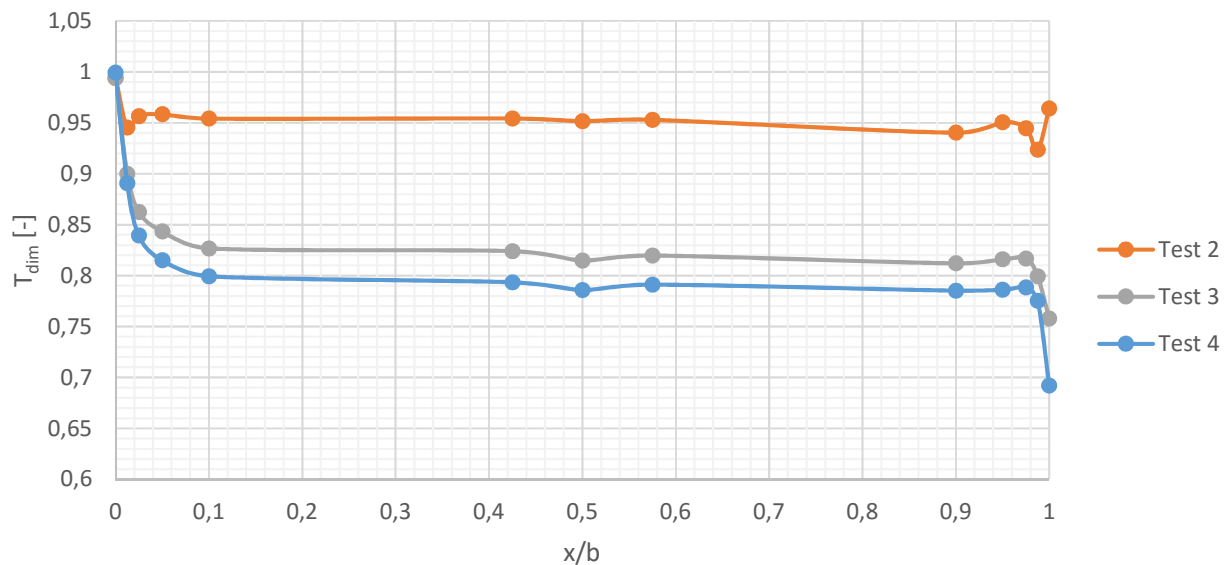


Figure 5.33. Horizontal temperature profiles in height 1.50 m.

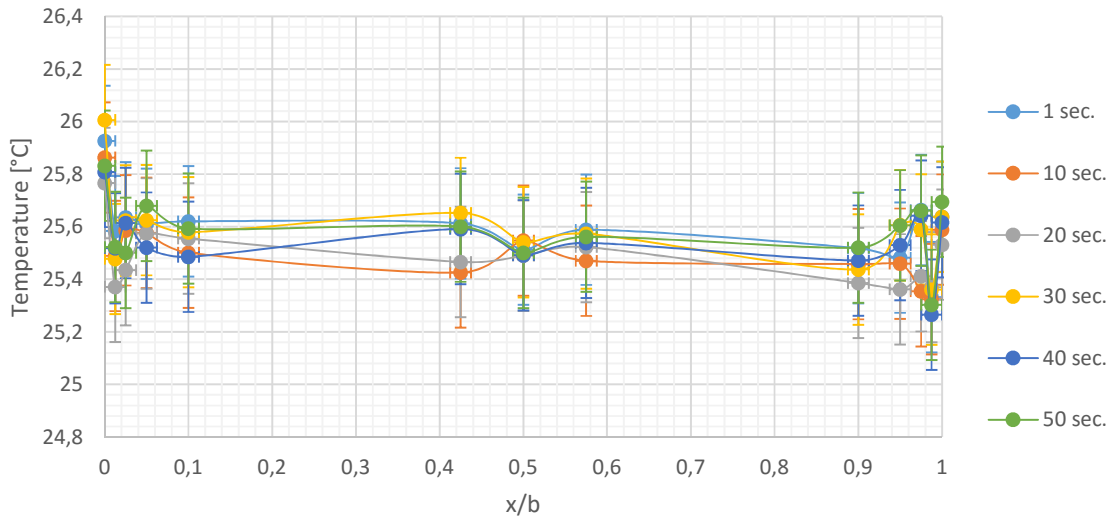


Figure 5.34. Stability in horizontal temperature profile in height 1.50 m for test 2.

A graph illustrating the stability at this height for test 2 is seen in figure 5.34. It can be said that the fluctuating temperatures are occurring both close to the cold and heated surface. Next is the temperature distribution in height 1.75 m shown in figure 5.35.

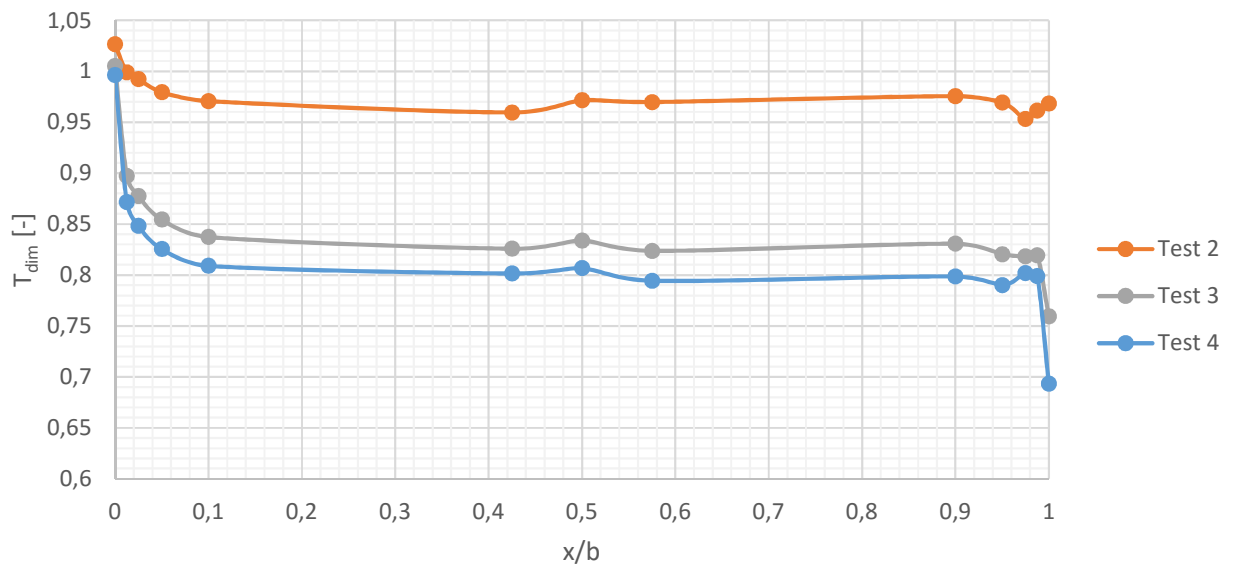


Figure 5.35. Horizontal temperature profiles in height 1.75 m.

The temperature drop in test 2 close to the heated surface is again disappeared, and the distribution is similar to what is seen in height 1.00 m. Close to the glass surface small temperature drops are now taking place for test 3 and 4. A closer look to the stability at this height shows that the temperature is fluctuating, but not in the same manner as for test 2 with

shifting location of high and low peaks. Figure 5.36 shows the stability for test 3 and figure 5.37 for test 4.

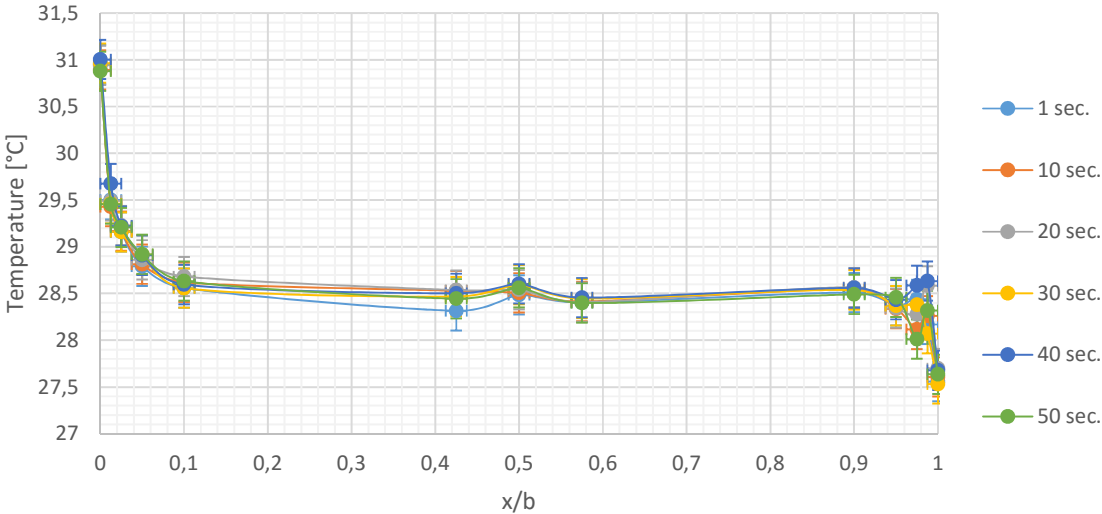


Figure 5.36. Stability in horizontal temperature profile in height 1.75 m for test 3.

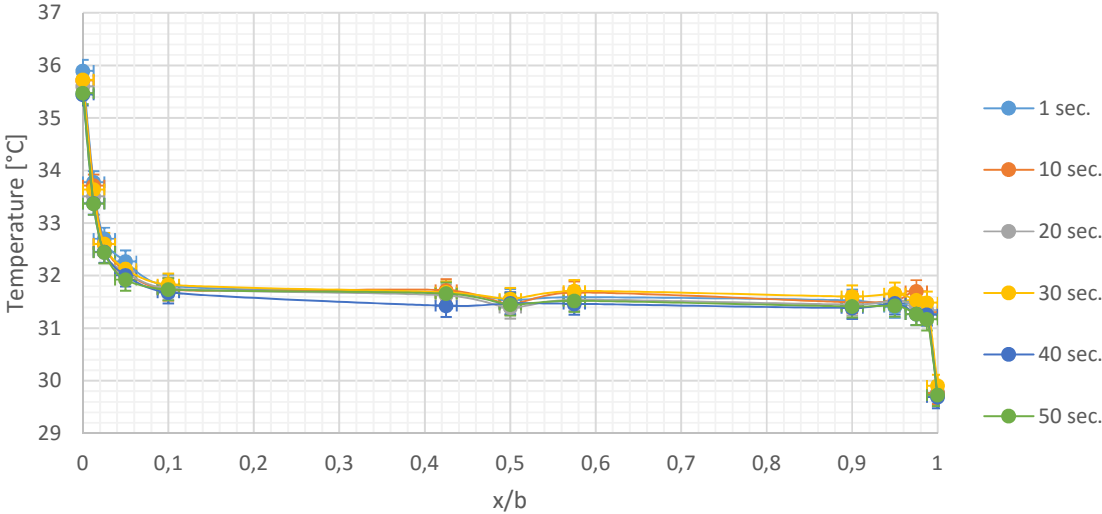


Figure 5.37. Stability in horizontal temperature profile in height 1.75 m for test 4.

The horizontal temperature profile in height 2.00 m will not be shown, since it shows the same tendencies as in height 1.75 m. More interesting is the temperature profiles in height 2.25 m, see figure 5.38 on the facing page.

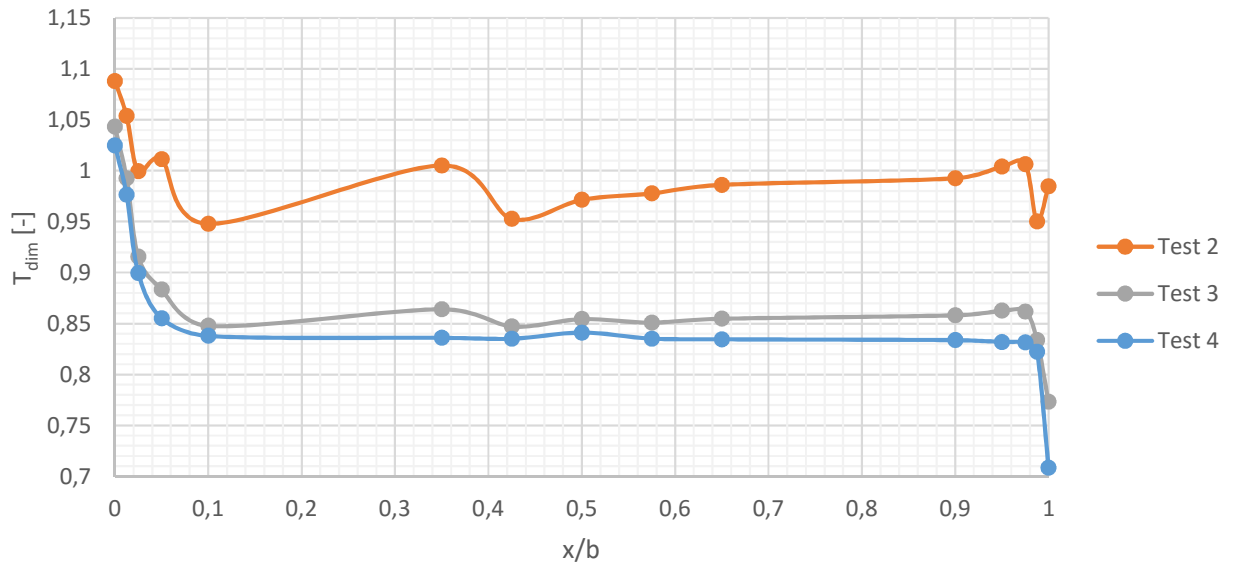


Figure 5.38. Horizontal temperature profiles in height 2.25 m.

It should be noted that an extra measurement point is located in the vicinity of the center, and as it can be seen an obvious temperature rise is occurring in test 2 at $x/b = 0.35$, but it is not known if this is occurring in the other heights as well. What can be concluded, is that the fluctuating temperatures in the center are disappearing and a more stable flow is obtained when the Rayleigh number is increased.

From the horizontal temperature profiles it can be concluded that a case of extreme recirculation in the entire channel is happening for all three tests observed due to the temperature decrease close to the heated surface and the temperature increase close to the colder surface compared with the surface temperatures. This case of recirculation might be occurring at the same time as other smaller regions having reversed flow conditions different locations in the channel, see figure 1.4 on page 4.

As mentioned previously the vertical temperature profiles may also indicate the flow conditions inside the channel. A graph comparing the vertical temperature profiles in the center is shown in figure 5.39 on the following page.

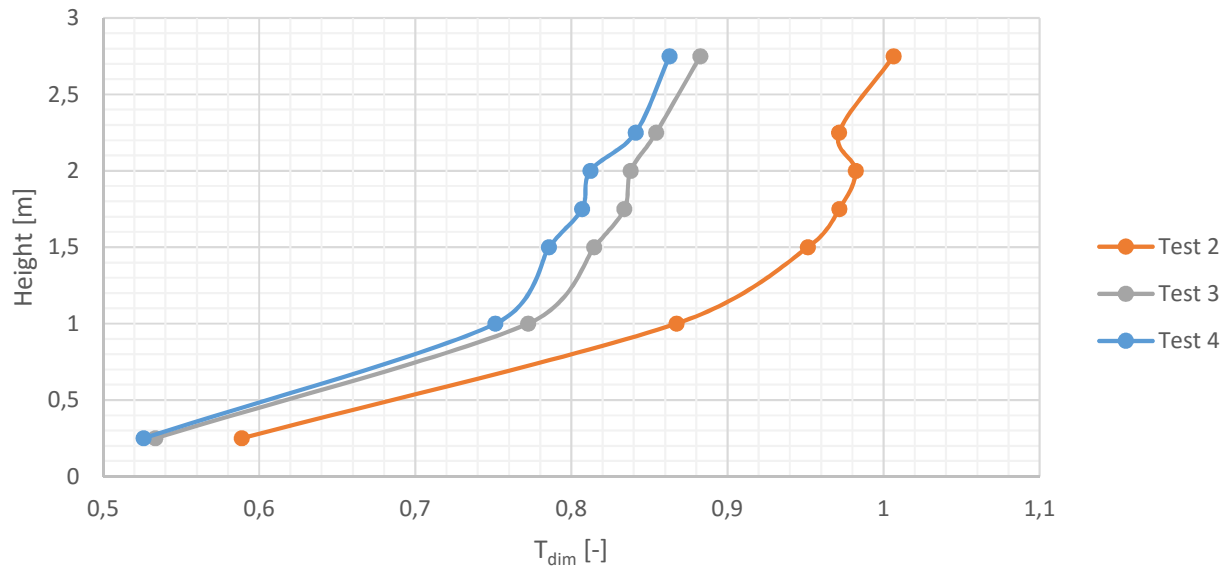


Figure 5.39. Vertical temperature profiles in center.

The vertical temperature gradient in test 2 has a temperature drop in height 2.25 m and as it is explained in *section 5.1* on page 39 a temperature drop in the vertical gradient can be due to a recirculating flow. Test 3 and 4 has no temperature drops, but exhibits only increasing temperature with increasing height, although with different slopes. This observation is also found to be consistent with the horizontal temperature profiles.

The stability in the center is found to be steady. Figure 5.40 shows the dynamic vertical temperature profiles in test 2.

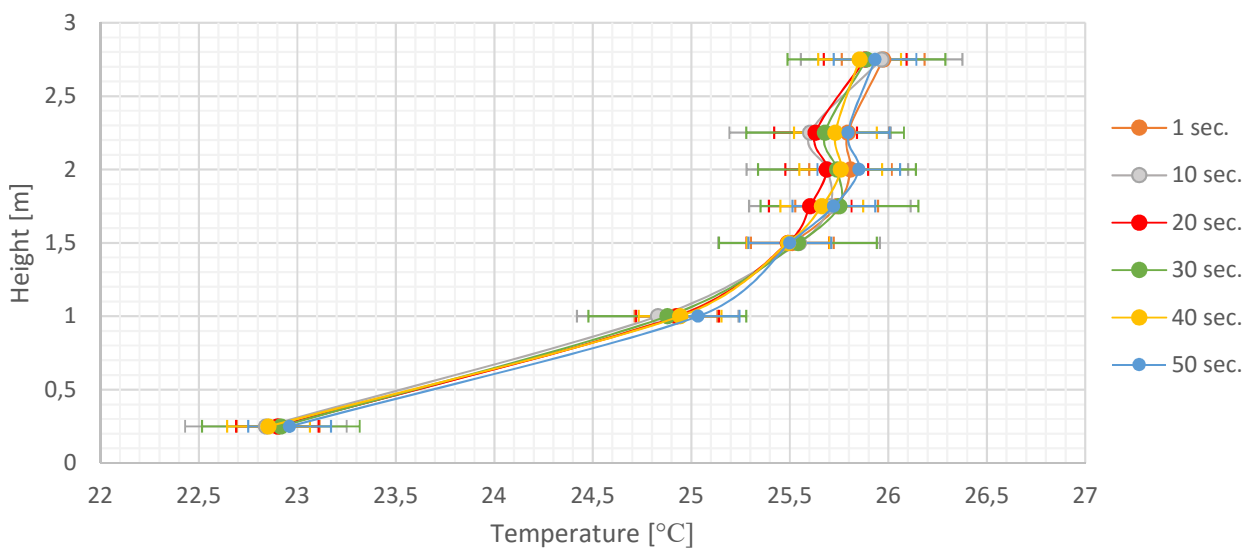


Figure 5.40. Stability of vertical temperature profile in the center for test 2.

It is discovered that all the measurements are within the error. From the perspective that recirculation happens and collapses in a periodic manner, the implication of recirculation in test 2 in the center is weakened since the temperature measurements imply steady conditions. The temperature drop might be a consequence of the extreme recirculation happening in the entire channel which is found to be steady also. The same stable flow is found in tests 3 and 4, the graphs are shown in *appendix*.

Next is shown the vertical temperature gradients for test 2 close to the heated surface in figure 5.41. It is chosen to use the 5 min average since the flow is proven to be sufficiently stable at these distances, see *appendix E* on page 139.

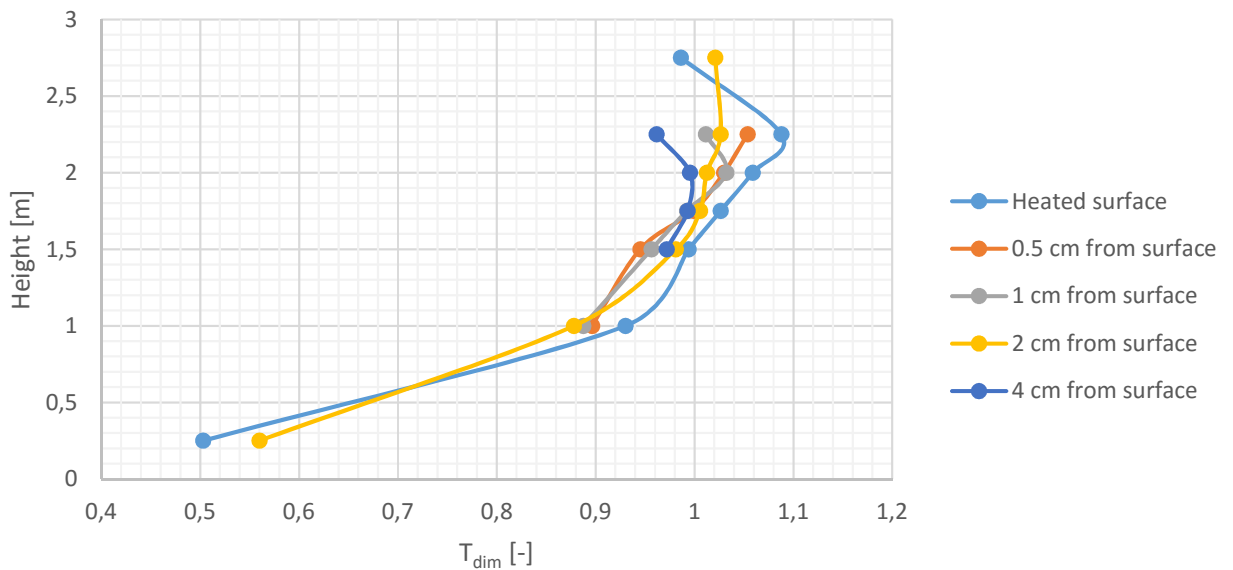


Figure 5.41. Vertical temperature profiles close to heated surface for test 2.

Here it is observed that 0.5 cm from the heated surface the temperature gradient only increases until the last point in 2.25 m. Then moving 1 cm from the surface a temperature drop is found in height 2.25 m indicating that this point is outside of the boundary layer. 2 cm from the heated surface the temperature drop is again disappeared but then once again occurring 4 cm from surface. Distances 0.5 cm and 1 cm from the surface have lower temperatures in height 1.50 m compared to the two points further way indicating a recirculation flow as it is also seen in the horizontal temperature profiles, as it happens again in height 2.25 m for the distance 1 cm from the surface.

Figure 5.42 on the next page shows the stability at the heated surface for test 2.

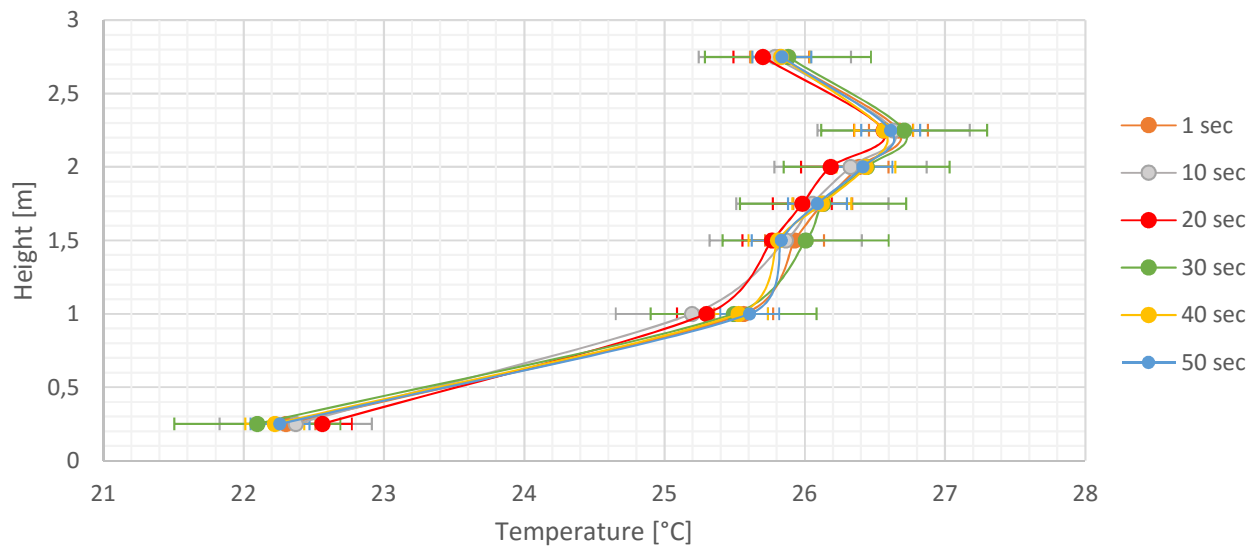


Figure 5.42. Stability of vertical temperature profile at the heated surface for test 2.

As the figure is showing the temperature at the heated surface are assumable stable and fluctuations are all within the measurement error, and the same stability conditions are found in tests 3 and 4. Figure 5.43 illustrates the vertical temperature gradients close to the heated surface in test 4.

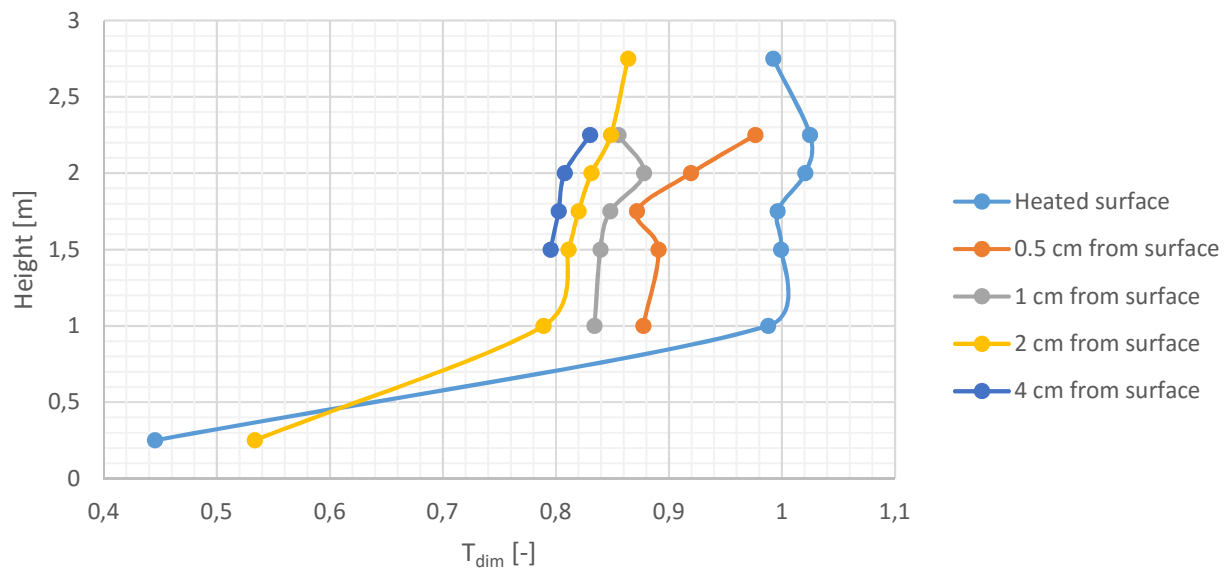


Figure 5.43. Vertical temperature profiles close to heated surface for test 4.

The vertical temperature gradient 0.5 cm from the heated surface have a temperature decrease in height 1.75 m and 1 cm from the surface a drop in height 2.25 m. This might be caused by

the inaccuracy of the measurements but it can also indicate recirculation. The other gradients increases as the height increase consistent with the theory of a standard channel flow. The vertical temperature gradients close to the heated surface for test 3 can be found in *appendix F* on page 145, which shows the same conditions as test 4.

From the horizontal temperature profiles it is observed that recirculation conditions are taking place in different heights. Next are the stability of vertical temperature profiles 0.5 cm from the glass surface shown for test 2 and 4 in figures 5.44 and 5.45.

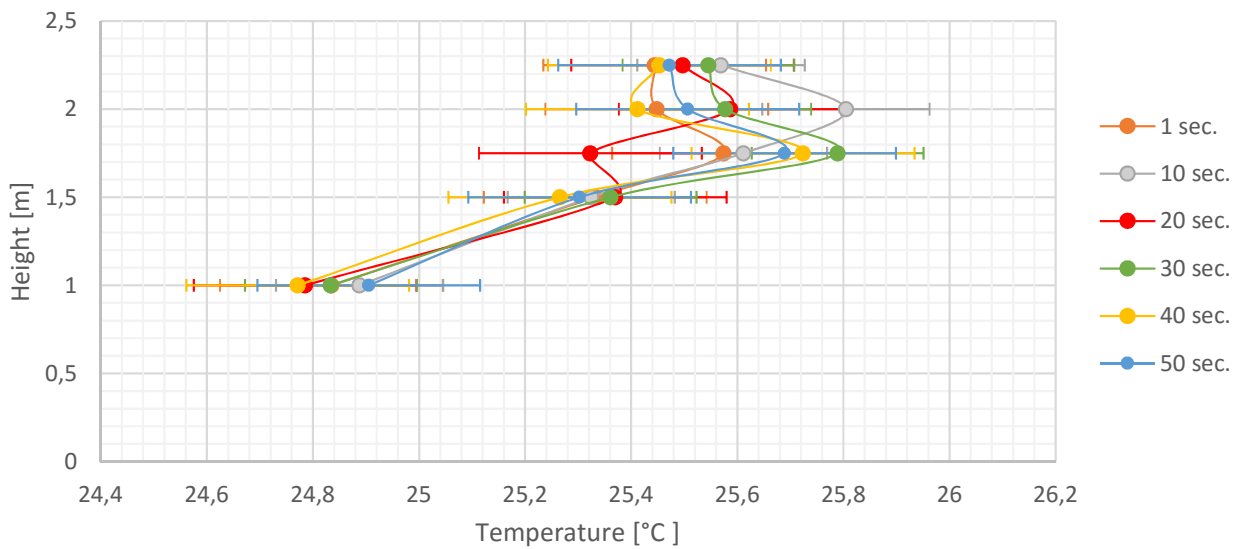


Figure 5.44. Stability of vertical temperature profile 0.5 cm from the glass surface for test 2.

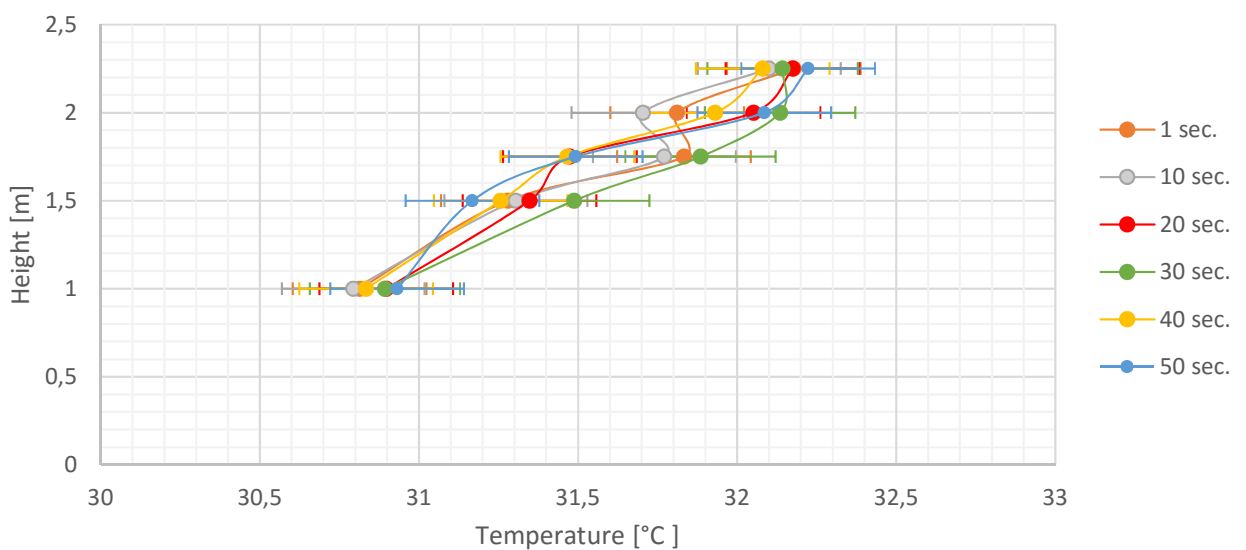


Figure 5.45. Stability of vertical temperature profile 0.5 cm from the glass surface for test 4.

It is seen that test 2 exhibits more dynamic behavior than test 4. The first instantly measurement in test 2 contains a temperature drop in height 2.00 m that then appears in height 2.25 m after 10 s and in height 1.75 m after 20 s where after the drop appears in height 2.00 m the next 30 s-40 s again. The measurements are in many points outside of the error bar indicating that the fluctuating behavior is actually occurring and is not due to a measurement error. In test 4 a temperature reduction is found for only two instantly measurements namely the 1 s and 10 s measurement in only one height 2.00 m. For this test more points are found within the measurement error. The stability 1 cm from the glass surface reveals the same tendencies, and will therefore not be shown here. But the condition changes when one moves 2 cm from the surface, see figures 5.46 and 5.47 on the next page as it is also observed in test 1.

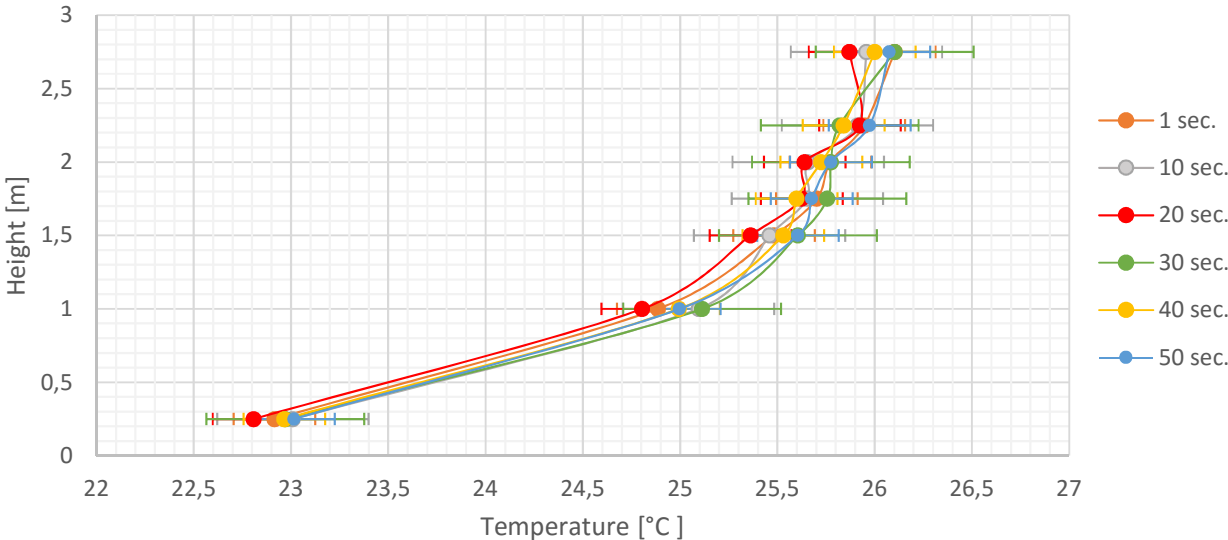


Figure 5.46. Stability of vertical temperature profile 2 cm from the glass surface for test 2.

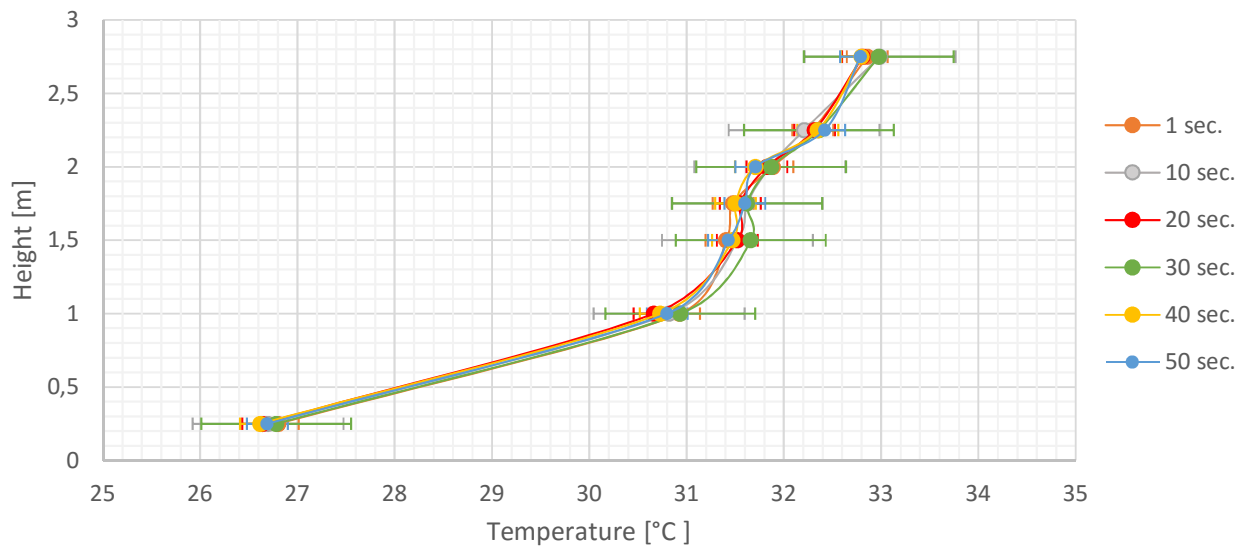


Figure 5.47. Stability of vertical temperature profile 2 cm from the glass surface for test 4.

Notice how the temperature only rises with no drops and the stability is much greater for both tests; all points are located within the measurement error. If the other distances is proved to have recirculation then it can be said, that the recirculating flow is within the limit of the boundary to the glass wall to 1 cm from the surface.

5.2.2 Group 2: Change of Inlet Temperature

Group 2 is a comparison of tests 1 and 5, see table 5.3 for the different test conditions.

	Test 1	Test 5
Ra_H [-]	$9.98 \cdot 10^{11}$	$7.11 \cdot 10^{12}$
Gr_H [-]	$1.34 \cdot 10^{12}$	$9.55 \cdot 10^{12}$
Re_H [-]	$8.03 \cdot 10^5$	
$Gr_H/Re_H^2 - ratio$ [-]	2.08	14.81
$T_{heater,SP}$ [°C]	30.00	
$T_{heater,meas.}$ [°C]	26.08	25.95
$T_{inlet,SP}$ [°C]	Ambient air	15.00
$T_{inlet,meas.}$ [°C]	24.59	15.76
ACH [h^{-1}]	4.00	
$T_{heater,meas.} - T_{inlet,meas.}$ [°C]	1.49	10.18
$T_{heater,meas.} - T_{glass,meas.}$ [°C]	0.69	1.11

Table 5.3. Test conditions for group 2. All values are averages of the last 5 min of measurements.

The mean values of the dimensionless numbers are taken according to the heated surface. As for group 1 a graph is made to illustrate the surface temperatures in both tests, see figure 5.48.

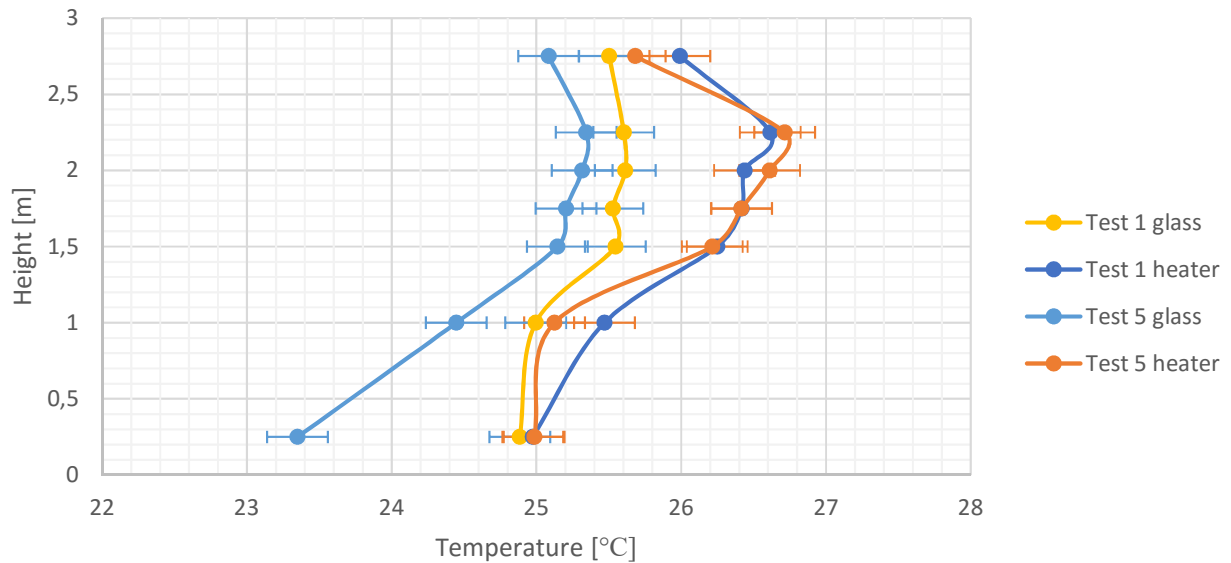


Figure 5.48. Temperature distribution on heated and cold surface for group 2.

From the graph it is observed that the two graphs representing the heated surface are quite similar except in height 1.00 m. This deviation can be due to a measurement error or the dynamic behavior of the heaters. It is noted how the glass surface has at all times lower temperatures in test 5 than test 1. The lower temperatures might be due to shifting and

uncontrollable ambient conditions at the test location, but most of all due to the lower inlet temperature that affects the fluid temperature inside the channel and the surfaces.

Comparison of Rayleigh Numbers

The two figures 5.49 and 5.50 show the calculated Rayleigh numbers for tests 1 and 5.

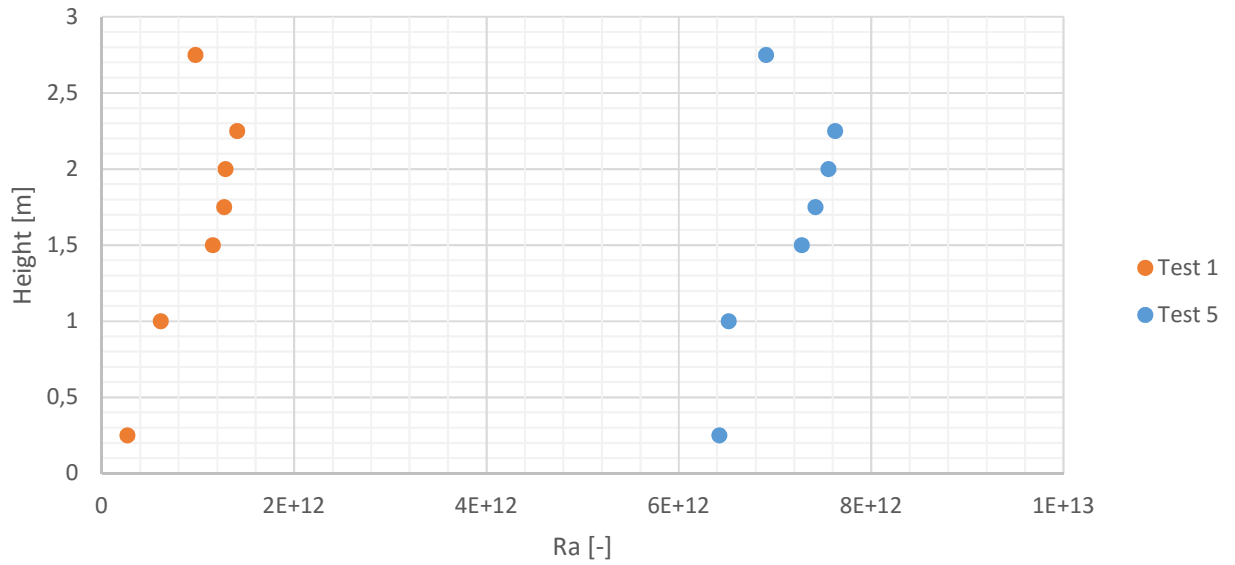


Figure 5.49. Rayleigh numbers according to the heated surface.

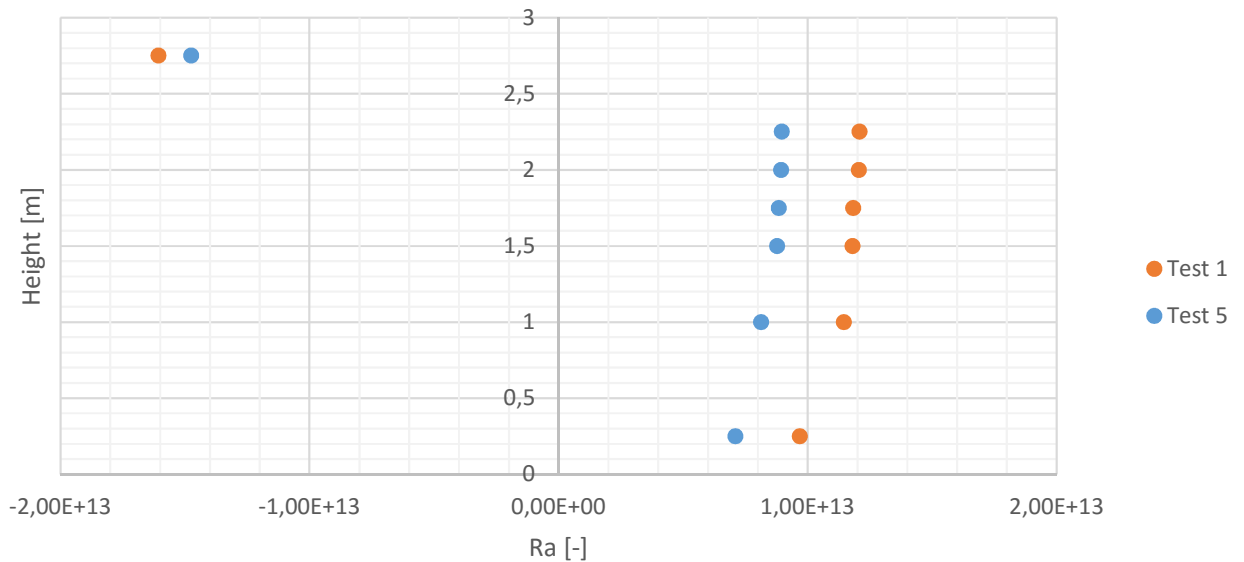


Figure 5.50. Rayleigh numbers according to the glass surface.

The Rayleigh number is above the criterion 10^9 when looking upon the absolute values

indicating that the flow is in transition to or is turbulent. It is observed that with lower inlet temperature, a higher temperature difference is achieved between the surface and the inlet leading to a higher Rayleigh number. For both cases the Rayleigh number increases with height indicating that the flow becomes buoyancy dominated along the height.

Comparison of Gr/Re^2 -ratio

Figures 5.51 and 5.52 on the next page show the calculated Gr/Re^2 -ratios for tests 1 and 5 according to the heated surface and the glass surface, respectively.

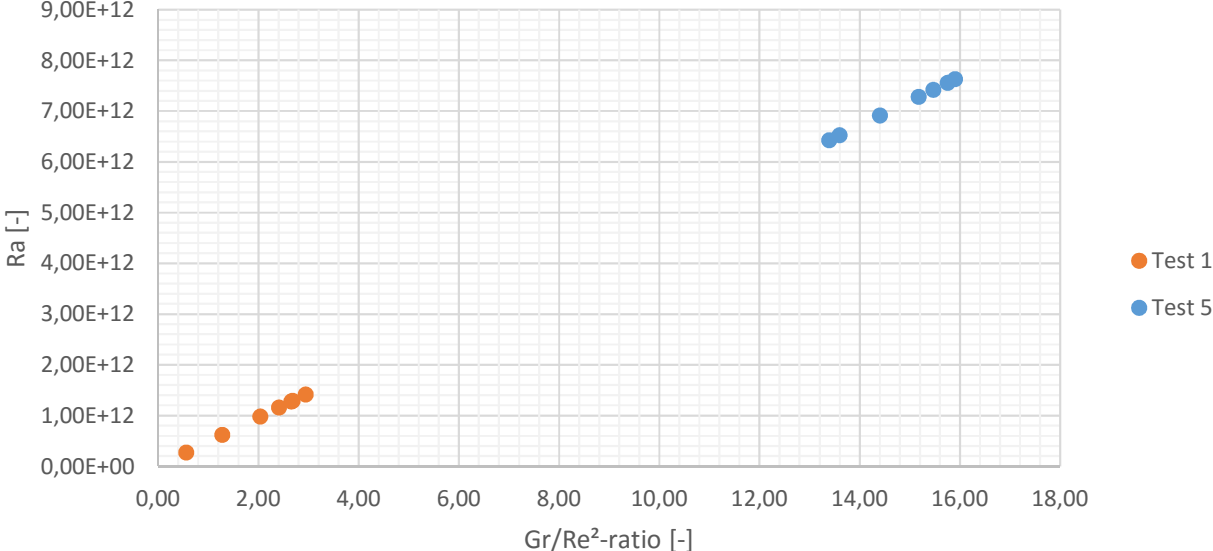


Figure 5.51. Gr/Re^2 -ratios according to the heated surface.

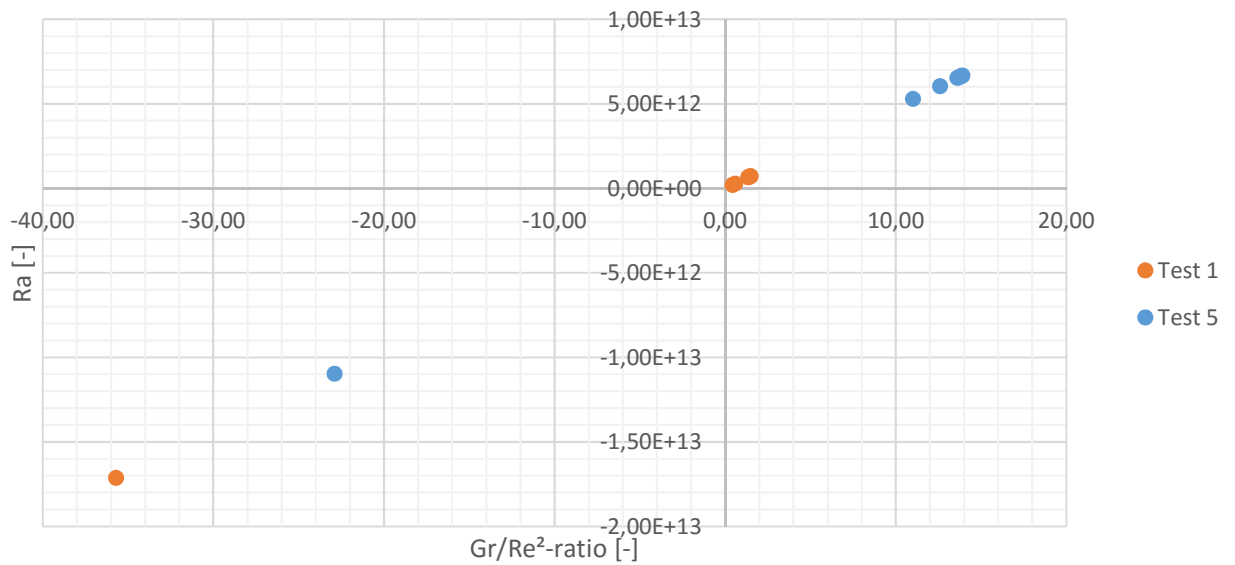


Figure 5.52. Gr/Re^2 -ratios according to the glass surface.

The figures show what is expected; with increasing Rayleigh number the Gr/Re^2 -ratio increases, again only absolute values is studied due to the direction of the flow. The Gr/Re^2 -ratio according to the heated surface for test 1 has a minimum of 0.56 that increases as one moves upward in the channel with a maximum of 2.94, implicating that the buoyancy forces becomes more enhanced upward in the channel. It might be concluded that the flow initially is very similar to mixed convection regime and moving upward with increasing buoyancy forces becoming more natural convection dominated. For test 5 the flow is assumed to be of natural convection conditions in the entire channel.

Flow Structure Indicated by Temperatures

The horizontal temperature profile in height 1.00 m is shown in figure 5.53 on the following page.

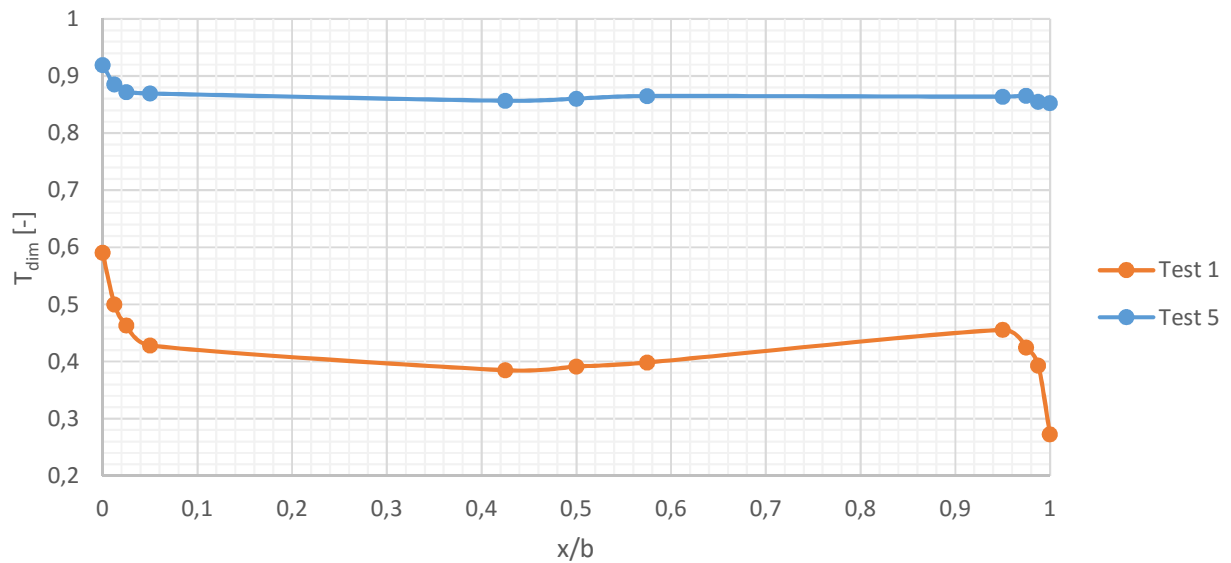


Figure 5.53. Horizontal temperature profiles in height 1.00 m.

In *section 5.1* on page 39 the graph showing the horizontal temperature profile in test 1 which is also shown here is described as resembling a standard channel flow when one wall is heated above the other; The air is heated up following an upward stream along the heated wall, and reversed at the colder surface. The same tendency is found in test 5 but with much lower gradients. This is due to the lower inlet temperature, lower surface temperature at the heated wall at exactly this height and lower glass surface temperature.

The stability at this height for test 1 is shown in figure 5.4 on page 42 and it is observed to be stable varying in one point with 0.3 °C but within the measurement error limit. The stability at height 1.00 m for test 5 is shown in figure 5.54 on the next page.

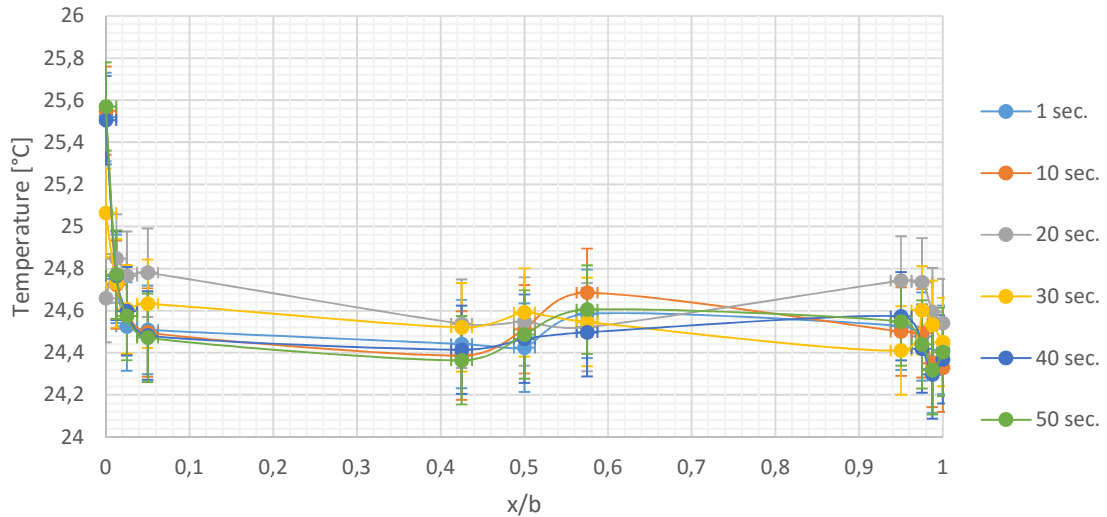


Figure 5.54. Stability in horizontal temperature profile in height 1.00 m for test 5.

From this graph it is discovered that the dynamics of the flow resembles test 1. The flow acts unstable with different locations of peak temperatures, and variation in one point up to 0.2 °C. The instability of the measurements might be due to low measurement accuracy, but if it is compared to the stability in tests 3 and 4 it might be said to indicate a fluctuating air pattern. In general the stability of test 5 shows similar tendencies as test 1; fluctuations are seen in heights 1.00 m and 1.50 m in the entire horizontal plane, but moving upward in the channel the dynamic behavior is more or less restricted to the half close to the colder surface. Due to the resemblance it is chosen not to discuss the stability of test 5 further more in the present study. However, graphs showing the stability for test 5 can be found in appendix G on page 153.

Figure 5.55 on the next page illustrates the comparison of horizontal temperature profiles in height 1.50 m.

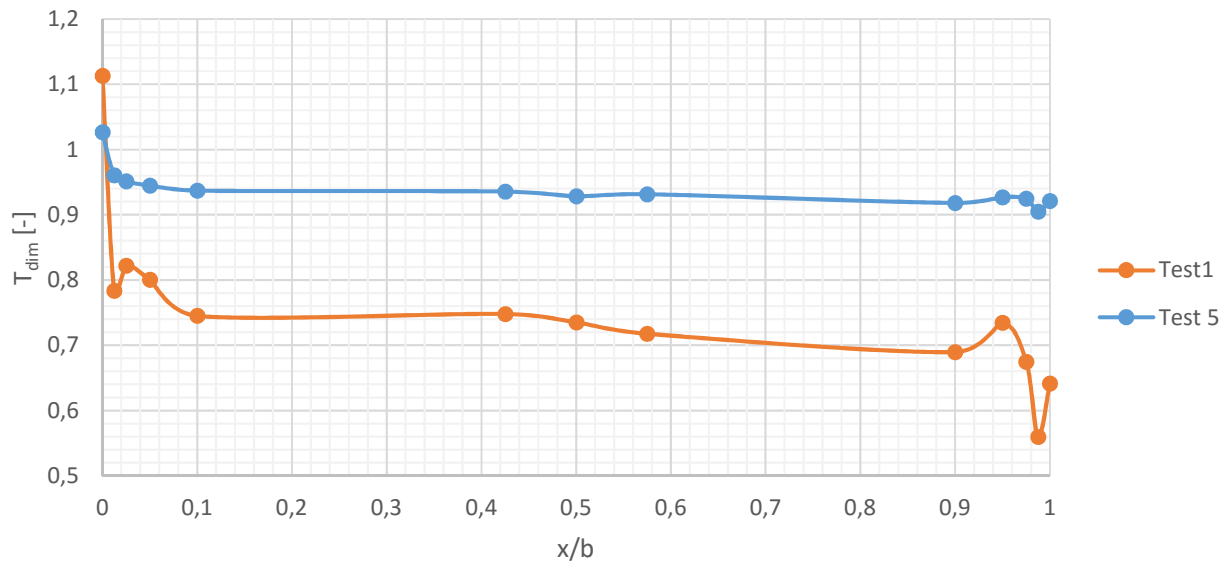


Figure 5.55. Horizontal temperature profiles in height 1.50 m.

In height 1.50 m test 1 has developed two peak temperatures close to each surface that might be an indication of recirculating flow. Although the same observation is found close to the glass surface in test 5 it is much more pronounced in test 1.

Next is the temperature profiles in height 1.75 m showed in figure 5.56.

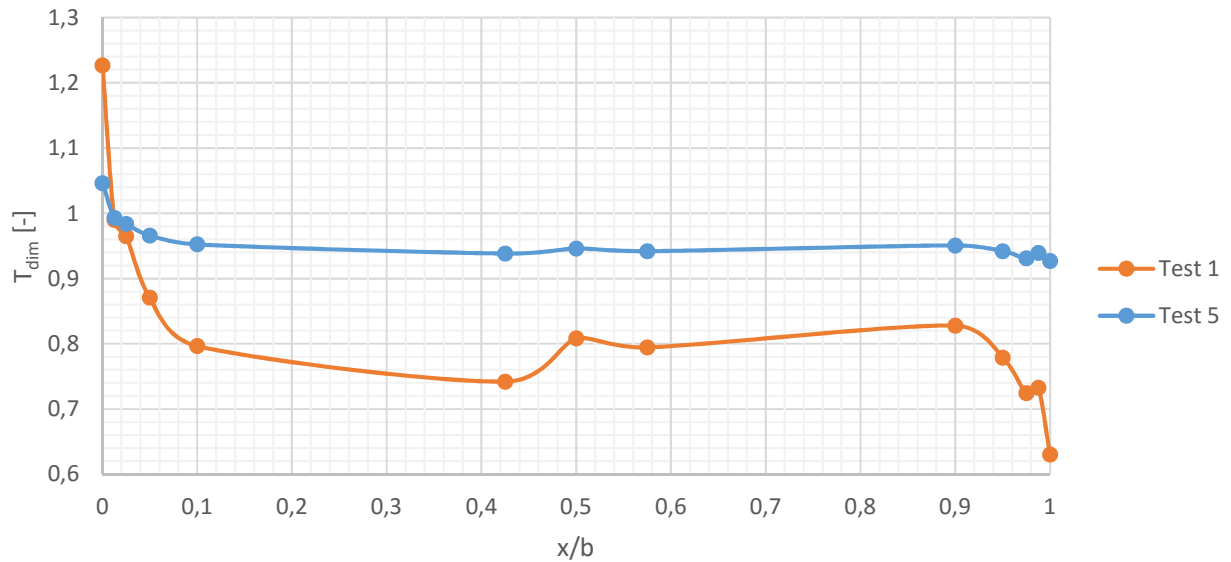


Figure 5.56. Horizontal temperature profiles in height 1.75 m.

Moving upward in the channel to height 1.75 m the peaks seems to be reduced. In the vicinity

of the center the temperature has changed from being almost constant to having a temperature drop in $x/b = 0.425$. Comparing the temperature increase from height 1.50 m to 1.75 m in both tests, the increase is found to be higher in test 1, which can be due to higher heat transfer caused by the possible recirculating flow occurring due to enhanced buoyancy forces [Gau et al., 1992].

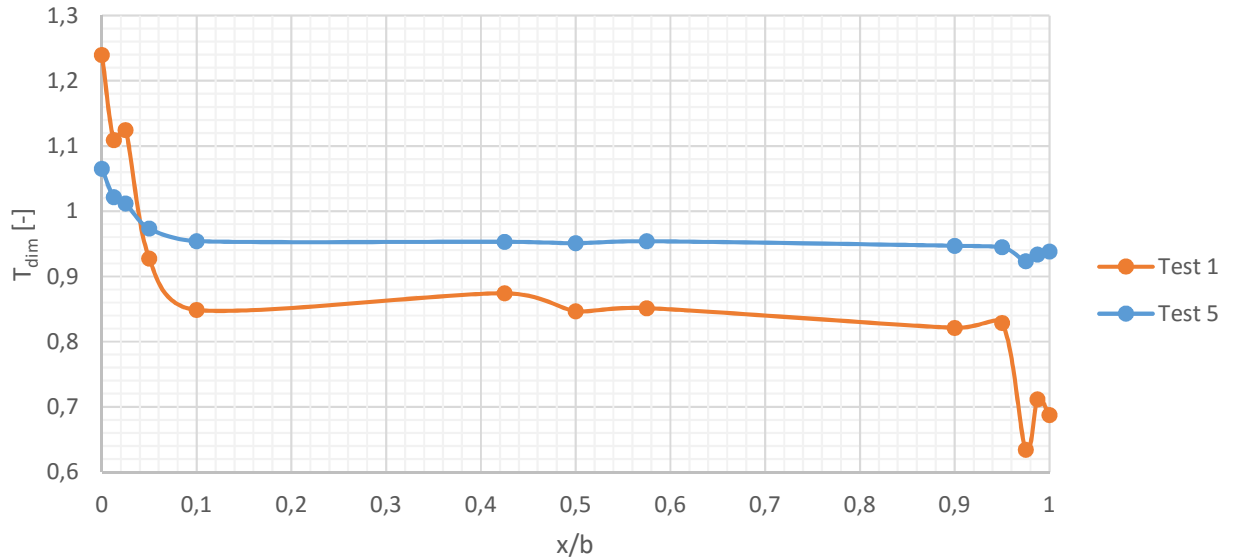


Figure 5.57. Horizontal temperature profiles in height 2.00 m.

In height 2.00 m the temperature drop in $x/b = 0.975$ is again increased like in happens in height 1.50 m, see figure 5.57, whereas the flow for test 5 resembles the flow in the lower heights.

The last horizontal temperature profile is shown in figure 5.58 on the following page.

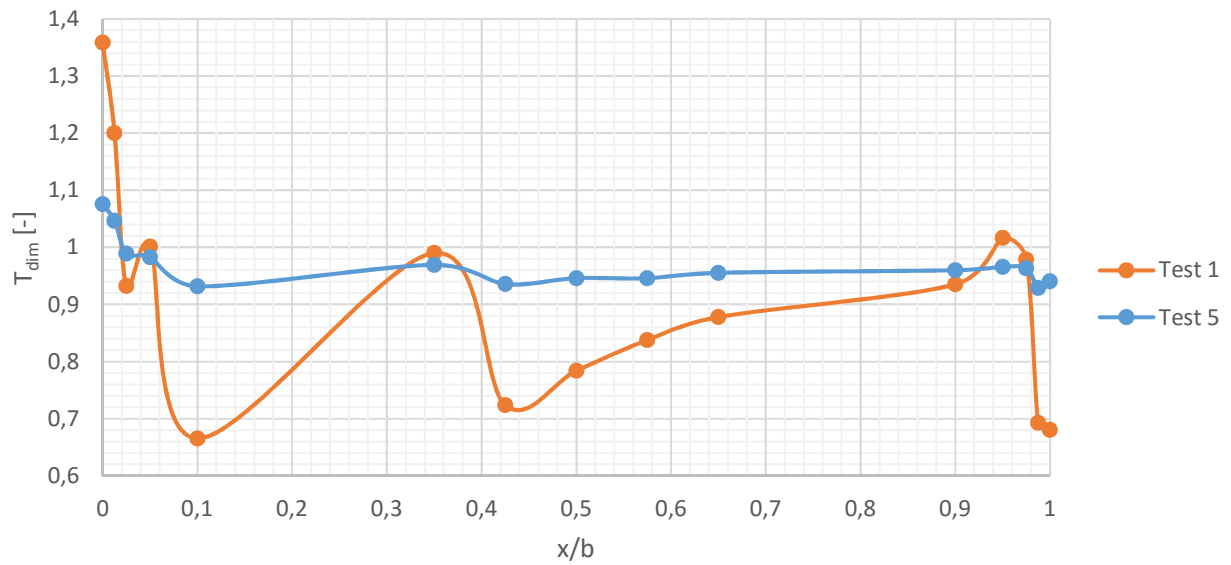


Figure 5.58. Horizontal temperature profiles in height 2.25 m.

Here it is observed that the temperature fluctuations happening in the entire channel have decreased in test 5 compared to test 1.

As for group 1 the vertical temperature profiles is analyzed. Figure 5.59 illustrates the vertical temperature profiles in tests 1 and 5.

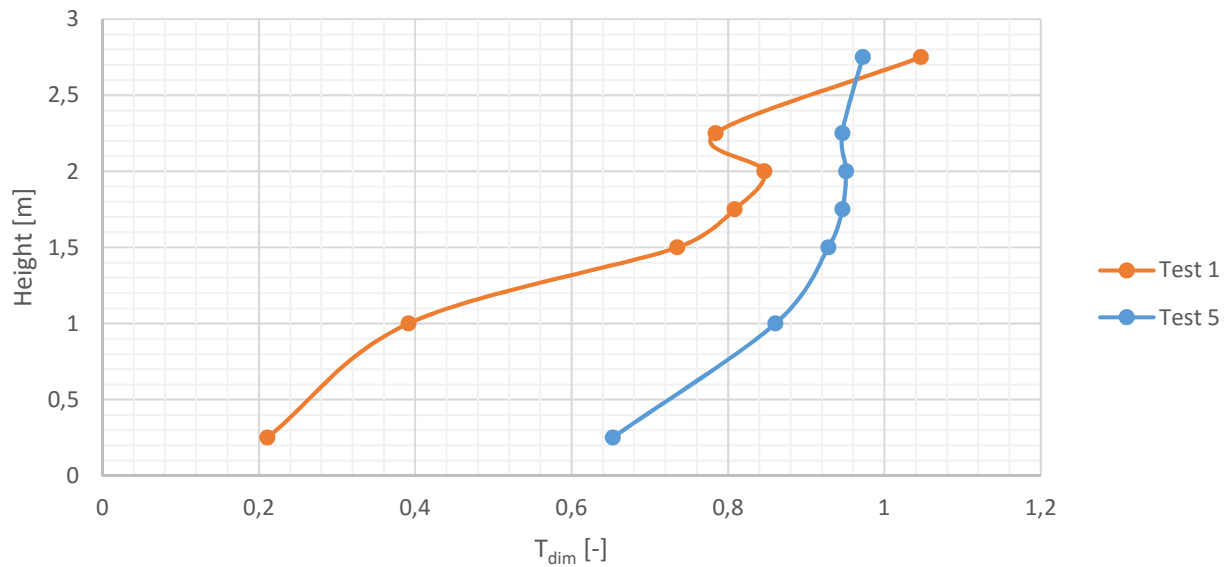


Figure 5.59. Vertical temperature profiles in center.

From the vertical temperature profile it is seen that the temperature drop in height 2.25 m

indicating flow reversal has disappeared as the Rayleigh number is increased in test 5. This implication agrees with the horizontal temperature profiles shown above, where the symptoms of recirculation is much greater in test 1.

From the horizontal temperature profiles a very weak indication of recirculation is observed close to the colder surface in test 5. For this reason, the stability at the glass surface and distances 0.5 cm, 1 cm, 2 cm and 4 cm from the surface is shown in figures 5.60, 5.61, 5.62, 5.63 and 5.64 on page 83.

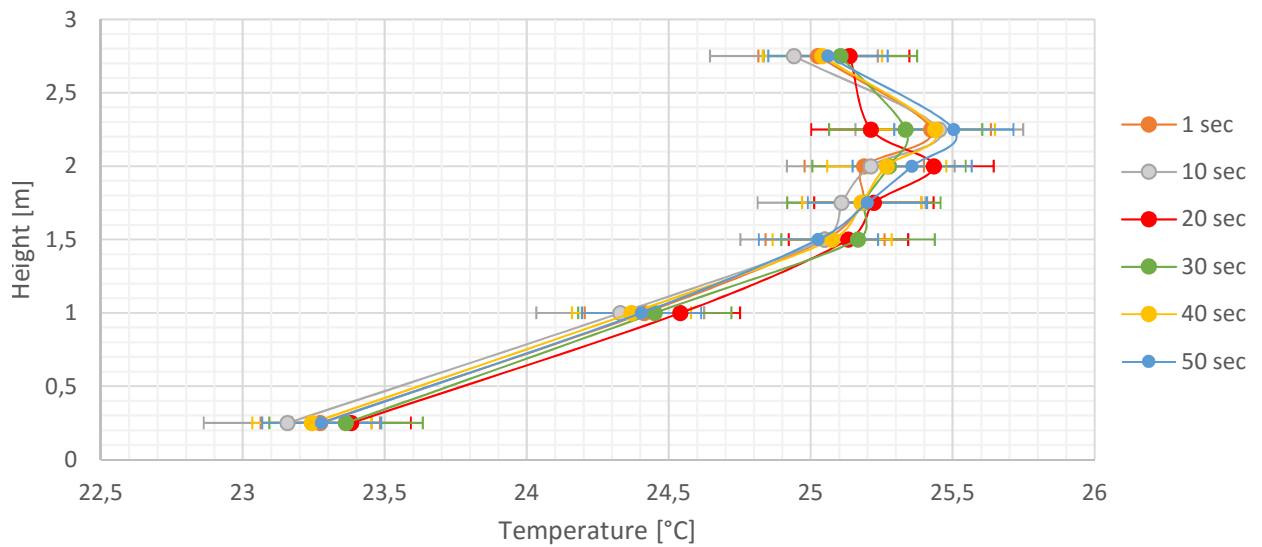


Figure 5.60. Stability of vertical temperature profile at glass surface for test 5.

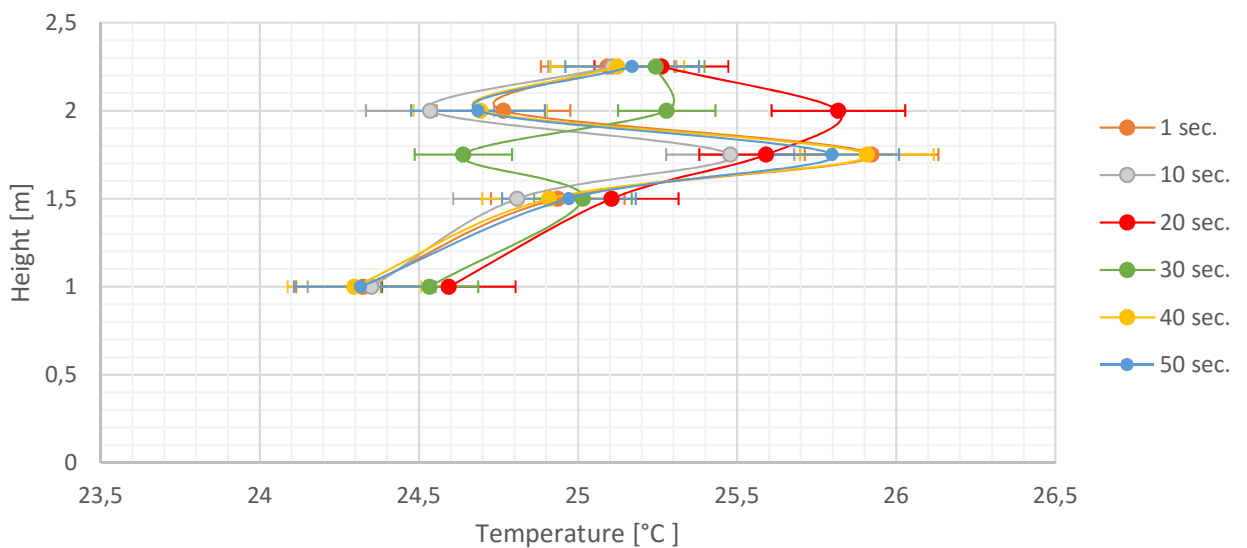


Figure 5.61. Stability of vertical temperature profile 0.5 cm from the glass surface in test 5.

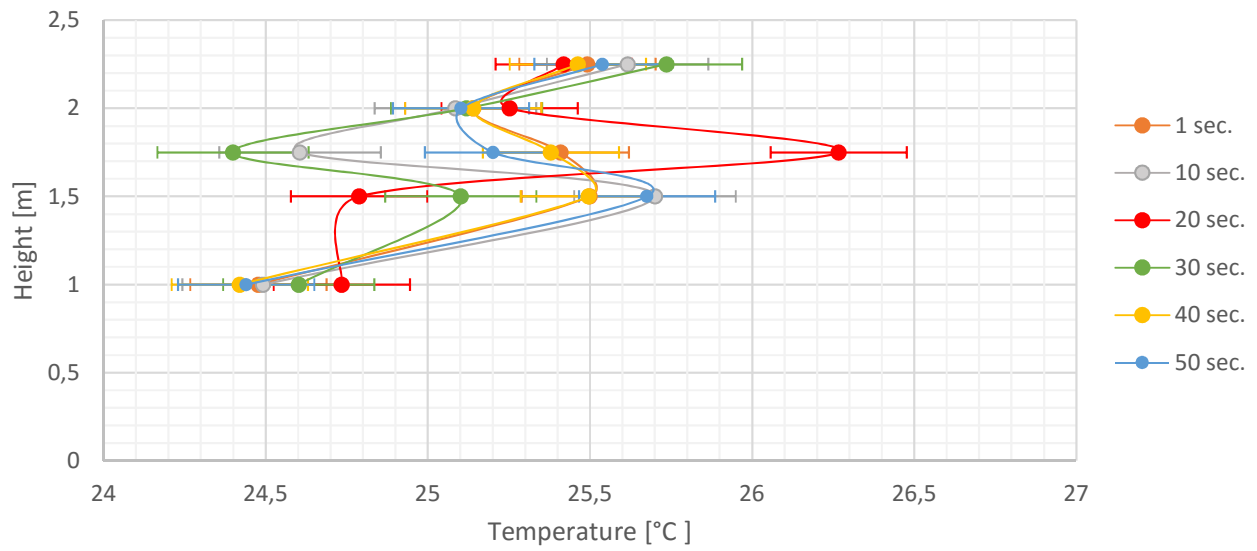


Figure 5.62. Stability of vertical temperature profile 1 cm from the glass surface in test 5.

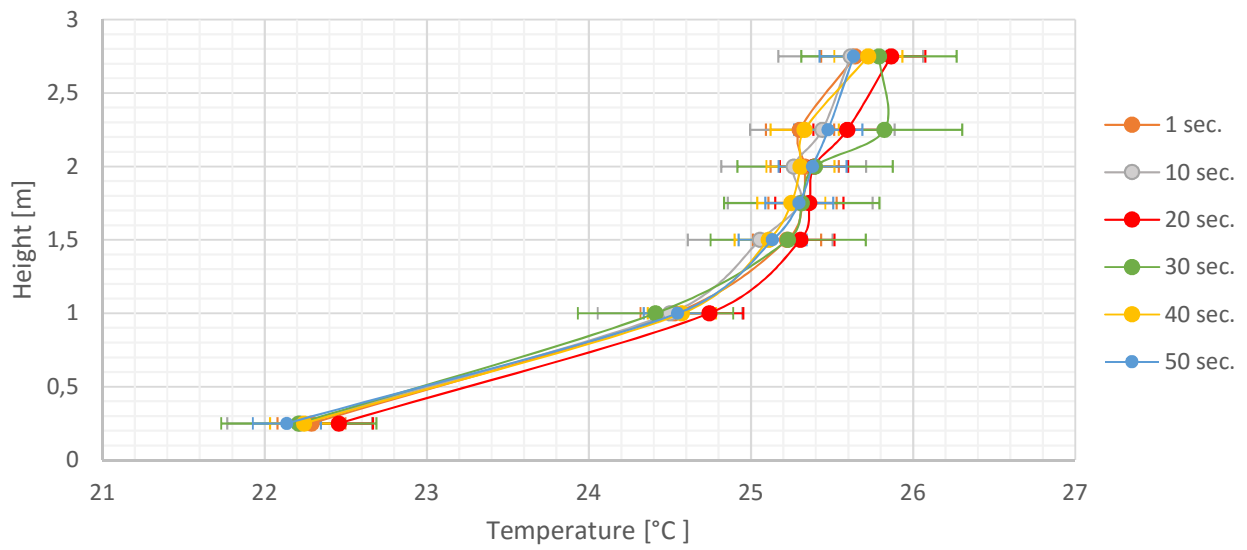


Figure 5.63. Stability of vertical temperature profile 2 cm from the glass surface in test 5.

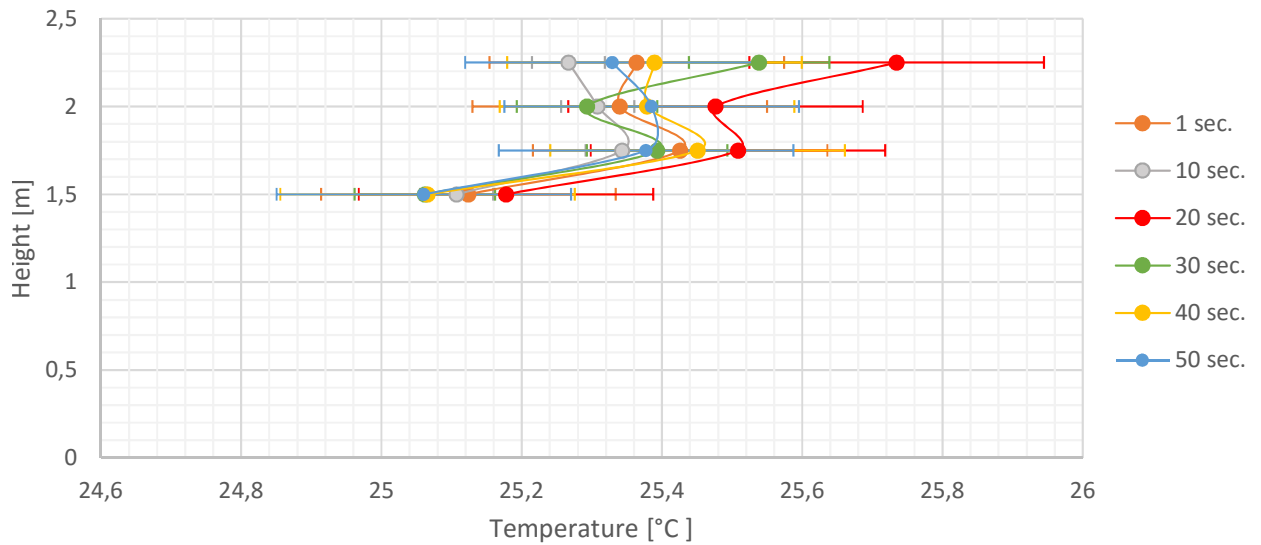


Figure 5.64. Stability of vertical temperature profile 4 cm from the glass surface in test 5.

The stability implicates that a recirculating flow is actually occurring in test 5. However, this implication is weakened when looking at the horizontal temperature profiles compared to test 1. This implies that the recirculation might be happening for test 5, but not as strong as seen in test 1 with lower Rayleigh numbers. The fluctuations in the graphs shown above for distances 0.5 cm, 1 cm and 4 cm are larger than the measurement error and are therefore considered as temperature variations happening in the channel. Whereas, the fluctuations at the glass surface and 2 cm from the surface are within the measurement error and the flow is considered steady at these points. This phenomenon is also found in test 1; the flow is oscillating from 0.5 cm to 1 cm, then found steady 2 cm from the surface and again dynamic 4 cm from the surface. It is not clear why in fact this is happening, but it is observed to be consistent with all the tests implicating that it might be a measurement error.

5.2.3 Remarks Regarding Rayleigh Number Dependency

By increasing the Rayleigh number the buoyancy forces become stronger and the flow obtains natural convection conditions. From the temperature measurements it is seen that areas of recirculation inside the channel appears with the lowest achieved Rayleigh numbers in test 3 and 1 and these areas disappear as the Rayleigh number increases. With the highest achieved Rayleigh numbers the flow inside the channel resembles what will be distinguished as a standard channel flow when one surface has higher temperatures than the other; the air moves upward in the channel close to the heated wall, this is seen when the temperature of the free fluid is lower than the surface, and then moves downward close to the glass wall causing a clockwise natural convection loop in the entire channel. This case of extreme recirculation happens for all the presented tests but with much greater appearance with higher Rayleigh numbers caused by the increase of heated surface temperature.

Decreasing the inlet temperature from approximately 25 °C in test 1 to 15 °C in test 5 it

is obvious that the Rayleigh number increases due to the higher temperature difference between the surface temperature and the inlet temperature. Increasing the Rayleigh number also increases the Gr/Re^2 -ratio implicating that the buoyancy forces has become enhanced. With the lower Rayleigh number obtained in test 1 indications of regions with recirculation is observed by temperature drops close to the heated and colder surface in horizontal temperature profiles, by the temperature deformation in the vertical profile in the center of the cavity and by the fluctuating behavior presented in *section* 5.1 on page 39. However, this is just an implication rather than a proven fact. Analyzing the stability of test 5 there are also found signs of recirculation, but comparing the horizontal temperature profiles with test 1 they seem to be of lesser size. Areas of recirculating flow might happen in test 5, but if this is the case their force have decreased.

In the literature study in *chapter* 3 on page 15 it is discovered that increasing Rayleigh number and Gr/Re^2 -ratio increases the buoyancy forces that is one of the main characteristics for when recirculation is a possibility. The opposite is found in the present study, like it was found by [Ospir et al., 20012]; with the lowest obtained Rayleigh numbers or Gr/Re^2 -ratio implications of regions containing recirculation are more pronounced than the higher achieved numbers. The small regions of recirculation are dominated by local buoyancy forces, and the disappearing areas of recirculation with increasing Gr/Re^2 -ratio might be due to an increase in the global buoyancy forces that dominates the flow. It is worth mentioning, that the difference between the obtained results and observations in the literature study may be a consequence of the heating system or different aspect ratios, as it is found that this also has an influence.

5.3 Air Change Rate Influence on Channel Flow

In the following section an effort is being done to find the range of when the possible recirculation flow found in test 1 disappears by increasing the air flow rate in the channel. By increasing the air flow rate the flow is expected to become less buoyancy driven and the forced convection effects becomes more dominant. An experiment is conducted with the same boundary conditions as for test 1 but with an ACH of 8 h^{-1} , this is named group 3.

5.3.1 Group 3: Influence of ACH

Table 5.4 is made to give an overview of the test conditions for test 1 and 6.

	Test 1	Test 6
Ra_H [-]	$9.98 \cdot 10^{11}$	$1.79 \cdot 10^{12}$
Gr_H [-]	$1.34 \cdot 10^{12}$	$2.41 \cdot 10^{12}$
Re_H [-]	$8.03 \cdot 10^5$	$1.61 \cdot 10^6$
$Gr_H/Re_H^2 - ratio$ [-]	2.08	0.93
$T_{heater,SP}$ [°C]	30.00	
$T_{heater,meas.}$ [°C]	26.08	26.02
$T_{inlet,SP}$ [°C]	Ambient air	
$T_{inlet,meas.}$ [°C]	24.59	23.44
ACH [h^{-1}]	4.00	8.00
$T_{heater,meas.} - T_{inlet,meas.}$ [°C]	1.49	2.58
$T_{heater,meas.} - T_{glass,meas.}$ [°C]	0.69	0.19

Table 5.4. Test conditions for group 3. All values are averages and the dimensionless numbers are according to the heated surface.

As for the other two groups the temperature distribution on the heated and the glass surface is shown to provide a better understanding of the boundary conditions for this group, see figure 5.65 on the following page.

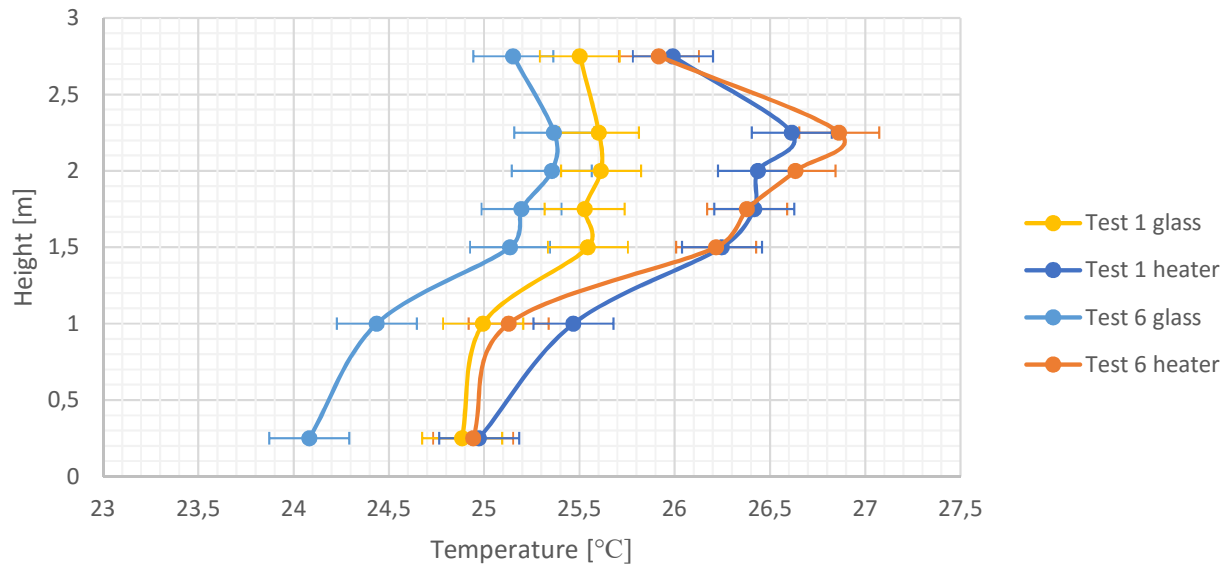


Figure 5.65. Temperature distribution on heated and cold surface for group 3.

It is observed that the temperature gradient obtained on the heated surface resembles quite well, but a difference of approximately $0.4\text{ }^{\circ}\text{C}$ is found between the measured glass surface in the two tests. This can be due to a measurement error, varying ambient conditions or simply the fact that the ACH is increased.

Dimensionless Numbers to Indicate Flow Condition

Looking at the equation for calculating Rayleigh number it is recognized that it is independent of any velocity variable, but since the air flow rate influences the temperatures in the channel, an effect is also seen in Rayleigh numbers. Figure 5.66 and 5.67 on the next page show the calculated Rayleigh numbers for test 1 and 6 according to the heated and the glass surface, respectively.

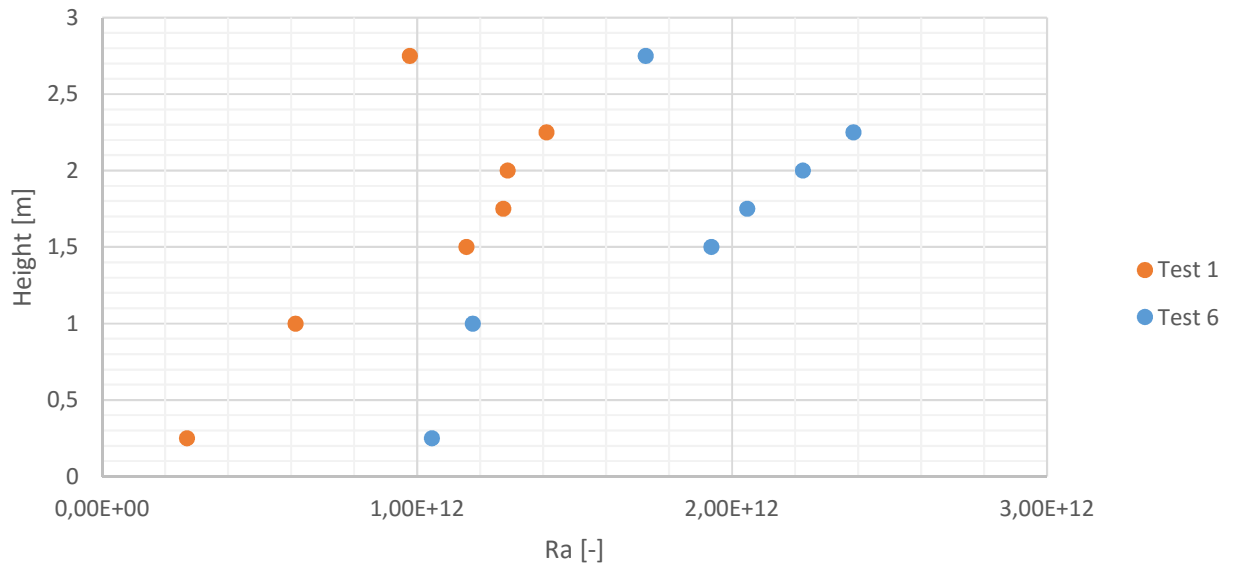


Figure 5.66. Rayleigh numbers according to the heated surface.

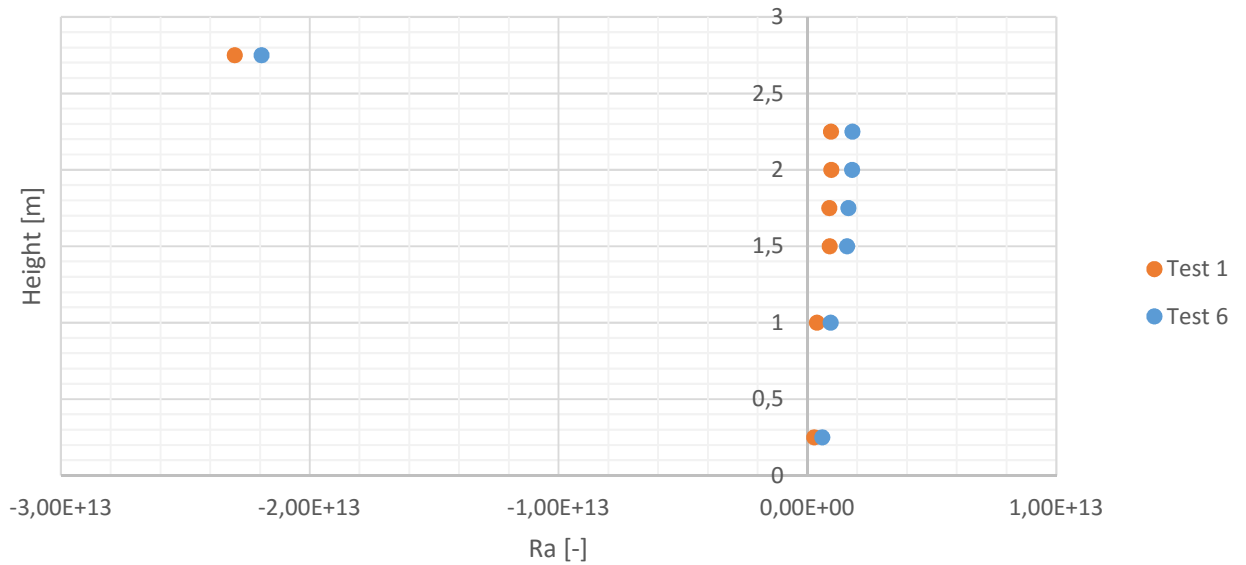


Figure 5.67. Rayleigh numbers according to the glass surface.

From the figures it is discovered that by increasing the ACH the Rayleigh numbers increases. This is caused by the increase in the temperature difference between the surface and the inlet temperature. The Rayleigh numbers are found to be above the criterion 10^9 stated in [Incopera og Dewitt, 2011] indicating that the flow is in transition to or is turbulent for both tests. Once again only absolute values are considered.

Unlike the Rayleigh number, the Gr/Re^2 -ratio has a velocity component involved, namely in

the calculation of Reynolds number. Figures 5.68 and 5.69 illustrates the Gr/Re^2 -ratio for the two tests according to the ACH.

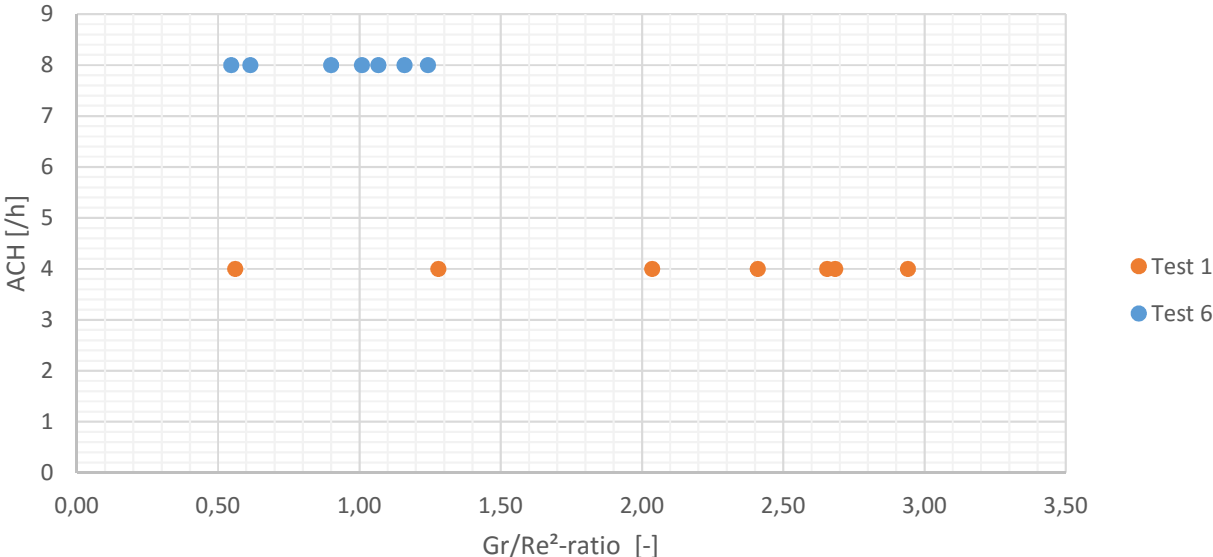


Figure 5.68. Gr/Re^2 -ratios according to the heated surface.

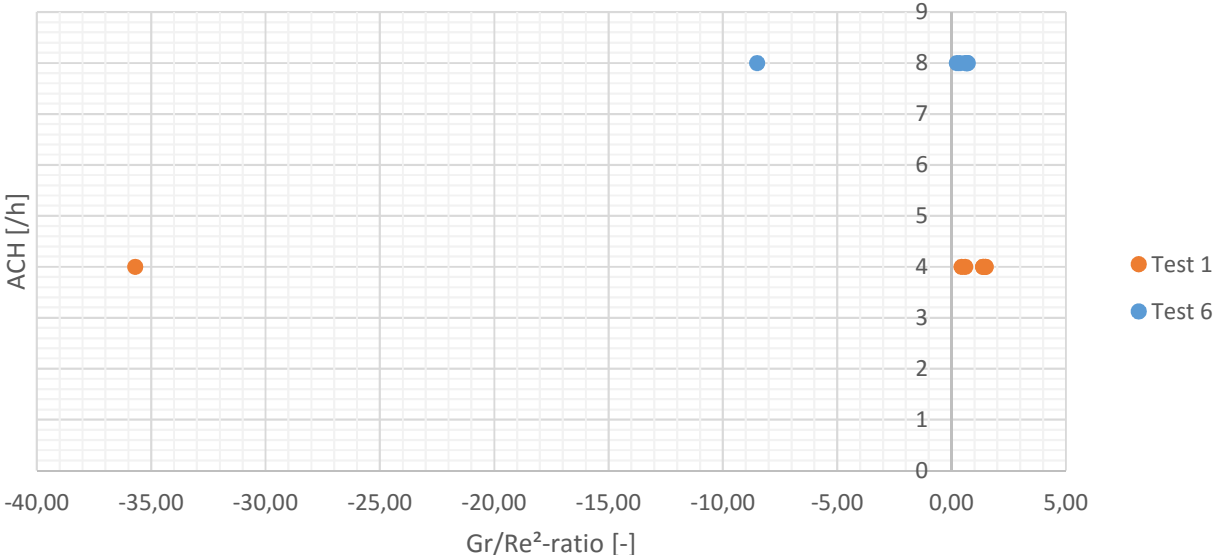


Figure 5.69. Gr/Re^2 -ratios according to the glass surface.

As it is expected the ratio has decreased by increasing ACH. The Gr/Re^2 -ratio now lies within a region where both forced and natural convection dominates. At the region close to the inlet the physical process is dominated by forced convection and a value lower than $Gr/Re^2 < 1$ is obtained. Moving upward in the channel the air is heated leading to an increase of Gr/Re^2 -

ratio, where the natural convection starts to dominate. This phenomenon happens for both tests but the buoyancy forces are greater in test 1.

Temperature Profiles

First is the comparison of the horizontal temperatures profiles in height 1.00 m shown in figure 5.70.

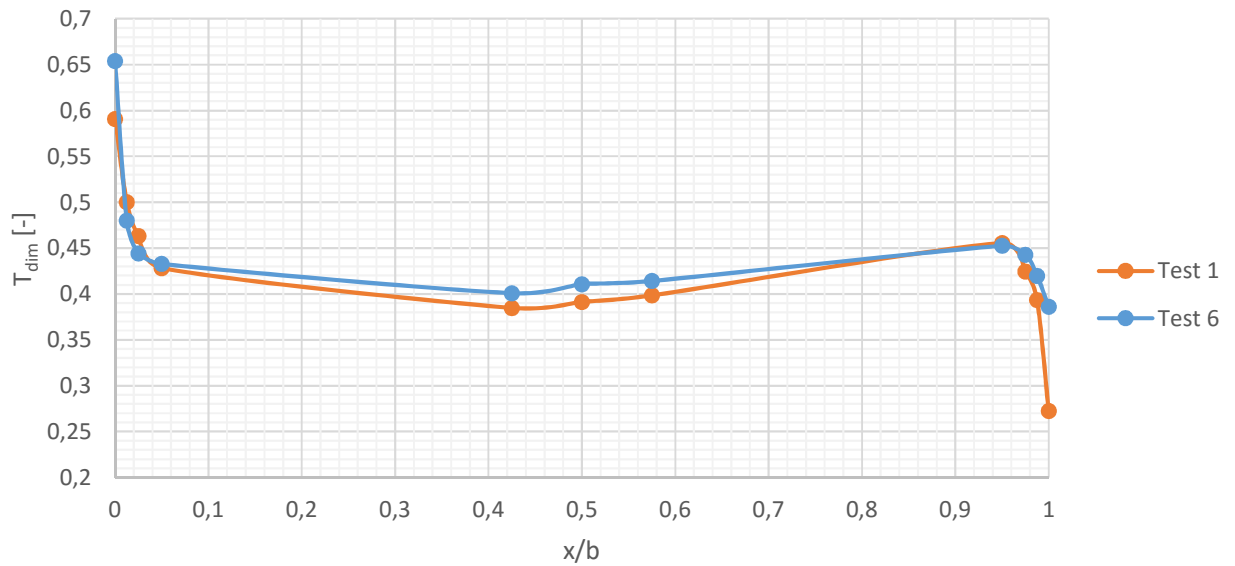


Figure 5.70. Horizontal temperature profiles in height 1.00 m.

Except from the surface temperatures the temperature distribution is the same for both tests. Recall from *section 5.1* on page 39 the stability for test 1 is proved to be stable. Figure 5.71 on the next page shows the stability for test 6 in height 1.00 m.

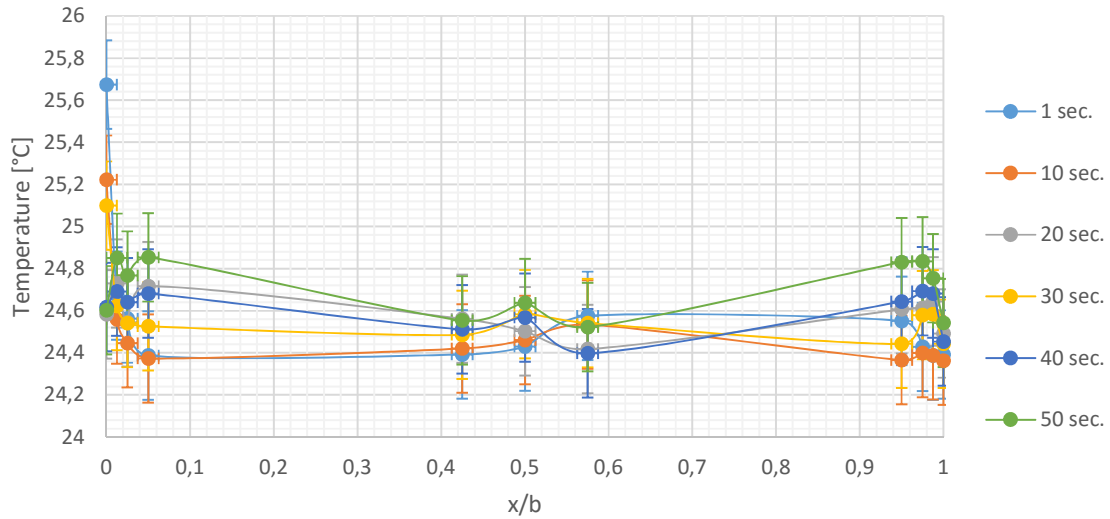


Figure 5.71. Stability in horizontal temperature profile in height 1.00 m for test 6.

A more dynamic behavior is observed from the graph. Both close to the heated surface and the glass surface temperature variations in one point is found to be outside of the measurement error indicating that the flow is unstable.

Figure 5.72 shows the horizontal temperature gradient in height 1.50 m.

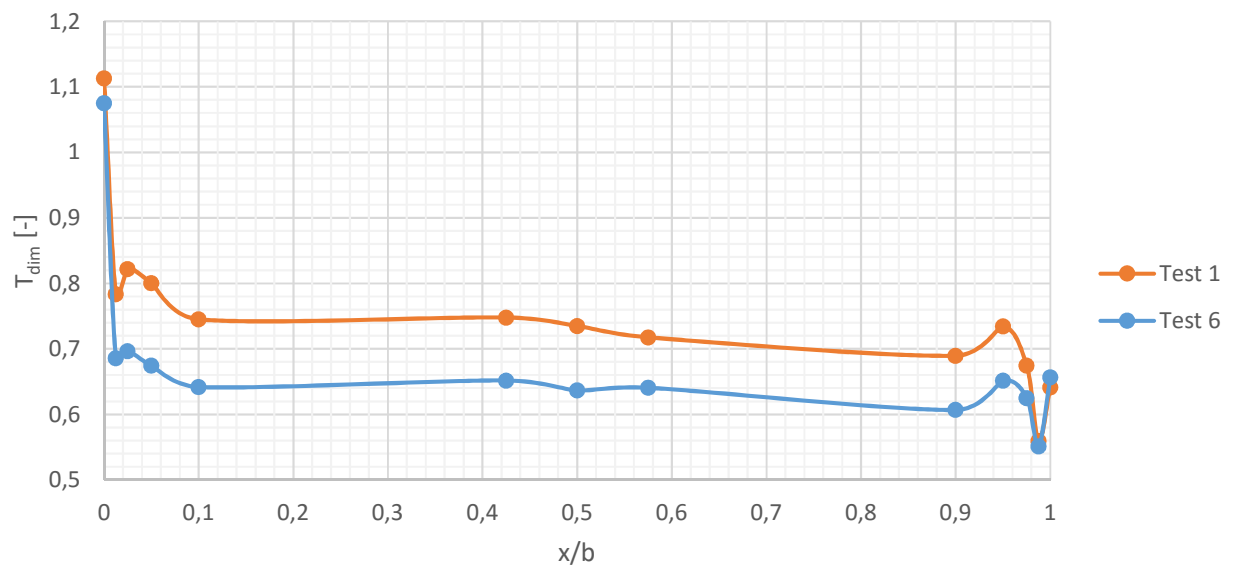


Figure 5.72. Horizontal temperature profiles in height 1.50 m.

Again, the two profiles exhibits the same behavior, but the gradient from $x/b = 0.9875$ to $x/b = 0.95$ is greater in test 1. For test 1 the stability is said to be steady and the fluctuations is within the limit of the measurements error.

Figure 5.73 shows the stability at this height for test 6.

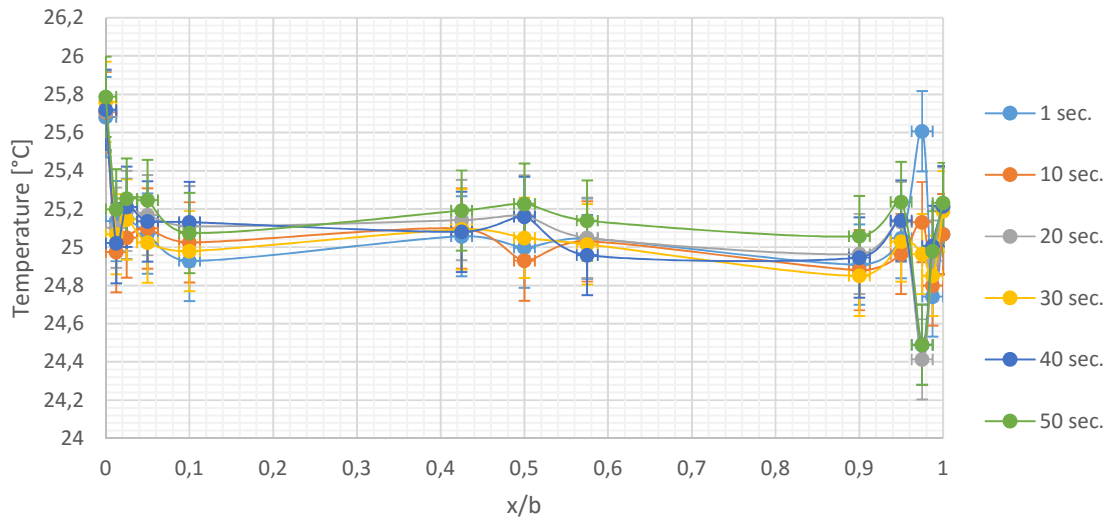


Figure 5.73. Stability in horizontal temperature profile in height 1.50 m for test 5.

As before, the fluctuating temperatures close to the colder surface are showing dynamic behavior outside of the measurement error. The flow is now observed to be more stable at the heated surface.

In heights 1.75 m and 2.00 m the tendencies of the horizontal temperature profiles are the same and is for that reason not showed. Also the stability of test 6 demonstrates the same pattern as it is found in height 1.50 m, with flow acting dynamic close to the glass surface and more steady conditions in the rest of the channel width. Graphs showing the stability can be found in *app:test18*. As for the other tests height 2.25 m revealed interesting flow patterns, see figure 5.74 on the following page.

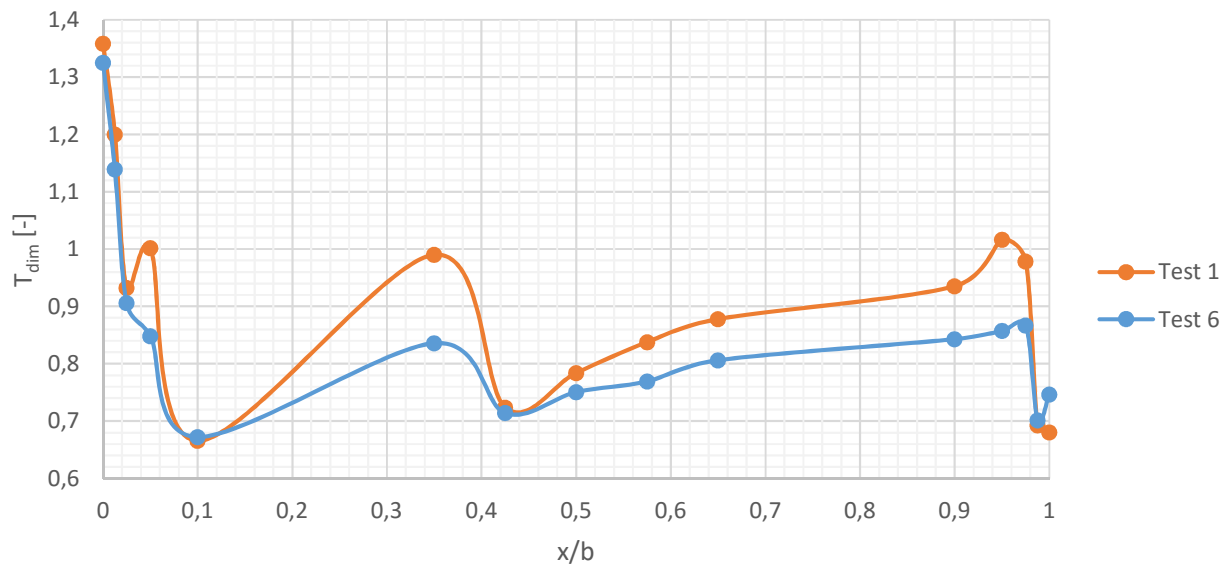


Figure 5.74. Horizontal temperature profiles in height 2.25 m.

The oscillating temperatures along the channel width seems to be decreased with increasing ACH. Also at this height the stability is shown to be steady and within the possible measurement error. But this is not the case for test 6, see figure 5.75.

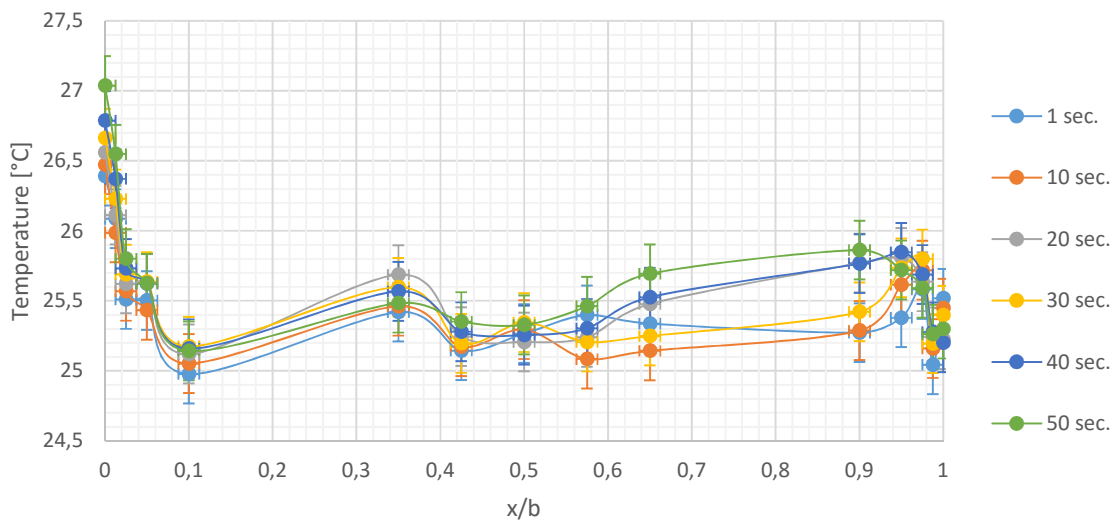


Figure 5.75. Stability in horizontal temperature profile in height 2.25 m for test 6.

The half closest to the colder surface demonstrates highly fluctuating temperatures varying in one point with up to 0.5 °C. First of all it should be mentioned that the general air flow pattern in both test 1 and 6 is similar to a case with extreme recirculation. From the literature it is found that obtaining this recirculating flow occurring in the entire channel leads to a backflow

at the outlet. Therefore, the fluctuations found close to the glass wall in height 2.25 m might be caused by this extreme recirculation. The fluctuating behavior might also be due to a secondary reversed flow at this region. Both theories are only implications rather than a proven fact.

Next are the vertical temperature profiles presented. First is the distribution at the center of the channel shown in figure 5.76.

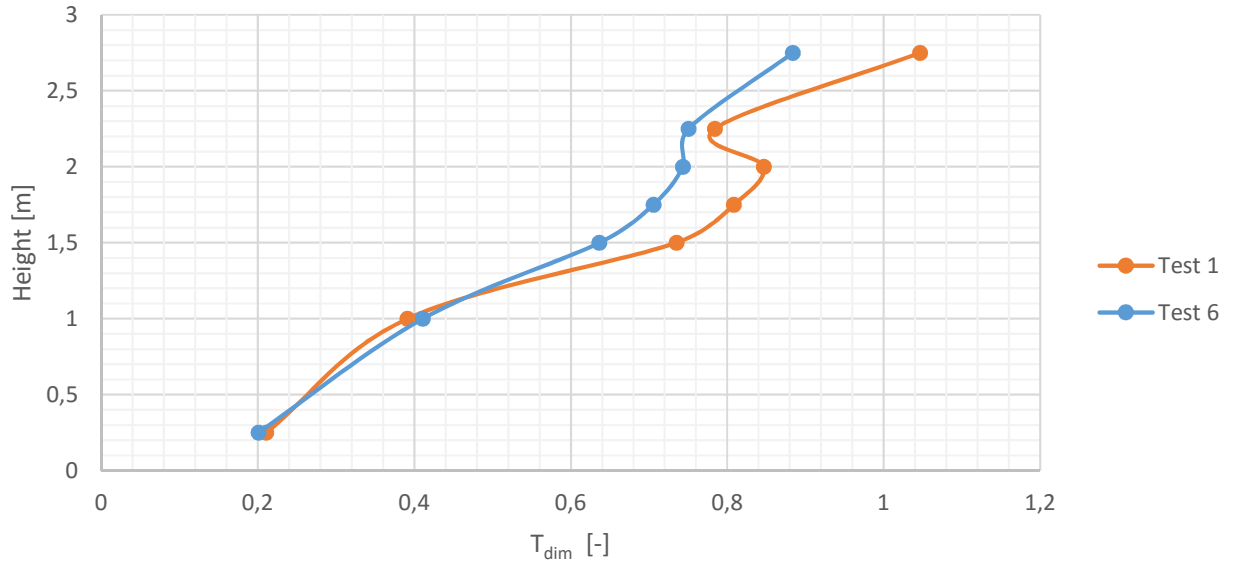


Figure 5.76. Vertical temperature profiles in center.

Although test 6 up till now has shown more indications of recirculating flow the vertical temperature profiles in the center weaken this statement. The temperature drop in height 2.25 m found in test1 is not appearing in test 6. But the horizontal temperature profiles indicated that the recirculation happens close to the glass surface, and for that reason a closer look will be given.

In *section 5.1* on page 39 the stability of the vertical temperature profiles for test 1 showed that the flow acted unstable in distances 0.5 cm and 1 cm from the glass surface and is more steady in distances 2 cm and 4 cm. Figures 5.77, 5.78, 5.79 and 5.80 on page 95 show the stability for test 6 in the vertical temperature gradients close to the glass surface.

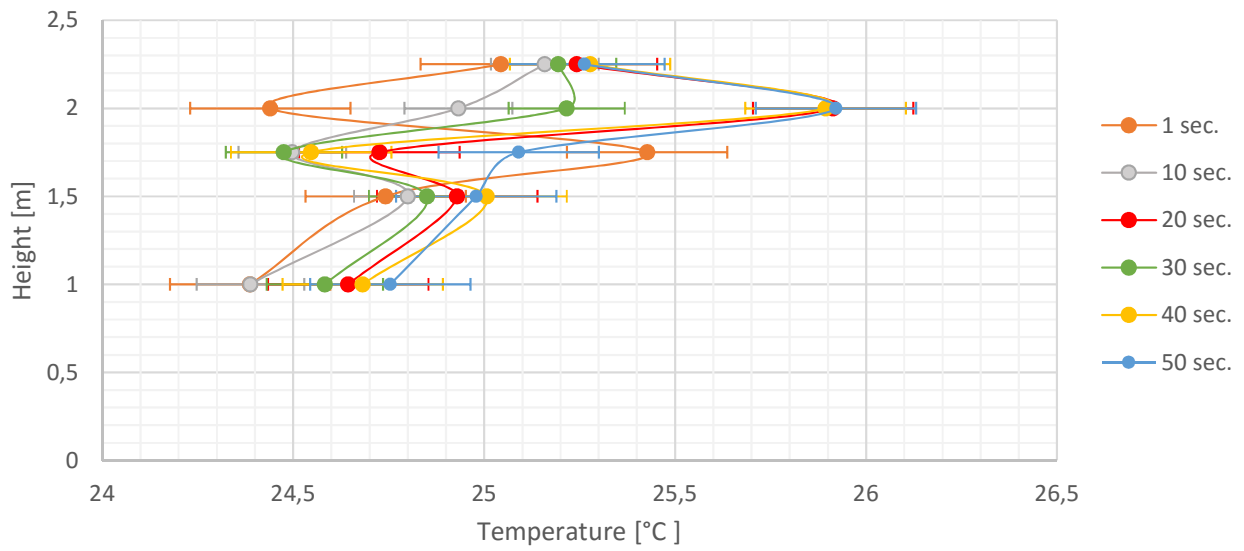


Figure 5.77. Stability of vertical temperature profile 0.5 cm from the glass surface in test 6.

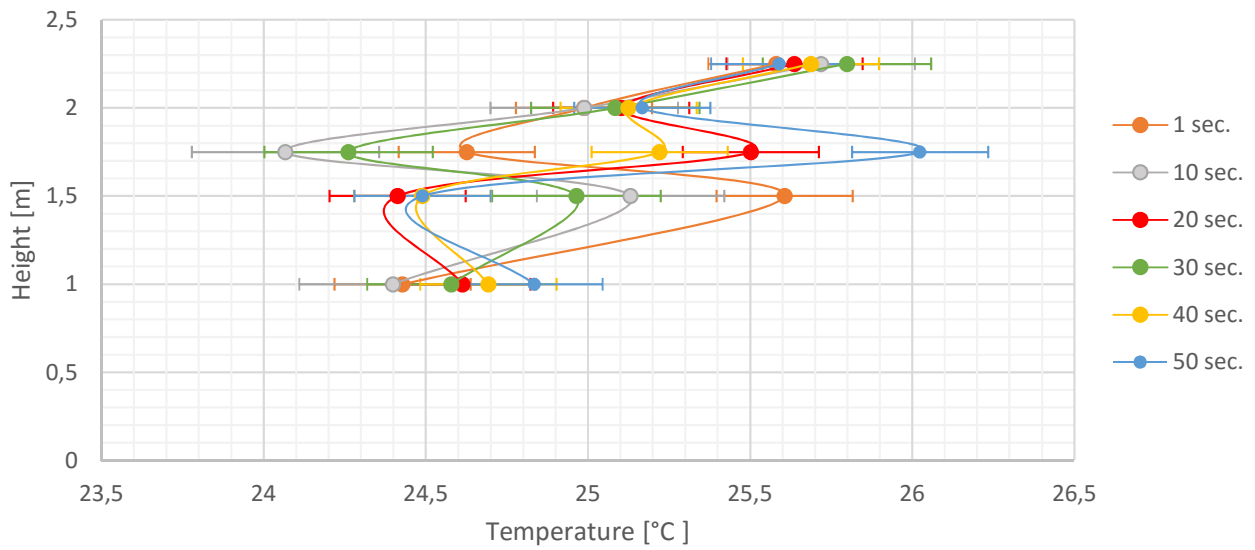


Figure 5.78. Stability of vertical temperature profile 1 cm from the glass surface in test 6.

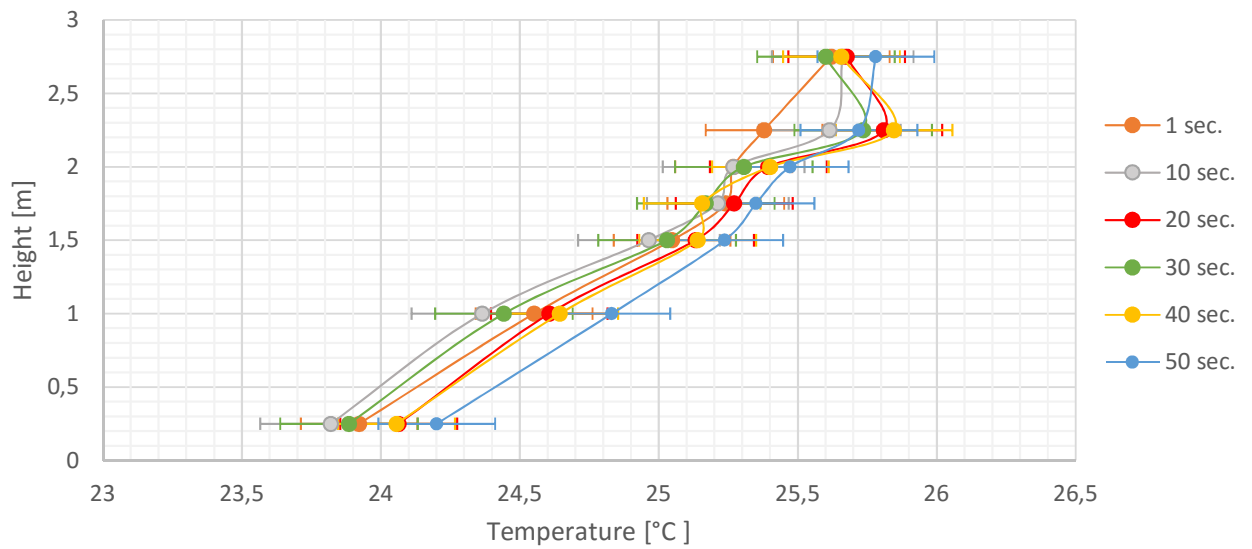


Figure 5.79. Stability of vertical temperature profile 2 cm from the glass surface in test 6.

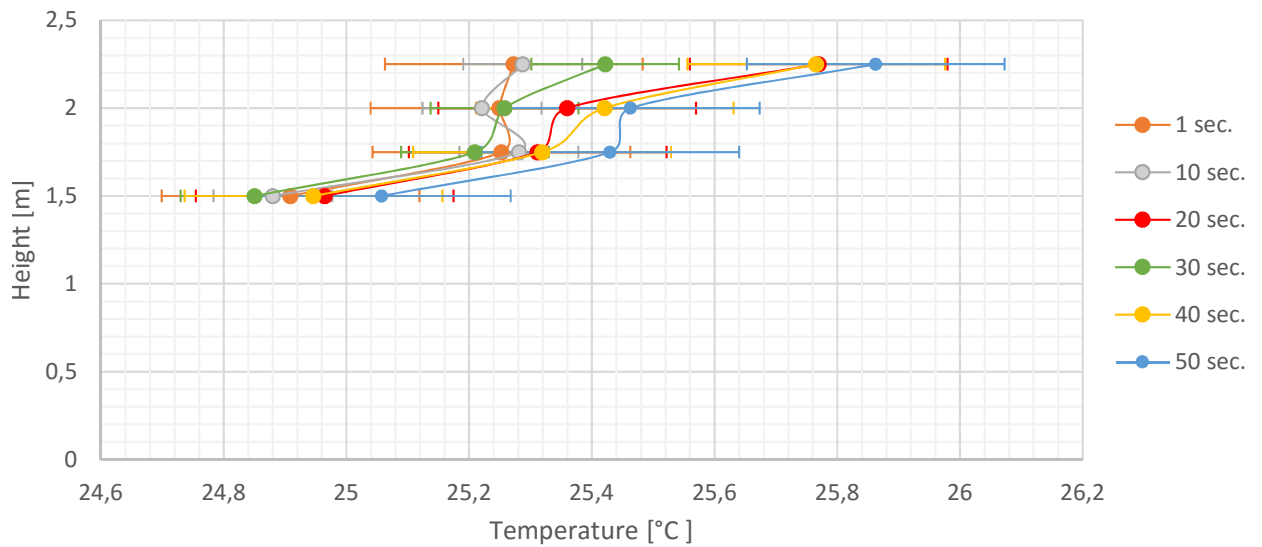


Figure 5.80. Stability of vertical temperature profile 4 cm from the glass surface in test 6.

From the graphs it is concluded that test 6 shows the same tendencies as test 1; the flow is unstable in distances 0.5 cm and 1 cm from the surface and again found stable from 2 cm. The difference between test 1 and 6 is found in the how much the temperatures are fluctuating, which is observed as much greater in test 6.

5.3.2 Remarks Regarding the Influence of ACH

Increasing the air flow rate in the cavity leads to an increase of Rayleigh number but a decrease in the buoyancy forces measured by Gr/Re^2 -ratio. The same air flow pattern is achieved but with a decrease in Gr/Re^2 -ratio the flow is found to be more dynamic close to the glass surface. In the center of the cavity the deformation in the vertical temperature profile is found to be decreased. A comparison of the dimensionless vertical temperature profiles close to the glass surface can be found in *appendix J* on page 171 and will not be further discussed.

The only literature that deals with increase of air flow rate is [Gau et al., 1992], where the flow was visualized. It was found that the penetration depth of the recirculating flow moved upward closer to the outlet with increasing flow rate, but the width of the region increased. Due to lack of measurements this cannot be concluded in the present study.

Thickness of Boundary Layer

As mentioned earlier the convective heat transfer strongly depends on the thickness of the boundary layers. For this reason it is interesting to calculate the thickness of the boundary layer analytical by a method developed by [Eckert og Jackson, 1950] and later analyzed by [Heiselberg og Sandberg, 1990], and compare the calculated results with the experimental results obtained during this study.

[Eckert og Jackson, 1950] obtained the formula describing the thickness of the boundary layer using the integrated momentum equation for the boundary layer and empirical relation of the shearing stress on the wall and heat transfer coefficients derived from forced convective flow. The relation is widely used, although it has not been proved entirely satisfactory, but was found to be appropriate, since it was assumed to be sufficient to predict the flow with an accuracy of 10 % from an engineering perspective [Heiselberg og Sandberg, 1990].

The thickness of the boundary layer was calculated according to equation 6.1.

$$\delta = 0.566 \cdot y \cdot Gr_y^{-\frac{1}{10}} \cdot Pr^{-\frac{8}{15}} [1 + 0.494 \cdot Pr^{\frac{2}{3}}]^{\frac{1}{10}} \quad (6.1)$$

Where:

δ		Thickness of boundary layer [m]
y		Vertical distance [m]
Gr_y		Local Grashof number [-]

The following analysis of the thickness of the boundary layer is presented for test 1. Due to the back flow near the glass surface which is found in *section 5.1* on page 39 the calculated distances are inverted. Grashof number is calculated according to the surface and the temperature in the center in each height.

The calculated thickness of the boundary layer is presented in figure 6.1 on the next page.

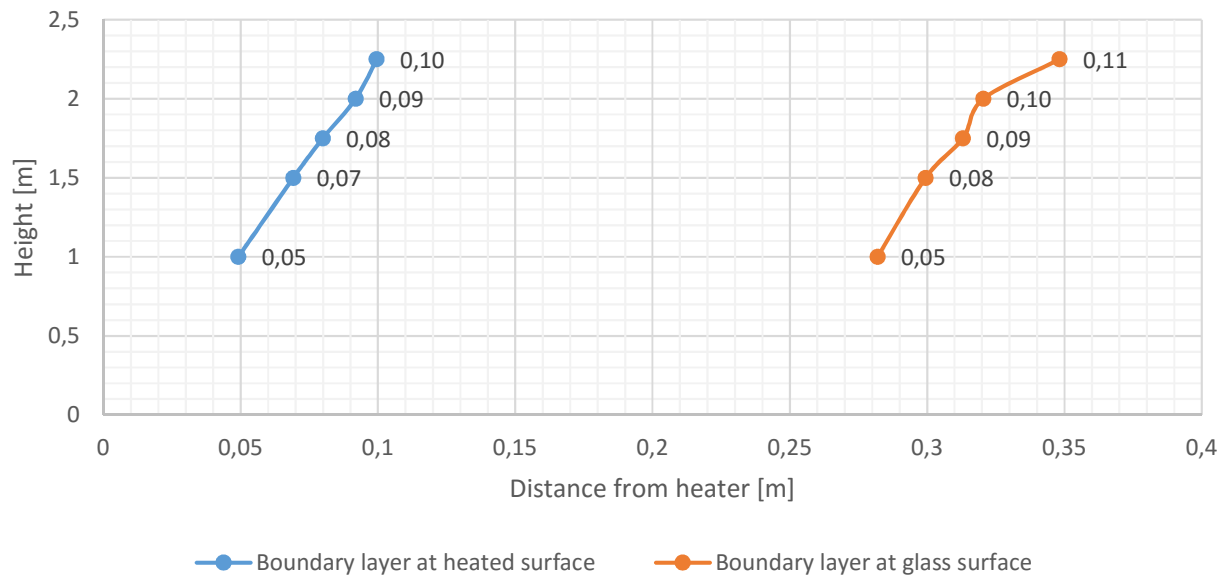


Figure 6.1. Thermal boundary layer thickness calculated analytical.

It is seen that the boundary layer grows almost proportional from the bottom of the channel to the top, and ends with a thickness of 0.10 m at 2.25 m height at the heated surface. This is found reversed near the glass wall that has a maximum thickness of 0.11 m in height 1.00 m

A comparison with the horizontal temperature profiles is done, and these can be found in figure 6.2 on page 100. The following table 6.1 is made in order to give a clear overview of the different distances obtained by the analytical solution and what is observed in the experiment.

Height [m]	Analytical		Experimental	
	Heated surface [m]	Glass surface [m]	Heated surface [m]	Glass surface [m]
1.00	0.05	0.11	0.02	> 0.02
1.50	0.07	0.10	≈ 0.04	–
1.75	0.08	0.09	> 0.04	–
2.00	0.09	0.08	> 0.04	–
2.25	0.10	0.05	–	0.02

Table 6.1. Calculated and observed boundary layer thicknesses.

Close to Heated Surface

Close to the heated surface the peaks are found to be within the limit of measurement error except in height 2.25 m, which is why they are not considered. In height 1.00 m the last measurement point is located 0.02 m from the surface, and from the surface until this point a temperature gradient is achieved. It is therefore not proven if the thermal boundary layer ends at 0.02 m or it extends to the calculated distance 0.05 m.

Without taking the peak values into account the boundary seems to be ending 0.04 m from the surface in height 1.50 m in the experiment. In height 1.75 m the horizontal temperature profile

is decreasing all the way to 0.17 m from the surface, so it is assumed that the boundary layer ends between 0.04 m and 0.17 m. At height 2.00 m the same tendency is found as in height 1.50 m, and it is again assumed to end at 0.04 m.

The fluctuating temperatures in height 2.25 m in the half of the cavity close to the heated wall made it difficult to conclude anything about the boundary layer. If recirculation flow is appearing at this height, the boundary layer thickness is affected due to entrainment of free flow from the core and the thickness may have decreased comparing to the lower level.

The boundary layer thickness calculated according to the analytical solution seems to be in acceptable agreement with the experiment, but the observations are just implications rather than proven facts due to the lack of measurement points in the horizontal plane and also the inaccuracy of the measurements.

Close to Glass Surface

In test 1 the flow is found to be highly dynamic close to the glass surface with peaks in almost every measured height, only heights 1.00 m and 2.25 will be analyzed. In height 1.00 m the thickness might extend to a distance more than 0.02 m from the surface, and in height 2.00 m a peak is found 0.02 m from the surface. Both observations are relatively in agreement with the analytical solution, but again due to lack of measurement points and error nothing can be concluded.

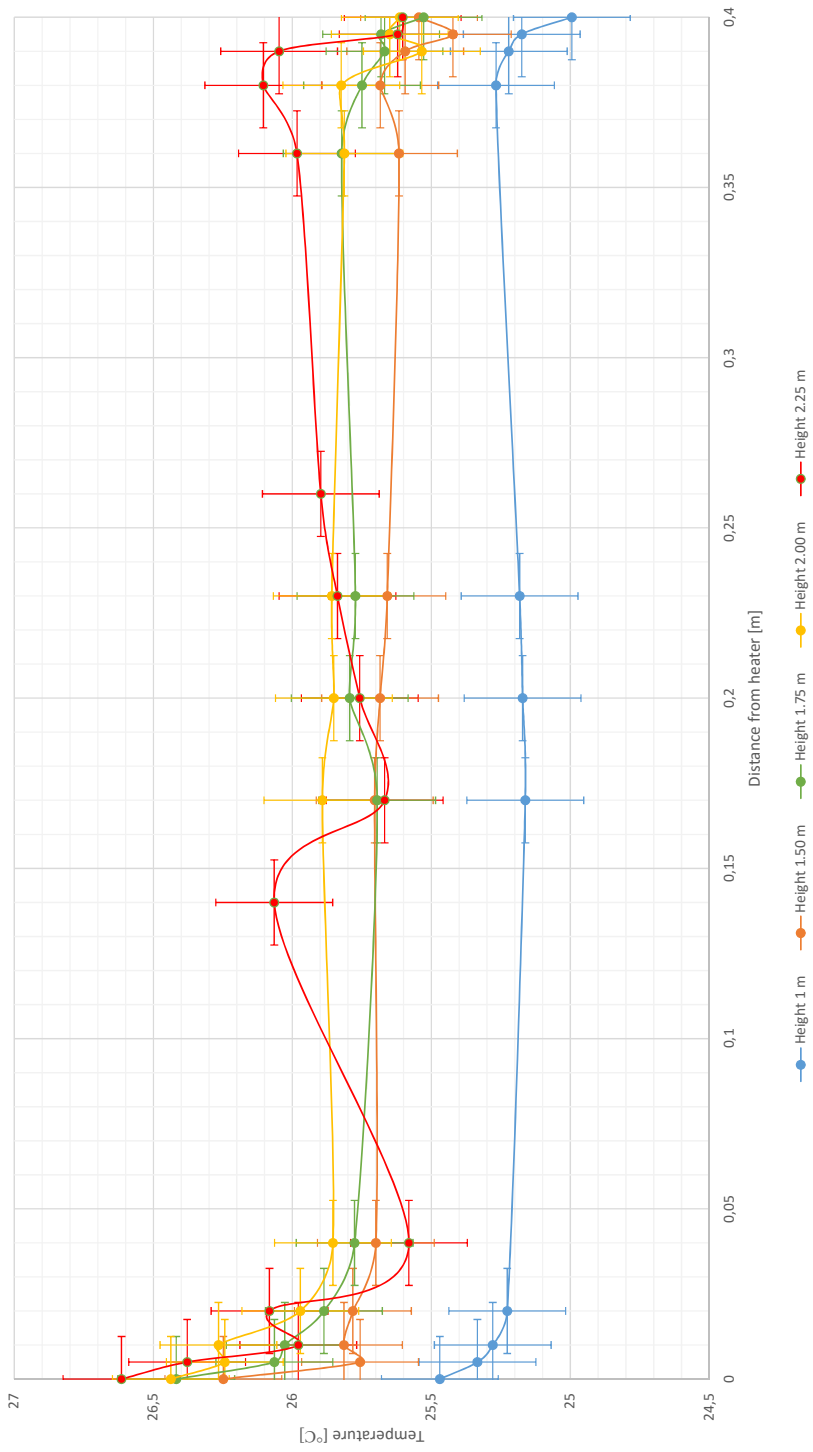


Figure 6.2. Horizontal temperature profiles for test 1.

Part III

Numerical Study

The purpose of the numerical study is to obtain similar results as in the experiment and by this validate the model. A further investigation can then be performed.

Numerical solution of Flow Inside a Vertical Channel

Besides from analyzing the air flow pattern by experimental work and analytical solutions, a numerical model is a useful tool to predict various values that describe the air flow pattern in the channel. The CFD (Computational Fluid Dynamics) program Ansys Fluent 15.0 is used in this study for this analysis. The program uses the numerical finite volume method and provides solutions in each volume.

The purpose of the numerical study is to validate a computational solution performed by comparing the predictions against the experimental results to address the simulation uncertainty and the degree of accurate representation. Two simulations are performed with the same boundary conditions as test 1 and the results are presented after explanation of the numerical solution technique.

7.1 Numerical Solution Technique

The description of the numerical solution technique is a common part of the work made in cooperation with two other master students, but is then later changed and extended. The following section is based on [Ansys, Inc.] unless else is stated.

The geometry model of the channel is designed according to the test facility during the experimental study. The inlet is set at the bottom of the glass surface and the outlet at the top. Both of them they have an area of 0.105 m^2 . The geometry and the mesh are created by using the software ICEM. The model geometry is presented in figures 7.1 and 7.2 on the following page.

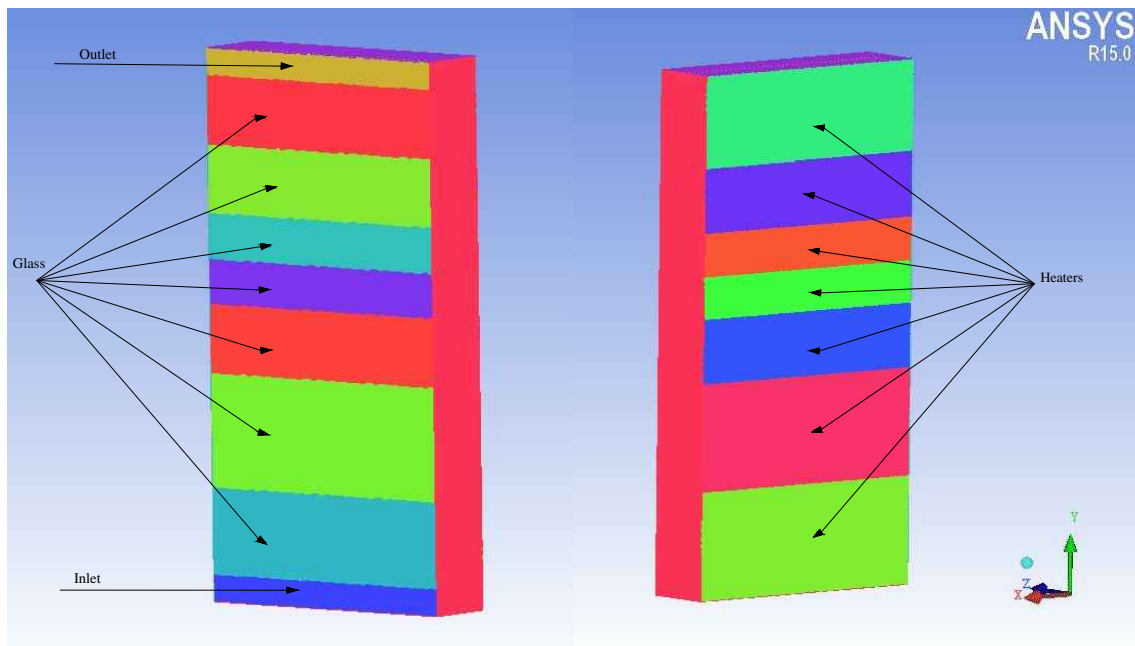


Figure 7.1. Front view of geometry model.

Figure 7.2. Back view of geometry model.

Both the heated and the glass surface is divided into 7 parts according to where the surface temperatures are measured in the experiments.

7.1.1 Mesh features

For the mesh generation it is selected to use unstructured patch dependent mesh with quadratic cells for the surfaces and volume, and prism layers near the boundaries to the heated wall and the glass. The boundary layers in free convection play an important role because the solution gradients in that area are very high. To capture the phenomenon of convection a fine mesh should be used but applying this has as a drawback at time and convergence. Instead, adding prism layers near the walls would be a time and cost effective solution.

The prism layer sizes are selected according to the measurement points in the experiments. Recall from figure L.1 on page 178 the first point is located at the surface, the second 0.5 cm from the surface, the third 1 cm, fourth 2 cm and the last 4 cm from the surface. The total length is then 4 cm divided in 8 layers with exponential growth.

At the end a grid of 5,994,240 cells is achieved with a minimum cell size of $8.95 \cdot 10^{-8} \text{ m}^2$ and a maximum cell size of $3.76 \cdot 10^{-7} \text{ m}^2$. The mesh quality is checked and the minimum quality obtained is 0.95, in a range from 0 to 1, where 0 corresponds to low quality.

7.1.2 General decisions

The steady state simulation is chosen with respect to the computational time and to the criterion of easier convergence.

The gravity exists in the y-axis of the geometry model and the pressure based solver is chosen for a low speed incompressible flow as it happens for the fluid in the channel. By using the pressure-based solver the pressure field is extracted by solving a pressure or pressure correction

equation, which is obtained by manipulating continuity and momentum equations, this will be further discussed later.

7.1.3 Properties of the fluid material

The fluid is chosen to be the air. As for its density, the Boussinesq approximation, given by the equation 7.1 is used.

$$\rho = \rho_0(1 - \beta\Delta T) \quad (7.1)$$

Where:

ρ_0		Constant density of the flow [kg/m ³]
β		Thermal expansion coefficient [K ⁻¹]
ΔT		Temperature difference [K]

According to Boussinesq approximation, the density differences can be neglected for small temperature gradient, so the density can be treated as a constant value in all the solved equations, except for the buoyancy term in the momentum equation. This density treatment is considered sufficiently accurate as long as the changes in density are small like it happens in a closed domain with natural convection and will lead to faster convergence.

The other properties of air such as the thermal conductivity λ [Wm⁻¹K⁻¹] and the specific heat capacity C_p [Jkg⁻¹K⁻¹] are treated as constant values because according to [Pasut og Carli, 2012], it is not worthy to treat these values as a function of the density. This treatment increases the computational time without any significant improvement of CFD prediction. The changes of λ and C_p are only 2.6 % and 0.1 % respectively at a temperature of 293.15 K.

7.1.4 Governing Equations

The airflow in the cavity is the result of natural convection, therefore it is driven by buoyancy forces. It can be described by the equations of mass, momentum and energy conservation, together with the definition of the turbulent flow variables [Baldinelli, 2009]. The general form of the governing equation for mass conservation is shown in equation 7.2.

$$\frac{\partial \rho}{\partial t} + \nabla \cdot (\rho \vec{v}) = S_m \quad (7.2)$$

Where:

t		Time [sec]
\vec{v}		Velocity vector [m/s]
S_m		Source term

The momentum conservation is solved by equation 7.3.

$$\frac{\partial}{\partial t}(\rho \vec{v}) + \nabla \cdot (\rho \vec{v} \vec{v}) = -\nabla p + \nabla \cdot (\bar{\tau}) + \rho \vec{g} + \vec{F} \quad (7.3)$$

Where:

p	Static pressure [Pa]
$\bar{\tau}$	Stress tensor [Pa]
$\rho \vec{g}$	Gravitational body force
\vec{F}	Gravitational external body force [N]

Energy conservation is solved according to equation 7.4.

$$\frac{\partial}{\partial t}(\rho E) + \nabla \cdot (\vec{v}(\rho E + p)) = \nabla \cdot \left(k_{eff} \nabla T - \sum_j h_j \vec{J}_j + (\bar{\tau}_{eff} \cdot \vec{v}) \right) + S_m \quad (7.4)$$

Where:

k_{eff}	Effective conductivity [W/mK]
\vec{J}_j	Diffusion flux of species j [kg/m ² - s]
h_j	Heat transfer coefficient [W/m ² K]

7.2 Turbulence Modelling

The right choice of a turbulence modelling method is of great importance since it ensures the accuracy of the model. Therefore, for the simulation of the vertical channel the k- ϵ realizable model is selected. It is suitable for a wide range of flows, such as the channel flow and layer flow. Moreover, it has good performance for flows involving rotation, boundary layers under strong adverse pressure gradients, separation and recirculation [Safer et al., 2005]. Moreover, the chosen turbulence model, except the turbulence flow, is able to deal with the laminar and the transitional flow.

In general, the k- ϵ model is a two equations Reynolds averaged Navier-Stokes based model. It uses two more transport equations for the kinetic energy k and the dissipation rate ϵ . These equations are presented in 7.5 and 7.6.

$$\frac{\partial}{\partial t}(\rho k) + \frac{\partial}{\partial x_j}(\rho k u_j) = \frac{\partial}{\partial x_i} \left[\left(\mu + \frac{\mu_t}{\sigma_k} \right) \frac{\partial k}{\partial x_j} \right] + G_k + G_b - \rho \epsilon - Y_M + S_k \quad (7.5)$$

$$\frac{\partial}{\partial t}(\rho \epsilon) + \frac{\partial}{\partial x_j}(\rho \epsilon u_j) = \frac{\partial}{\partial x_j} \left[\left(\mu + \frac{\mu_t}{\sigma_\epsilon} \right) \frac{\partial \epsilon}{\partial x_j} \right] + \rho C_1 S_\epsilon - \rho C_2 \frac{\epsilon^2}{k + \sqrt{\nu \epsilon}} + C_{1\epsilon} \frac{\epsilon}{k} + C_{3\epsilon} G_b + S_\epsilon \quad (7.6)$$

Where:

k	Turbulent kinetic energy
ϵ	Dissipation rate
G_k	Generation of turbulent kinetic energy due to the mean velocity gradients
G_b	Generation of turbulent kinetic energy due to the buoyancy
Y_M	Contribution of the fluctuating dilatation in compressible turbulence to the overall dissipation rate
S_ϵ	Source term
$\sigma_k - \sigma_\epsilon$	Turbulent Prandtl numbers for k and ϵ

The eddy viscosity is calculated from equation 7.7.

$$\mu_t = \rho C_\mu \frac{k^2}{\epsilon} \quad (7.7)$$

Where:

μ_t	Turbulent viscosity
C_μ	Value calculated by the model

The values of the model constants are given in Table 7.1. These default values have been derived by data fitting for a wide range of turbulent flows.

$C_{1\epsilon}$	C_2	σ_κ	σ_ϵ
1.44	1.9	1.0	1.2

Table 7.1. The constants values in the k- ϵ realizable model.

Near-wall Treatment

The following section is based on both [Ansys, Inc.] and [Tu et al., 2013].

The near-wall treatment is essential for such problems like boundary layer flow and a modelling procedure often used is the wall functions. In this approach, the near-wall boundary is not explicitly determined within the numerical model, but is joined by the wall functions. The wall functions are generated by dimensionless variables with respect to the local conditions at the wall; y is the distance normal to the wall and U is the time-averaged velocity parallel to the wall, then the dimensionless wall distance y^+ and dimensionless velocity U^+ is described by the log-law relation

$$U^+ = \frac{1}{\kappa} \ln(Ey^+) \quad (7.8)$$

$$y^+ = \frac{\rho C_\mu^{1/4} k_P^{1/2} y_P}{\mu} \quad (7.9)$$

Where:

κ	Von Karman constant (=0.4187)
E	Emperical constant (=9.793)
U_P	Mean velocity of the fluid at the wall-adjacent cell centroid, P
k_P	Turbulence kinetic energy at the wall-adjacent cell centroid, P
y_P	Distance from the centroid of the wall-adjacent cell to the wall, P

In general the near wall region can be divided into three main layers; the inner layer closest to the wall is called *viscous sublayer*, and here the viscosity plays an important role in momentum and heater transfer, the flow is distincted as laminar. Then a layer called *buffer layer* is formed, where the effect of molecular viscosity and turbulence are equally important. The outer layer is called the *fully-turbulent layer* and as the name suggest turbulece has the greatest effect on the flow. The dimensionless distance to the outer layer is determined by the mentioned log-law relation, whereas the *viscous sublayer* is obtained by a linear relationship between the y^+ and U^+ written as

$$y^+ = U^+ \quad (7.10)$$

For this relation the shear stress is assumed to be approximately constant and equivalent to the wall shear stress τ_w . In Ansys Fluent the linear relation is used whenever $y^+ < 11.225$ and the low-law relation is employed when $y^+ > 11.225$. Since the purpose of the wall functions is to relate the flow parameters to the first noden and thereby removing the requirement to determine the structure in between, the lower limit of the dimensionless distance must be carefully located in such way that it does not fall into the *viscous sublayer*, but also the upper limit must be carefully placed in order to get a sufficient resolution. In [Tu et al., 2013] it is stated that *an adequate boundary layer resolution generally requires at least eight to ten grid nodel points in the layer*. The degree of resolution can be determined by plotting the ratio of turbulent diffusion and the molecular diffusion (due to molecular viscosity), which is normally found to be high within the boundary layer.

For the near wall region in the k- ϵ model, the standard wall function is used. The standard wall function implies that the near wall cells lies completely in the logarithmic region of the boundary layer. It corresponds to the region where the turbulent shear stress is dominant.

7.2.1 Radiation Model

The thermal radiation heat transfer between the surfaces was calculated by the *surface-to-surface* radiation model, since the model is appropriate for enclosure radiative heat transfer. The model assumes all surfaces to be grey and diffuse. Emissivity and absorption of a grey surface are independent of wavelength. By Kirchhoffs law it is known that the emissivity is

equal to the absorption and for a diffuse surface, the reflectivity is independent of outgoing and incoming directions. For this model any absorption, emission and scattering is ignored (hence the name of the model) only surface-to-surface radiation is considered.

The heat transfer is calculated according to the view factors. These are calculated automatically and accounts for the surfaces size, separation distance and orientation. The basis of the view factors can either be face-to-face or cluster-to-cluster. The cluster-to-cluster basis gathers surfaces into clusters and calculates a common view factor for each cluster. This option is suitable for complex geometry with a high number of surfaces. Since the model only has six surfaces it is chosen to use the face-to-face basis. This relates to the boundary conditions chosen for each wall, where only the two main walls were selected to participate in the view factor calculation, namely the heated wall and the glass. In this setting the number of faces per surface cluster was set to one, as each wall is considered as one surface.

There are two methods for calculating the view factors: Ray tracing and Hemicube. The Hemicube is more accurate than the Ray tracing method since it divides the surfaces into subsurfaces, calculate a view factor for each subsurface and sums them for the whole surface. The Hemicube is recommended for large complex geometries, and since the model is simple it is chosen to use the ray tracing method and considered sufficient.

The reflected energy flux of a surface depends on the incident energy flux of its surrounding surfaces and it can be expressed as the energy flux from all the other surfaces. The reflected energy of a surface k is given by equation 7.11, [Jiru et al., 2011].

$$q_{out,k} = E_k + \rho_k q_{in,k} \quad (7.11)$$

The amount of the incident energy from a surface j onto the surface k , is given by the view factor F_{jk} . In other words, the view factor can be expressed as the fraction of energy emitted by surface i directly on a surface k . For N surfaces, the incident energy flux is given by equation 7.12

$$q_{in,k} = \sum_{j=1}^N F_{kj} q_{out,j} \quad (7.12)$$

Therefore, the radiosity of a surface k can be expressed by equation 7.13.

$$q_{out,k} = E_k + \sum_{j=1}^N F_{kj} q_{out,j} \quad (7.13)$$

7.3 Boundary Conditions

- Inlet

The inlet is set to be a velocity inlet since the velocity is known in advance. The velocity and the air temperature are set according to the measured values during the experimental study. As for the turbulent quantities of k (kinetic energy) and ϵ (dissipation rate) of the inlet, they are derived from empirical correlations among the turbulent intensity I , the length scale l and the inlet velocity u as they are presented in the equations 7.14 and 7.15.

The turbulence length scale is set to depend on the hydraulic diameter D_h (which is calculated to be 0.1337 m for a rectangular inlet) and the turbulence intensity is set to 10 %. The velocity profile is uniform by default.

$$k = \frac{3}{2}(u \cdot I)^2 \quad \text{with} \quad I = 0.16(Re)^{-1/8} \quad (7.14)$$

$$\epsilon = C_\mu^{3/4} \frac{k^{3/2}}{l} \quad \text{with} \quad l = 0.07D_h \quad (7.15)$$

- Outlet

The outlet is modelled as a pressure outlet with the same turbulent quantities values as the inlet, taking into consideration the uncertainty if the flow is fully developed or not. Another benefit is that by using pressure outlet, its pressure is extrapolated from the interior. The back flow is not calculated during the experiments, so it is set to be normal to boundary, as an option for back flow direction specification method. Its temperature is set from the average temperature for each case of the experiments.

- Walls

The walls are taken as adiabatic walls without heat fluxes and no-slip shear conditions. This indicates that the air sticks to the walls and the velocity will be zero at the boundary walls. All the momentum will be lost when the fluid molecules hit the wall. Concerning the heaters, which are used to create a temperature distribution, are set as having no-slip shear conditions and having a temperature range as they had during the measurements.

- Radiation

Regarding the boundary conditions for the radiation, only the surfaces that were defined previously to section 7.2.1 on page 108 were used.

7.4 Discretization Scheme

At the expense of the assumption of incompressible fluid, the solution of the governing equations yields a lack of an independent equation for pressure. Since fluid flow is driven by the contribution of pressure gradients in the momentum equation and the additional equation provided by the continuity, the system is self-contained; there are four equations with four independent variables (u, v, w, p), but without an independent equation to calculate the pressure. Although the continuity and momentum equations are the only two equations needed to solve the velocity and pressure field in an incompressible flow, the continuity

equation is a kinematic constraint on the velocity field rather than a dynamic equation. One possible way to bridge the velocity and pressure field is to construct the pressure field by assuming continuity conservation.

The SIMPLE scheme is essentially a guess-and-correct method for calculating the pressure field through the solution of a pressure corrector. The pressure correction equation is deduced from the continuity equation. Figure 7.3 shows the sequence of operations in a SIMPLE scheme iterative process.

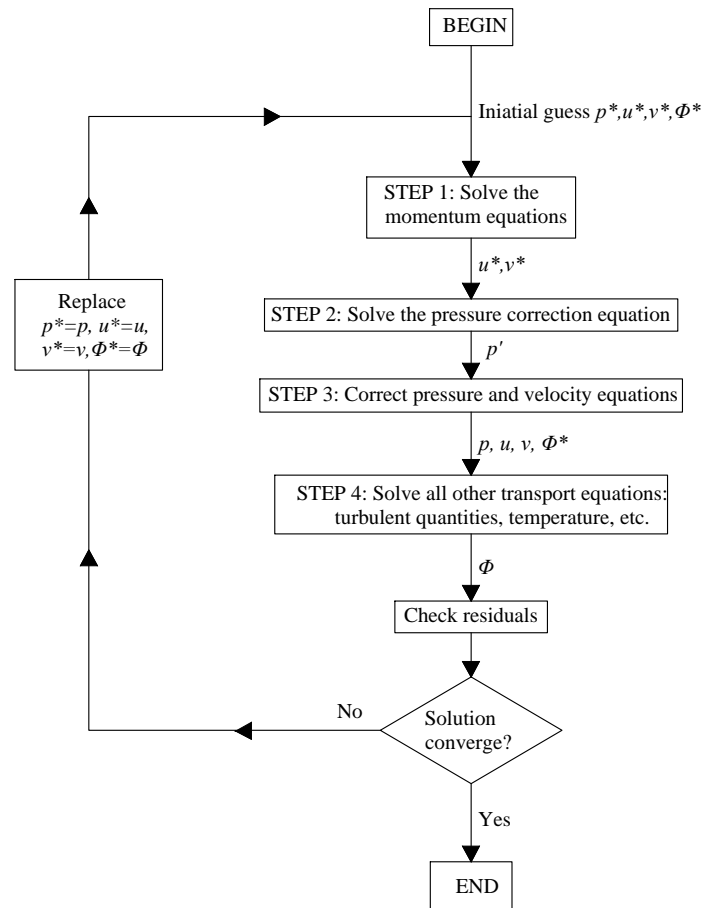


Figure 7.3. Iteration procedure for SIMPLE scheme.

The following spatial discretization is used:

- Gradient: Least squares cell based
- Pressure: Second order
- Momentum: Second order upwind
- Turbulent kinetic energy: First order upwind
- Turbulent dissipation rate: First order upwind
- Energy: Second order upwind

In order for the solution to be considered converged, the sum of the absolute normalised residuals for all of the cells in the domain are set to be less than 10^{-9} for all the variables.

7.5 Numerical Results and Discussion

As mentioned the numerical study is conducted with the same boundary conditions as in test 1. The boundary conditions are once again listed in table 7.2 to give an overview of the test condition.

	Test 1
Ra_H [-]	$9.98 \cdot 10^{11}$
Gr_H [-]	$1.34 \cdot 10^{12}$
Re_H [-]	$8.03 \cdot 10^5$
$Gr_H/Re_H^2 - ratio$ [-]	2.08
$T_{heater,SP}$ [°C]	30.00
$T_{heater,meas.}$ [°C]	26.08
$T_{inlet,meas.}$ [°C]	24.59
ACH [h ⁻¹]	4.00

Table 7.2. Test conditions for test 1

The CFD files can be found in *appendix N* on page 183.

Except from the inlet/outlet boundary conditions explained earlier another test is simulated with reversed boundary conditions. The two types of choice regarding inlet/outlet are explained as

- According to general knowledge and theory about natural convection in a vertical channel: The inlet is set as inlet velocity and outlet as a pressure outlet (like presented in the previous chapter)
- According to experimental set up: The inlet is now set as a pressure inlet and outlet as a inlet velocity but with change in flow direction. This is the closest resemblance to the experiment, but due to uncertainties in the actual experiment that is not transferred to the numerical model, the accuracy of prediction might be less.

First are the horizontal temperature profiles illustrated in figures 7.4, 7.5, 7.6, 7.7 and 7.8 on page 115.

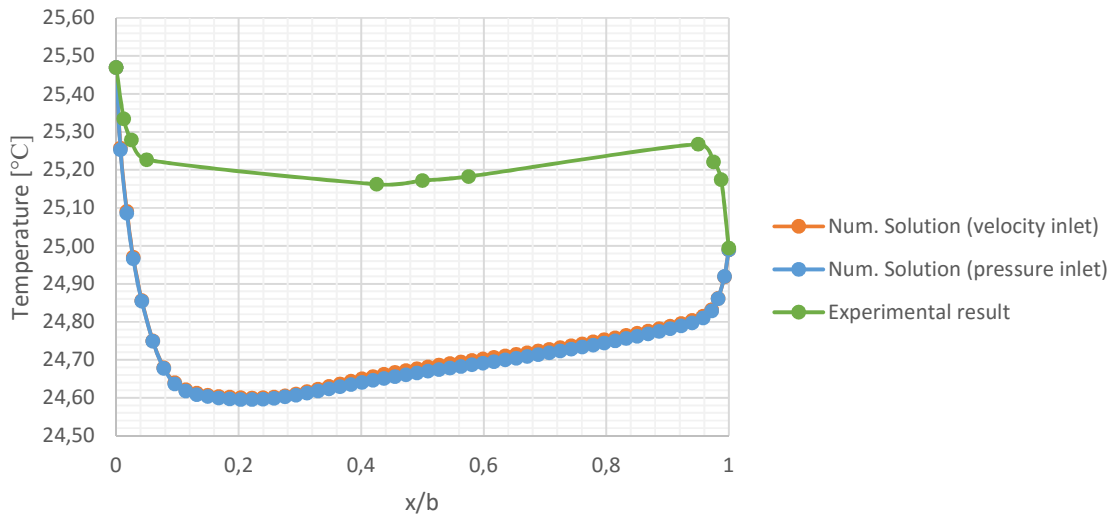


Figure 7.4. Horizontal temperature profile in height 1.00 m.

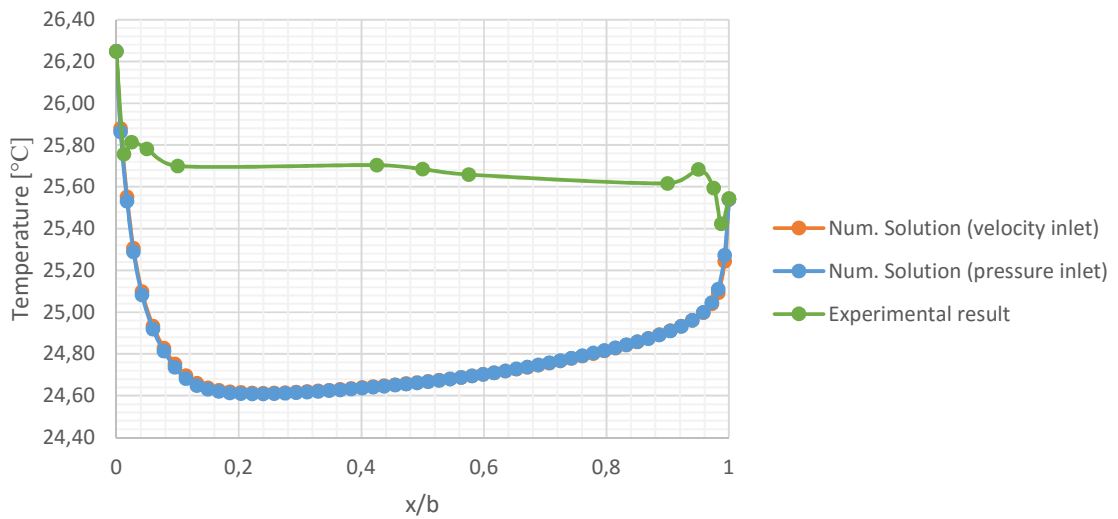


Figure 7.5. Horizontal temperature profile in height 1.50 m.

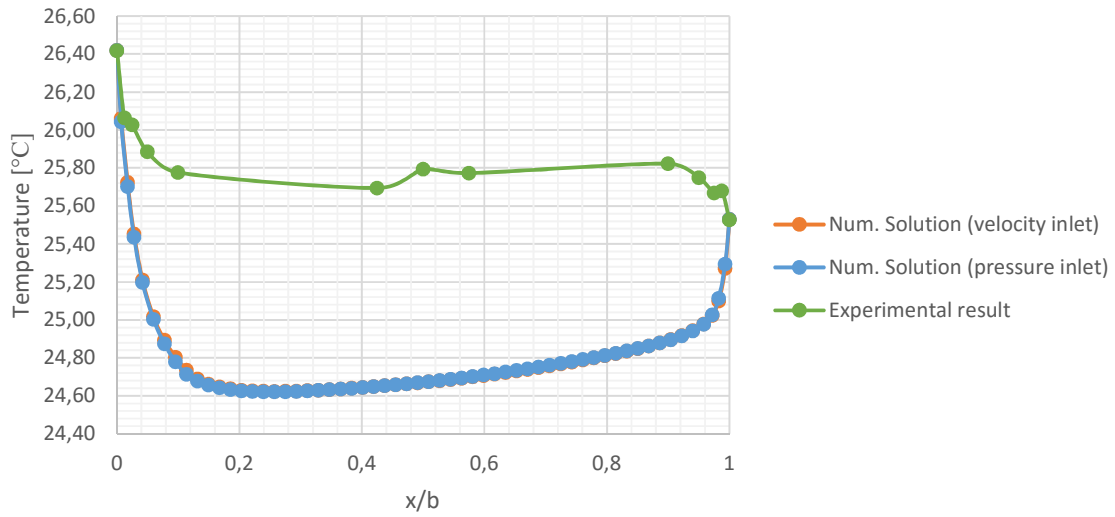


Figure 7.6. Horizontal temperature profile in height 1.75 m.

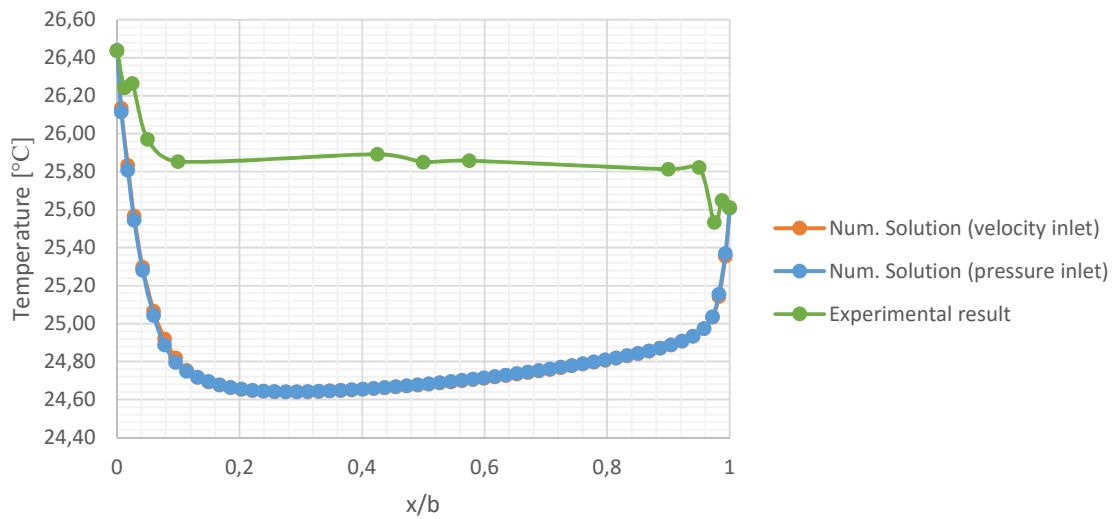


Figure 7.7. Horizontal temperature profile in height 2.00 m.

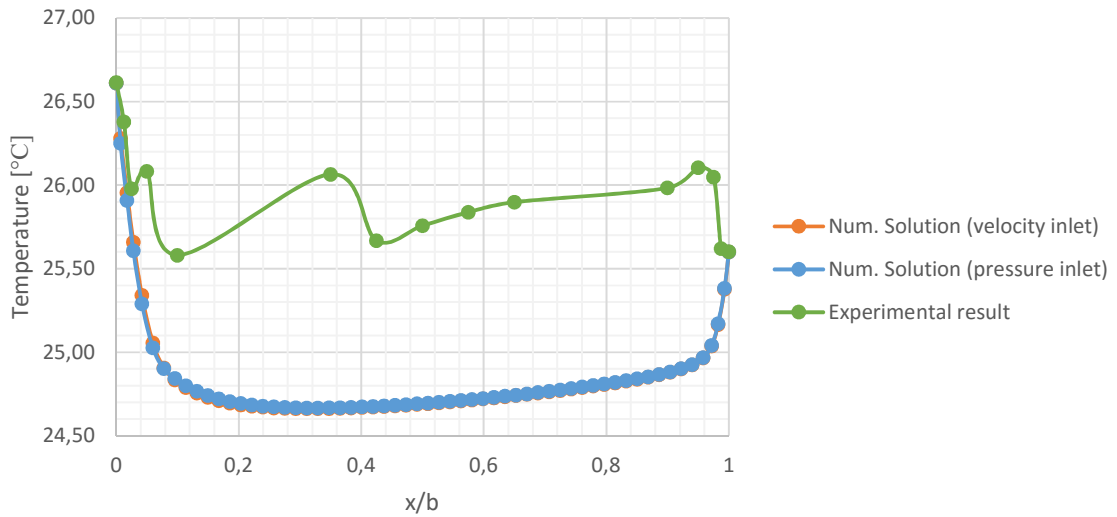


Figure 7.8. Horizontal temperature profile in height 2.25 m.

First of all it is observed in all height that both surface temperatures are predicted correctly. This is due to the fact that the boundary conditions for the wall is set as a constant temperature and not i.e. a heat flux. Throughout all heights it is further discovered that the numerical model is not able to predict the same kind of flow pattern as it is found in the experiment. In the experiment the horizontal temperature profiles revealed that the flow accelerated along the heated wall and reversed at the top having a upstream direction close to the colder wall. The numerical model predicted the flow as a standard channel flow with the same type of temperature distribution on close to the surfaces, indicating that the flow appears to have only downstream direction. Although the flow pattern is observed to be different, the predicted temperatures are within a limit of 10 % which means that the prediction is regarded as accomplished. A contour plot of the temperatures is presented in figures 7.9 and 7.10 on the following page.

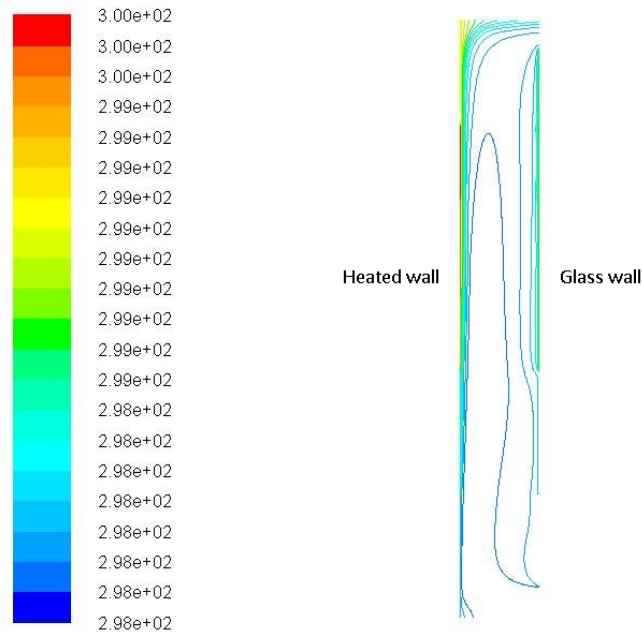


Figure 7.9. Contour plot of temperature in K for the test with velocity inlet.

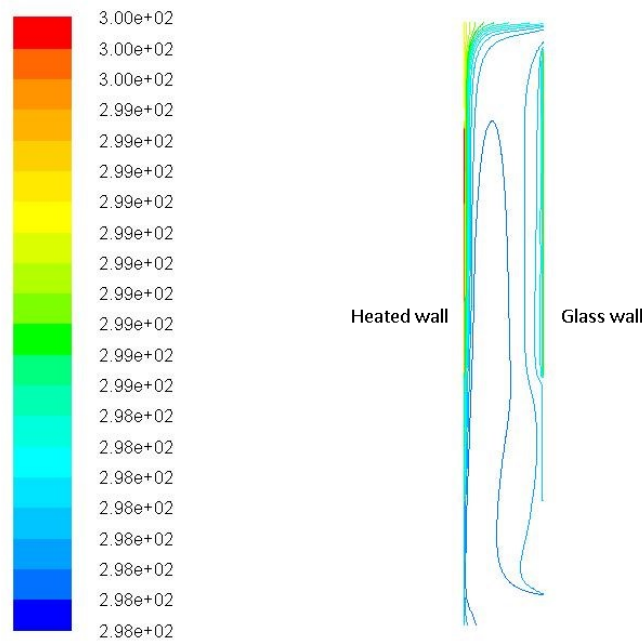


Figure 7.10. Contour plot of temperature in K for the test with pressure inlet.

Besides from comparing the numerical solution to the experimental results, the two models exhibit truly similar conditions both in terms of air flow pattern and predicted temperatures.

The difference of the obtained numerical results and the experimental results might be a consequence of the chosen grid size, that can average the gradient from the boundary layers or due to turbulent model limitations.

7.5.1 Further investigation of Numerical Results

Although there are no experimental results regarding the velocities in the experiment, it is chosen to show the horizontal velocity profiles obtained in the two numerical simulation. For this presentation only the y-velocity is presented. The y-velocity is especially interesting because this is the flow direction in the channel. Positive y means the flow is going from the bottom to the top.

Figures 7.11, 7.12, 7.13, 7.14 and 7.15 on page 119 show the velocity profiles for the two simulated situations.

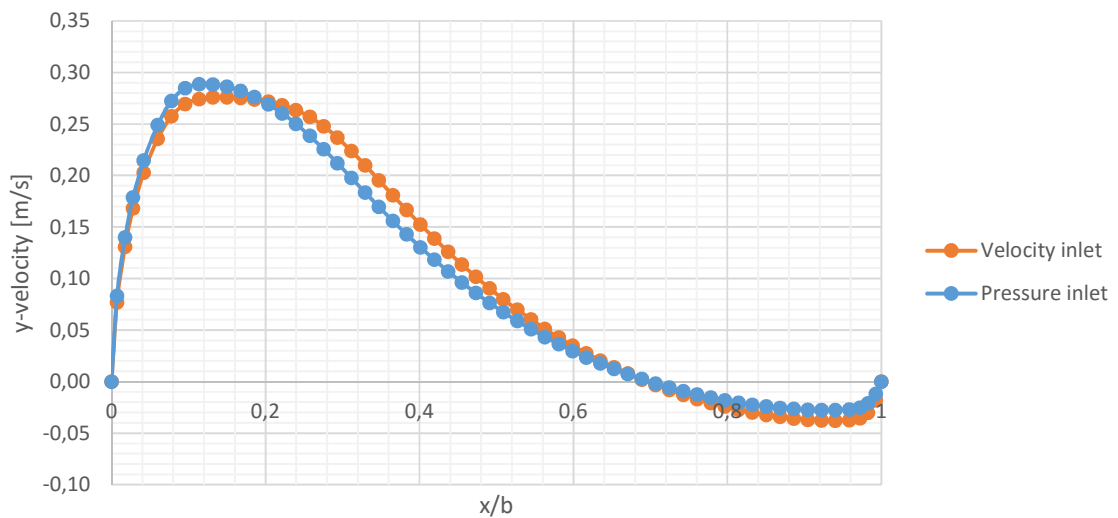


Figure 7.11. Horizontal velocity profile in height 1.00 m.

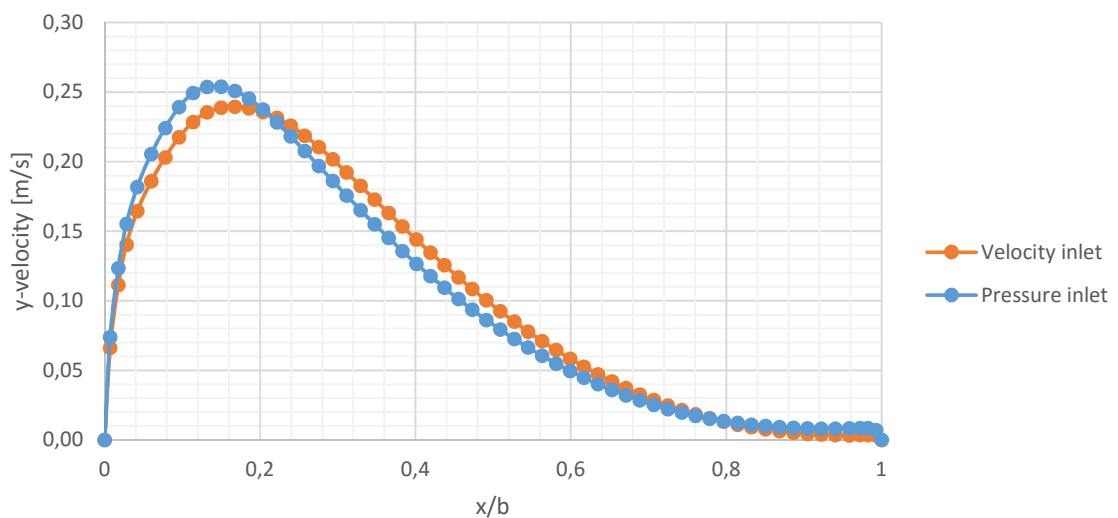


Figure 7.12. Horizontal velocity profile in height 1.50 m.

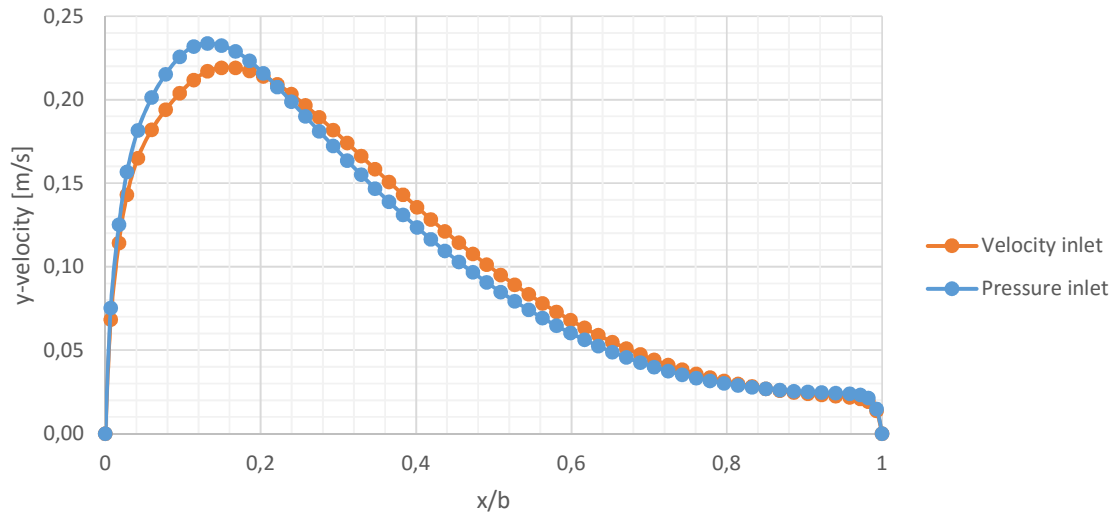


Figure 7.13. Horizontal velocity profile in height 1.75 m.

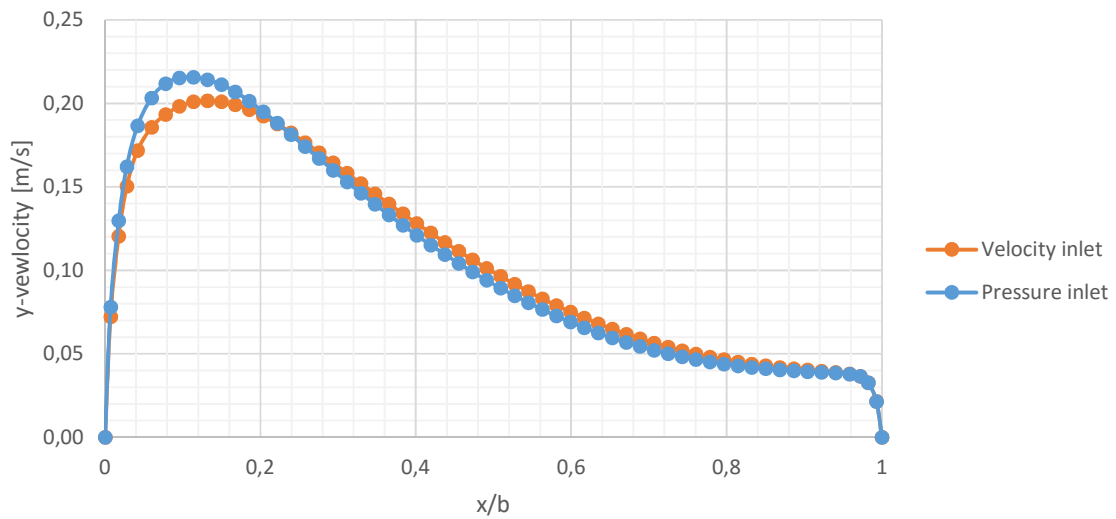


Figure 7.14. Horizontal velocity profile in height 2.00 m.

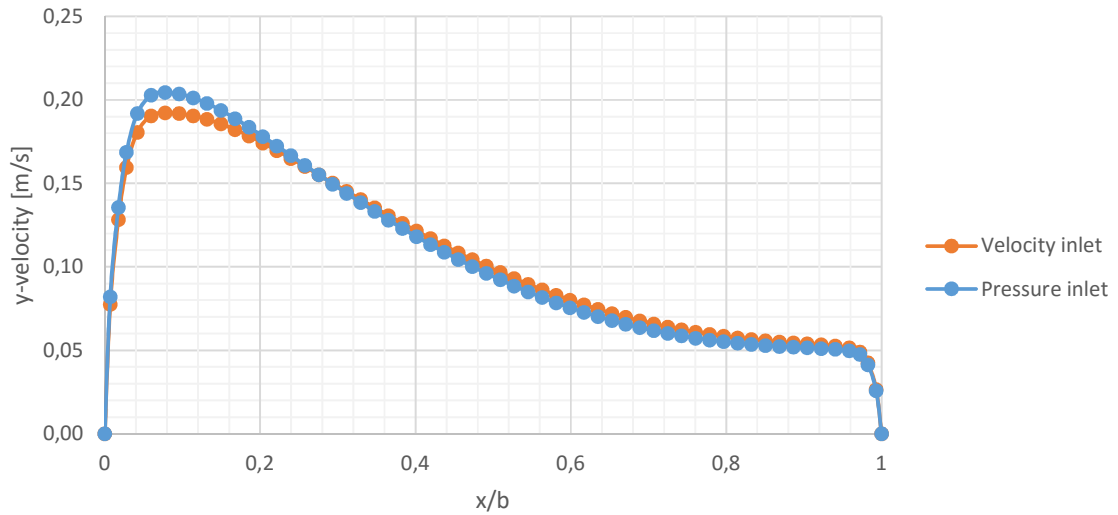


Figure 7.15. Horizontal velocity profile in height 2.25 m.

As it is mentioned before the no-slip condition is chosen for the walls and in the horizontal velocity profiles this effect is seen with zero velocity component at the surfaces.

In height 1.00 m negative velocities are found close to the colder surface indicating that a reversed flow is occurring at this region. The velocity distribution close to the heated wall demonstrates the characteristics as known from theory. Moving upward in the channel the negative velocities change direction and becomes greater along the height. The velocity boundary layer develops with increasing thickness along the channel height close to the glass wall. An interesting observation is found in height 1.50 m. At this height the highest velocity is found from the five investigated heights. This means that the air is accelerated along the heated wall until 1.50 m and then relatively decelerates after that point.

Vector plots of the y-velocity for both cases are found in figures 7.16 and 7.17 on the following page.

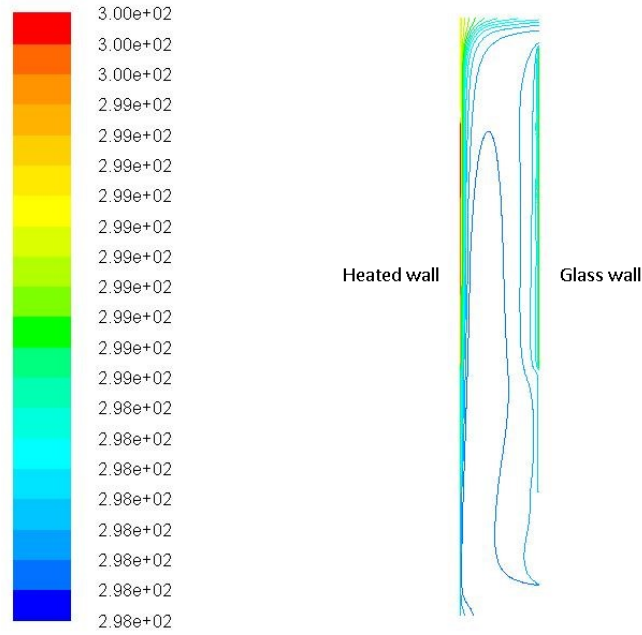


Figure 7.16. Vector plot of y-velocity in m/s for the test with velocity inlet.

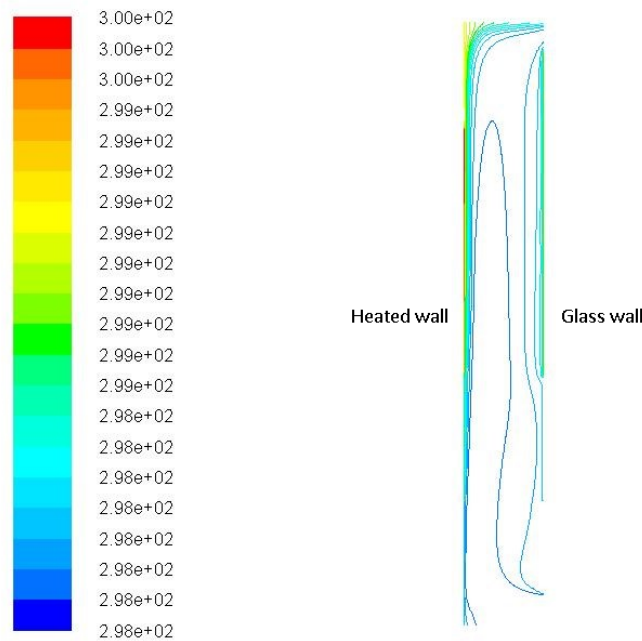


Figure 7.17. Vector plot of y-velocity in m/s for the test with pressure inlet.

In the literature study of [Ayinde et al., 2008] and the present experimental study it is found that the flow inside a vertical channel acts as 2D. It is therefore chosen to investigate this assumption by the numerical solution as well.

The results of the 3D study is taken in height 1.75 m. Three horizontal velocity and temperature distributions are compared; in the center and ± 10 cm from the center, see figures 7.18 and 7.19

on the next page.

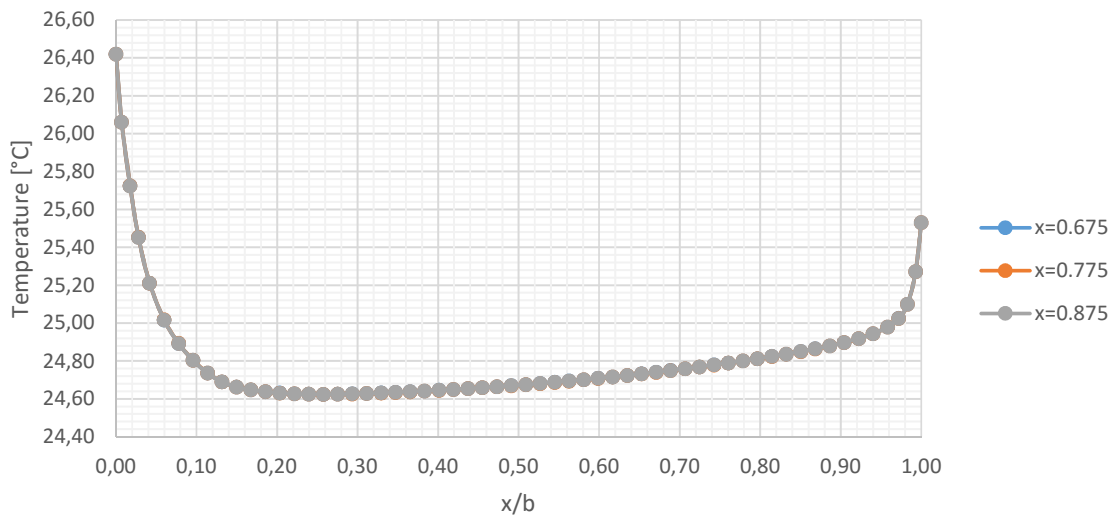


Figure 7.18. Horizontal temperature profile in height 1.75 m in the center and $> pm$ 10 cm.

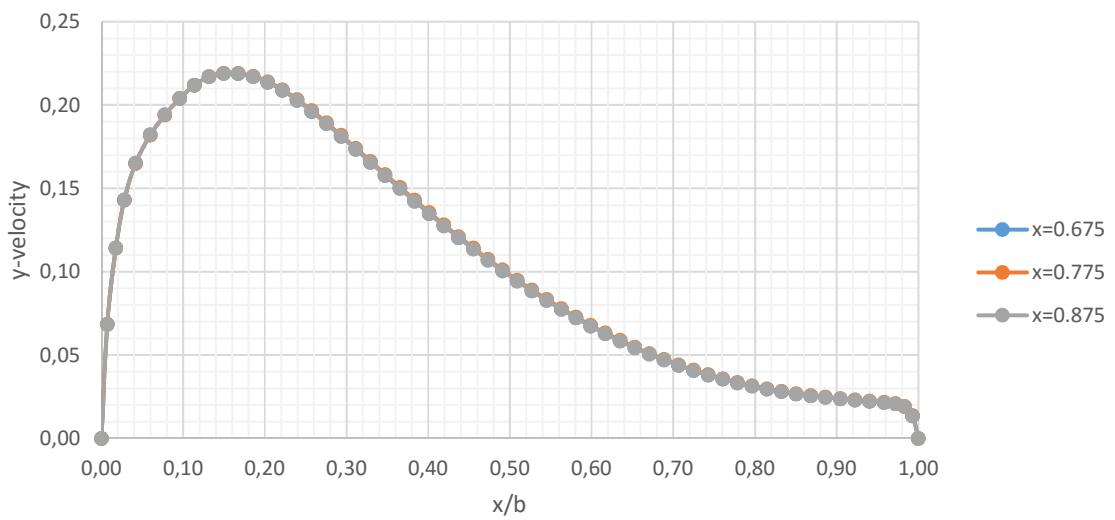


Figure 7.19. Horizontal velocity profile in height 1.75 m in the center and $> pm$ 10 cm.

From these two graphs it can be concluded that the flow is also 2D in the numerical model.

Conclusion

The turbulent natural convection flow regime inside a vertical parallel-plate channel with one heated surface was studied and analyzed in the present work. The objective of the study was especially to find more information about recirculating flow and an effort was being done in order to estimate when the recirculation appeared by experimental work.

During the literature study two main types of recirculating flow was found; Extreme recirculation that was appearing in the entire channel when one wall was subjected to temperatures higher than the other. In this case the air moved upstream close to the heated wall and in a reversed direction close to the colder wall. The other case showed smaller regions of recirculation flow. This could appear several places in the channel at the same time and also accompanied by the extreme recirculation. The presence of those two types of flow was found when the buoyancy forces were strong and the air flow rate was low. It was therefore found to be related to the dimensionless parameters Rayleigh number, Reynolds number and Gr/Re^2 -ratio in both appearance and penetration length. Vertical velocity profiles was also found to be an indication of recirculation flow that might have deformation if recirculation is appearing due to mixing of the air. The literature study proved that recirculation is a possibility and not just an assumption for turbulent natural convection.

Experimental work was conducted on a test facility made as a vertical parallel-plate channel that could resemble a DSF. One wall was made of an aluminum plate with attached heating mats at the back that could supply heat, the other wall was made of glass. The channel width was set to 0.40 m and the height was 3.03 m resulting in an aspect ratio of 7.5. The inlet and outlet set up was chosen according to lesser disturbance to the natural convection; the air was extracted at the top of the channel by a fan and the inlet was open to the ambient, but had the possibility of being cooled. Measurements of temperature distributions made it possible to analyze the flow pattern. The experimental work covered the modified Rayleigh number $Ra^*(b/H)$ $9.98 \cdot 10^{11}$ to $1.17 \cdot 10^{13}$, which was found to be higher than values obtained in the literature, but it also covered another aspect ratio.

The experimental data has been grouped according to the objective of the analysis and what has been proved in the literature:

- Study the Rayleigh number dependency

- Study the influence of change in ACH

It is worth mentioning that all of the presented tests indicated conditions like extreme recirculation due to the asymmetrically heated walls. By studying the effect of increasing Rayleigh number the flow was observed to be more stable. Indications of regions with recirculation was found in the tests with the lowest Rayleigh number and those implications disappeared as the Rayleigh number increased. The indications were observed due to peaks close to the surfaces and instability in the time-evolution, but also deformations in the vertical temperature profiles. This remark was found not to be in agreement with the observations in the literature, but it was discussed that the global buoyancy driven flow was dominating with high Rayleigh numbers and not allowing local buoyancy forces to drive.

From theory it is known that by increasing the inlet velocity, the forced convection condition will increase. This was also observed in the present study by the low Gr/Re^2 -ratio. Although an effort was being done to not reach a situation with recirculation flow, some implications of flow reversal maintained. I.e. the transient dynamic behavior close to the glass surface, deformation of vertical temperature profiles and peaks fluctuating along the horizontal plane.

All things considered, the experimental study did only imply that recirculation was occurring rather than proved. The high uncertainties regarding the measurements and experimental set up may be the cause of the effects. A more detailed experimental analyze is needed in order to prove the appearance of recirculation.

Furthermore, a numerical solution was studied. The model resembles the test facility and the boundary conditions was chosen according to this. The turbulence model Realizable $k-\epsilon$ was chosen due to the fact that it was found to be acceptable sufficient at predicting recirculation flow. The simulation was conducted in steady state and the mesh contained 5,994,240 cells. The predicted temperatures was found to be in an acceptable limit of less than 10 %. Although the same air flow pattern with air heated up along the heated wall and reversed direction at the colder wall was not achieved, the model was said to be validated.

8.1 Future Work

The study of turbulent natural convection in vertical parallel-plate channel has many applications seen from an engineering point of view. An example is the flow inside a DSF. DSFs are especially designed to increase the use of natural ventilation, and since the experimental set up in fact was mechanically ventilated, a future study regarding the applicability of the experimental results from a natural ventilation perspective would decrease the limitations of when the observed flow structure happens.

In the literature study it was found that the appearance of recirculation flow was dependent on the aspect ratio of the channel and an investigation of this problem would further improve the study.

Limitations regarding the measurements concerns measurement errors, lack of measurements and lack of other measurement techniques. Velocity measurements could either confirm or dismiss the indications found from the temperature distributions.

Another problem found in the present experimental work was that the flow was found

oscillating from 0.5 cm to 1 cm, then found steady 2 cm from the surface and again dynamic 4 cm from the surface. This phenomenon was found in almost every test. It is not clear why in fact this is happening, but it seems to be consistent with all the tests implicating that it might be a measurement error.

At last, although the numerical model was validated, a further improvement and investigation of the model would enhance the validation, i.e. an effort should be done in order to capture the extreme recirculation.



Bibliography

- Ansys, Inc.** Ansys, Inc. *Ansys Fluent Help File*.
- Ayinde, Said, og Habib, 2008.** Taofeek F. Ayinde, Syed A. M. Said, og Mohammed A. Habib. *Turbulent Natural Convection Flow in a Vertical Channel with Anti-Symmetric Heating*. *Heat Mass Transfer*, 44, 1207–1216, 2008.
- Badr, Habib, Anwar, Ben-Mansour, og Said, 2006.** H. M. Badr, M. A. Habib, S. Anwar, R. Ben-Mansour, og S. A. M. Said. *Turbulent natural convection in vertical parallel-plate channels*. *Heat and Mass Transfer*, 43(3), 73–84, 2006.
- Baldinelli, 2009.** G. Baldinelli. *Double skin façades for warm climate regions: Analysis of a solution with an integrated movable shading system*. *Building and Environment*, 44(6), 1107–1118, 2009.
- Dantect Dynamics, 2008.** Dantect Dynamics. *Measurement Principles of LDA*. URL: <http://www.dantecdynamics.com/measurement-principles-of-lda>, 2008. Downloaded: 15-06-2015.
- Eckert og Jackson, 1950.** E. R. G. Eckert og Thomas W. Jackson. *Analysis of Turbulent Free-Convection Boundary Layer on Flat Plate*. NACA, 2207, 1–22, 1950.
- Gau, Yih, og Aung, 1992.** C. Gau, K. A. Yih, og W. Aung. *Reversed flow structure and heat transfer measurements for buoyancy-assisted convection in a heated vertical duct*. *Journal of Heat Transfer*, 114, 928–935, 1992.
- Habib, Said, Ahmed, og Asghar, 2002.** M. A. Habib, S.A.M. Said, S.A. Ahmed, og A. Asghar. *Velocity Characteristics of Turbulent Natural Convection in Symmetrically and Asymmetrically Heated Vertical Channels*. *Experimental Thermal and Fluid Science*, 26, 77–87, 2002.
- Heiselberg og Sandberg, 1990.** Per Kvols Heiselberg og Mats Sandberg. *Convection from a Slender Cylinder in a Ventilated Room*. *Indoor Environmental Technology* No 5, R9044, 1–20, 1990.

- Incopera og Dewitt, 2011.** Frank Incopera og David Dewitt. *Fundamental of Heat and Mass Transfer*. ISBN: 978-0470-50197-9, 7th edition. John Wiley and Sons, 2011.
- Jiru, Tao, og Haghghat, 2011.** Teshome Edae Jiru, Yong-X Tao, og Fariborz Haghghat. *Airflow and heat transfer in double skin facades*. Energy and Buildings, 43(10), 2760–2766, 2011.
- Larsen, 2008.** Olena Kalyanova Larsen. *Double-Skin Facade - Modelling and Experimental Investigations of Thermal Performance*, 2008.
- Marcondes, Melo, og Gurgel, 2006.** F. Marcondes, V. S. Melo, og J. M. Gurgel. *Numerical analysis of natural convection in parallel, convergent, and divergent open-ended channels*. International Journal of Numerical Methods for Heat and Fluid Flow, 16(3), 304–323, 2006.
- Ospir, Popa, Chereches, Polidori, og Fohanno, 2012.** Dan Ospir, Catalin Popa, Cristian Chereches, Guillaume Polidori, og Stephane Fohanno. *Flow visualization of natural convection in a vertical channel with asymmetric heating*. International Communications in Heat and Mass Transfer, 39, 486–493, 2012.
- Pasut og Carli, 2012.** Wilmer Pasut og Michele De Carli. *Evaluation of various CFD modelling strategies in predicting airflow and temperature in a naturally ventilated double skin façade*. Applied Thermal Engineering, 37, 267–274, 2012.
- Poirazis, 2004.** Harris Poirazis. *Double Skin Façades for Office Buildings*, 2004.
- Safer, Woloszyn, og Roux, 2005.** Nassim Safer, Monika Woloszyn, og Jean Jacques Roux. *Three-dimensional simulation with a CFD tool of the airflow phenomena in single floor double-skin facade equipped with a venetian blind*. Solar Energy, 79(2), 193–203, 2005.
- Sealens, 2002.** Dirk Sealens. *Energy performance assessment of single storey multiple-skin facades*, 2002.
- Sparrow, Chrysler, og Azevedo, 1984.** E. M. Sparrow, G. M. Chrysler, og L. F. Azevedo. *Observed flow reversals and measured-predicted nusselt numbers for natural convection in a one-sided heated vertical channel*. Journal of Heat Transfer, 106, 325–332, 1984.
- Tu, Yeoh, og Liu, 2013.** Jiyuan Tu, Guan-Heng Yeoh, og Chaoqun Liu. *Computational Fluid Dynamics - A Practical Approach*. ISBN: 978-0-08-098243-4, 2nd edition. Elsevier Ltd., 2013.
- Yilmaz og Gilchrist, 2007.** Turgut Yilmaz og Alastair Gilchrist. *Temperature and Velocity Field Characteristics of Turbulent Natural Convection in a Vertical Parallel-Plate Channel with Asymmetric Heating*. Heat Mass Transfer, 43, 707–719, 2007.
- Zollner, Winter, og Viskanta, 2002.** E. Zollner, E. R. F. Winter, og R. Viskanta. *Experimental studies of combined heat transfer in turbulent mixed convection fluid flows in double-skin-façades*. Heat and Mass Transfer, 45, 4401–4408, 2002.

Wide Cavity

The following graphs shows the calculated $Ra^{-1/4}$. For all tests it is found to be lower than $\frac{b}{H} = 0.13$, and it is concluded that the cavity acts as wide.

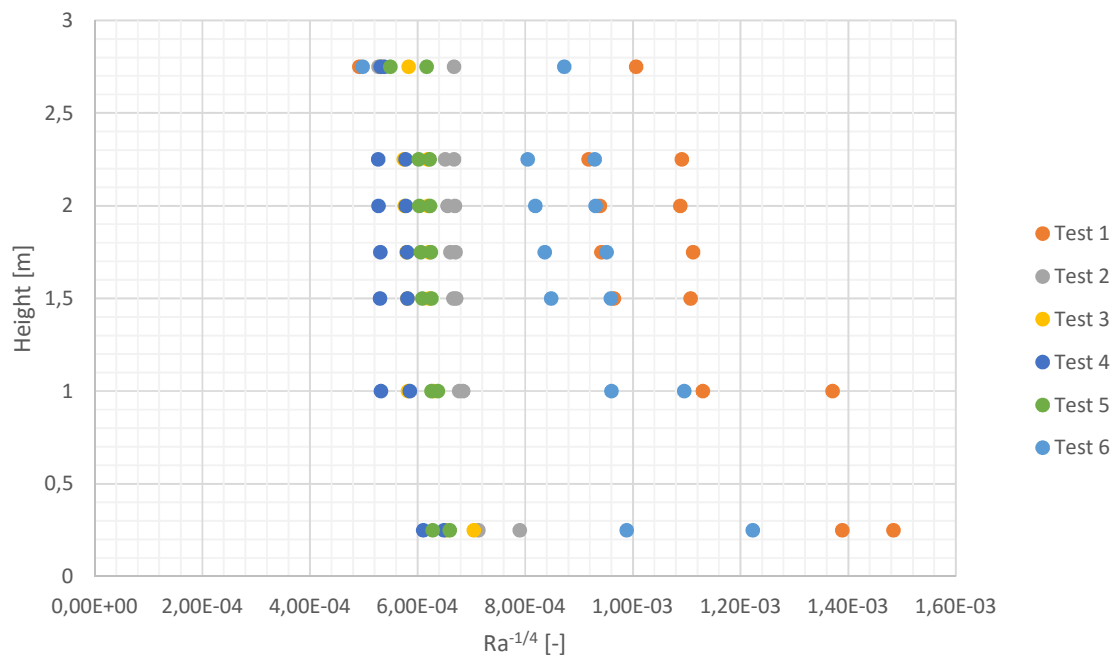


Figure A.1. Calculated $Ra^{-1/4}$ numbers for each test according to height.

B

Positions of Thermocouples

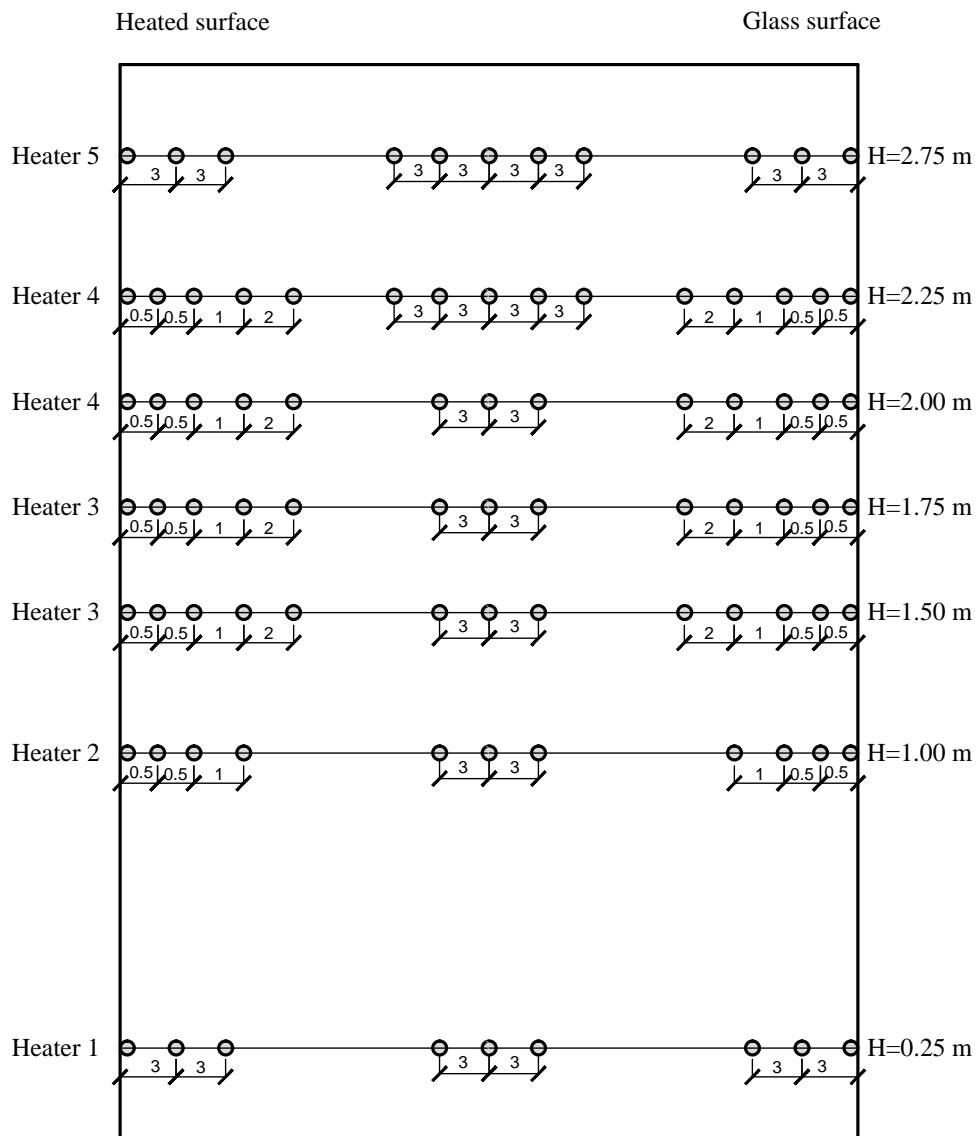


Figure B.1. Positions of thermocouples in channel.

C

2D Thermal Pictures

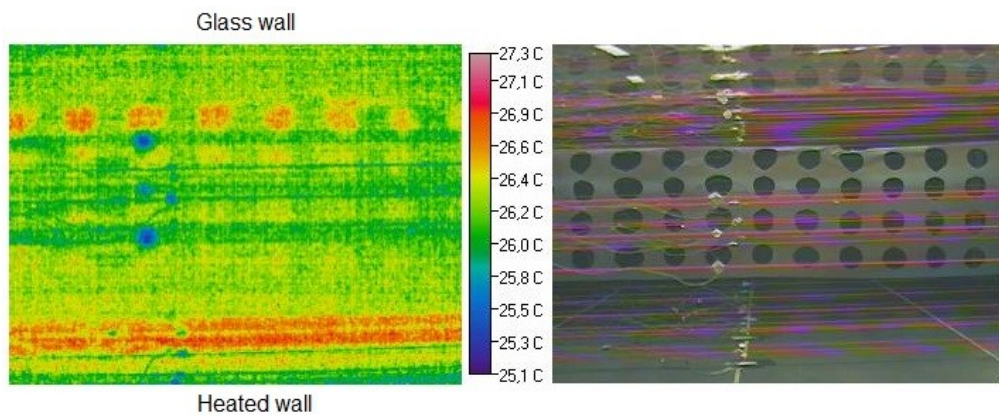


Figure C.1. Picture caputered in the center of the channel.

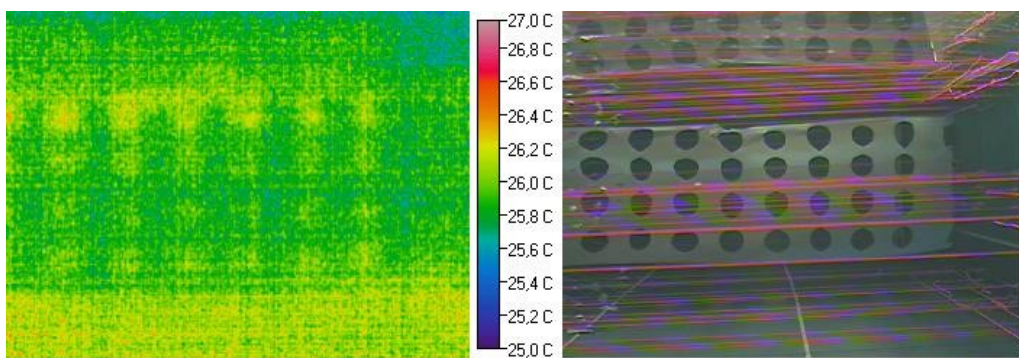


Figure C.2. Picture caputered to the right.

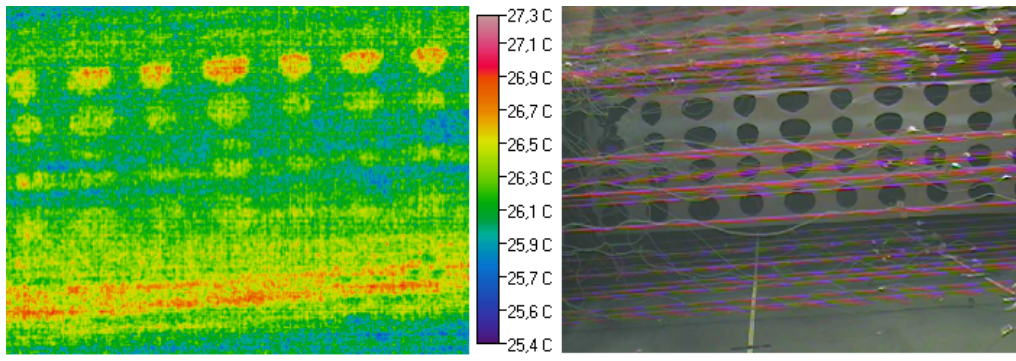


Figure C.3. Picture caputered to the left.

Test 1

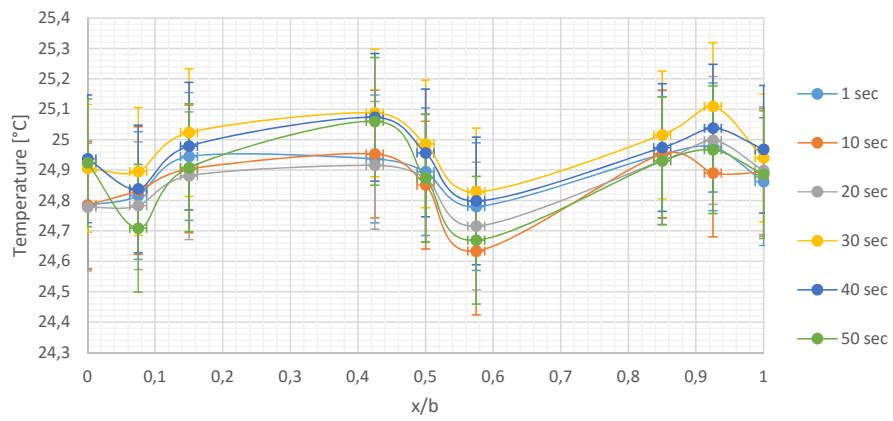


Figure D.1. Stability in horizontal temperature profile in height 0.25 m.

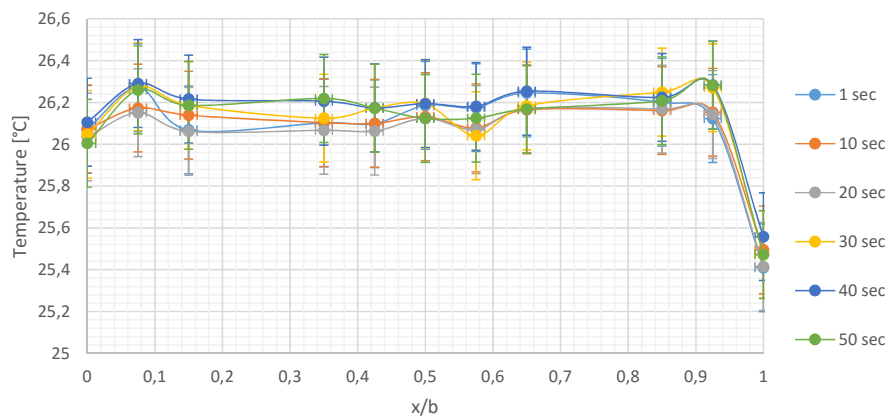


Figure D.2. Stability in horizontal temperature profile in height 2.75 m.

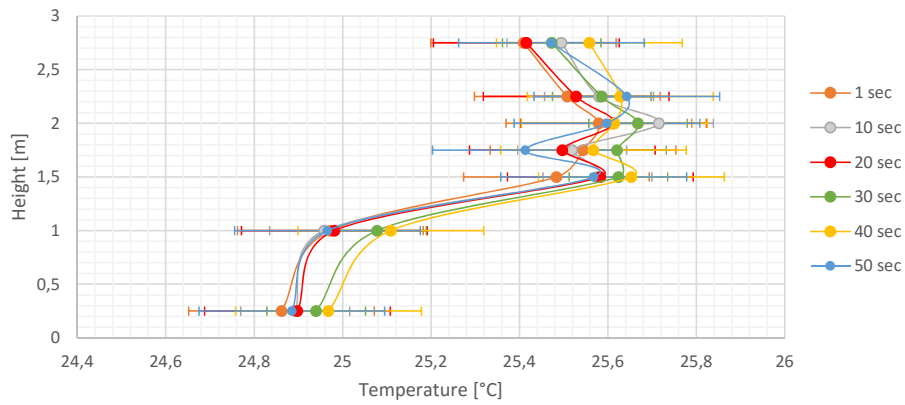


Figure D.3. Stability in vertical temperature profile at the glass surface.

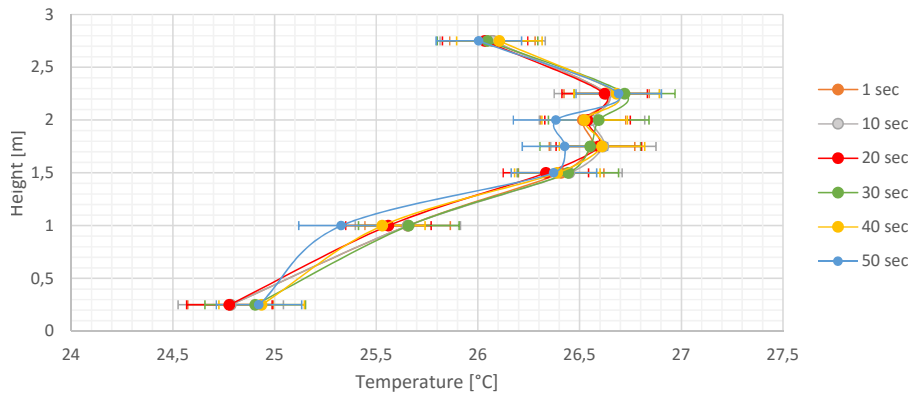


Figure D.4. Stability in vertical temperature profile at the heated surface.

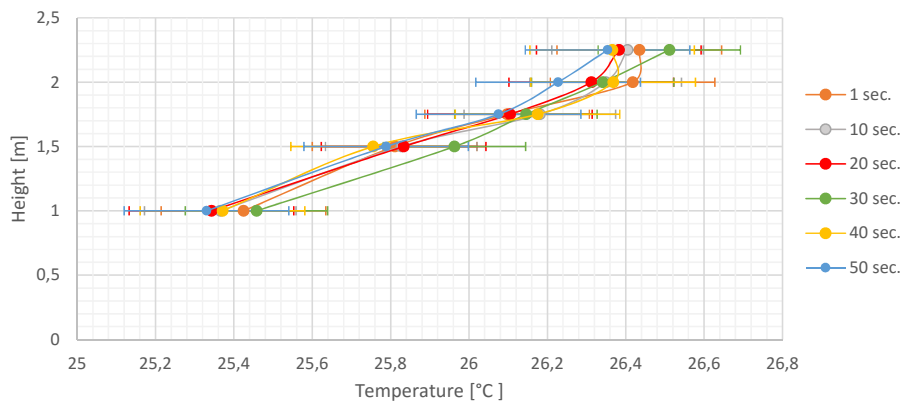


Figure D.5. Stability in vertical temperature profile 0.5 cm from the heated surface.

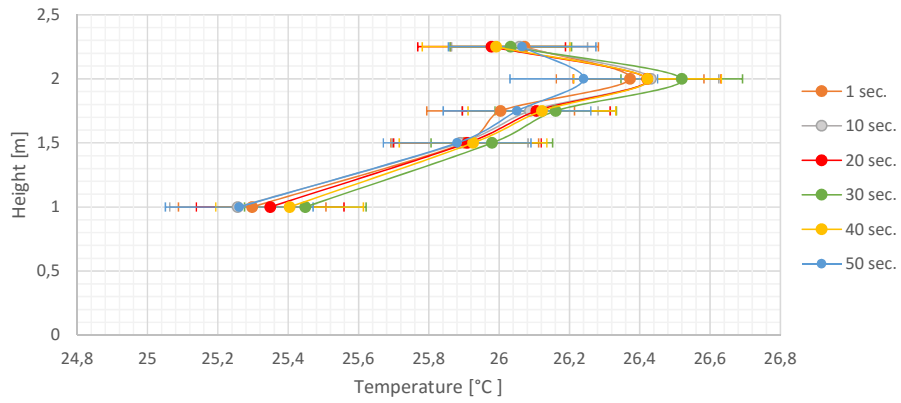


Figure D.6. Stability in vertical temperature profile 1 cm from the heated surface.

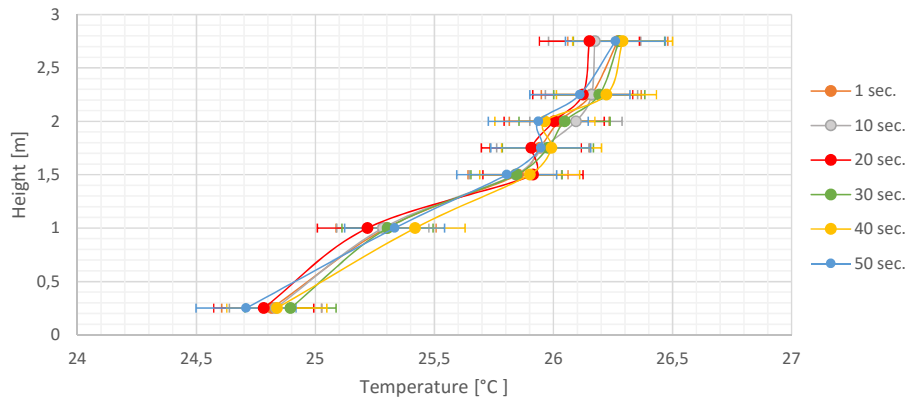


Figure D.7. Stability in vertical temperature profile 2 cm from the heated surface.

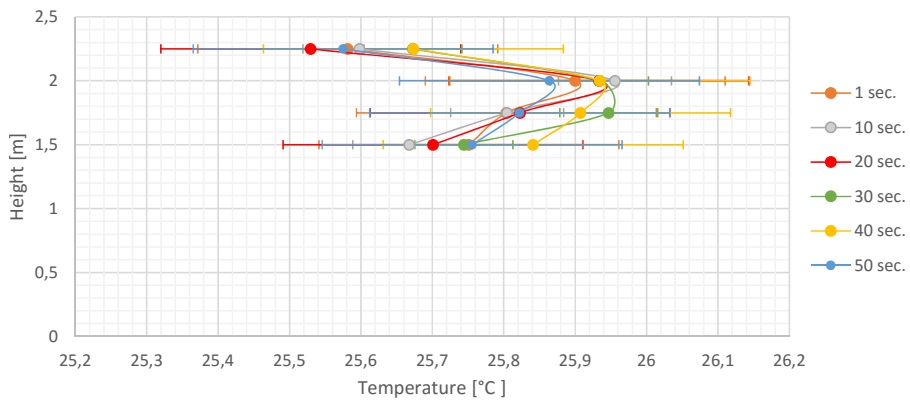


Figure D.8. Stability in vertical temperature profile 4 cm from the heated surface.

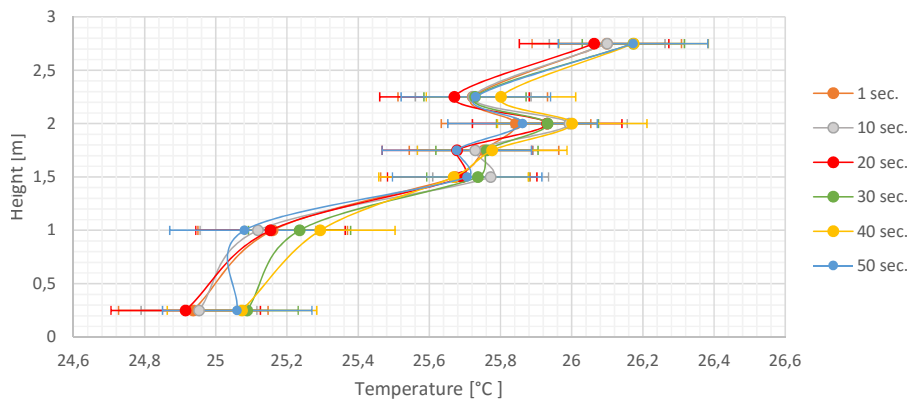


Figure D.9. Stability in vertical temperature profile 17 cm from the heated surface.

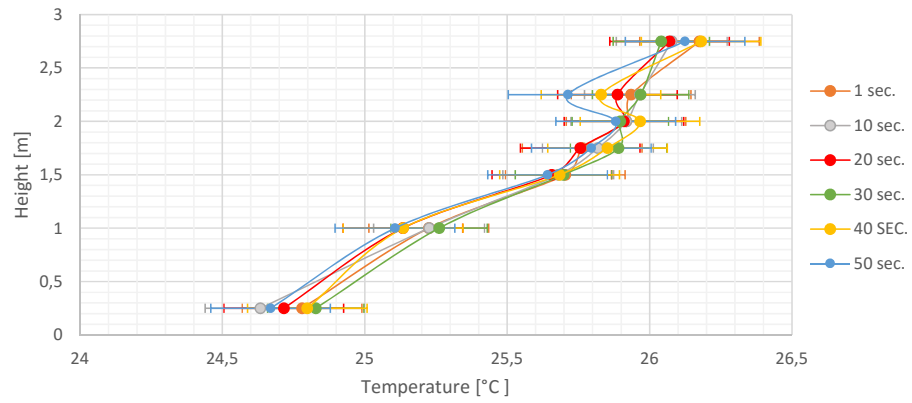


Figure D.10. Stability in vertical temperature profile 17 cm from the glass surface.

Test 2

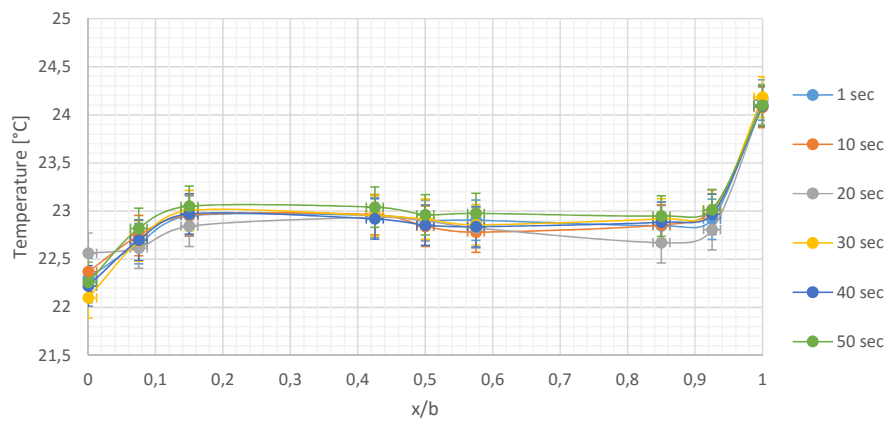


Figure E.1. Stability in horizontal temperature profile in height 0.25 m.

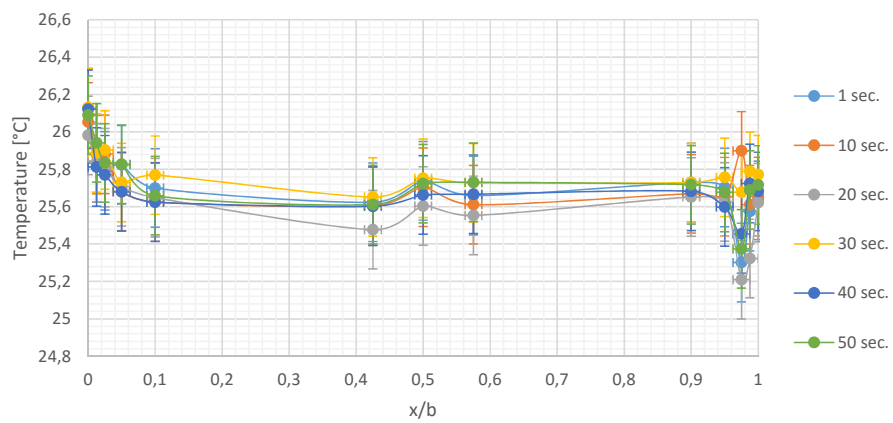


Figure E.2. Stability in horizontal temperature profile in height 1.75 m.

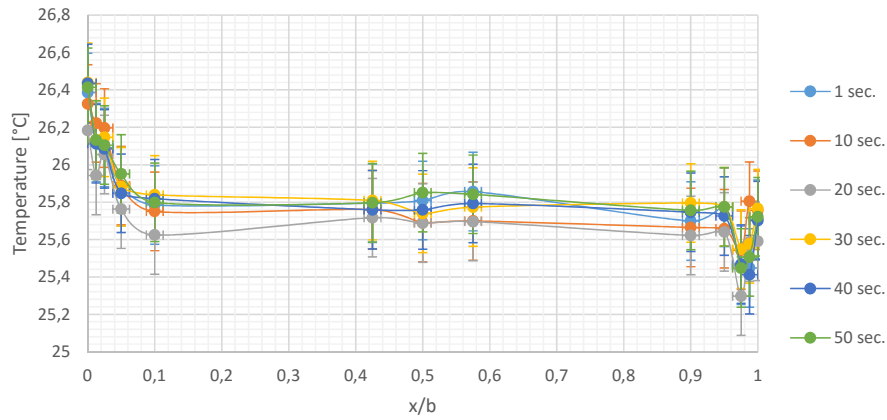


Figure E.3. Stability in horizontal temperature profile in height 2.00 m.

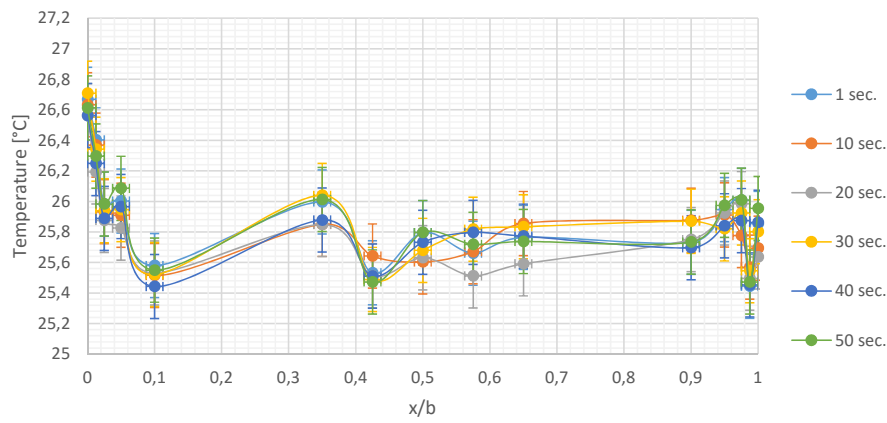


Figure E.4. Stability in horizontal temperature profile in height 2.25 m.

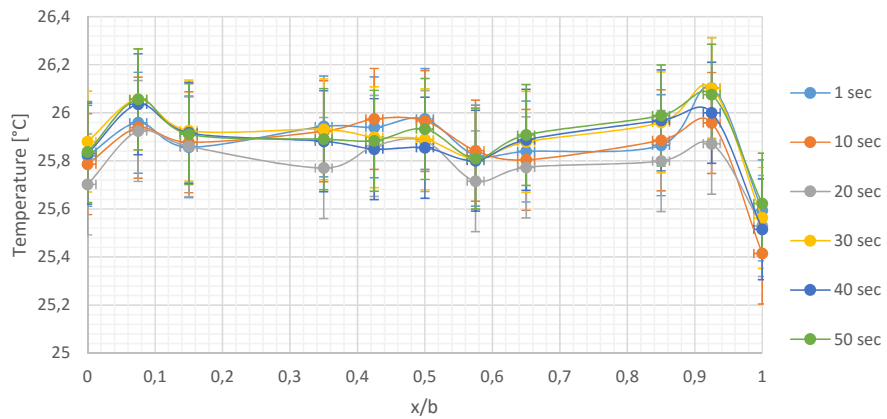


Figure E.5. Stability in horizontal temperature profile in height 2.75 m.

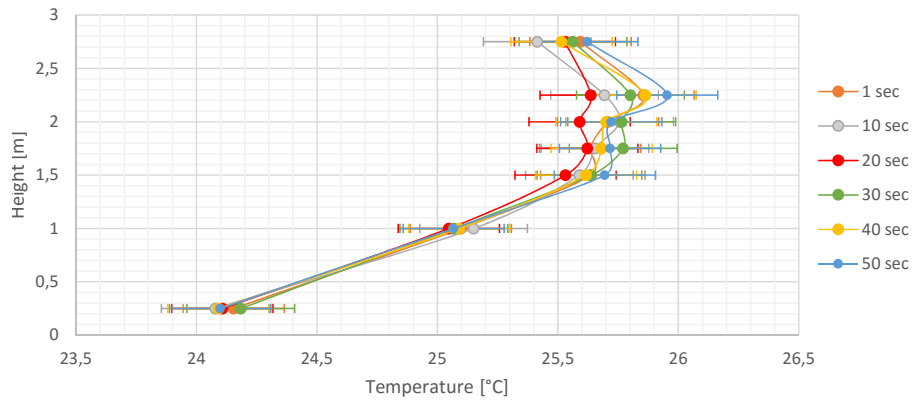


Figure E.6. Stability in vertical temperature profile at the glass surface.

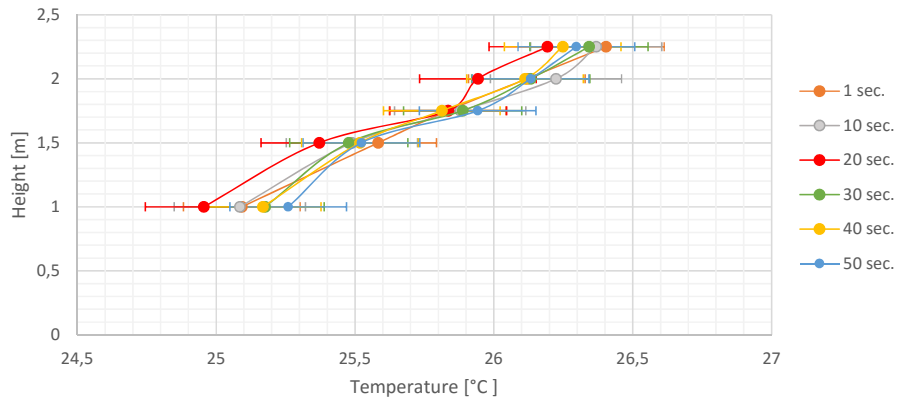


Figure E.7. Stability in vertical temperature profile 0.5 cm from the heated surface.

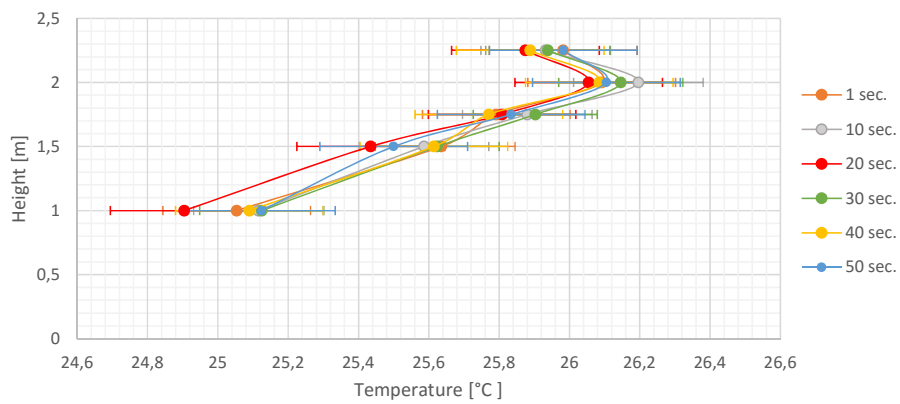


Figure E.8. Stability in vertical temperature profile 1 cm from the heated surface.

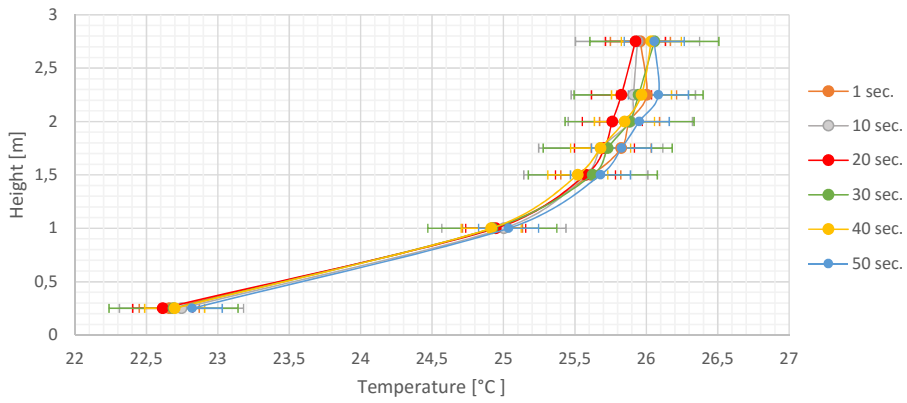


Figure E.9. Stability in vertical temperature profile 2 cm from the heated surface.

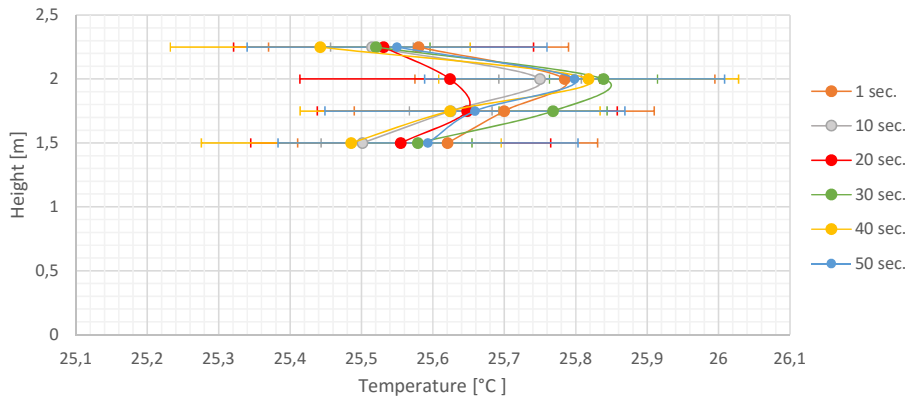


Figure E.10. Stability in vertical temperature profile 4 cm from the heated surface.

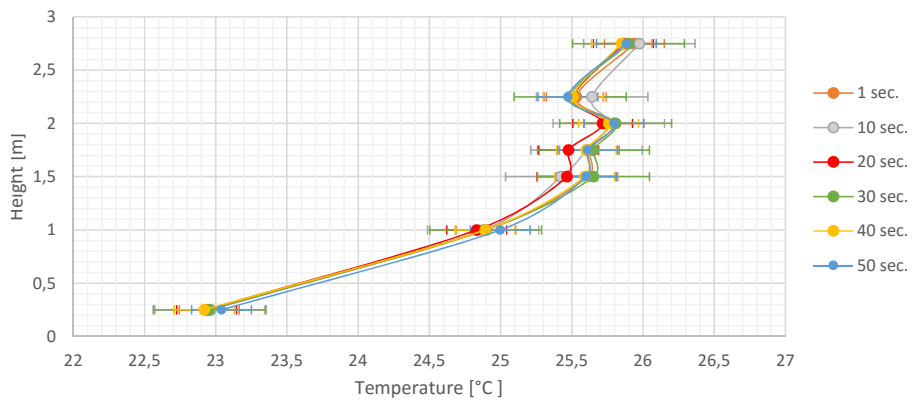


Figure E.11. Stability in vertical temperature profile 17 cm from the heated surface.

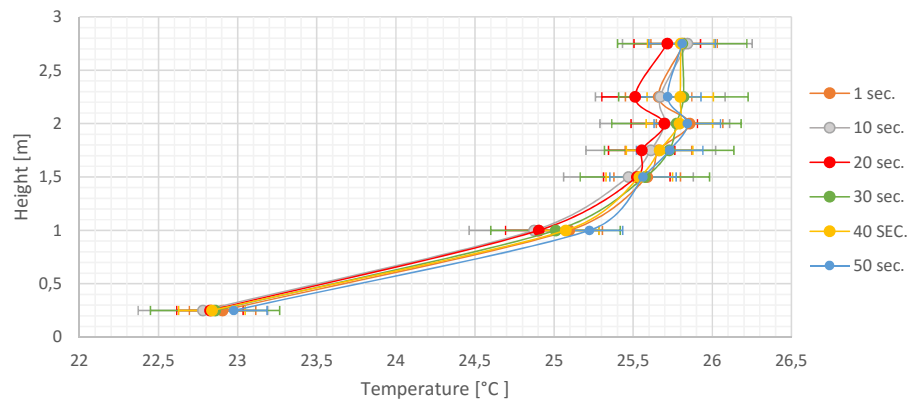


Figure E.12. Stability in vertical temperature profile 17 cm from the glass surface.

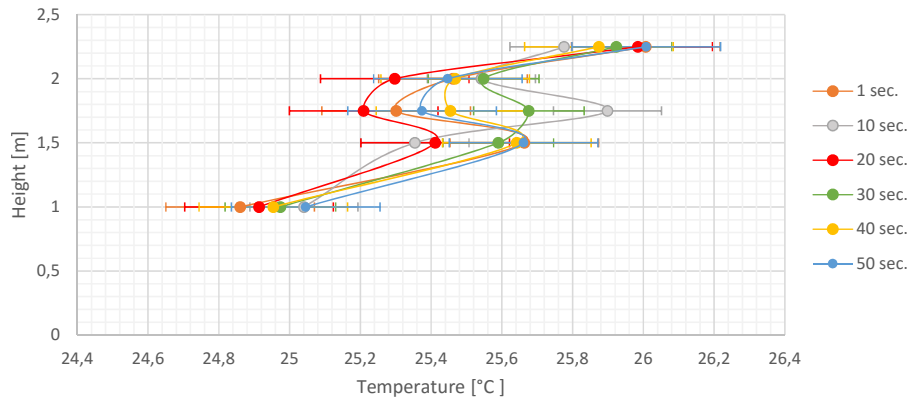


Figure E.13. Stability in vertical temperature profile 1 cm from the glass surface.

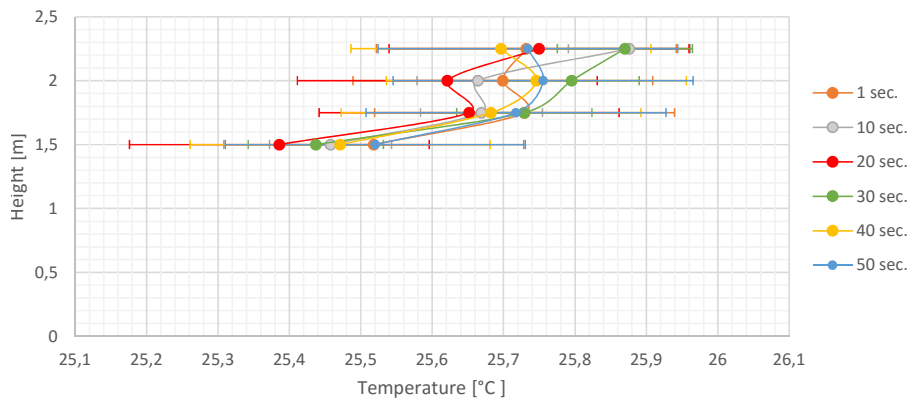


Figure E.14. Stability in vertical temperature profile 4 cm from the glass surface.

Test 3

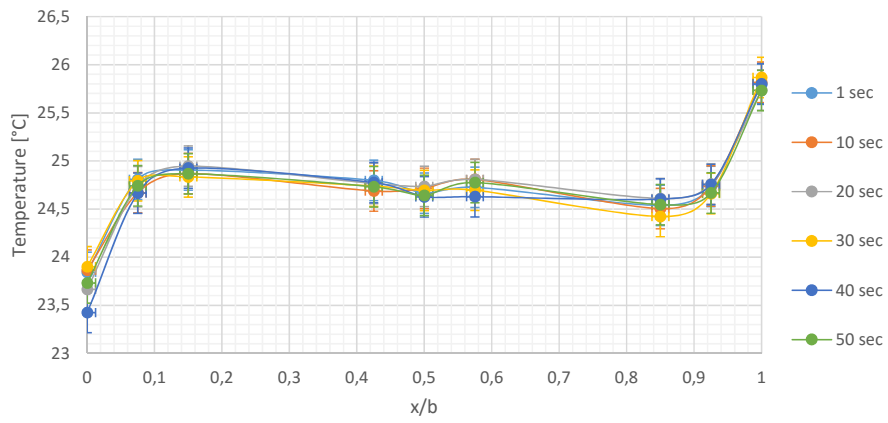


Figure F.1. Stability in horizontal temperature profile in height 0.25 m.

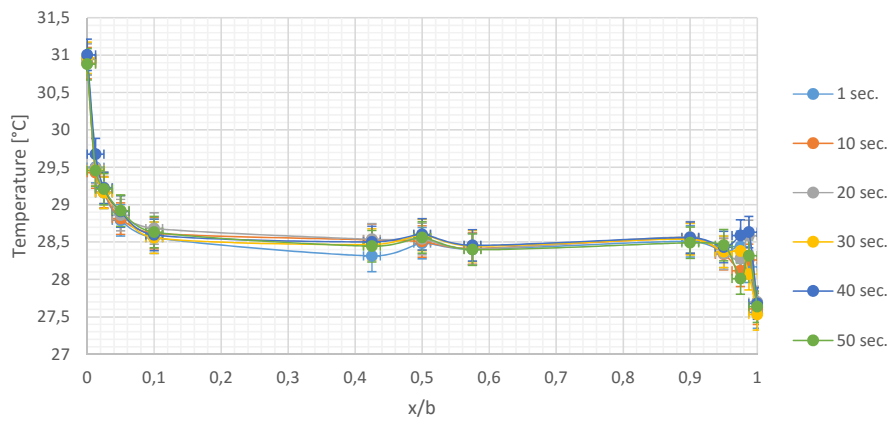


Figure F.2. Stability in horizontal temperature profile in height 1.75 m.

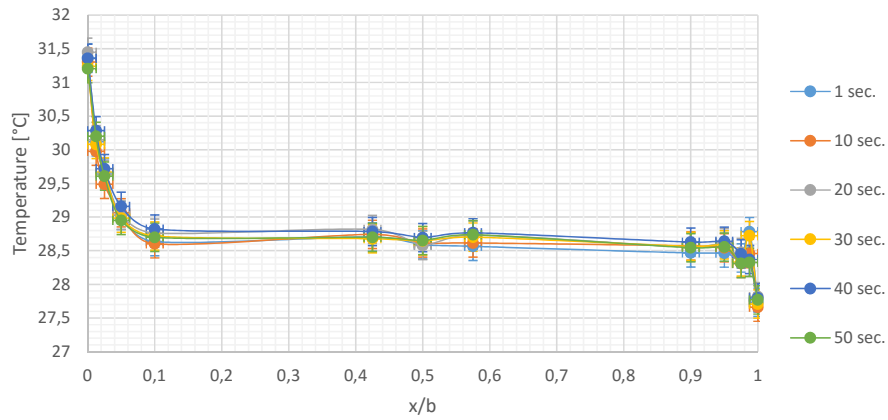


Figure F.3. Stability in horizontal temperature profile in height 2.00 m.

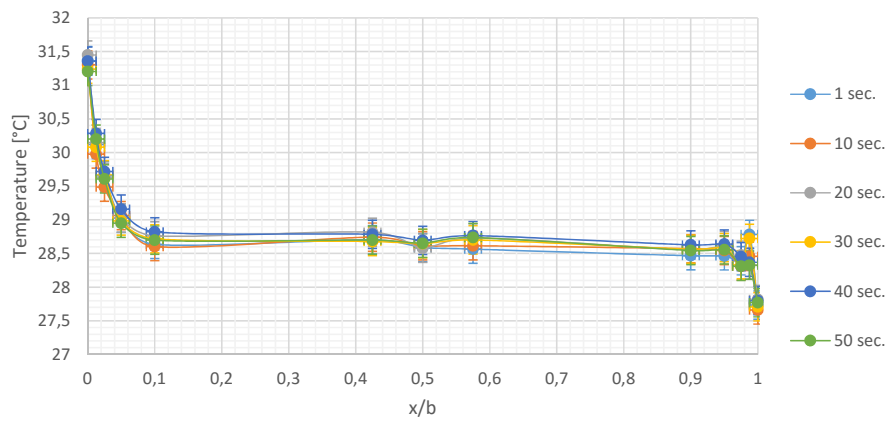


Figure F.4. Stability in horizontal temperature profile in height 2.25 m.

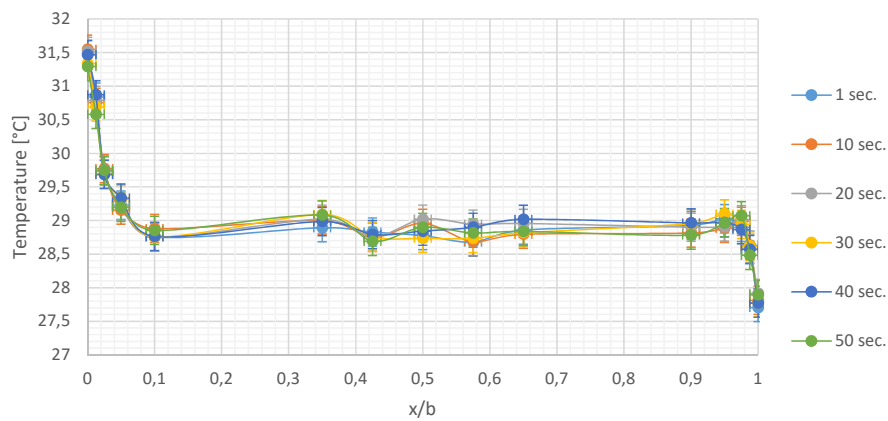


Figure F.5. Stability in horizontal temperature profile in height 2.75 m.

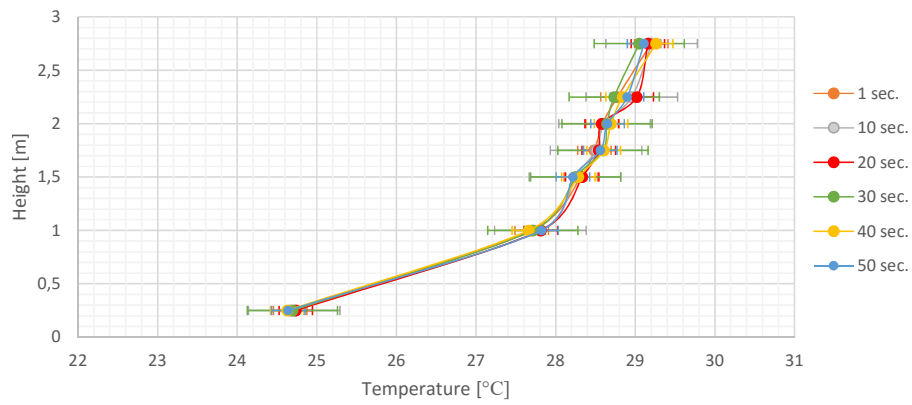


Figure F.6. Stability in vertical temperature profile in the center.

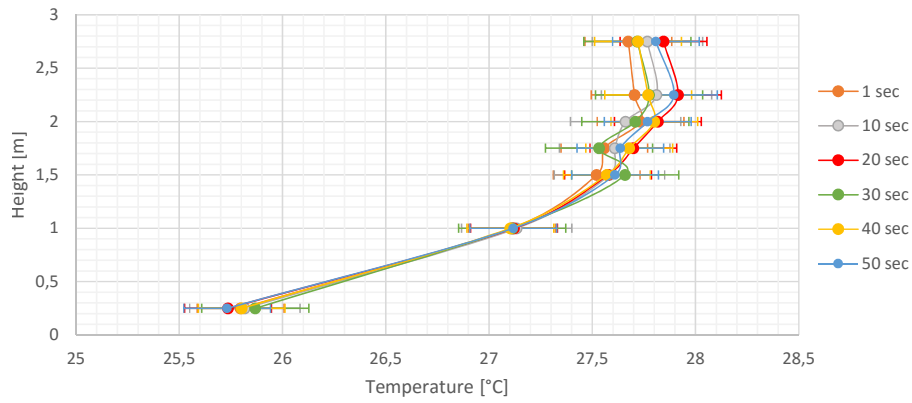


Figure F.7. Stability in vertical temperature profile at the glass surface.

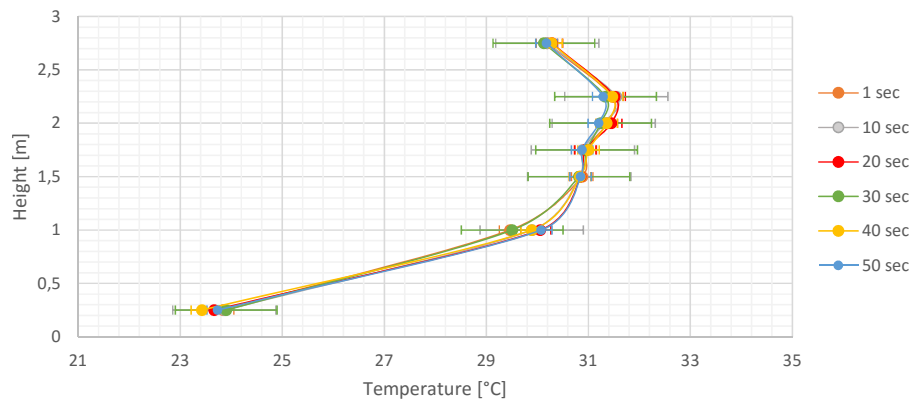


Figure F.8. Stability in vertical temperature profile at the heated surface.

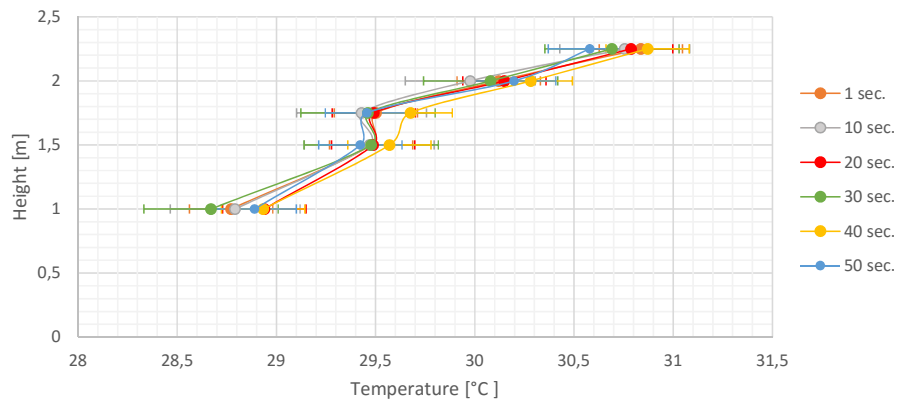


Figure F.9. Stability in vertical temperature profile 0.5 cm from the heated surface.

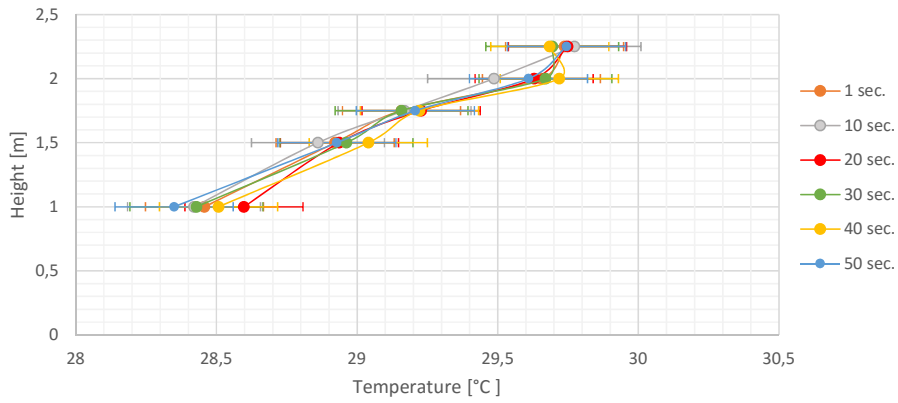


Figure F.10. Stability in vertical temperature profile 1 cm from the heated surface.

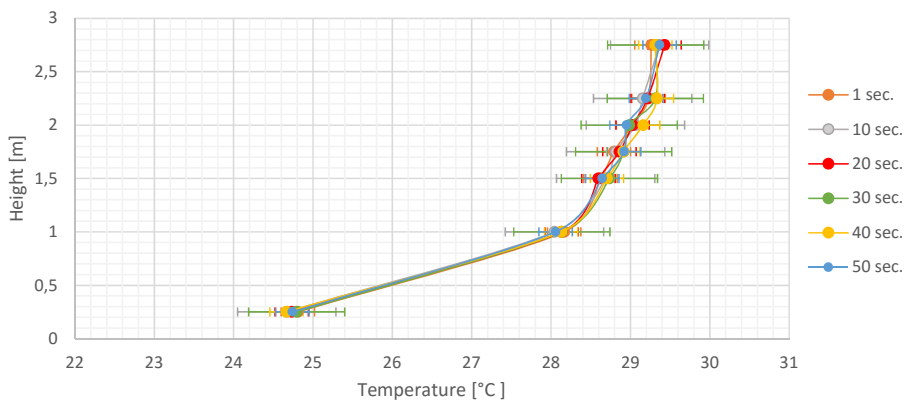


Figure F.11. Stability in vertical temperature profile 2 cm from the heated surface.

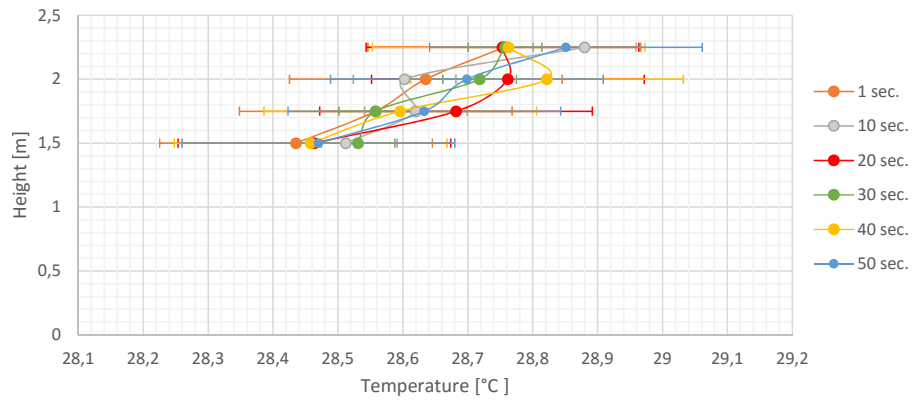


Figure F.12. Stability in vertical temperature profile 4 cm from the heated surface.

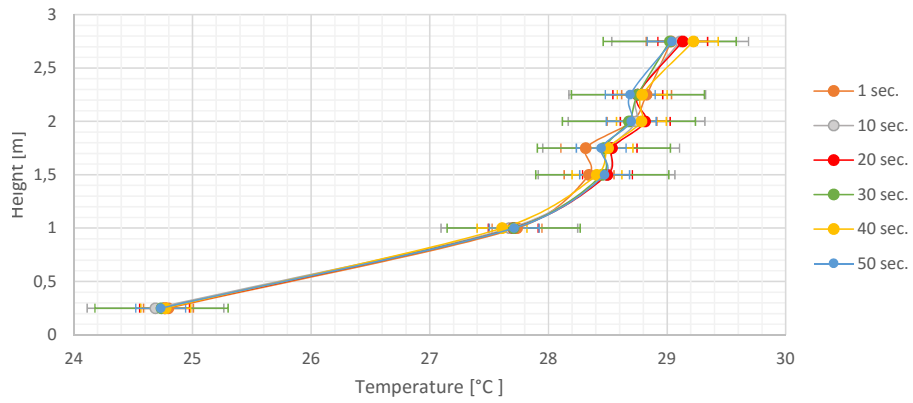


Figure F.13. Stability in vertical temperature profile 17 cm from the heated surface.

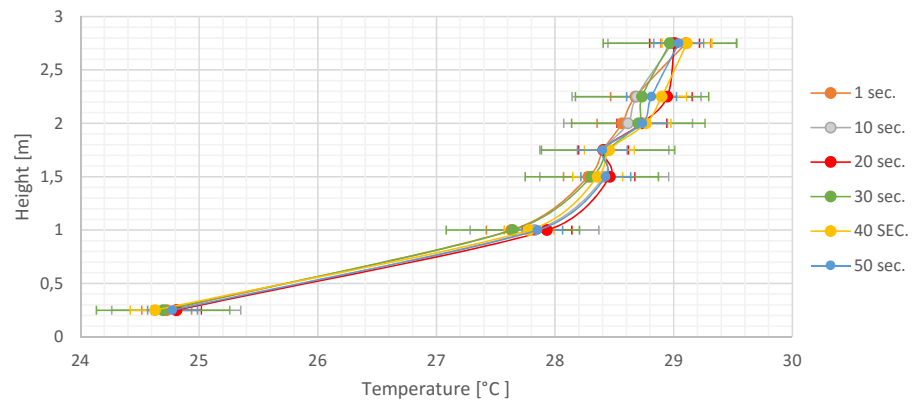


Figure F.14. Stability in vertical temperature profile 17 cm from the glass surface.

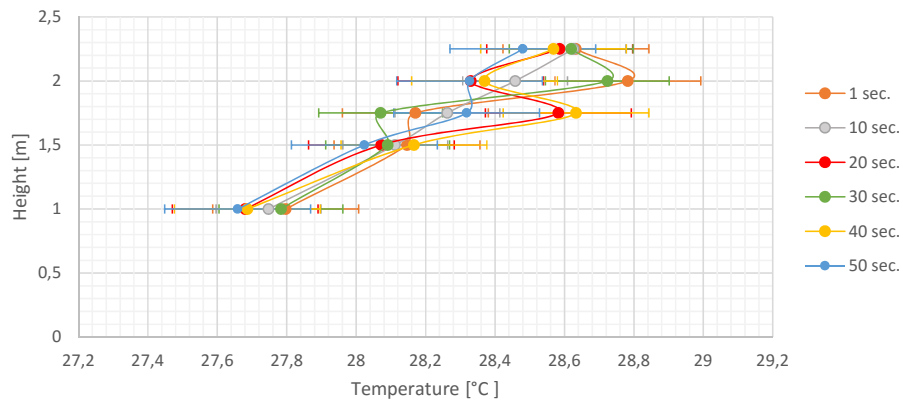


Figure F.15. Stability in vertical temperature profile 0.5 cm from the glass surface.

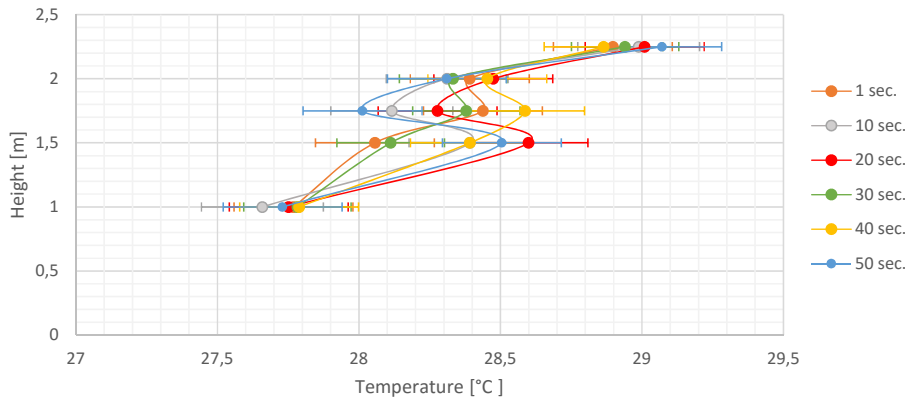


Figure F.16. Stability in vertical temperature profile 1 cm from the glass surface.

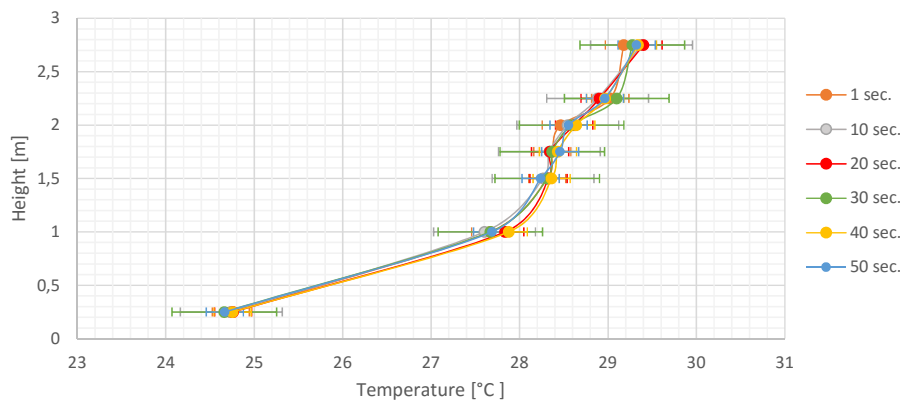


Figure F.17. Stability in vertical temperature profile 2 cm from the glass surface.

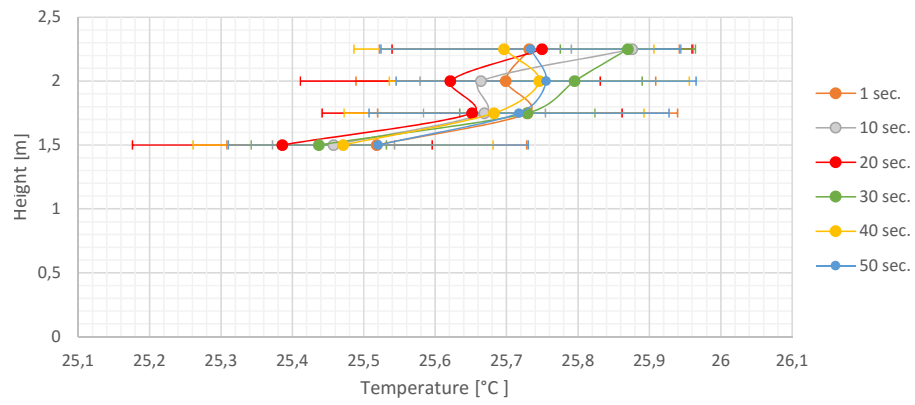


Figure F.18. Stability in vertical temperature profile 4 cm from the glass surface.

Test 4

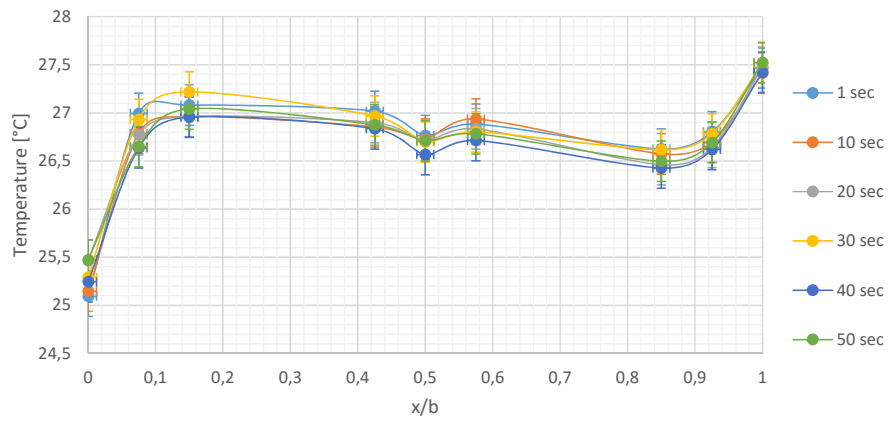


Figure G.1. Stability in horizontal temperature profile in height 0.25 m.

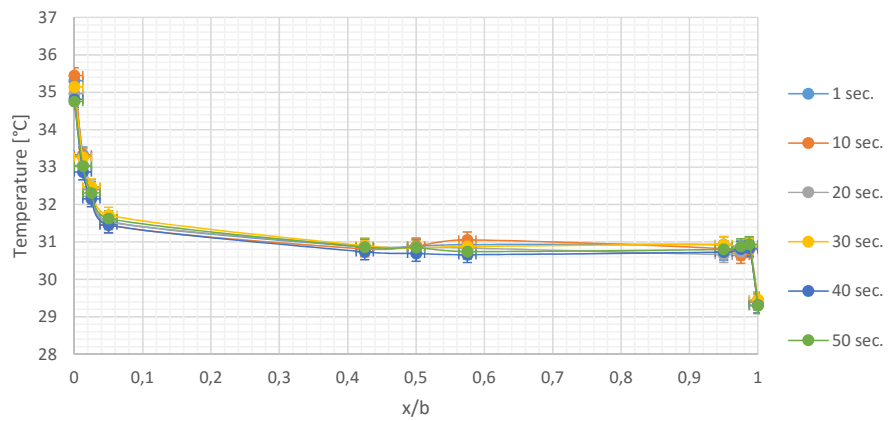


Figure G.2. Stability in horizontal temperature profile in height 1.00 m.

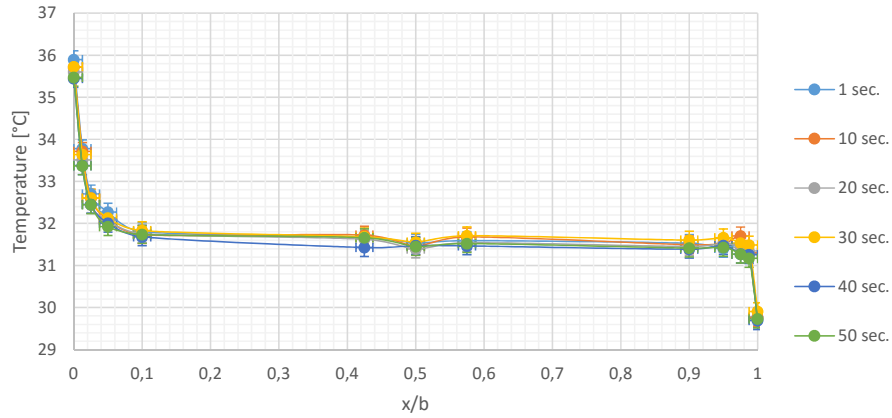


Figure G.3. Stability in horizontal temperature profile in height 1.75 m.

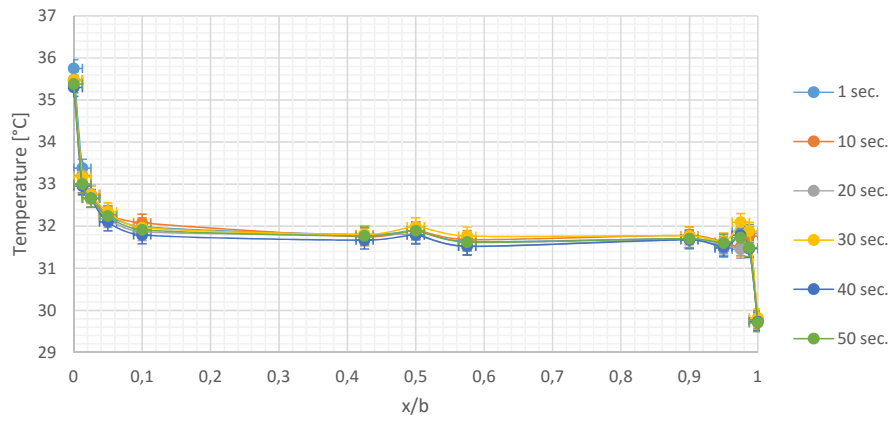


Figure G.4. Stability in horizontal temperature profile in height 2.00 m.

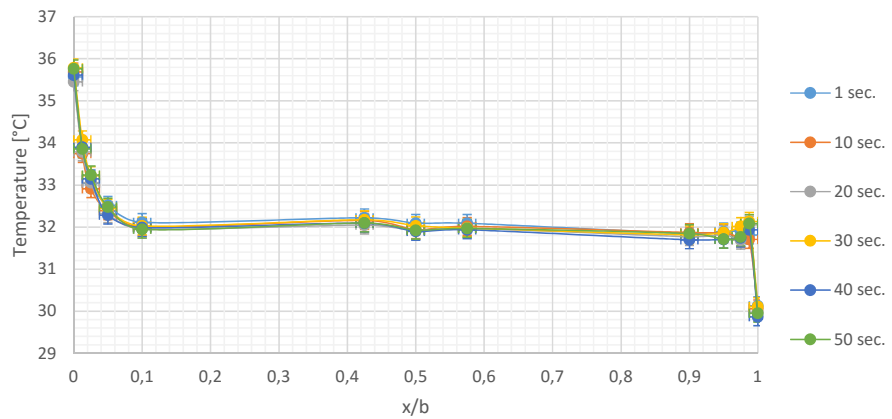


Figure G.5. Stability in horizontal temperature profile in height 2.25 m.

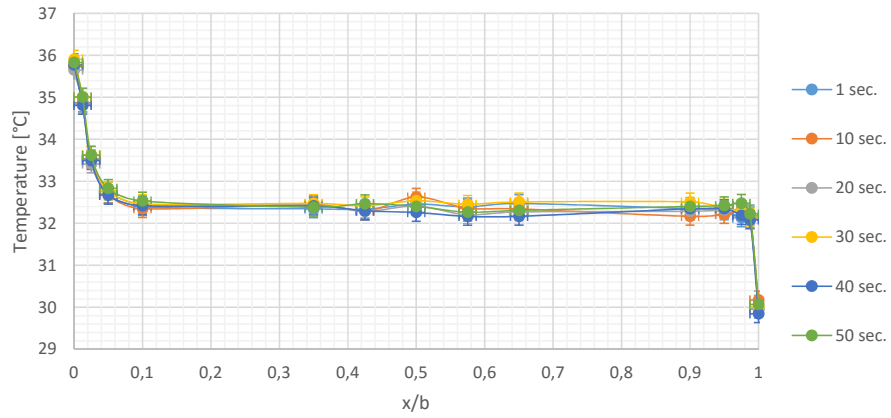


Figure G.6. Stability in horizontal temperature profile in height 2.75 m.

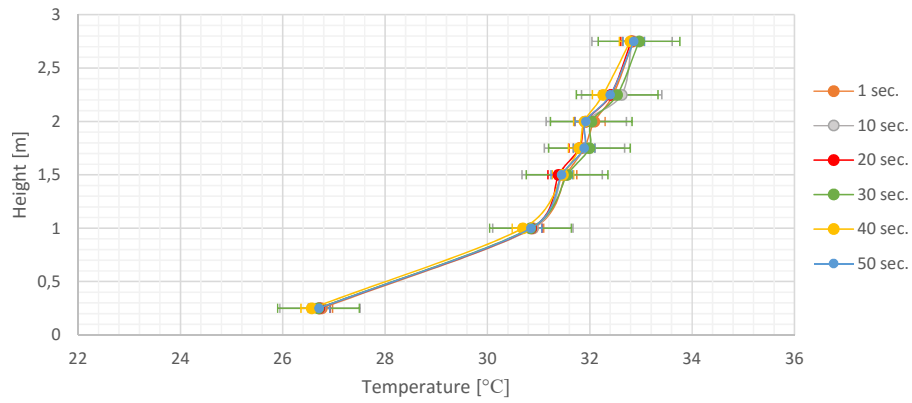


Figure G.7. Stability in vertical temperature profile in the center.

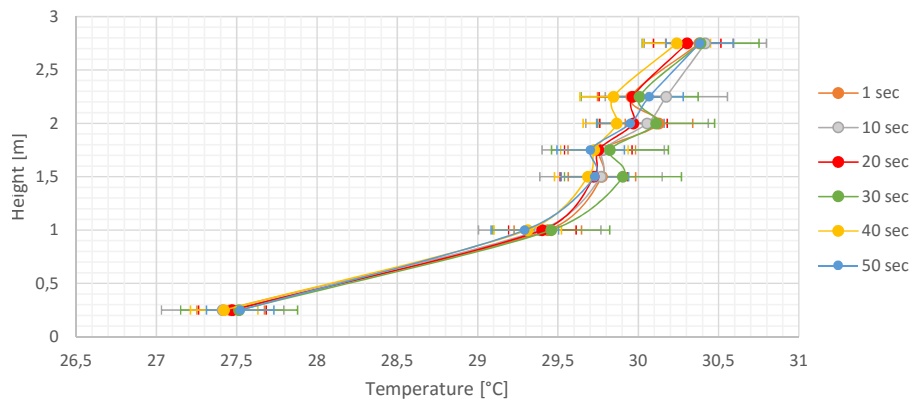


Figure G.8. Stability in vertical temperature profile at the glass surface.

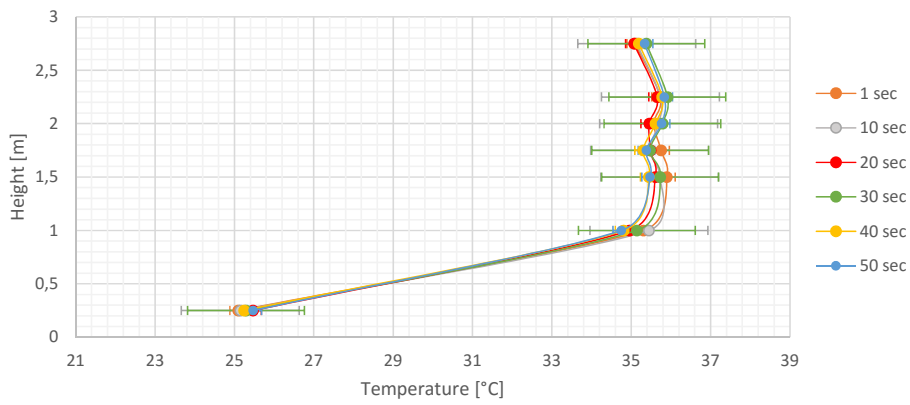


Figure G.9. Stability in vertical temperature profile at the heated surface.

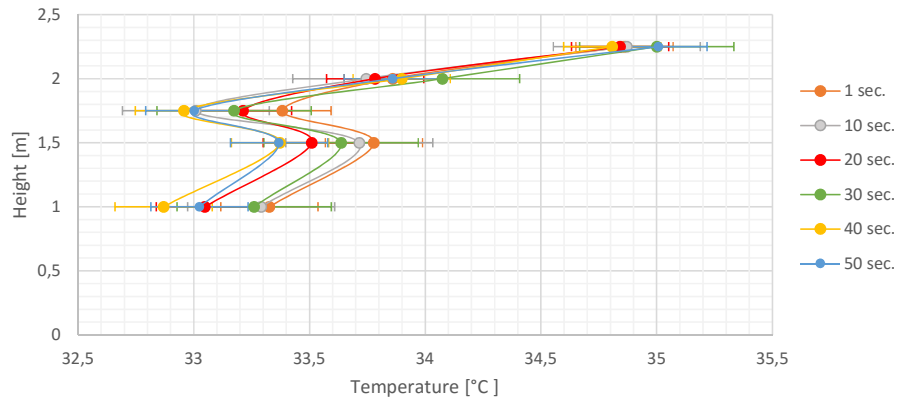


Figure G.10. Stability in vertical temperature profile 0.5 cm from the heated surface.

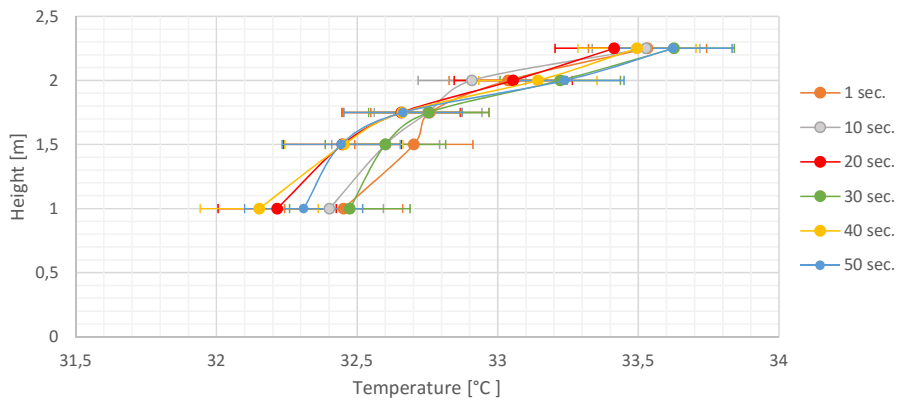


Figure G.11. Stability in vertical temperature profile 1 cm from the heated surface.

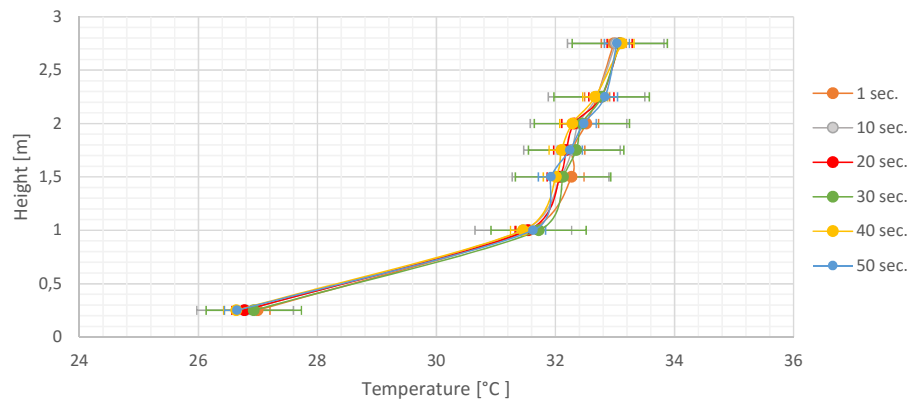


Figure G.12. Stability in vertical temperature profile 2 cm from the heated surface.

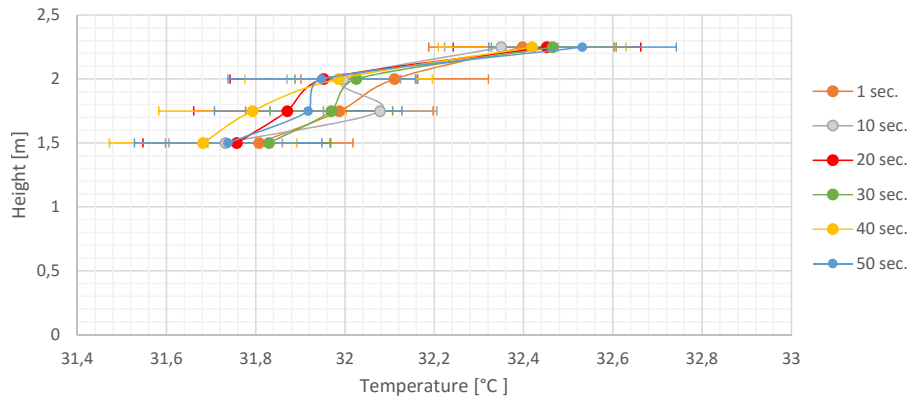


Figure G.13. Stability in vertical temperature profile 4 cm from the heated surface.

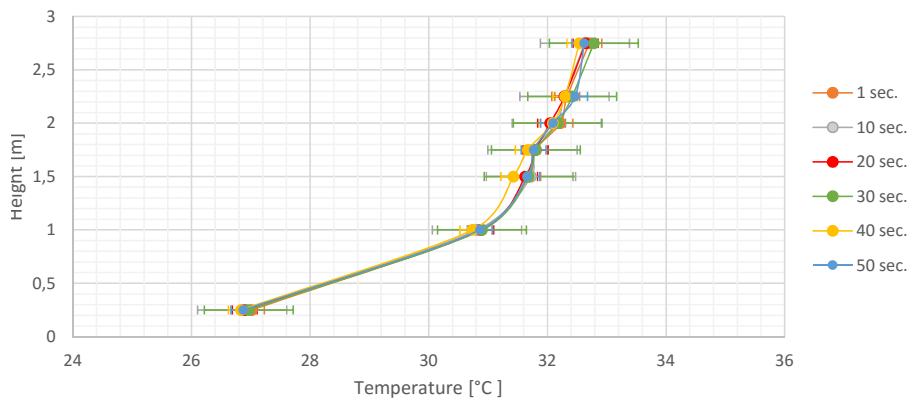


Figure G.14. Stability in vertical temperature profile 17 cm from the heated surface.

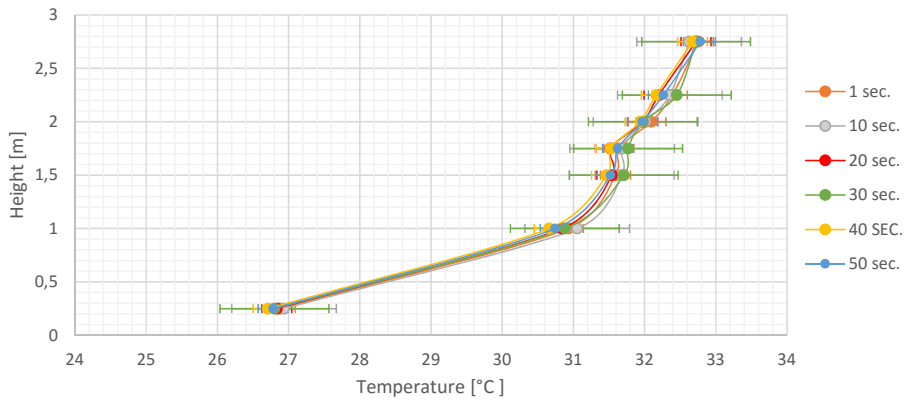


Figure G.15. Stability in vertical temperature profile 17 cm from the glass surface.

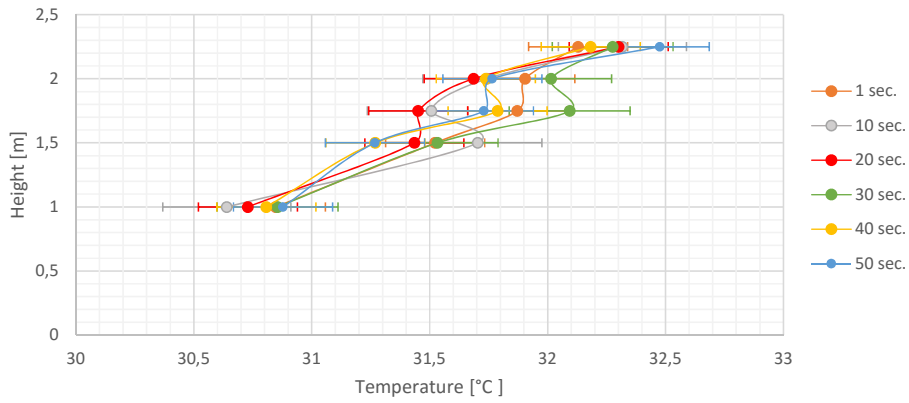


Figure G.16. Stability in vertical temperature profile 1 cm from the glass surface.

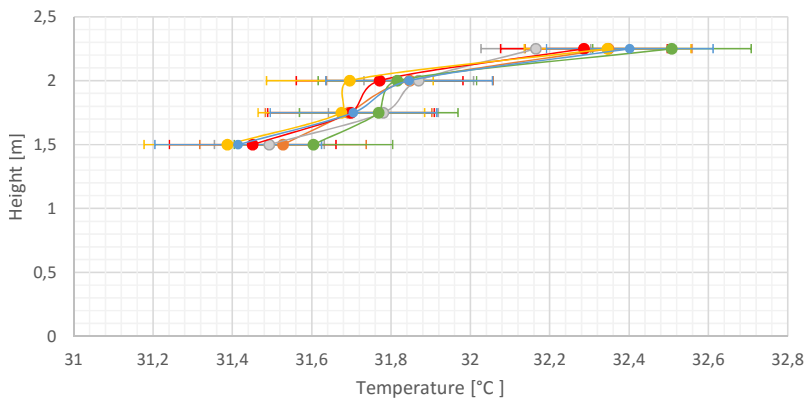


Figure G.17. Stability in vertical temperature profile 4 cm from the glass surface.

Test 5

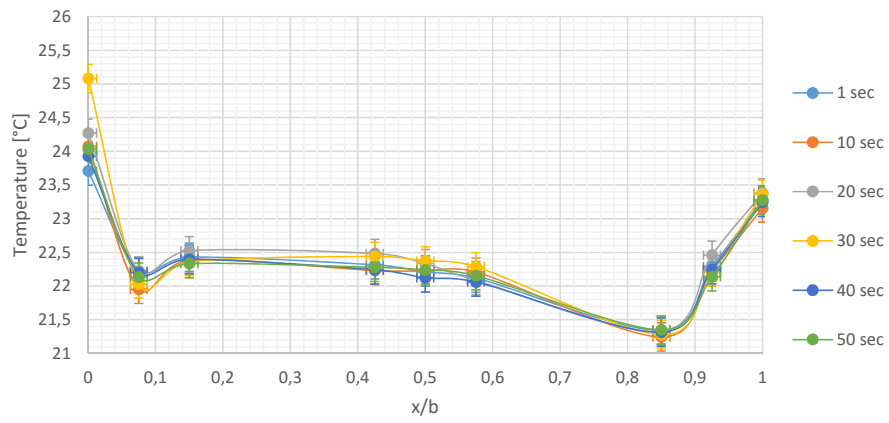


Figure H.1. Stability in horizontal temperature profile in height 0.25 m.

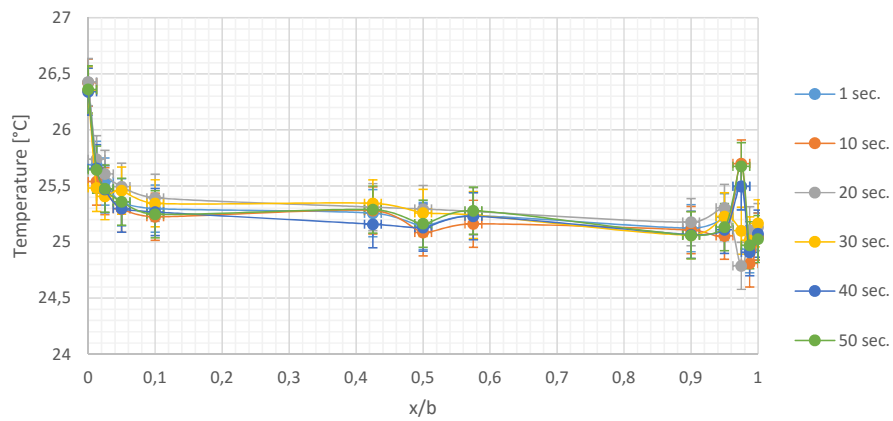


Figure H.2. Stability in horizontal temperature profile in height 1.50 m.

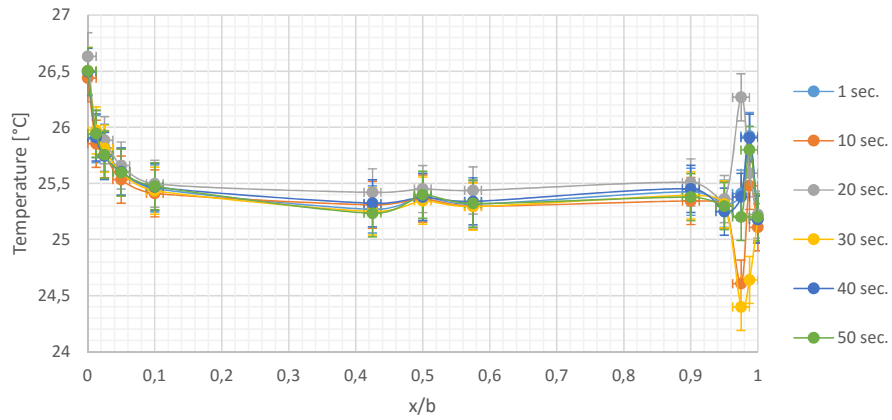


Figure H.3. Stability in horizontal temperature profile in height 1.75 m.

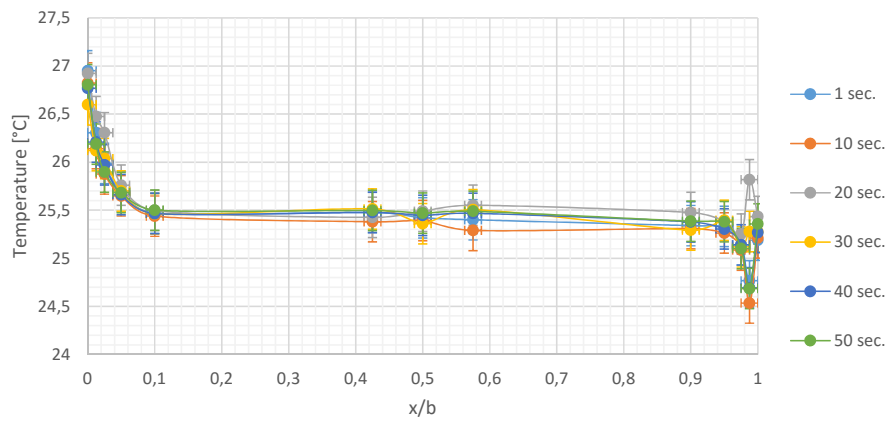


Figure H.4. Stability in horizontal temperature profile in height 2.00 m.

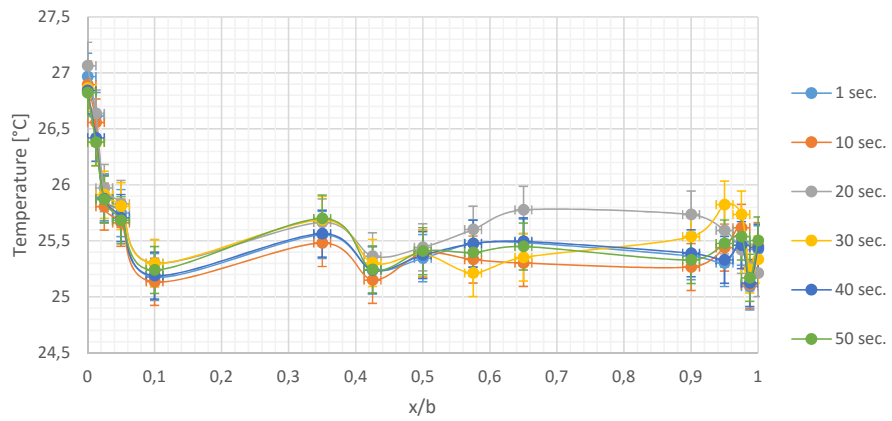


Figure H.5. Stability in horizontal temperature profile in height 2.25 m.

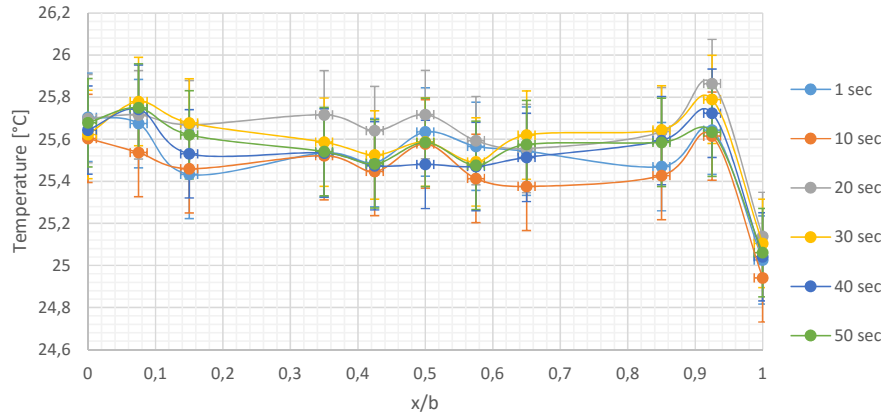


Figure H.6. Stability in horizontal temperature profile in height 2.75 m.

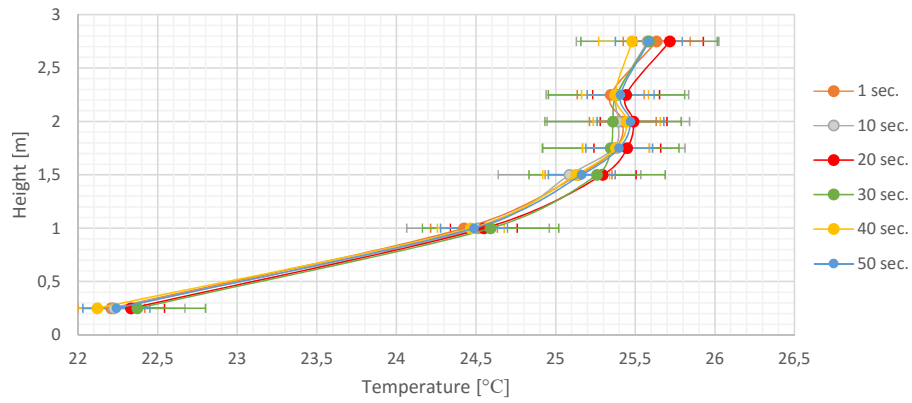


Figure H.7. Stability in vertical temperature profile in the center.

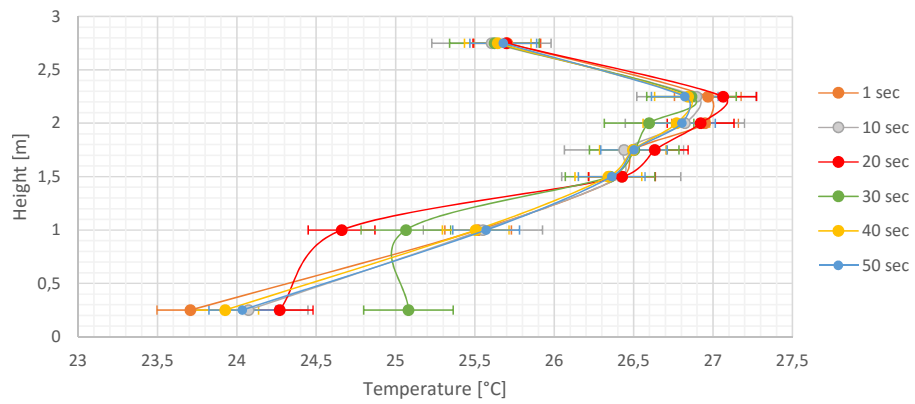


Figure H.8. Stability in vertical temperature profile at the heated surface.

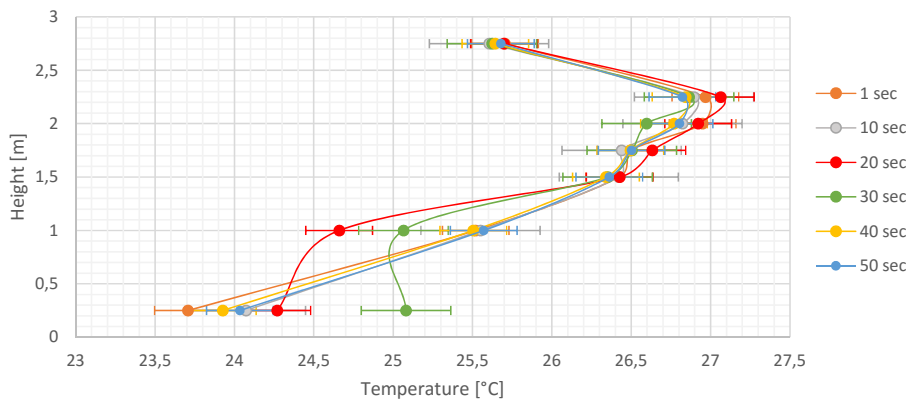


Figure H.9. Stability in vertical temperature profile 0.5 cm from the heated surface.

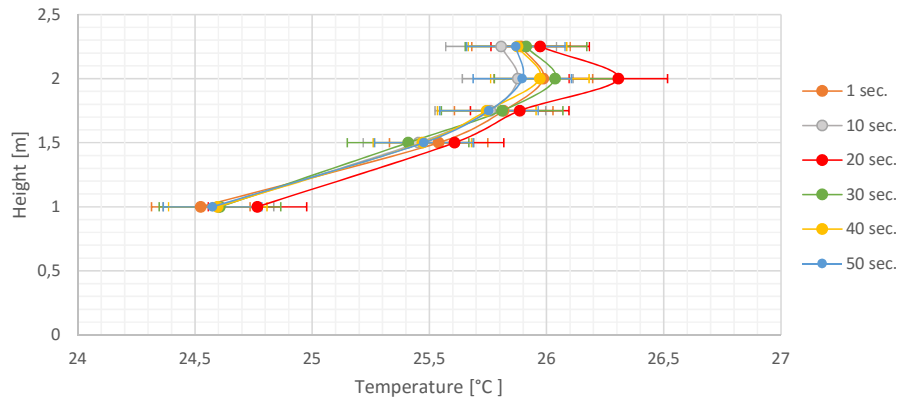


Figure H.10. Stability in vertical temperature profile 1 cm from the heated surface.

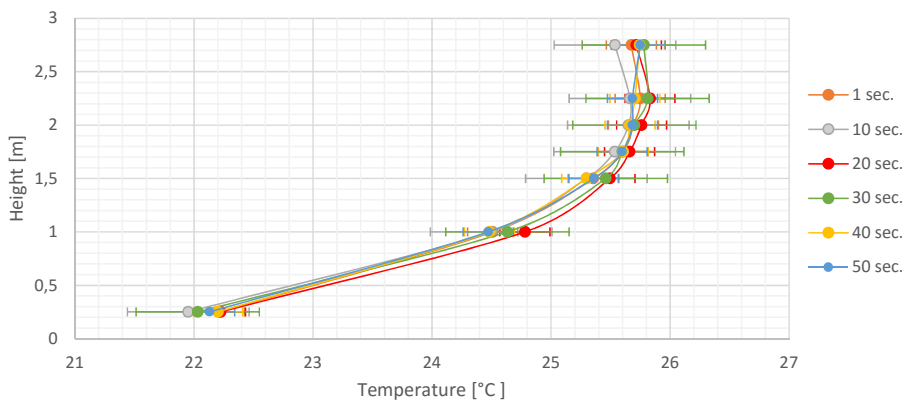


Figure H.11. Stability in vertical temperature profile 2 cm from the heated surface.

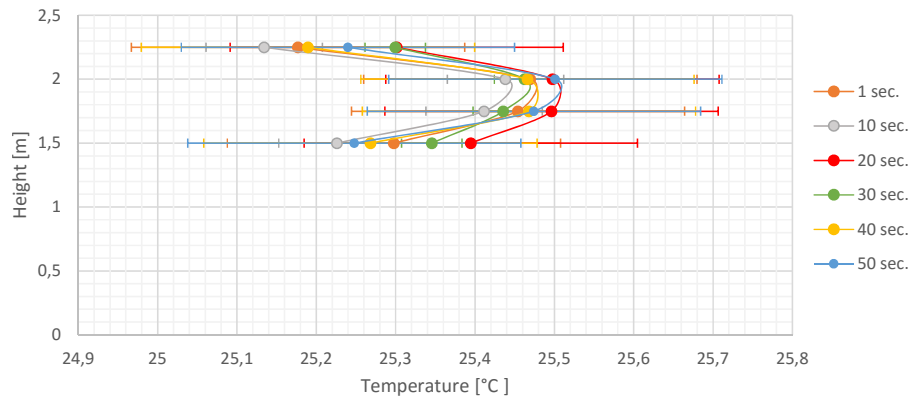


Figure H.12. Stability in vertical temperature profile 4 cm from the heated surface.

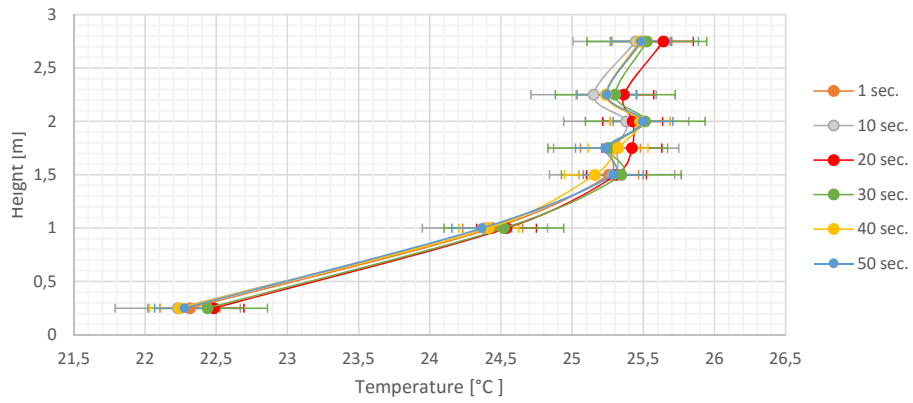


Figure H.13. Stability in vertical temperature profile 17 cm from the heated surface.

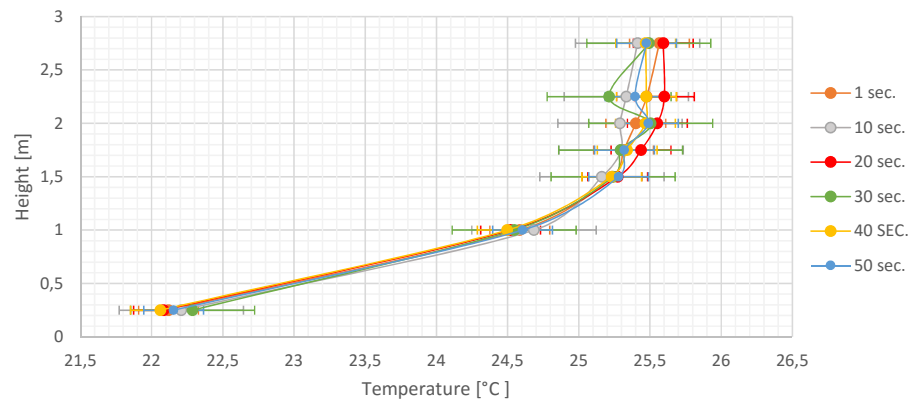


Figure H.14. Stability in vertical temperature profile 17 cm from the glass surface.

Test 6

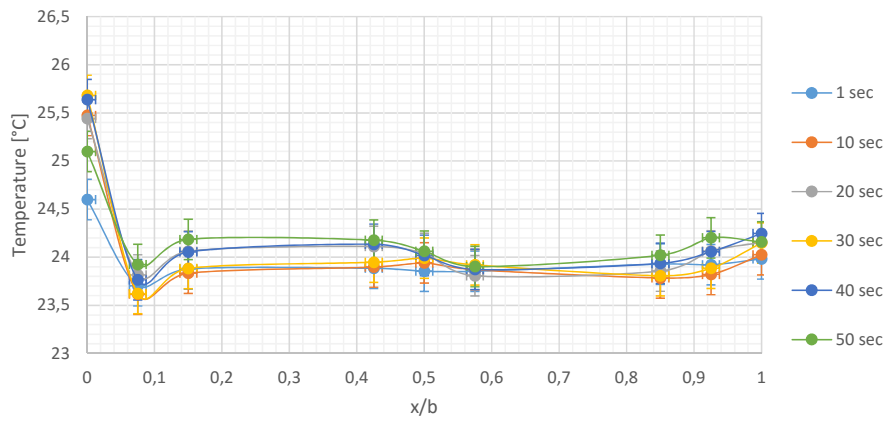


Figure I.1. Stability in horizontal temperature profile in height 0.25 m.

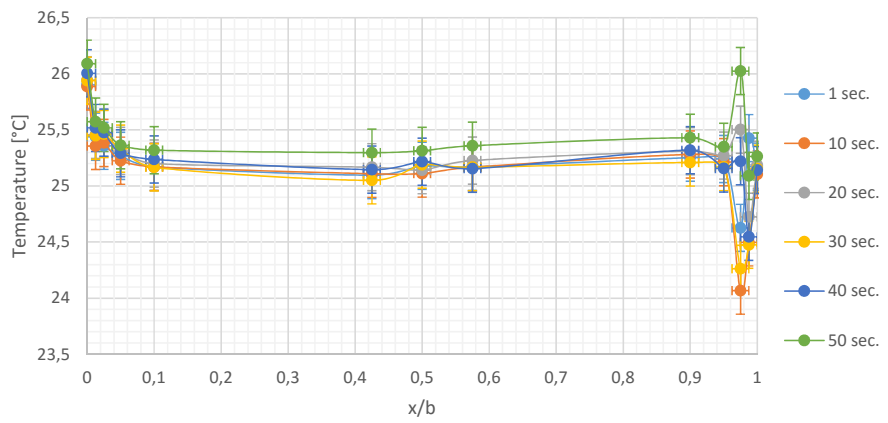


Figure I.2. Stability in horizontal temperature profile in height 1.75 m.

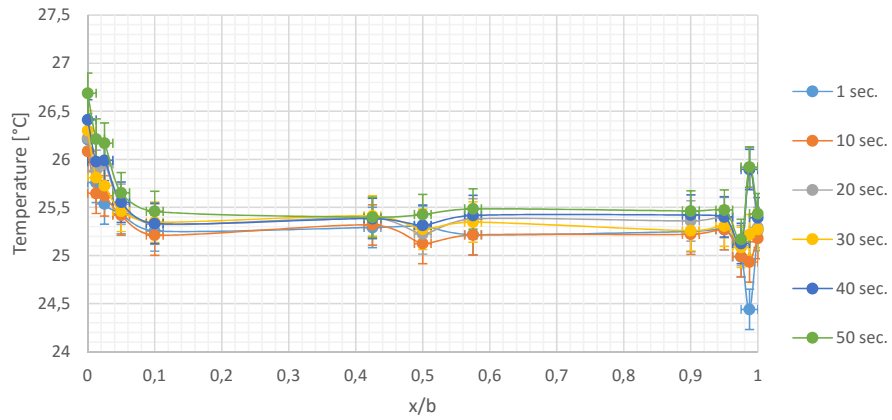


Figure I.3. Stability in horizontal temperature profile in height 2.00 m.

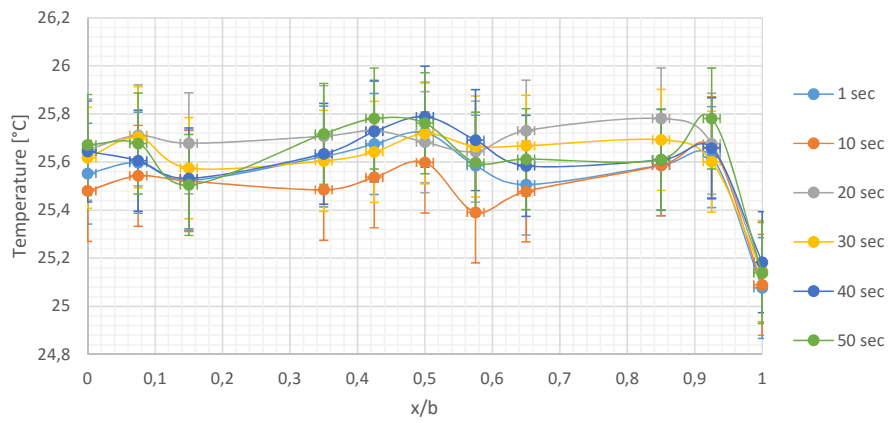


Figure I.4. Stability in horizontal temperature profile in height 2.75 m.

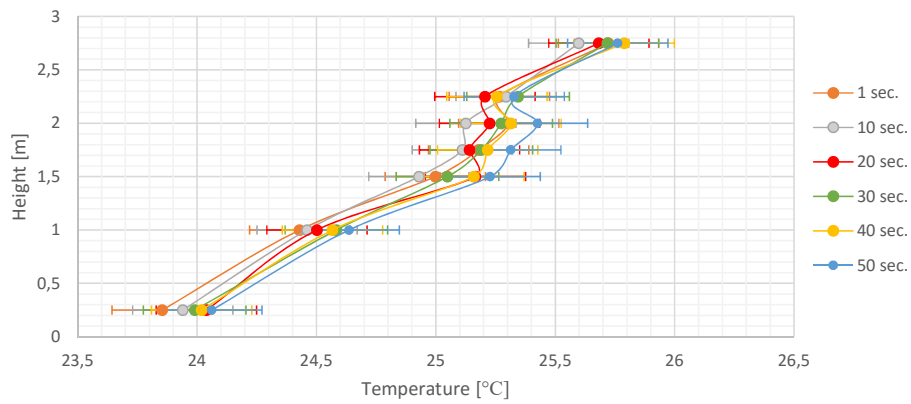


Figure I.5. Stability in vertical temperature profile in the center.

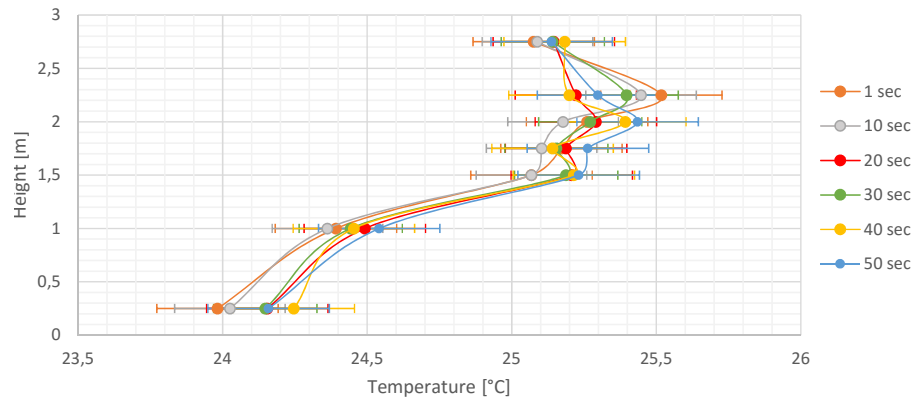


Figure I.6. Stability in vertical temperature profile at the glass surface.

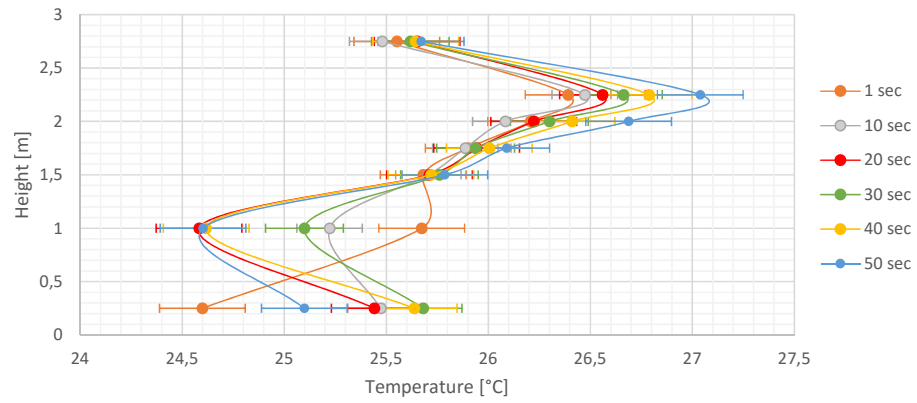


Figure I.7. Stability in vertical temperature profile at the heated surface.

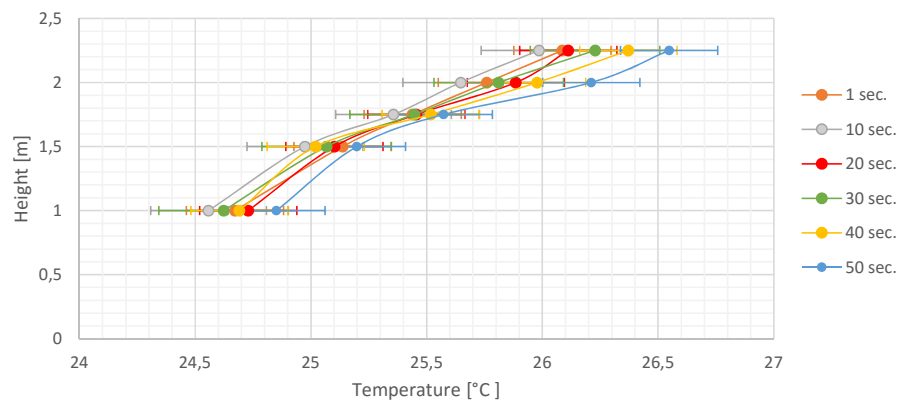


Figure I.8. Stability in vertical temperature profile 0.5 cm from the heated surface.

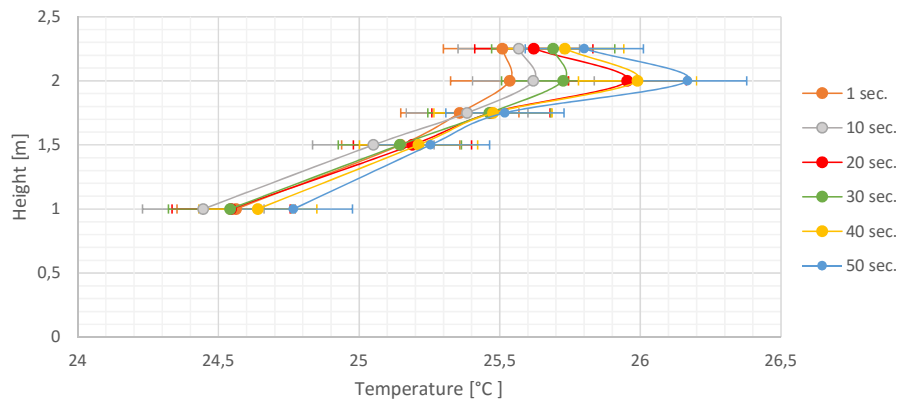


Figure I.9. Stability in vertical temperature profile 1 cm from the heated surface.

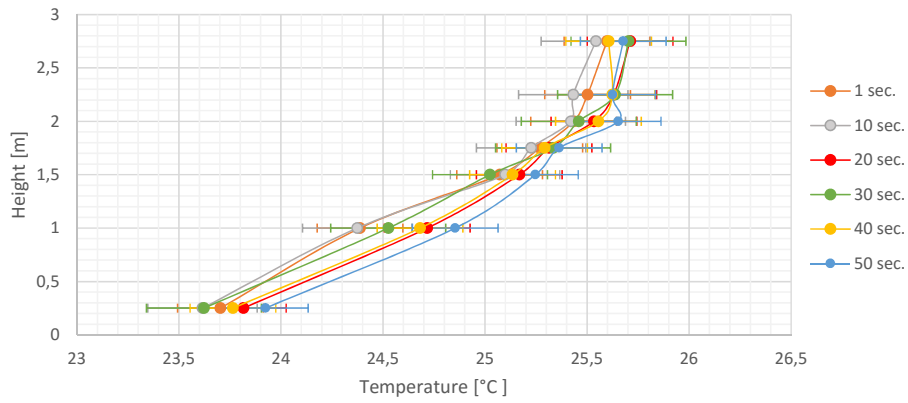


Figure I.10. Stability in vertical temperature profile 2 cm from the heated surface.

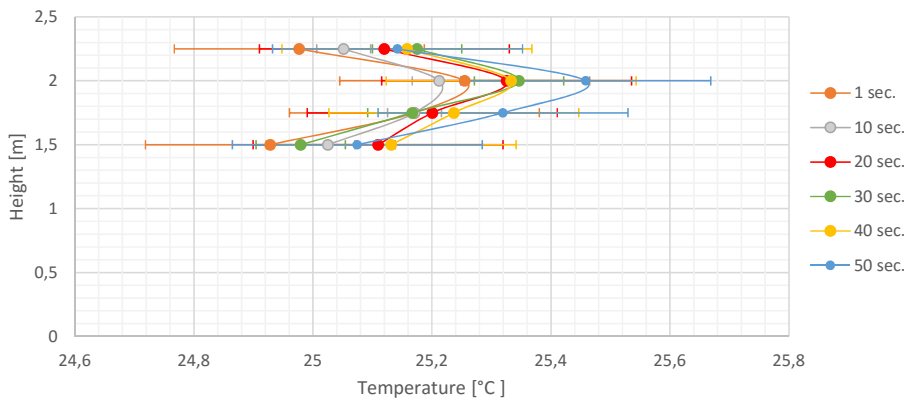


Figure I.11. Stability in vertical temperature profile 4 cm from the heated surface.

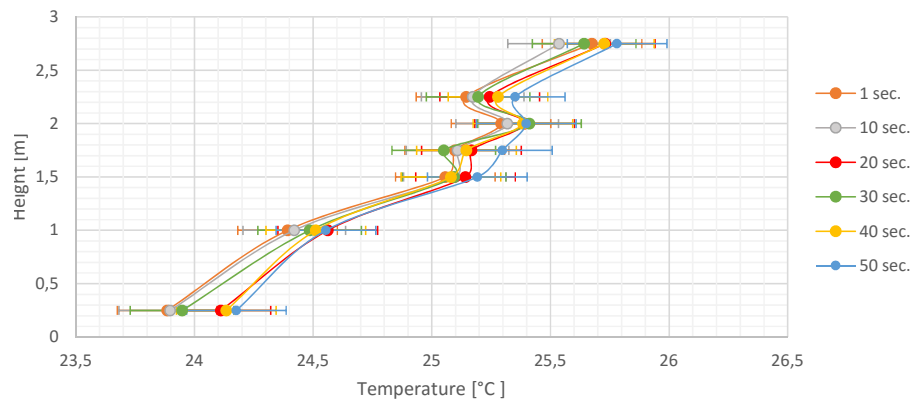


Figure I.12. Stability in vertical temperature profile 17 cm from the heated surface.

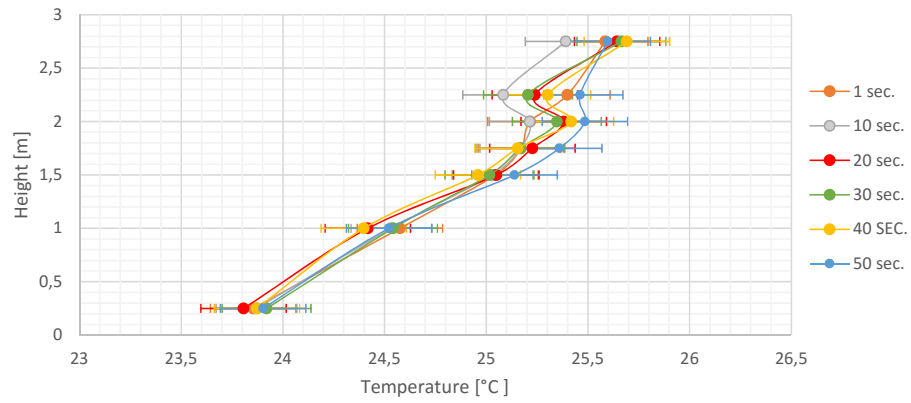


Figure I.13. Stability in vertical temperature profile 17 cm from the glass surface.

Comparison Close to Glass Surface of Group 3

Vertical dimensionless temperature profiles close to the glass surface:

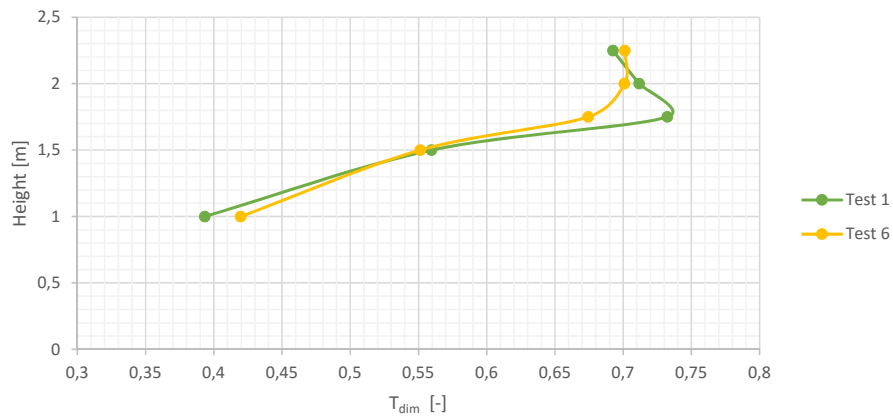


Figure J.1. Vertical temperature profiles 0.5 cm from glass surface.

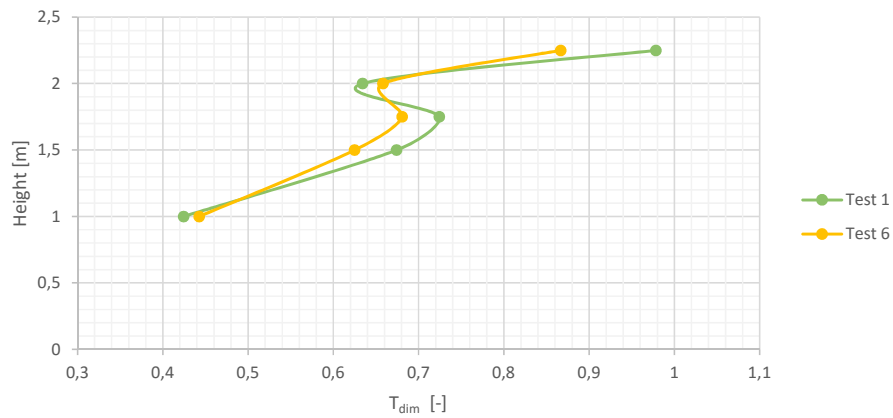


Figure J.2. Vertical temperature profiles 1 cm from glass surface.

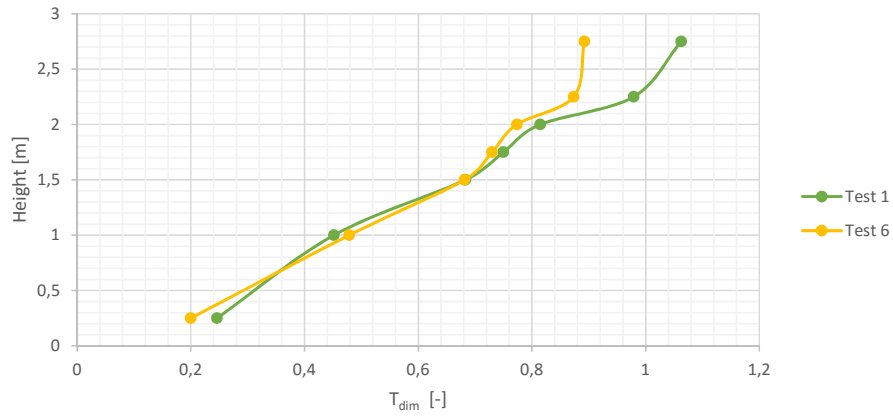


Figure J.3. Vertical temperature profiles 2 cm from glass surface.

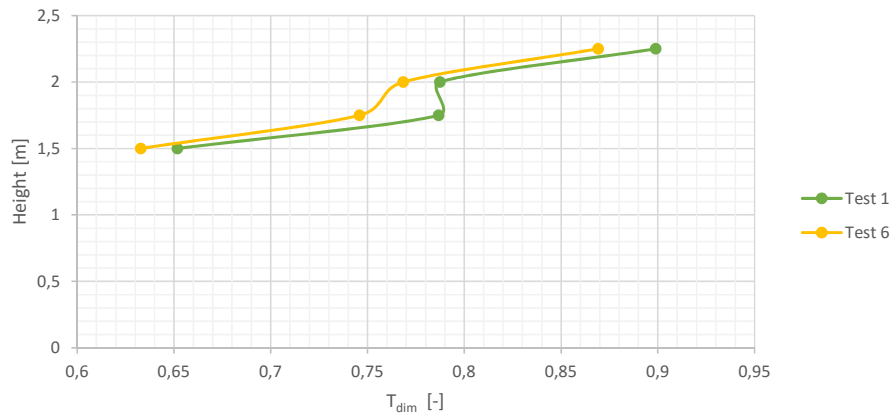


Figure J.4. Vertical temperature profiles 4 cm from glass surface.

First Period of Experimental Work

The test facility was constructed for the purpose of studying the convective channel flow. Since it was a test facility a lot of trial and error processes have occurred throughout the entire project period. The first six months of this project the experimental work was conducted in cooperation with two other master students, who finished June 2015. A lot of tests have been disregarded due to different errors, but in the following section the results from 8 tests conducted in the first six months are shown.

From theory it was known that recirculation flow appears when the buoyancy forces are strong. For this reason it was chosen to have high surface temperature at the heated wall. Furthermore, the ACH was set very low also due to known theory. The cooler for the inlet temperature was installed after the six months, so for these tests the inlet air temperature was not controlled.

The location of the thermocouples was also changed after six months. The initially locations can be found in *appendix L* on page 178. Table K.1 shows the test conditions for those eight tests, and also the mean Rayleigh number and mean Gr/Re^2 - *ratio*.

Test number	Temperature [°C]	ACH [h ⁻¹]	Ra [-]	Gr/Re^2 -ratio [-]
1	35	1.5	$4.01 \cdot 10^6$	$5.98 \cdot 10^{-6}$
2	35	3.0	$3.64 \cdot 10^6$	$1.33 \cdot 10^{-5}$
3	35	5.0	$3.43 \cdot 10^6$	$4.61 \cdot 10^{-6}$
4	39	1.5	$5.66 \cdot 10^6$	$8.46 \cdot 10^{-5}$
5	45	1.5	$6.86 \cdot 10^6$	$1.02 \cdot 10^{-4}$
6	49	1.5	$1.01 \cdot 10^7$	$1.52 \cdot 10^{-4}$
7	53	1.5	$1.03 \cdot 10^7$	$1.54 \cdot 10^{-4}$
8	53	10.0	$1.23 \cdot 10^7$	$4.13 \cdot 10^{-6}$

Table K.1. Test conditions for previous tests.

The same channel flow structure was obtained throughout every test when looking at the temperature distribution both horizontal and vertical. The flow was found to resemble the condition of extreme recirculation flow. Figure K.1 on the following page shows the horizontal temperature profile for test 7 as an example of how all profiles looked like.

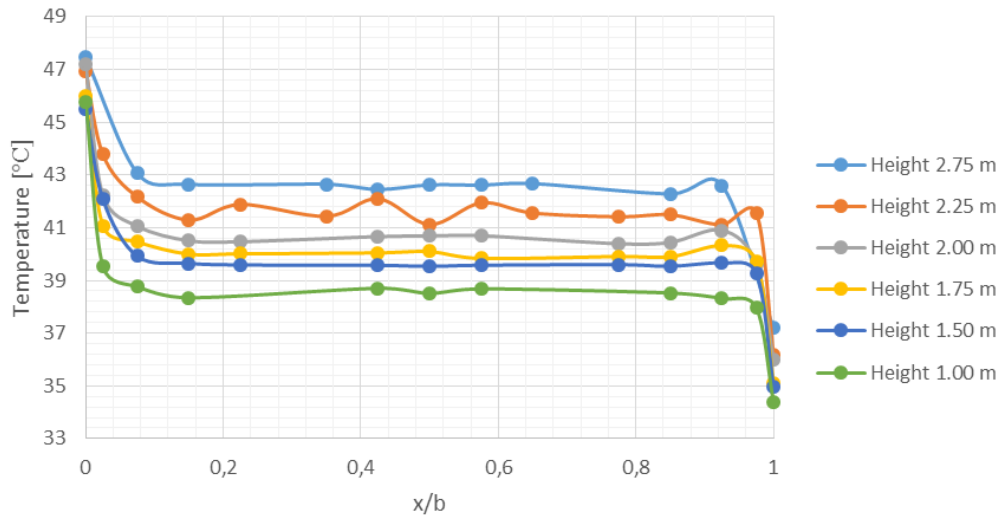


Figure K.1. Horizontal temperature profiles for test 7.

The reason why the tests showed the same tendencies might be due to the locations of the thermocouples. From the study which is presented in this report, the recirculation was found to happen close to the surface, and maybe it was simply not captured for these eight tests.

Except from temperature measurements the velocity field was also measured by a LDA system (Laser Doppler Anemometer). Explanation of the LDA measuring system can be found in *appendix M* on page 179.

Velocity measurements was conducted for case 7 in the test rig. Velocity profiles were measured in four different heights. Due to the height of the traverse system it was not possible to get lower elevations than 1.53 m, which was approximately the middle of the channel. The velocity was measured for 30 sec of interval with 1000 samples, each point three times.

The next figure K.2 on the facing page shows the horizontal velocity profiles in heights 1.53 m, 1.70 m, 1.83 m and 1.93 m.

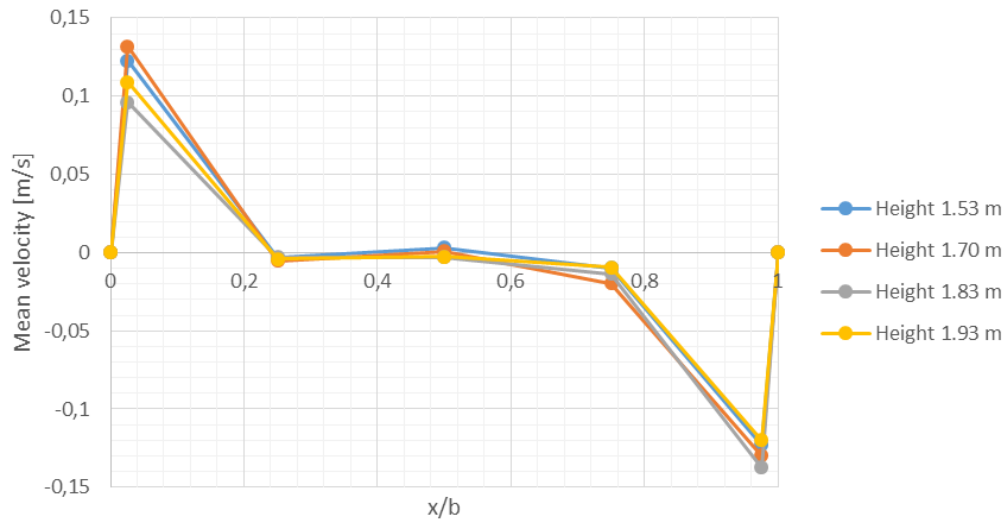


Figure K.2. Velocity profiles.

It was seen that the air accelerated downstream near the heated surface and decelerated upstream near the glass surface representing a case of extreme recirculation like it was found in [Ayinde et al., 2008] and [Habib et al., 2002]. The air exceeded the inlet velocity which was calculated to be approximately 0.005 m/s, thus the acceleration of the air was caused by the convective heat transfer. The almost zero velocities in the vicinity of the centerline indicated that the air was removed from the core to the boundary layer, creating a large vortex in the channel, and the velocities were a consequence of the convective heat transfer. In [Ayinde et al., 2008] two different Rayleigh numbers were tested, and increasing the Rayleigh number caused a higher gradient in the horizontal profile, but in none of the presented literatures was found the same nearly uniform zero velocities close to the center, but only in the complete center.

The turbulence intensity was also found to be highest in the center for all four heights like cited in [Habib et al., 2002]. The results can be seen in figure K.3 on the next page.

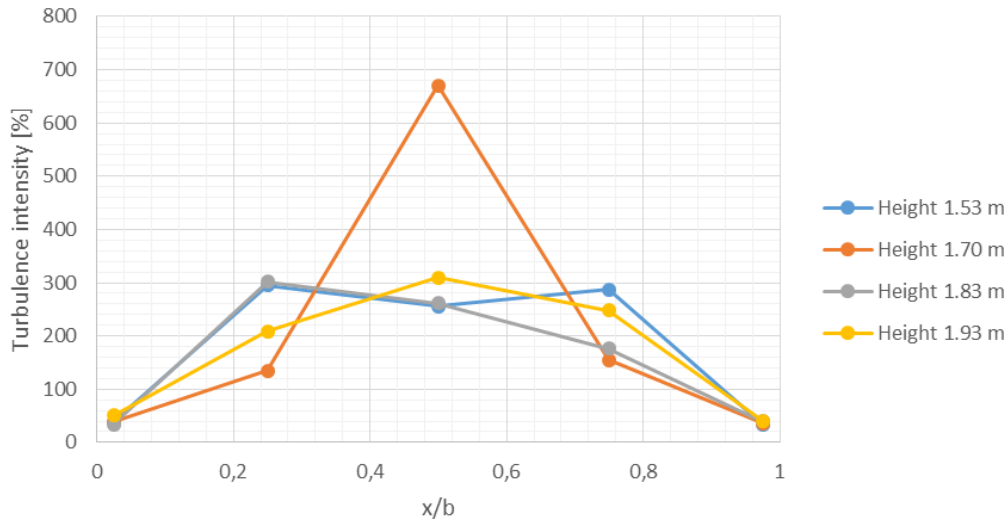


Figure K.3. Turbulence intensity for velocity measurements.

According to [Ayinde et al., 2008] the highest velocities was found in the mid plane of the channel for both aspect ratios, which was in a reasonable good agreement with these results, but it was not a clear declaration because of the lack of measurements in greater heights. Furthermore it was also seen in this study that the absolute peak velocities were the same near the hot and the cold surface for each height. The results in [Yilmaz og Gilchrist, 2007] did not resemble these results, as the extreme recirculation and backflow near the colder surface was not found. It should be mentioned that the aspect ratio was 20 compared to this case, which was 7.5, and much greater velocities were obtained in [Yilmaz og Gilchrist, 2007]. Due to the fact that the cavity in [Yilmaz og Gilchrist, 2007] was more narrow than in this study, the surfaces had greater interaction i.e. the radiation to the cold surface was greater causing a different flow regime.

L

Positions of Thermocouples First Measurement Period

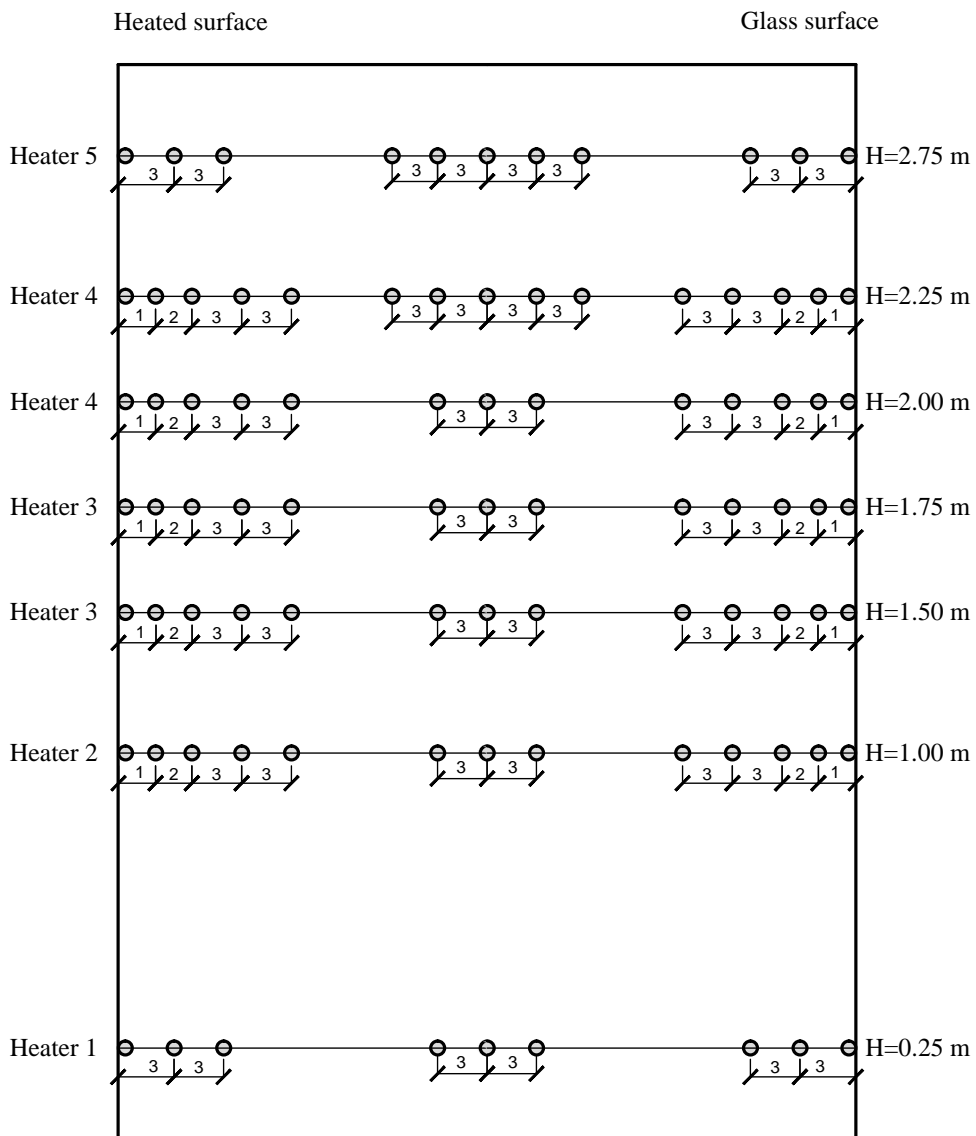


Figure L.1. Positions of thermocouples in channel.

Velocity Measurements

The following section is based on [Dantec Dynamics, 2008].

An 1D type of Laser Doppler Anemometer (LDA) which was equipped with a burst spectrum analyzer (BSA) was used to measure the air velocity in the vertical channel. The LDA is an optical non-intrusive instrument that measures the particle flow in gases and fluids. The principle of the LDA is shown in figure M.1. It consists of a continuous wave laser, transmitting optics including a beam splitter and a focusing lens, receiving optics as a focusing lens, an interference filter and a photodetector, and at last a signal processor.

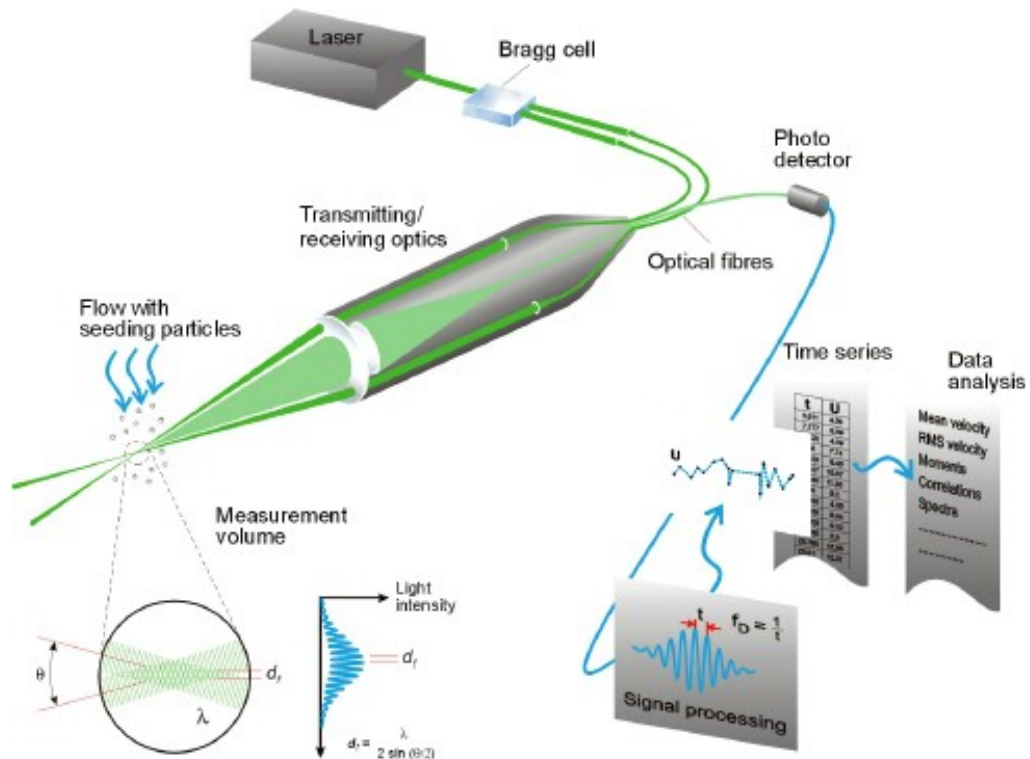


Figure M.1. LDA principle. [Dantec Dynamics, 2008]

As the figure is showing a Bragg cell is used as the beam splitter that creates vibrations, which generate acoustical waves acting like an optical grid. From this, two laser beams are produced with equally intensity but different frequencies. The laser beams are brought to the probe, where after the lens force them to intersect in a probe volume, the measurement volume showed in figure M.1 and this volume is only a few millimeters long. Fringes, which are parallel planes of high light intensity, are created in the measurement volume due to interference between the two laser beams. When seeding particles pass this area the scattered light contains a Doppler shift, the Doppler frequency, which is proportional to the velocity measured perpendicular to the probe volume. The scattered light is then sent back to the lens and focused on a photo-detector, that analysis the light intensity according to frequency and speed of the particle, since velocity equals distance divided by time.

The locations where the LDA probes conducts the velocity measurements has to be known with high accuracy. For that reason a 2D traverse mechanism were used to know the coordinates with high accuracy.

Fog droplets generator was used to create particles that can be traced by the LDA. It was needed to take into consideration that the smoke machine warms the incoming air, so the smoked air entered into the cavity was warmer than the ambient air. For that reason, the smoke was streamed into a 1 m long tube to ensure that the smoke, after it was generated and before entering the cavity, was cooled off and resembled the ambient air.

The inlet of the cavity was a free ambient air inlet, and the air temperature could vary according to the ambient conditions. For that reason, in order to reduce this uncertainties and to have the almost same ambient conditions during the measurements, the measurements were performed by using two DANTEC Flow LDA laser probes. The first laser was positioned steady in the middle of the cavity at the height of 1.20 m from the inlet height and the second was placed on the traverse mechanism and measured the velocities for different locations as it is illustrated in figure M.2. Only measurements from the second laser were used when the first laser with constant location showed a nearly steady state.

Also, it has to be mentioned that the laser, which was located steadily had a lens suitable for measuring distances up to 160 mm and the second one located on the traverse system had a lens that measured distances up to 400 mm. For each measuring point, the readings of 89 thermocouples were taken. The purpose of these readings was to compare the effect of adding smoke to the measurements conducted without smoke.

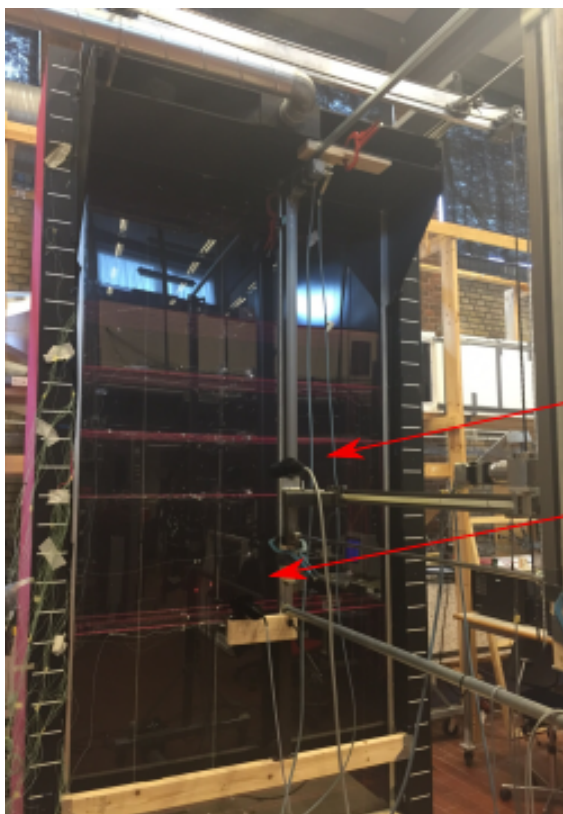


Figure M.2. Position of two lasers for velocity measurements.

To ensure that the first measuring position of the laser probe was in accordance with the measuring location of the thermocouple, the probe was traversed towards the heating wall, and it was assumed that it was coincident with the wall surface when the signal amplitude of the probe was at maximum [Yilmaz og Gilchrist, 2007]. From that point, the laser probe was moved to the first wanted location.

N

Electronic Appendix

Two folders are found in the CD:

- Experimental Study
- Numerical Study

In the folder experimental study, all calculations and graphs is to be found.

The CFD model can be found in the numerical study folder.